Title
Instrumentation for Treatment of Cancer Using Proton and Light-Ion Beams

Authors
Chu, W.T.
Ludewigt, B.A.
Renner, T.R.

Publication Date
1993-02-01

LBL-33403
UC-406
Preprint

Lawrence Berkeley Laboratory
UNIVERSITY OF CALIFORNIA

Accelerator & Fusion Research Division

Submitted to Review of Scientific Instruments

Instrumentation for Treatment of Cancer Using Proton and Light-Ion Beams

W.T. Chu, B.A. Ludewigt, and T.R. Renner

February 1993

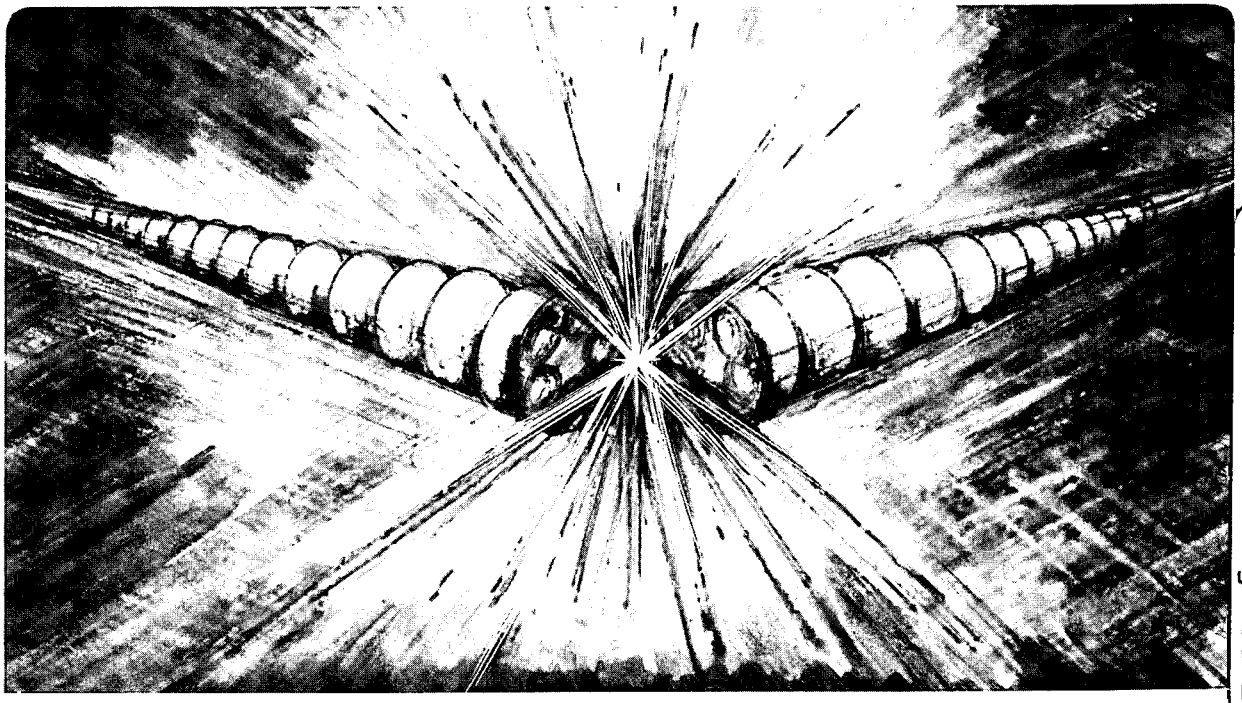

Prepared for the U.S. Department of Energy under Contract Number DE-AC03-76SF00098

DISCLAIMER

LBL-33403

Instrumentation for Treatment of Cancer Using Proton and Light-Ion Beams

W. T. Chu, B. A. Ludewigt, and T. R. Renner

Lawrence Berkeley Laboratory

University of California, Berkeley, CA 94720

February 1993

Submitted to the Reviews of Scientific Instrument for publication.

This work is supported by the Director, Office of Energy Research, Office of High Energy and Nuclear Physics, of the U.S. Department of Energy under Contract No. DE-AC03-76SF00098 and in part by the National Institute of Health under Grant No. CA49562.

Abstract

Clinical trials using accelerated heavy charged-particle beams for treating cancer and other diseases have been performed for nearly four decades. Recently there have been worldwide efforts to construct hospital-based medically-dedicated proton or light-ion accelerator facilities. To make such accelerated heavy charged-particle beams clinically useful, specialized instrument must be developed to modify the physical characteristics of the particle beams in order to optimize their biological and clinical effects. This paper reviews the beam modifying devices and associated dosimetric equipment developed specifically for controlling and monitoring the clinical beams.

I. INTRODUCTION

I.A. Rationale for Using Heavy Charged-Particle Beams to Treat Human Cancer

Radiations used for treatment of human cancer and other diseases come from either sources external to the patient body or from implanted radioactive sources within the patient body. X rays were the first external radiation used for such purposes. Until the 1970s many hospitals used gamma rays from radioactive isotopes, such as ^{60}Co, or megavoltage x rays from betatrons. Modern hospitals now use mainly bremsstrahlung photons produced when high-energy electrons from an electron linear accelerator (LINAC) interact in a target material. High-energy electrons themselves are also directly used for patient treatment. The above are called *conventional radiation* since photons and electrons have been widely used in radiotherapy.

In recent years, other types of radiations, especially of nuclear and subatomic particles, have been clinically evaluated. The types of particle radiation of interest in this review are accelerated atomic nuclei, such as hydrogen, helium, carbon, neon, silicon and argon nuclei. The medical community calls the radiation of these accelerated nuclei *heavy charged-particle* radiation. *Heavy* because they are heavier than the particles of conventional radiation, and *charged* to distinguish them from the other neutral particles, such as neutrons, which have also been clinically evaluated. Protons (nuclei of hydrogen atoms, $m_p \approx 1836\ m_e$) represent the lightest of the nuclear particles. Heavier-nuclei beams are sometimes called by clinicians *heavy-ion* radiation. When first available for clinical use, any nuclear particles heavier than protons were called heavy ions. More recently, the nuclei with an atomic number equal to or smaller than that of neon nuclei are called *light ions*, leaving the name *heavy ions* to heavier ones such as silicon and argon nuclei. Active clinical research is pursued worldwide using heavy charged-particle radiation to take advantage of its dose-localizing effect due to the Bragg peak (see Sec. I.A.1. below) and biological advantage over conventional radiation (see Sec. I.A.2. below).[1-4] Clinical advantages of negative pions ($m_\pi \approx 267\ m_e$) are also being studied as the penetrating pions deposit a large amount of energy at the end of their flight path due to the Bragg peak and nuclear "star" formation.[5-7] The negative pions are the lightest member of the heavy charged-particle family. Even though the dose distributions of fast neutron beams do not have the dose localizing advantage,[8] clinical trials are also underway using beams of fast neutrons of tens of MeV to exploit their radiobiological advantages over photons due to the fast neutron's high LET (linear energy transfer) characteristics.[9-13] The use of antiproton beams for treatment of human cancer has been proposed[14]; however, actual implementation of their clinical use has not yet materialized. In this paper, the discussion will be concerned mainly with instrumentation for treatment of cancer using proton and light-ion beams.

I.A.1. Physical advantage of heavy charged-particle radiation

I.A.1. a. Bragg peak and distal dose falloff

When energetic heavy charged particles enter an absorbing medium, they are slowed down by losing their kinetic energy mainly through ionizing the medium. The energy loss per unit mass per unit area of the absorber, or specific ionization (usually expressed in keV/μ in water) increases with decreasing particle velocity, giving rise to a sharp maximum in ionization near the end of the range, known as the Bragg peak.[15] As shown in Fig. 1, when a beam of monoenergetic heavy charged particles enters the patient body, the depth-dose distribution is characterized by a relativelylow dose in the entrance region (plateau) near the skin and a sharply elevated dose at the end of the range (Bragg peak). The range can be adjusted, so that the Bragg peak occurs in the target volume as shown in the figure. A pristine beam with a narrow Bragg peak makes it possible to

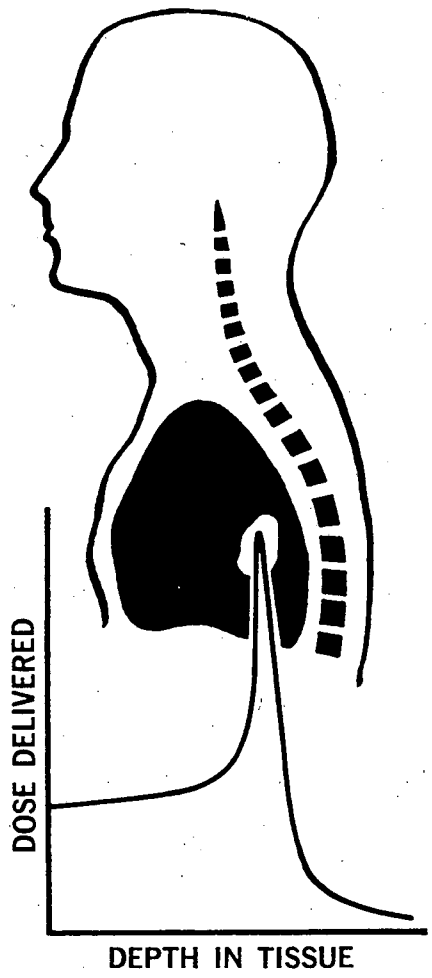

Fig. 1. Schematically shown is a Bragg curve, the relative dose as a function of the penetration depth. The range of the beam may be adjusted to place the Bragg peak inside the target volume. The dose beyond the target volume is very small, thereby any critical structures distal to the target, such are the spinal cord, are protected. The entrance dose, the dose upstream of the target, is also low compared with the peak dose.
(XBL 737-969)

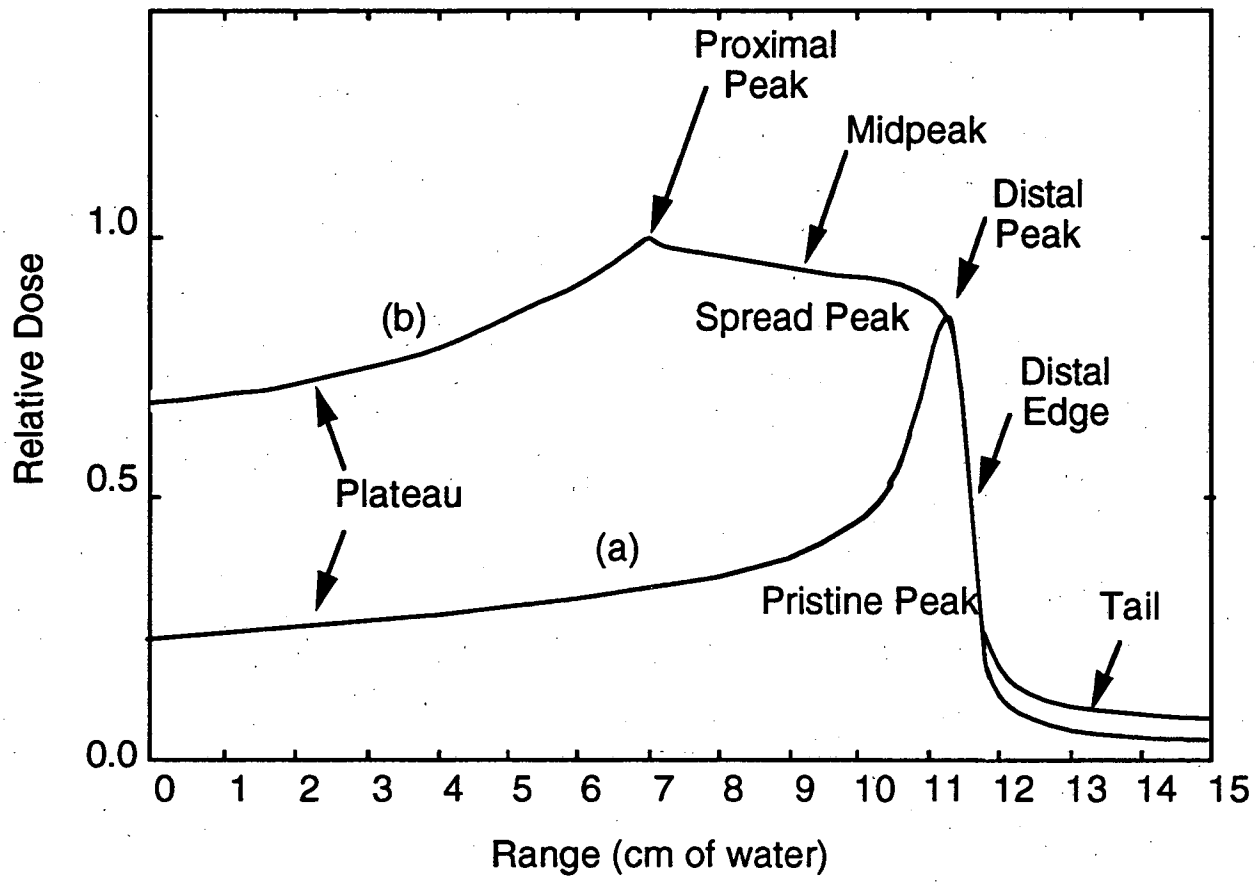

Fig. 2. Shown are the *physical* dose distributions as a function of penetrating depth of (a) a pristine beam and (b) a beam whose energy is modulated to widen the stopping region. Such a curve with a spread-out Bragg curve has several regions referred to as the plateau, the proximal peak, the midpeak, the distal region, the distal dose-falloff edge, and the tail. A uniform biological dose distribution within the spread-out peak region is obtained by compensating for the variation in the relative biological effectiveness of the radiation as a function of penetrating depth, as depicted in Fig. 4.

irradiate a very small localized region within the body with an entrance dose lower than that in the peak region.[1, 16, 17] If the Bragg peak is spread out to cover an extended target by modulating the energy of the particles, as shown in Fig. 2, the ratio of peak-to-plateau decreases[18]; however, the *biologically effective* dose in the spread-out peak can still be greater than the entrance dose[19] (see Sect. I.A.2). In contrast, commonly used gamma-rays and fast neutrons, in penetrating the patient body, impart nearly exponentially decreasing dose distributions, giving higher doses at the entrance region and in the intervening tissues and lower doses in the target volume itself as indicated in Fig.

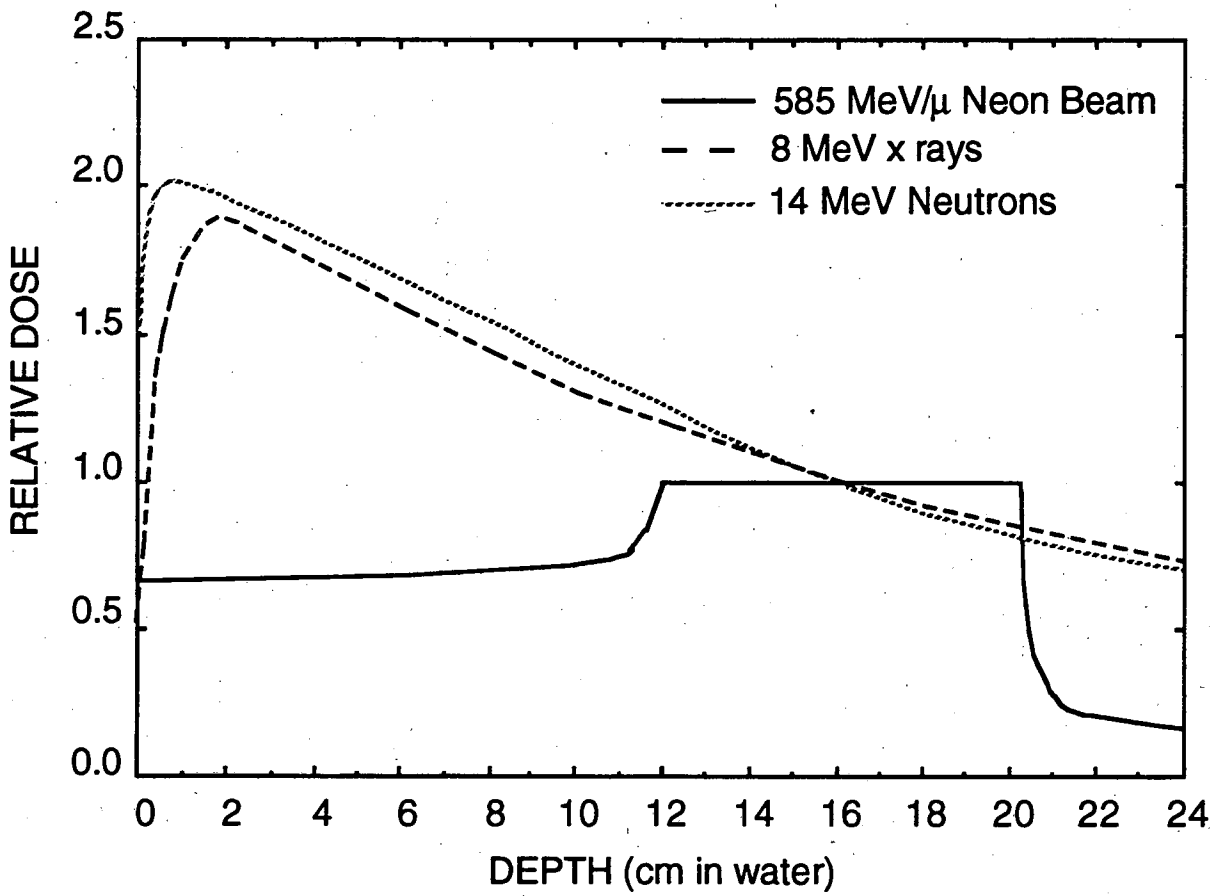

Fig. 3. The dose deposition of several types of radiation as a function of penetrating depth in water are compared. The doses are normalized at the midpeak of the heavy charged-particle beam.

3. The radiation dose beyond the target volume only gradually decreases irradiating critical organs and healthy tissues there. For the heavy charged-particle beams, the radiation dose abruptly decreases beyond the Bragg peak, sparing any critical organs and healthy tissues located downstream of the target volume from unwanted radiation. Examples of spread-out *Bragg ionization curves* of several heavy charged particles are shown in Fig. 4.

I.A.1. b. Multiple scattering and lateral dose falloff

Another physical advantage of *heavier* charged particles is that they suffer significantly less multiple scattering than *lighter* ones while penetrating the absorbing medium (see I.C.3.a). The result is that the heavier charged-particle beams exhibit sharper lateral dose falloffs at the field boundary. This is an important property to be exploited in clinical application as many tumors are immediately adjacent to critical organs, which must be spared of unwanted radiation as much as possible.

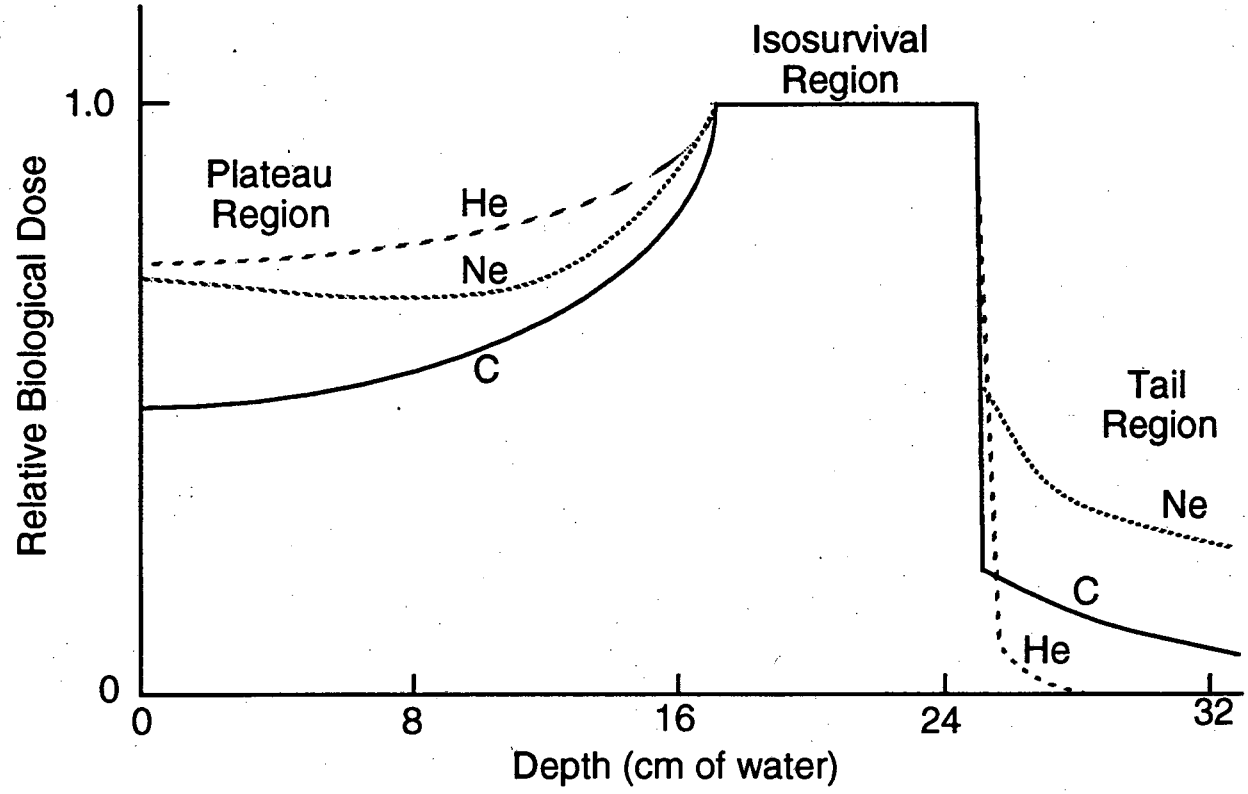

Fig. 4. The relative *biological* dose of spread-out Bragg peaks of helium, carbon, and neon ion beams as a function of penetrating depth in water are shown for comparison. The doses are normalized at the isosurvival region and the figure shows the different relative entrance, plateau, and tail doses for these beams.

I.A.1. c. Dose localization

These superior dose localization capabilities of heavy charged-particle beams suggest the possibility of depositing a higher dose into the target volume while reducing the unwanted radiation in surrounding critical tissues. The clinical expectation is increased local control with a decrease in normal-tissue complications.

Based on the physical advantage of dose localization, Robert R. Wilson proposed as early as 1946 the rationale for using accelerated heavy charged-particle beams for radiotherapy of human cancer and other diseases.[20] The radiobiological rationales to use protons in radiotherapy have been reviewed by Raju recently.[21] A year later, when the 184-Inch Synchrocyclotron was completed by E. O. Lawrence and his associates[22] at the Radiation Laboratory of the University of California, Berkeley, now the Lawrence Berkeley Laboratory (LBL), the first biological investigations with high-energy nuclei were begun by Cornelius A. Tobias and John H. Lawrence.[1] These

investigations were followed by the first human therapeutic exposure to proton, deuteron, and helium-ion beams at the Radiation Laboratory in December 1954.[23, 24] In the early part of 1970s, clinical trials using accelerated proton beams to test their dose-localization advantages in treating human diseases began in the U. S.,[25, 26] Sweden,[27, 28] and the Soviet Union.[29] Clinical trials using accelerated light and heavy ions to treat human cancers started at LBL in November 1977.[30, 31] The past efforts and current plans worldwide in clinical trials using the protons and heavier ions for treatment of cancer are summarized in Sec. I.B.

I.A.2. Biological rationale for clinical use of light and heavy ions

I.A.2.a. LET and oxygen effect

In radiotherapy, *local control* of a tumor means remission of the treated disease and its non-recurrence at the same site over five years. The failure in local control of tumors treated with conventional radiation is often due to its inability to completely eradicate anoxic (deprived of dissolved gaseous oxygen) tumor cells which are resistant to conventional radiation. Regrowth of the cells in the anoxic core of the tumor results in the failure of the local control.[32] In 1967, Tobias and Todd gave the scientific justification for utilizing light and heavy ion beams to reduce this radiobiological oxygen effect.[33] Ions with higher atomic charges (Z) produce higher linear energy transfer (LET), *i.e.*, the energy loss of the penetrating particle per unit distance in absorbing material, often expressed in an energy loss per unit thickness of water-equivalent material (keV/μ). Beams having higher LET exhibit the biological advantages of lower oxygen effect, as indicated in Fig. 5. The oxygen enhancement ratio (OER) is defined as the ratio of the absorbed dose of a given radiation to produce a certain biological endpoint in an anoxic cell population to that needed to achieve the same biological endpoint for an oxic cell population. In the case where the endpoint is cellular inactivation, for example, the value of OER tells you how much more radiation is required to inactivate anoxic cells (usually found in tumor cores) compared with well oxygenated cells (usuallyfound in healthy tissues surrounding the tumor volumes). Based on this scientific rationale, radiobiological investigations were conducted on physical and biological factors of various high-LET radiations, such as light and heavy ions, negative pions, and fast neutrons, crucial for radiotherapy.

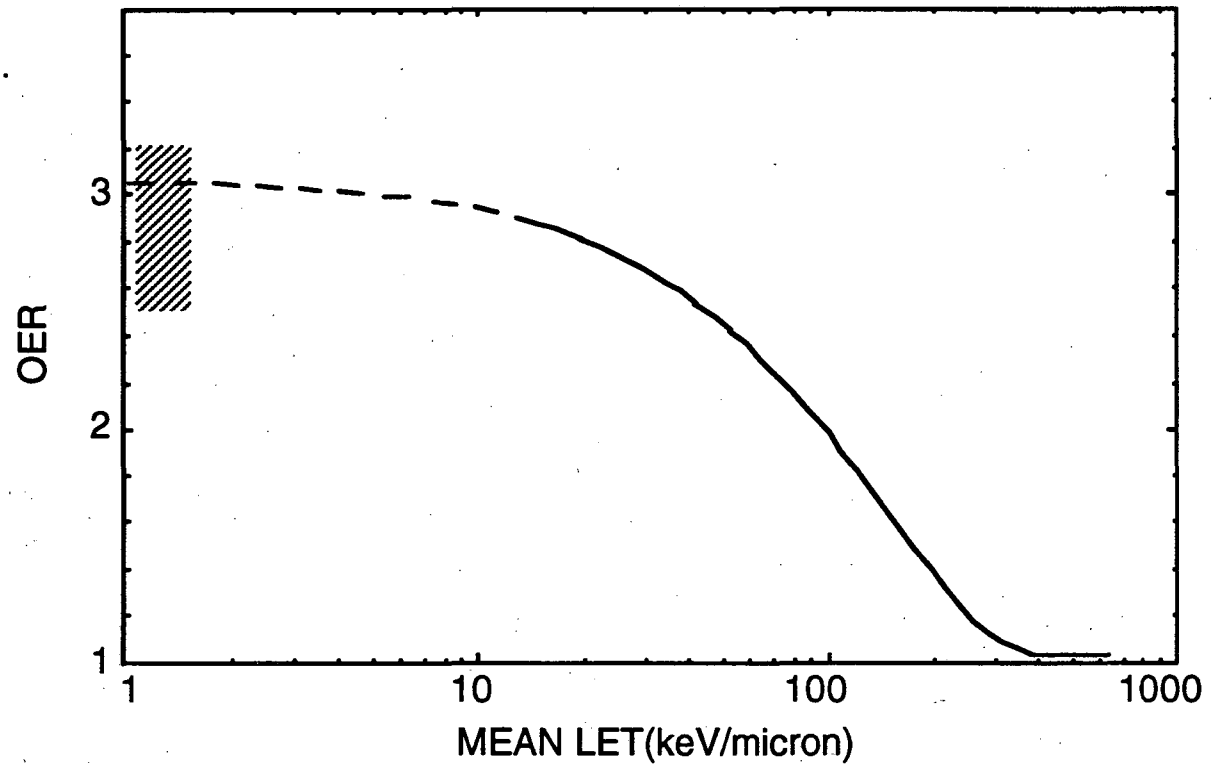

Fig. 5. The variation of the oxygen enhancement ratio (OER) is shown as a function of the linear energy transfer (LET) of the radiation. The lower the OER the lower the resistance of oxygen-deprived cells to inactivation by radiation. The shaded area represents the measured OER for x rays. The solid curve is a generalized fit to data using various ions and energies.

I.A.2.b. Radiobiological rationale for clinical use of light and heavy ions

With advances in accelerator design in the early 1970s, it became possible to examine the biological effects of high-energy light and heavy ions. Synchrotrons at Berkeley[34] and Princeton[35,36] accelerated ions with atomic numbers between 6 and 18, at energies that permitted the initiation of several biological studies.[37-39] The higher relative biological effectiveness (RBE) of these high-Z ion beams indicated a high likelihood of an enhanced therapeutic potential when compared with lower-Z ion beams.[40-42] The RBE is defined as the ratio of absorbed dose of a reference radiation to that of a radiation in question required to produce the same biological endpoint, other conditions being equal.[43] The RBE of each ion has been studied in some detail with a variety of biological endpoints.[44-47] Biology experiments performed mainly at LBL show that the RBE of a heavy charged-particle beam is not a simple function of LET[48, 49] as shown in Fig. 6. In general, the values of RBE and the degrees of dose localization increases from protons to silicon ions. The

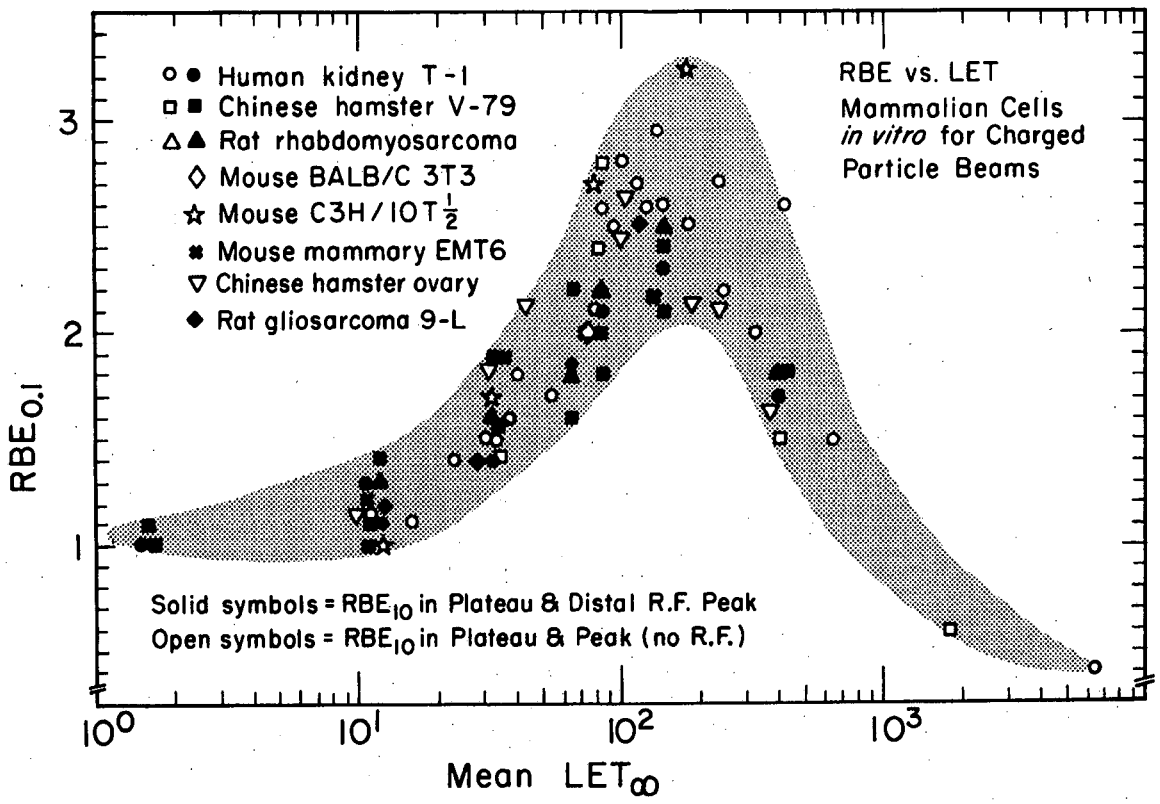

Fig. 6. A graph of the radiobiological effectiveness (RBE) of a radiation field versus its LET. A simple relationship does not exist between the two, even though LET is usuallly used to describe of the differences in radiation damage by various light ions. The data is from a number of experiments using a number of ions, energies and cell types. The shaded area shows the general trend of the data. (XBL 7810-3663)

radiobiological rationale for using these high-Z particles for radiotherapy,[50-53] as understood today, can be summarized as follows: (a) The high resistance of hypoxic cells relative to oxic cells is reduced when irradiated with high-LET radiation. (b) Slowly proliferating cells (in G_0 or long G_1 phase in cell cycle) show a similar increase in sensitivity, if irradiated with high-LET radiation. (c) Overall treatment time with high-LET radiation can be shortened since fewer fractions of larger doses may be used instead of multiple fractions of small doses when the surrounding normal tissue damage in a fewer fraction can be kept comparable to that of a standard low-LET fraction.[54] The last point should be compared with the fact that there is an advantage in using multiple, small fractions of low-LET radiation for sparing late damage.[55]

It is advantageous to treat tumors with high-LET radiation if they have the following properties[54, 56]: (a) High intracellular repair — whether of sublethal or potentially lethal damage,[57] repair is less after high-LET irradiation. (b) Poor cell cycle redistribution — if redistribution of the resistant phases of the cell cycle were rapid, conventional low-LET radiotherapy would be as effective. (c) Poor reoxygenation during treatment — if reoxygenation was good, conventional radiotherapy would be as effective. These three factors all lead to more cell killing in tumors treated with high-LET than with low-LET radiation. (d) Rapid proliferation in tumors — it is easier to give treatments in shorter overall times with high-LET radiation. Cutting down the number of treatments also benefits individual patients as well as the management of the clinic.

I.A.3. Clinical trial using heavier ions

The construction of the Bevalac accelerator complex at LBL, in which the SuperHILAC injects heavy-ion beams into the Bevatron, expanded the opportunity for medical studies with heavy charged-particle beams.[58] Clinical trials for treating human cancer using neon and other ions have been in progress at the LBL Bevalac since 1977.[3, 4] Future clinical trials using light and heavy ions are planned in Darmstadt, Germany and Chiba, Japan, as discussed in Sec. I.B. below.

I.A.4. Needs for beam-delivery technologies

To test their therapeutic potential adequately, the *physical and biological* advantages of heavy charged-particle beams must be fully exploited for clinical application. One must develop technologies to deliver optimum radiation dose distributions, *i.e.*, delivering a maximum dose to the tumor, and at the same time, minimizing the radiation dose delivered to surrounding sensitive, normal structures of the body. Many beam modifying instruments and beam delivery methods, which have been developed to optimize the physical dose distribution within the patient body, are the topics of this review. There are several earlier review papers on dosimetry equipment and methods for heavy charged-particle beams,[59-64] and for dosimetric procedures.[65-69] This review concentrates on the discussion of instrumentation developed for the modification, control, and monitoring of the clinical beams.

I.B. General Overview of Worldwide Interests in Heavy Charged-Particle Radiotherapy

In recent years, there has been increased interest in the medical community throughout the world to build *dedicated medical* accelerators employing beams of energetic protons and light and heavy ions. In 1991 Sisterson reviewed the clinical use of protons and ion beams from a worldwide perspective.[70] A summary of updated situation and future plans in this fast moving field is given below. From the large number of new facilities either under construction or in operation around the

world one can conclude that interest in radiation therapy with proton beams has increased dramatically in the last few years.

I.B.1. On-going proton and helium-ion trials

Clinical studies underway using low-LET radiation, namely accelerated protons and helium ions, are discussed first.

•From 1975 to 1987, the 932-MeV helium-ion beam from the 184-Inch Synchrocyclotron at LBL was used for treatment of cancer patients, for precision high dose radiotherapy[71] of tumors adjacent to critical central nervous system structures,[72, 73] for treatment of malignant ocular tumors,[74-78] for irradiation of intracranial lesions,[79-81] and more recently for stereotactic radiosurgery,[82] such as the treatment of arteriovenous malformations (AVM).[83] After 1987, the LBL helium-ion programs have been continued at the Bevatron.[84] More than 2200 patients have been treated using helium ions. The proton beam from the 184-Inch Synchrocyclotron was used for pituitary irradiation of patients;[24, 85-90] however, the topics of interest in this article are mainly the treatment of cancer patients and the earlier pituitary trials will not be further discussed.

•Massachusetts General Hospital and Massachusetts Eye and Ear Infirmary have used the 160-MeV protons at the Harvard Cyclotron Laboratory (HCL)[91] to treat more than 4000 patients.[55, 92-97]

•From 1957 to 1968, the 185-MeV protons from the 230-cm synchrocyclotron at the Gustaf Werner Institute in Uppsala, Sweden was used to treat a limited number of patients with stereotactic radiosurgery of the brain[98] and for the treatment of cancer.[99-101] They have upgraded a 200-MeV modified three-sector, variable-energy cyclotron (SFSC-200), and began treating AVM patients in 1991 at the Theodore Svedberg Laboratory.[102, 103]

•In Russia (formerly U.S.S.R.), medical proton trials have been in progress at three institutes.[104] Beginning in 1969, the Institute of Theoretical and Experimental Physics (ITEP) in Moscow has used proton beams from the synchrotron for patient treatments,[105, 106] and since 1982 three treatment rooms have been available for clinical trials.[107] The proton energy is variable between 70 and 200 MeV.[108, 109] About 2000 oncological, neurosurgical, ophthalmological,[110] and endocrinological patients have been treated.[111-113] In 1989, the reconstruction of a 680-MeV cyclotron was finished at the Joint Institute of Nuclear Research (JINR) in Dubna,[114] and patients have been treated using a degraded proton beam.[115] At the Central Research Roentgenoradiology Institute using the 1000-MeV proton beams from the synchrocyclotron of the Leningrad Institute for Nuclear Physics (LINPH) in Gatchina, near Leningrad, intracranial diseases have been treated using plateau radiation.[116-120] These Russian facilities have treated more than 2500 patients, one-third of all the patients treated worldwide.[121]

•Very active proton therapy programs are in progress in Japan.[122] Between 1979 and 1991 the National Institute of Radiological Sciences (NIRS) in Chiba has treated 75 patients using 70-MeV

protons (to be upgraded to 90 MeV).[123] In 1983 a clinical study of proton radiotherapy was initiated at the Particle Radiation Medical Science Center (PARMS) of the University of Tsukuba, Japan using the 250-MeV protons obtained by degrading the 500-MeV protons from the booster synchrotron of the High Energy Physics Laboratory (KEK).[124] PARMS employs two treatment rooms, one with a vertical beam line and the other with a horizontal beam line, and has treated more than 200 patients between 1983 and 1991.[125-128]

•The Paul Scherrer Institute (PSI, formerly the Swiss Institute of Nuclear Research, SIN) at Villigen, Switzerland, is currently treating eye melanomas with protons at the Ophthalmological Therapy Installation (OPTIS) employing 72-MeV protons from one of the injector cyclotrons. OPTIS is a collaborative project between PSI and the Ophthalmological Hospital of Lausanne University,[129, 130] and since 1984 used protons to treat patients.[131, 132] PSI is in mid-construction of a large-field proton treatment system.[133]

•The treatment of patients started in 1991 at the Centre Antoine-Lacassagne in Nice, France which has reinstalled its Medicyc cyclotron[134] to produce a 63-MeV proton therapy beam.[135] Eight major radiotherapy centers in southeastern France have formed a cooperative group to exploit this capability.[136] This facility is also preparing to start neutron therapy in 1992.

•The Medical Research Council Cyclotron Unit at the Clatterbridge Hospital, Merseyside, U.K., uses 62.5-MeV protons from a fixed energy AVF cyclotron (Scanditronix MC60) to treat ocular melanoma patients. Patients have been treated since its opening in 1989.[137, 138] Boosting the energy to 180 MeV using a drift tube LINAC (DTL) technology has been recently proposed.[139] The energy of the proton beam may be increased to 200 or 250 MeV at a later date by adding more accelerating tanks.

•One especially notable initiative in the U.S. is the commissioning of a 250-MeV proton synchrotron at the Loma Linda University Medical Center in Loma Linda, California.[140-143] The accelerator was designed and built by the Fermi National Accelerator Laboratory.[144, 145] It is the *first* dedicated proton accelerator facility built for a hospital. The proton facility has three rotating-gantry rooms, two fixed horizontal beam-line rooms, one for small-field treatments (eye and brain) and large-field treatments, and the other for research. The first patient was treated in the eye beam in October 1990, and the second beam line, the horizontal beam line with a 250-MeV beam was put into clinical use in March 1991. The patient treatments began in June 1991 using the beam delivered by one of the gantries.

•Four hospitals and the three oncological centers of the Paris area (Assistance Publique, Institut Gustave Roussy, Institut Curie, and Centre René Hugenin) have created the Centre de Protonthérapie d'Orsay (CPO) by converting the 200-MeV proton cyclotron at Orsay exclusively for medical use. It provides a 73-MeV eye treatment beam and a 200-MeV large field treatment beam.[146] The medical programs have started in 1991.[147, 148]

•Proton therapy started at Louvain-la-Neuve since 1991 using a 85-MeV proton beam at the cyclotron of the University of Louvain.[149, 150]

I.B.2. Planned proton facilities

Discussed below are clinical proton facilities either under construction at various existing accelerator laboratories or being planned for dedicated medical use.

•The National Accelerator Centre, Faure, South Africa, a proton facility with a 200-MeV variable-energy sector cyclotron, is developing a horizontal clinical beam line. Personnel from the Groote Schuur Hospital of the University of Cape Town plan to treat patients.[151]

•The medical community in Japan is aggressively pursuing acquisition of new dedicated proton facilities. A new dedicated medical synchrotron with an energy variable in steps of 120, 180 and 230 MeV is planned for construction at Tsukuba. The designed beam intensity is 20 nA, which corresponds to 1.25×10^{11} protons per second. Two modes of extraction, fast and slow, are planned. Two treatment rooms with horizontal and vertical (up and down) beams are planned.[152, 153] The construction of a 250-MeV AVF separate-sector cyclotron is coming to a near completion at the Osaka University in Japan. The machine is planned to be used for medical sciences as part an interdisciplinary research program.[154] However, anticipating the beam-time demand for this machine by the physics community, they are contemplating another new facility. There is also a proposal to build a 250-MeV synchrotron for medical use at Kyoto.[155]

•Several medical accelerators have been designed in Russia.[119, 156] Specially notable are designs of a very compact synchrotron, accelerating protons to 200 MeV with a high magnetic field of 5~10 Tesla, the orbit length of 4.7 m, and repetition rate of 10 Hz, developed at the Institute of Nuclear Physics (INS) in Novosibirsk,[157] and a negative hydrogen ion (H^-) synchrotron for proton therapy facility, conceived at ITEP, that permits multiple extractions to facilitate the beam sharing among six treatment rooms.[158, 159] ITEP has received funding for a dedicated medical proton synchrotron, and construction is scheduled to start in 1992.[158, 160] At the same time, ITEP is developing a smaller (less than 500 m^2) version of 3-room proton therapy facility.

•There are several initiatives to build hospital-based dedicated proton accelerators in the U.S: notable examples are at the Massachusetts General Hospital in Boston,[161] and the University of California, Davis Cancer Center in Sacramento.[162] The University of Texas Southwest Medical Center is considering for clinical trials the use of 70-250 MeV proton beams extracted from the injection LINAC of the Superconducting Super Collider (SSC) in Waxahachie, Texas.[163, 164] The American Proton Development Corporation of Chicago has plans to build several dedicated proton medical accelerator facilities.[165]

•The Princess Margaret Hospital in Toronto, Canada has considered for clinical application a 3-Tesla isochronous superconducting cyclotron designed by the National Superconducting Cyclotron Laboratory of East Lansing, MI.[166, 167] One or two gantries are envisioned for the facility.

•The Indiana University Cyclotron Facility (IUCF) has a plan to use proton beams with energies from 185 to 200 MeV for clinical purposes.[168]

•The Forschungszentrum (KFA) in Jülich is building a new accelerator, a synchrotron and storage ring (COSY-Jülich), which is scheduled for operation in early 1993 and will deliver protons at energies of 50 to 2500 MeV. A medical application of the proton beam has been planned.[169]

•The Laboratori Nazionali di Legnaro (LNL), Padova, Italy has a plan to develop proton beam with an energy from 20 to 1000 MeV and use it for radiotherapy.[170]

•TRIUMF, Vancouver, Canada, plans to use protons of energies from 72 to 500 MeV for patient treatment.[171]

•There is a proposal to install a hospital-based proton therapy center in Antwerp, Belgium.[172]

•It is noteworthy that new designs of proton medical accelerators are being worked on. Ion Beam Application (IBA) of Belgium and Sumitomo Heavy Industries of Japan have proposed a compact, high-field isochronous cyclotron.[173-175] Hospital-based proton accelerators for radiation therapy have been proposed using LINACs[176, 177] and synchrotrons.[178]

I.B.3. Heavier ion facilities

Summarized below are existing, under construction, and planned clinical facilities for heavier ion beams.

•Clinical trials for treating human cancer using ion beams have been in progress at the LBL Bevalac since 1977.[4, 30] Ions of interest range from ^{4}He to ^{28}Si. ^{20}Ne ions with energies per nucleon of 450 and 585 MeV have been most commonly used. More than 450 patients have been treated in the clinical trial using neon-ion beams.

•The National Institute of Radiological Sciences (NIRS) in Chiba, Japan, is building the Heavy Ion Medical Accelerator at Chiba (HIMAC).[179-181] It will produce ion beams from ^{4}He to ^{40}Ar up to a maximum energy per nucleon of 800 MeV.[182] The target completion date is 1993. The HIMAC will have two treatment rooms, one with both a horizontal and a vertical beam, and the other with only a vertical beam. There will also be a secondary (radioactive) beam room, a biology experimental room, and a physics experimental room, all equipped with horizontal beam lines. All beam lines are of the fixed beam type, in contrast to rotating gantries. Adjacent to the HIMAC, the NIRS is planning to build a 200-bed hospital to be completed by 1995. At the Riken Ring Cyclotron facility, carbon-ion beams with energy per nucleon of 135 MeV have been used for the biophysics studies since 1990.[183] There is an initiative to construct another heavy ion machine in Kobe to accelerate ions as heavy as ^{12}C.[184]

•Preclinical studies to determine clinically important disease sites for heavy-ion beams have been started at SIS of GSI, Darmstadt, Germany, in collaboration with the University Clinic of Radiology, Heidelberg, and the German Cancer Research Center (DKFZ). A medical program is planned for the future.[185-188]

•The European Community (EC) has completed the feasibility study of constructing the European Light Ion Medical Accelerator (EULIMA). One of the accelerator types under consideration is a tandem cyclotron for accelerating light ions, from ^{4}He to ^{20}Ne, to a maximum energy per nucleon of 500 MeV.[189-191] The choice for the machine design is driven by the availability of an existing cyclotron in Nice, France, that may be used as the injector for a bigger sector-focused cyclotron to be constructed. However, the feasibility study included a study of a synchrotron as the accelerator of choice.[192-195] A synchrotron design considering specific site conditions of a Heidelberg site has been also proposed.[196]

•At the INFN–Laboratori Nazionali di Legnaro (LNL), Padova, Italy, low energy (in the range of 10 MeV/amu) radiobiology experiments of protons and various ions have been conducted since 1984. Now a superconducting post-accelerator (ALPI) is being built for the existing TANDEM-XTU, and there is a proposal to use the ALPI as an injector for a synchrotron (ADRIA), and use the light and heavy ions, such as ^{12}C, ^{20}Ne, ^{28}Si, and ^{40}Ar of an energy per nucleon from 100 to 1000 MeV for radiotherapy trials.[170]

•As mentioned above, KFA in Jülich is building the COSY-Jülich, which has the option to accelerate ^{4}He, ^{12}C, ^{16}O, and ^{20}Ne ions.[169]

•Biomedical research using heavy charged-particle beams is also under active consideration in Russia. A design study has been performed at ITEP[197] to accelerate light ions from ^{12}C to ^{20}Ne with energy per nucleon up to 500 MeV, and bring the light-ion beams to the treatment rooms to be constructed for the H^- accelerator discussed above.[158, 160]

I.B.4. Negative pion clinical trials

In discussing accelerated heavy charged-particle beams for radiotherapy, negative pion beams should be included for completeness. Clinical advantages of negative pions are also being studied as the penetrating pions deposit a large amount of energy at the end of their flight path due to the Bragg peak and nuclear "star" formation.[5, 7, 198] The pion beams exhibit physical and biological advantages similar to light ions; their dose boundaries are not as distinct as proton or light ion beams as the pions have smaller mass and suffer bigger scattering effects in penetrating patient body. In contrast to the fact that protons, light and heavy ions are primary particles, negative pions are secondary particles produced by the interactions of the primary beams, usually proton beams, with target materials.[199] Because of the lighter mass of pions, therapeutically useful pion beams, with a maximum range of approximately 30 cm in soft tissue, possess relatively low magnetic rigidities. To

collect most of the secondary pions produced in large solid angles and focus them into the target volumes, rather specialized multichannel pion applicators have been developed at Stanford[200, 201] and PSI (formerly SIN).[202, 203] Clinical trials using negative pions have been conducted at Los Alamos,[204-206] TRIUMF in Vancouver,[207, 208] and PSI.[209]

I.B.5. General remarks on future clinical particle accelerator facilities

Based on the increased interest in building dedicated medical accelerator facilities, the following general statements may be made:

•Although medical accelerators, often synchrotrons, are based on well-established technologies, much inventiveness is required to satisfy the clinical requirements, namely reliability, serviceability, compactness, and operation economy.

•The accelerator, although it is the basis of such a facility, represents only one-quarter to one-third of the total facility construction expense. What physically dominates the facility cost are the beam transport systems and the patient treatment facilities.

•In practice, the extracted beams are heavily modified before clinically used, and their clinical efficacy is largely determined by the devices that modify the beams. In addition, controlling the clinical beams and providing reliable dosimetry of the treatment are vital for the success of the treatment and for patient safety.

The discussion on medical accelerator designs is beyond the scope of this review. This review concentrates on the discussion of instrumentation developed for the modification, control, and monitoring of the clinical beams.

I.B.6. Abbreviation of names of clinical facilities and institutions

Following abbreviations of the clinical facilities and institutions will be used throughout this article.

EULIMA	European Light Ion Medical Accelerator
FNAL	Fermi National Accelerator Laboratory
GSI	Gesellshaft für Schwerionenforschung, Darmstadt, Germany
HCL	Harvard Cyclotron Laboratory, Cambridge, MA
HIMAC	Heavy Ion Medical Accelerator at Chiba, Japan
ITEP	Institute of Theoretical and Experimental Physics, Moscow
LBL	Lawrence Berkeley Laboratory, University of California
LLUMC	Loma Linda University Medical Center Proton Therapy Facility, Loma Linda, CA
MGH	Massachusetts General Hospital, Boston, MA
NIRS	National Institute of Radiological Sciences, Chiba, Japan

PARMS Particle Radiation Medical Science Center, University of Tsukuba, Japan
PSI Paul Scherrer Institute, Villigen, Switzerland (formerly SIN)
TSL Gustaf Werner Cyclotron, Theodore Svedberg Laboratory, Uppsala, Swed

I.C. Physical Parameters of Clinical Beams

The important physical parameters and effects of the accelerated particle beams that impact instrumentation design will be briefly introduced in this Section along with relevance of accelerator parameters to the instrumentation.

I.C.1. Medical accelerator parameters

As mentioned previously both synchrotrons and cyclotrons have been used to produce heavy charged-particle beams with sufficient energy to reach target volumes within the human body. In addition to the existing accelerator facilities, a number of design studies have been undertaken for a dedicated medical accelerator.[145, 210-216] Recently proton LINACs have been proposed for radiation therapy use.[176] A general conclusion of these works is that synchrotrons are well suited for rapid energy changes required for conformal 3D radiotherapy (see Sec. II.C.3), while cyclotrons are capable of producing beams at higher fluxes (particles per second); thereby, facilitating the production of radioactive beams (see Sec. V.A). For either type of accelerators, the particle species, the beam energy and its spread, the intensity, the beam size and divergence (emittance), and the time structure of the extracted beam have an impact on patient treatments.

The required range of the beam can be as large as the width of a human body for treatment of deep-seated tumors or as small as 1 cm for some eye treatments. For treating eye tumors or other diseases such as choroidal melanomas, a proton energy of ~75 MeV suffices for most applications.[217] A practical maximum beam range is 32 cm in water (a good approximation of body tissue in terms of the stopping power), which for protons and helium ions corresponds to an energy per nucleon of ≈215 MeV and for neon ions ≈550 MeV. For actual treatments a continuously variable range of energies is required which can be achieved by either changing the accelerated energy of the beam or by degrading the fixed beam energy after exiting the accelerator, as discussed in Sec. II.A and II.B.

The beam emerging from the accelerator is not truly monoenergetic, but has some energy spread or dispersion. Both the dispersion within a single pulse and that of several consecutive pulses of the extracted beam must be considered, since the treatment is always achieved using many accelerator pulses. Usually this dispersion is negligible for synchrotron beams, $\Delta E/E<10^{-4}$, with the pulse-to-pulse energy variation of $<10^{-3}$; but it can be significant in cyclotron beams, $\Delta E/E>10^{-2}$. This energy spread along with the range straggling contributes to the finite width of the Bragg peak and the deterioration of the steepness of the distal dose falloff of the spread-out Bragg peak.

Table 1

Particle Fluxes (in particles/second) required to deliver 1 Gy-liter/minute in two representative target volumes with given width of spread Bragg peaks

Particle	Target volume Area = 400 cm^2 Width = 2.5 cm	Target Volume Area = 50 cm^2 Width = 20 cm
^{1}H	1.0×10^{10}	3.3×10^{9}
^{4}He	3.4×10^{9}	1.1×10^{9}
^{12}C	6.7×10^{8}	2.2×10^{8}
^{20}Ne	3.0×10^{8}	1.0×10^{8}
^{28}Si	2.0×10^{8}	7.0×10^{7}

The beam flux required for a patient treatment depends on the size, shape, and depth of the target volume, the prescribed dose, and the desired treatment time. To minimize the effect of the motion of the target volume during a treatment, treatment times of less than one minute treatments are desirable, while several minutes are often acceptable. As an illustration, the beam fluxes for various particle beams to deliver 1 Gy into a target volume of 1 liter in 1 minute are listed in Table 1. Even for a given target volume, the intensities vary according to the target geometry, and two examples are given in the list.

In order to calculate a required beam flux in the accelerator, $I_{accelerator}$, the duty factor (the fraction of the accelerator cycle time in which beam is actually coming out of the machine) of the accelerator (η_d), the extraction efficiency (η_x), the beam transport efficiency from the accelerator to the treatment room (η_t), and the efficiency of generating the clinically useful radiation field (η_f) must be taken into account. The required particle flux in the accelerator is:

$$I_{accelerator} = \frac{I_{target}}{\eta_d \eta_x \eta_t \eta_f}, \qquad (1)$$

where I_{target} is the flux required inside the target volume.

The emittance of a beam is defined as the product of the area occupied by the beam in the plane perpendicular to the beam direction and the angular divergence of the beam. The emittance of the beam is unique to each accelerator and is usually an invariant during its transport without collimation.

The typical physical size of the beam from an accelerator is small (< 1 cm diameter) compared to the typical size of radiation fields required for patient treatments; hence, there is the need for laterally spreading the beam. When the beam is bent in a magnetic field, the energy dispersion of the beam leads to an increase in the physical size of the beam spot and an undesirable correlation of the particle energy and position. The magnitude of this effect is a function of the optical properties of the particular beam transport system.

The last important parameter of a particle beam is the time structure of the extracted beam because it may alter the biological effect of the radiation and impact the ability of the beam delivery system to deliver the desired radiation field. The dose-rate effects are discussed in Sec. I.D.1 and II.C.4.

I.C.2. Beam transport and delivery

The extracted beam is transported from the accelerator to the treatment room by the beam transport system, series of dipole and quadrupole magnets. The arrangement of magnets, vacuum chambers, and diagnostic instrumentation is called a beam line. The beam delivery system, located at the end of the beam line usually in the treatment room, modifies and monitors the beam to achieve the prescribed radiation dose distribution inside the target volume.

I.C.2.a. Beam transport

A stable and efficient transport of the beam from the accelerator to the treatment room is required for reproducible dosimetry and thereby reliable patient treatments.[218] The stability of the centroid of the beam position must typically be better than 1.0 mm. This requirement places constraints on the stability of the bending and focusing magnets needed to control the beam position and profile. The ease of adjusting the beam through the beam line, in what is called tuning a beam line, and the reproducibility of the beam-line tune are critical for efficient and reliable clinical operation. The analyzing power of the transport system is also important for physically separating particles with different momenta and charges for radioactive beam production as discussed in Sec. V.A.

I.C.2.b. Beam delivery systems

The beam delivery system, which monitors the beam and shapes it in three dimensions to irradiate the target volume, consists of devices introduced here and elaborated on in Sections II and III. In a typical treatment room the beam, after passing through a vacuum window at the end of the beam transport system, travels through several kinds of devices and several drift spaces (path length the beam travels unmodified) before entering the patient. These devices change the beam range (Sec.

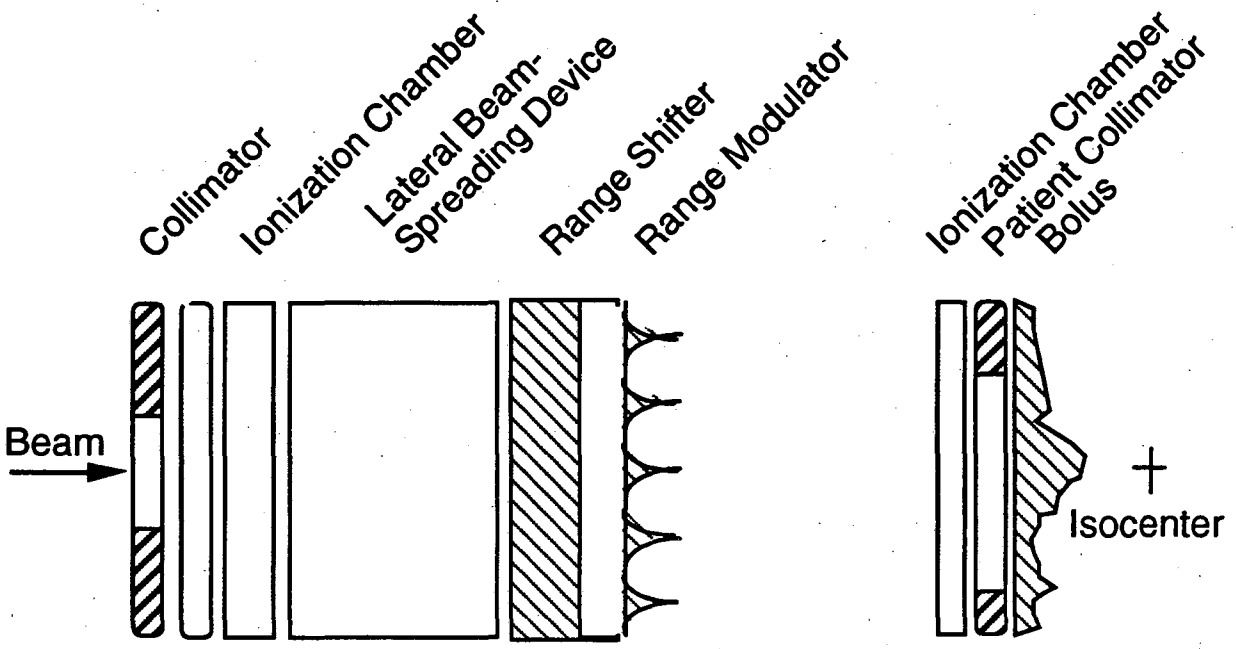

Fig. 7. A typical beam transport system is schematically shown. Beam spreading devices, monitoring devices, range modulation devices and field shaping devices are identified.

II.A), modulate the range (Sec II.B), spread the beam laterally (Sec II.C), and shape its lateral profile (Sec. II.D). Dose measuring devices (Sec. III.A and III.B) and beam monitoring devices (see Sec. III.D) are required for control of the radiation.

A general beam-line layout places a set of dose detectors and beam monitoring devices near the patient and at a position before the beam spreading device, as shown in Fig. 7. The beam spreading devices are usually located as far from the patient as is practical to minimize the effective source size and the angular divergence of the beam. The drift space interspersed between the beam modifying and monitoring devices in a clinical beam line is typically 3 meters or longer. One meter of a drift space in air is equivalent in stopping power to ~1.2 mm of water. Fragmentation of the heavier ions in this air path is negligible; however, multiple scattering can be significant for lighter ions, such as protons and helium ions.

The parameters of beam delivery systems in fact lead to competing requirements on the design and placement of the beam-line elements. An optimization process involving several parameters with clinical tradeoffs is often required. In general, the maximum field size, the field uniformity, the treatment time, the beam divergence, the lateral dose falloff (the *apparent* penumbra) of the field, thebackground radiation, and the beam fragmentation are important factors to consider. Furthermore, different clinical requirements necessitate different designs, which generally fall into

two categories: namely, beam lines for small and large radiation fields. Large radiation fields require more complex systems for laterally spreading the beam. The small beam spot extracted from the accelerator must be modified to cover areas as great as 30 cm x 30 cm with a dose uniformity within ±2%, and the dose rate on the order of 1-2 Gy/minute. The beam lines for small fields are simpler because they can often directly utilize the beam from the accelerator with minor modification, probably using a simple scatterer.

I.C.3. Effects of material in the beam path

Any material in the beam path can potentially modifies the beam because the material scatters the beam (multiple scattering), smears its energy (range straggling), and fragments some portion of it (nuclear fragmentation).

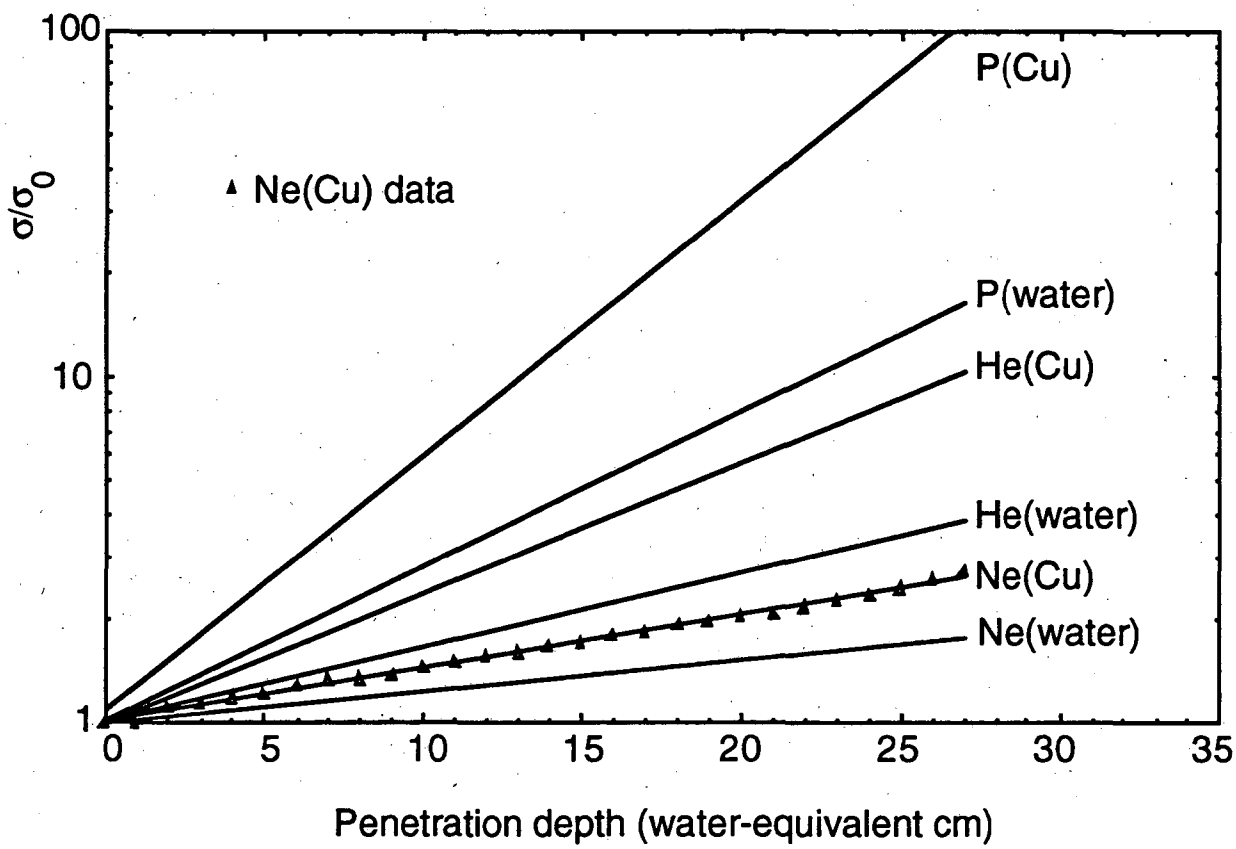

Fig. 8. Shown are the relative increases in beam lateral dose falloffs due to multiple scattering in water and copper for proton, helium-ion, and neon-ion beams. The lateral dose falloff (σ) is expressed in terms of the lateral dose falloff (σ_0) at the entrance of the absorber, and the penetration depth in water-equivalent thickness.

I.C.3.a. Multiple Scattering

Multiple scattering of the beam can be described as the small angle deflection of the beam particles due to collisions with the nuclei of the traversed material. These numerous small angle deflections lead to a divergence of the beam and to a lateral spreading of the particles away from the central trajectory. Elastic Coulomb scattering dominates this process with a small strong-interaction scattering correction. The angular distribution of the scattered particles is roughly Gaussian for small deflection angles. Multiple scattering of heavy charged particles in water can be described by the projected radial distribution of deflection y from the incident beam direction, which is a Gaussian with variance, σ_y given by:

$$\sigma_y = 0.0294 R^{0.896} Z^{-0.207} A^{-0.396}, \qquad (2)$$

where R is the water-equivalent thickness in cm, and Z is the charge of the particle with mass, A.[219] Fig. 8 shows the relative increases in the lateral dose falloff distance from the 90% to the 10% level due to multiple scattering in water and copper for proton, helium-ion, and neon-ion beams. The lateral dose falloff (σ) is expressed in terms of the lateral dose falloff (σ_0) at the entrance of the absorber, and the penetration depth in water-equivalent thickness. The width of the lateral dose falloff may be cut down by collimating the beam immediately before it enters the patient.

Table 2

Measured Widths of the Lateral Dose Falloffs of Helium-Ion Beams

	Collimator to phantom distance	
Residual Range	0 mm	100 mm
(mm)	width(mm)	width(mm)
60	1.5	1.9
90	2.4	2.7
120	3.4	3.8

An analysis of the measured lateral dose falloff for helium-ion beams[82] is summarized in Table 2. They show the measured widths of the lateral dose falloff between 90% and 10% dose points for a clinically used helium-ion beam of various residual ranges in water. The beam started out at an energy per nucleon of 230 MeV (the range of 31.6 cm in water), but the energy was degraded before clinical use, and the placement of the degrader was optimized to obtain the results in Table 2. For protons, the widths will be approximately twice as big as those shown for helium ions. The width is seen to increase essentially linearly with the residual range of the beam. The sharpest dose falloffs

are obtained when the final collimator is at the surface of the patient and when the shortest range is used. For a small beam, rarely it is necessary for the final collimator to be further than 10 cm from the patient surface. For treating small targets, where the sharpness of the lateral dose falloff is essential, the choice of the heavy charged-particle beam becomes important.[220]

I.C.3.b. Range Straggling

Range straggling is the dispersion of the path length of a particle beam due to statistical fluctuations in the energy-loss process.[221, 222] The end result is to produce a smearing of the range of the stopping particle beam. For a particle traveling in a direction x, with energy E and mean range R, the distribution of ranges, $s(x)$, is Gaussian,[223, 224]

$$s(x) = \frac{1}{\sqrt{2\pi}\sigma_x} e^{-(x-R)^2/2\sigma_x^2} \tag{3}$$

The variance, σ_x, in centimeters in the path length of a particle in water can be approximated with

$$\sigma_x = 0.012R^{0.951}A^{-0.5}, \tag{4}$$

where R is the water-equivalent thickness of the material the beam traverses.[219] In the region where this formula is valid ($2 < R < 40$ cm), σ_x is almost proportional to range, R, and inversely proportional to the square root of the particle mass number, A. For example if protons with a range of 30 cm pass through 25 cm of water, the variance in the range becomes 2.6 mm, or the *distal* dose falloff distance from 90% to 10% dose level is 4.4 mm, which may be unacceptable in certain clinical applications. Shown in Table 3 are some typical values of σ_x for ions with a range of 20 cm in water.

Table 3. Range Straggling in Water

Ion	σ_x (mm)
Protons	2.0
Helium	1.0
Carbon	0.6
Neon	0.5

The range straggling for heavier charged particles varies approximately inversely to the square-root of the mass of the particle. When expressed as a percentage of the total range, the rms range straggling is 1.0% for protons, 0.5% for helium ions, 0.3% for carbon ions and 0.25% for neon ions for most ranges of clinical interest. Minimizing range straggling and multiple scattering can be done by removing material from the beam line. For example magnetic deflection can eliminate the material needed to spread the beam in a scattering system (See Sec. II.C) or changing the accelerator energy can eliminate material degraders used to change the energy of the beam.

I.C.3.c. Beam Fragmentation

As a particle beam penetrates through matter the primary particles suffer fragmentation collisions, which decrease the number of primaries with the corresponding increase of lighter fragments.[225] Beam fragmentation refers to the process whereby the beam particle, called the projectile nucleus, after suffering a nuclear collision with a target nucleus is broken apart into several daughter particles. The remnants of the projectile nucleus emerge from the absorbing material with similar momenta as that of the original projectile nucleus. The target nuclei nucleus may also fragment, but these fragments have relatively lower energy and momentum and do not travel with the beam. The probability that a particle will undergo such a nuclear interaction has an exponential dependence on the length it travels. A nuclear interaction length, λ_I, is defined as the length in the material in which an interaction will occur with a probability of 1/e. It is related to the nuclear interaction cross section by:

$$\lambda_I = \frac{A_T}{\sigma \rho N} \tag{5}$$

where ρ is the mass density in g/cm^3, A_T and A_P are the target and projectile atomic masses respectively, N is Avogadro's number, and σ is the interaction cross section given by[226]:

$$\sigma = 78(\sqrt[3]{A_T} + \sqrt[3]{A_P} - 1.25)^2 \times 10^{-27}\, cm^2. \tag{6}$$

Table 4. Nuclear Interaction Lengths

Ion	λ_I (cm)
Protons	60.1
Helium	38.0
Carbon	24.4
Neon	19.5

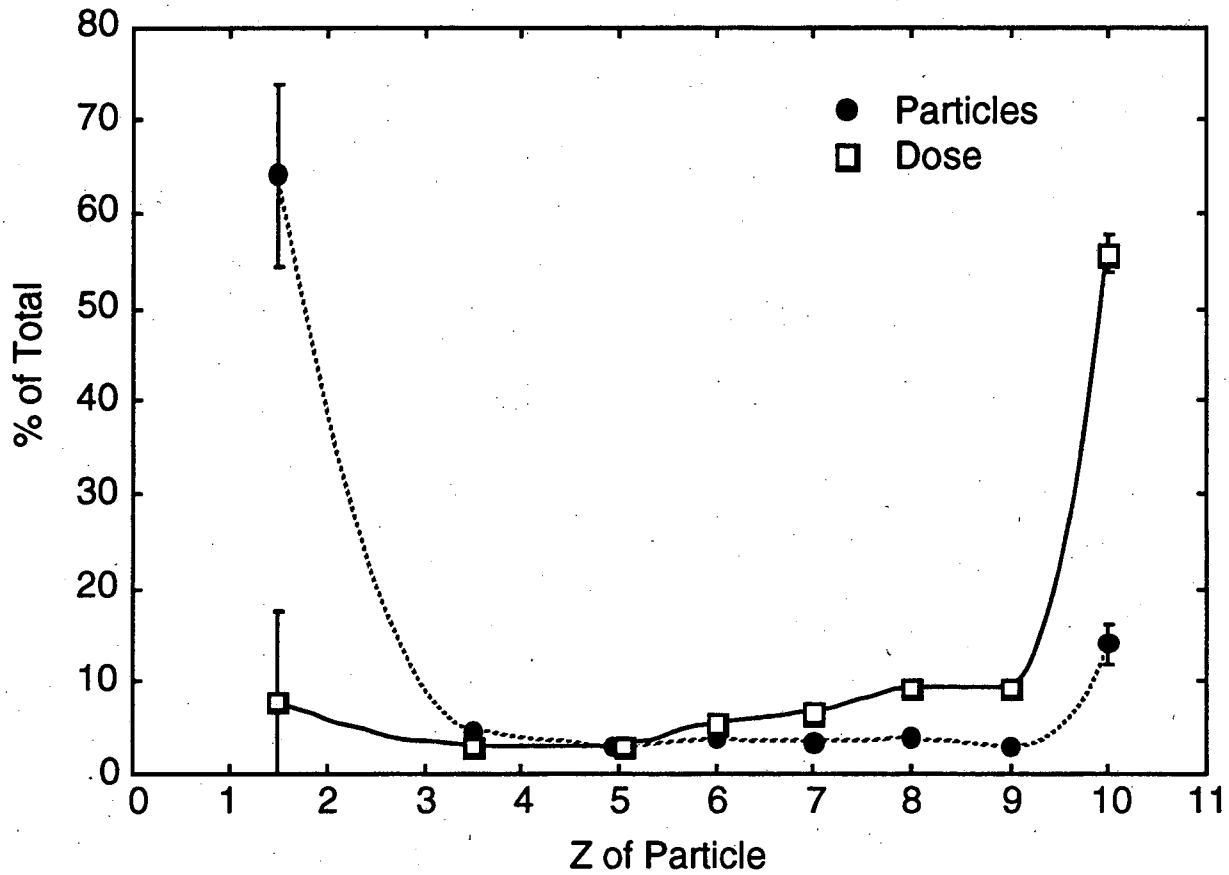

Fig. 9. The contributions of different atomic charges to the total particle flux and the total dose delivered are shown. The data was measured with the BERKLET using neon ions in the proximal peak region of a 12-cm spread out Bragg peak with a residual range of 28 cm in water. This corresponds to the beam traversing 16 cm of water. The data for low Z values (1~2 and 3~4) are lumped togeter.

For example for neon ions passing through 19.5 cm of water, 37% (≈1/e) would have fragmented; however, the contribution by the fragments to the dose is less than 37% since the fragments have lower Zs than the primary particles and the dose depends on the square of the particle charge, Z^2.. Fig. 9 shows the measured flux and dose contribution as a function of the particle charge for a neon-ion beam after traversing 16 cm of water. The Table 4 shows the calculated nuclear interaction length for several ion species in water at energies corresponding to clinically usable ranges.

For protons colliding with a water-like target material (e.g. tissue) the dominant interaction products are neutrons knocked out of the target nuclei. These neutrons are not easily stopped and contribute to the dose delivered beyond the stopping region of the primary projectile. Heavier

charged particles also produce such a neutron background. Even after accounting for the higher RBE of the neutrons produced, they contribute less than 0.5 % of the biological dose delivered to the patient by the charged particles.[227] Their contribution can exceed this in cases where the range of the beam is severely degraded upstream of the patient such as in the case where the beam is spread out by double scattering (Sec. II.C.1.b). Whole body exposure can then become an issue.

For helium-ion projectiles, neutrons and isotopes with A<4 are produced which have longer ranges than the primary particles. A single proton knocked out of the helium projectile leads to a triton with a range three times that of the original helium projectile. On the other hand, ^{3}He has a short range. This long-range dose can be significant depending on the clinical situation. Typically a tail dose, the dose beyond the Bragg peak, is only a few percent of the peak dose. Carbon and neon ions fragment into a larger number of nuclear species.[228] These fragments lead to a significant dose beyond the actual stopping range of the primary particles, and contribute significantly to the dose within the spread-out Bragg peak. In general, the heavier the nuclear projectile, the larger the dose delivered in the region beyond the Bragg peak when normalized to the dose delivered by primary ions at the proximal peak of the spread-out Bragg peak (defined below in Sec. I.D. 2.a). For neon-ion beams, depending on the energy, the physical tail dose immediately downstream of the distal peak can be as large as 30 % of the target dose.

An additional complication is that a fragmented beam has a radiobiological effect different from that of the primary beam. The LET distribution of the fragmented beam becomes quite complex as more of the primary beam fragments[229, 230]; hence, the biological effectiveness, since it is a function of the LET of the beam, is a function of the depth of the material penetrated.[231] For beams where the Bragg peak is spread out over some region (see Sec. I.D below), the composition of the beam and its biological effect is also a function of depth and must be accounted by adjusting the depth-dose distribution.

Accurate modeling of the fragmentation process has been hampered by the paucity of data on nuclear cross-sections for all the particles and energies required. Measurements have been done on several specific cases in support of some theoretical modeling of the needed cross-section data.[228] Another approach has been to actually measure the particles found in a beam for a particular clinical setting and use a cell survival model to predict the biological effects of the beam.[232] Some promising results have emerged, but are not complete enough yet to be applied clinically. The response of cells of different tissue to heavy charged particles has also been modeled based on photon data and limited animal experiment data with heavy charged particles. Actual clinical results have been the primary guide in determining biological effects of these beams and setting tolerance dose for normal tissues and estimating complication effects.

I.D. Clinical Parameters

In the clinical use of heavy charged-particle beams, the objective is to place a *biologically* uniform high-dose region accurately in the target volume while sparing the surrounding healthy tissues from unwanted radiation as much as possible. To assess clinically the prescribed and delivered treatment, various dosimetric quantities must be accurately known. These clinically pertinent quantities are discussed in this Section.

I.D.1. Dose and Dose Rate

The most important quantity measured in radiotherapy is absorbed dose, defined as the energy absorbed (not the incident energy) per unit mass of a material. In general, clinical situations encountered in radiation therapy using heavy charged-particle beams require an accuracy of the dose measurement to an accuracy of less than ±5% of overall uncertainty and reproducibility of ±2% precision.[233] Ideally the dose distribution is known at all points in the treatment volume and the surrounding tissues. The measurement of such dose distributions is called dosimetry, and the measuring instruments are dosimeters. The purpose of maintaining accurate dosimetry is twofold. The first is to establish reliable values of clinically effective doses for tumor control and tolerance doses for critical tissues. Secondly, maintaining accurate dosimetry traceable to a known standard facilitates the exchange of clinical information between institutions for intercomparison of the clinical data.

Protocols for heavy charged-particle beam dosimetry have been established by the American Association of Physicists in Medicine for protons and heavier ions,[234] and by the European Clinical Heavy Particle Dosimetry Group (ECHD) for proton beams.[235] They describe the methods of calculating the dose based on measurements using various dosimeters. Discussions of these methods are outside of the scope of this review, and the readers may refer to existing review articles on the heavy charged-particle dosimetry.[68]

The effect of the absorbed dose as a function of its delivery time, or dose-rate effect,[236, 237] has been of some concern in the development of dynamic beam delivery systems described in Sec. II.C. These systems deliver all or a substantial fraction of the required dose to a segment of the target in a relatively short time. The effective dose rate for some systems can be on the order of 10^6 Gy/min. For a dose-rate effect to be observed the temporal and spatial separation between particles must be small enough that there is an interplay between the damages in cell nuclei done by the energy loss of multiple particles. It is generally agreed that the dose-rate effect is not important for most of the beam delivery systems considered. Further discussions are presented in Sec. II.C.4.

I.D.2. Dose distributions

Ideally the three-dimensional dose distribution should be known in evaluating both the prescribed and delivered treatment. In practice, however, only subsets of the complete three-dimensional dose distribution may be known. The first subset of data, called a depth-dose curve, is the dose deposited as a function of the depth of penetration at some lateral position in the beam, usually along the central ray. The second subset is called the transverse dose distribution and measure the uniformity of the radiation transverse to the beam direction at a certain depth of penetration.

I.D.2.a. Depth-dose curves

Depth-dose curves for particle beams of unmodulated range are described in terms of several regions as depicted in Fig. 2. The relatively constant entrance dose region is called the plateau of the Bragg curve, while the region of high energy deposition is called the peak. This peak is where the primary particles are coming to a stop and their LET is highest. The energy deposition after the peak, *i.e.*, the dose deposited beyond the distal edge of the peak, is called the tail. The ratio of the peak to plateau doses for pristine (not modulated in range) beams in the energy range used clinically is about 4:1 for protons and 6:1 for neon ions. For proton beams the FWHM of this peak in water or soft tissue is typically 1.5 ~ 2.0 cm. The FWHM is only ≈5 mm for neon-ion beams.

In order to irradiate the extended width of the target volume to the highest dose, the sharp Bragg peak is swept across it by modulating the range of the beam. The resulting energy deposition curve is called a *spread-out Bragg peak* (hereafter called SOBP). The physical methods for modulating the range are discussed in Sec. II.B. The depth-dose distribution for modulated particle beams is also divided into several regions as shown in Fig. 2. The entrance region, as with the beams of unmodulated range, is called the plateau. It is followed by the proximal peak where the dose is at a maximum. This peak is the beginning of the region of stopping particles or high LET portion of the Bragg curve, which continues through the midpeak region and ends at the distal peak. This entire high LET region (SOBP) covers the depth of the target. The distal edge of the SOBP, again as in the Bragg peak, is where the dose sharply falls off due to the stopping of the remaining primary particles. Beyond the distal edge lies the tail dose region. Dose at this depth is from secondary particles created from nuclear interactions of the primary particles with the material. This does not imply that the dose arising from the fragments is confined only to the tail region. Fragmentation starts as the primary particles enter the material, therefore, the fragment dose builds up starting at the entrance. (See the discussion under Sec. II.B.)

The sharpness of the distal falloff, or distal edge, is one of the most clinically important attributes of heavy charged-particle therapy. The chance of local control without complication depends decisively on how closely this edge can be placed between the distal surface of the target volume and the critical tissues beyond. The sharpness of this edge varies from 1 mm for the particle beams used

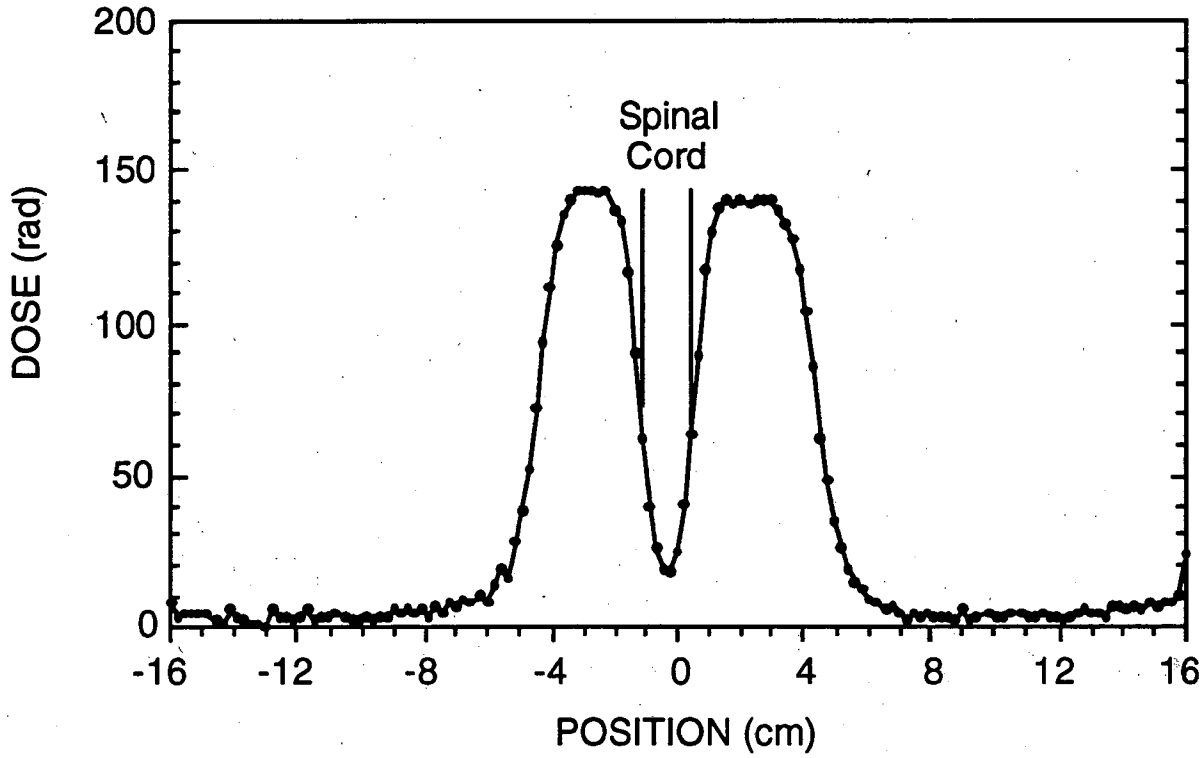

Fig. 10. A transverse dose profile of a helium-ion treatment field measured by a segmented ionization chamber. The gap in the middle results from the patient collimator which is shaped to spare irradiation of the spinal cord of the patient.

for ocular treatments to as much as 15 mm in beams with wider SOBP widths for deeper parts of the body. In general, as discussed in Sec. I.C.3.b above, the heavier charged particles have sharper distal edges. The accuracy of the placement of this edge in the body depends on the knowledge of the particle energy and the stopping power of the tissue the beam must penetrate. Uncertainties in determining the stopping power along the beam trajectory come primarily from the uncertainties (1 ~ 5%) in converting CT numbers to electron densities or stopping power values.[238-243] Several other clinically important parameters are the proximal-peak dose, the proximal-peak to plateau dose ratio, and the tail to proximal-peak dose. Normal tissue sparing upstream and downstream of the target for a given target dose are governed by these parameters.

I.D.2.b. Transverse Dose Profiles

A transverse profile of a 3-dimensional dose distribution is primarily a means of verifying that the transverse spreading of the beam is correct and that the radiation field uniformity satisfies clinical

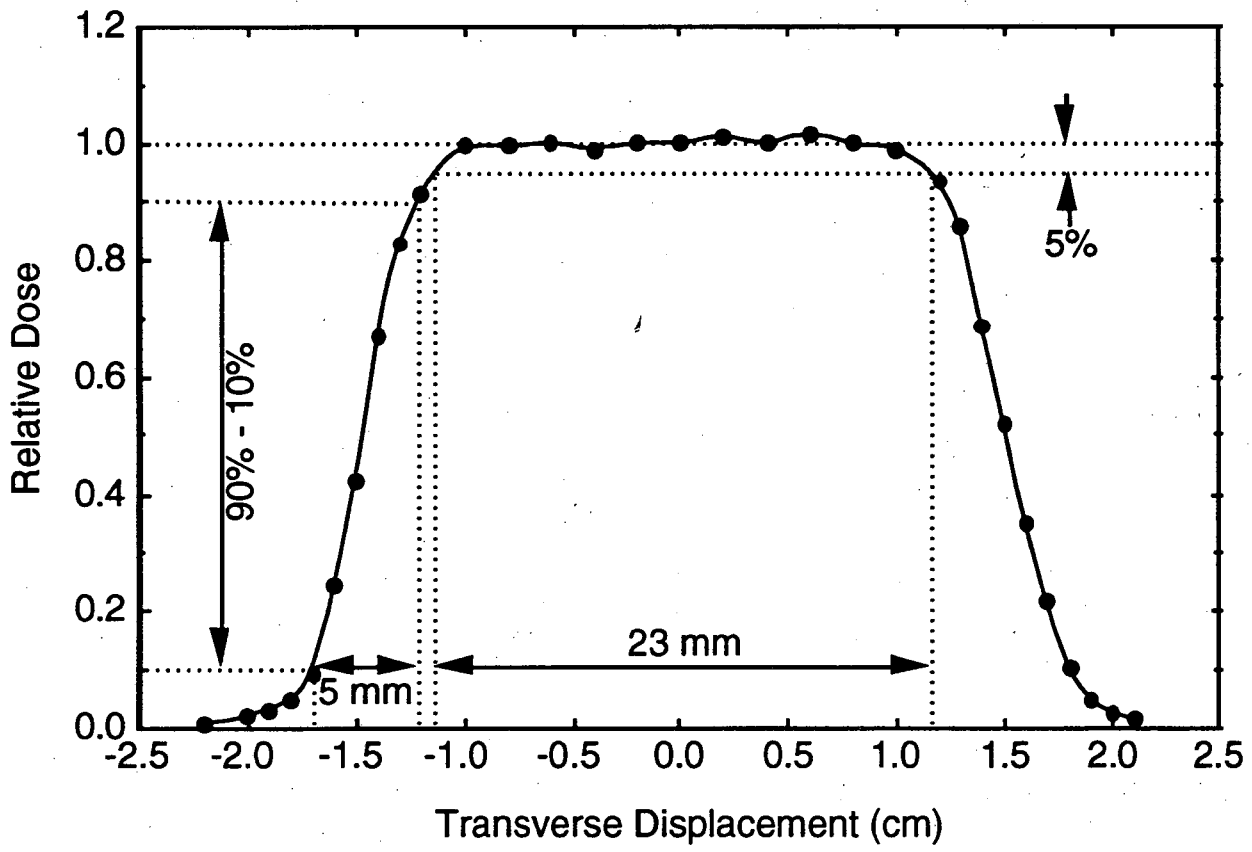

Fig. 11. The transverse profile of a helium ion treatment field shows the width of the lateral dose falloff and the uniformity of the treatment field at the front of the tumor at the proximal peak of the dose distribution.

requirements. If the radiation field has cylindrical symmetry, the transverse dose distribution can be measured along a line perpendicular to the central ray. Multisegmented ionization chambers (Sec. II.A.2.c), diode arrays (Sec. III.E.1.a), and multiwire proportional counters (Sec. III.D.3) can be used to measure these 1-dimensional profiles of the beam as shown in Fig. 10.

For arbitrary distributions it is prudent to monitor the entire radiation field cross-section immediately upstream of the patient. Two-dimensional, multi-segmented ionization chambers can measure such 2-dimensional dose distributions as discussed in Sec. II.B.3. Multiplane, multiwire chambers can also be used by sampling several one-dimensional projections of the dose profile at different orientations and reconstructing the 2-dimensional dose distribution from them as discussed in Sec. III.D.2.c. For irregularly-shaped treatment volumes, measuring the 3-dimensional dose distribution is ideal. Characterizing the radiation field in three dimensions can be done by sampling the dose in a water phantom by moving small detector around the 3-dimensional radiation field.

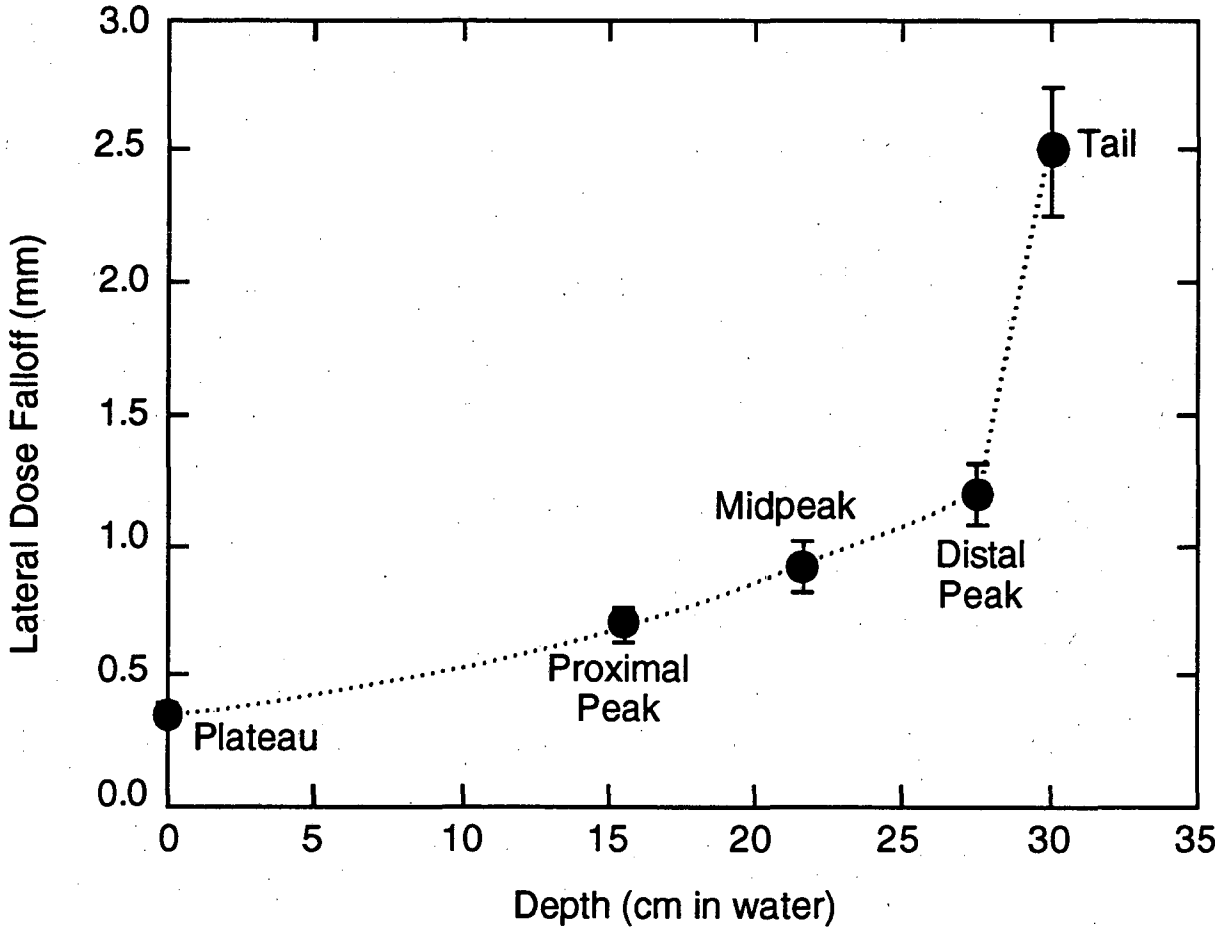

Fig. 12. Typical values of the width of the lateral dose falloff as a function of depth in water for a neon-ion treatment field. The increase of the falloff with depth arises mainly from multiple scattering of the beam in the patient tissue. The lines are drawn to guide the eye.

Such a method, however, assumes that the radiation field remains constant and requires a long data-collection time; furthermore, it is not usable for on-line monitoring purposes during a treatment.

The uniformity of the radiation across the treatment volume and the falloff of the dose at the edges of the treatment field are of particular clinical interest. The sharpness of the lateral dose falloff, often called the *apparent* penumbra, is of clinical importance because it determines the radiation exposure of the normal tissues adjacent to the target for a given dose within the target volume. Fig. 11 shows an example of the profile and lateral dose falloff of a large helium-ion treatment field. The lateral dose falloff, defined as the distance in which the dose falls from 90% to 10% of the central dose value, is shown in Fig. 12 as a function of depth in water for a neon-ion beam.The first factor determining the lateral dose falloff is the apparent finite source size of the radiation. The range-

shifting or range-modulating devices found in a treatment delivery system act as finite-size source, since particles traversing them are scattered, thus diffusing the beam and increasing its divergence. The increase in the lateral dose falloff also comes from the angular confusion in the rays leaving these devices because they act as multiple incoherent sources. The "source"-to-isocenter distance, SAD, should be increased as large as possible so that the radiation source may be regarded as a point-like source. Multiple scattering of the penetrating particles in a medium (e.g., tissue) also enlarge the lateral dose falloff with increasing depth. Finally, scattering off the edges of collimators causes an additional spreading of the lateral dose falloff.[244] The relative contributions of these in broadening the lateral dose falloffs depend on the beam beam-delivery system setup. Some can be reduced by changing the geometry, while others are inherent in the beam delivery system or caused within the patient and therefore can not be reduced.

I.D.3. RBE and LET

As mentioned above, the RBE of a heavy charged-particle beam is not a simple function of LET. The track structure of the energy deposition plays an important role.[245] Consequently, LET information alone can not serve as a simple predictor of the RBE of the radiation. Knowledge of the beam composition, *i.e.* the particle fluence as a function of charge and velocity is required.[228] Using current experimental methods, accurate determination of these quantities at a point in the treatment volume takes considerable effort. For this reason, averaged-LET distributions in the treatment volume as a function of depth and lateral position still remain useful in estimating clinical effects. A standard measure has been the weighted average of the LET of the particles with the dose they deliver, called the dose-averaged LET, L_D:

$$L_D = \int L\, D(L) dL \Big/ \int L\, \Phi(L) dL \qquad (7)$$

where $D(L)$ is the dose contributed by particles of a given LET, L, and $\Phi(L)$ is the fluence of particles with the given L. The dose is related to fluence and LET as:

$$D(L) = \frac{1.6 \times 10^{-7}\, \Phi L}{\rho} \qquad (8)$$

where ρ is the material density in g/cm^3, L is measured in keV/μm and Φ in particles/cm^2.

I.D.3.a. RBE and LET Distributions

The main function of a beam delivery system is to create a radiation field which produces uniform cell killing or a uniform biological response. Changes in the primary particle beam from fragmentation lead to changes in the biological effectiveness of the radiation. Fig. 13 shows a measurement of RBE as a function of depth. Measurements at various lateral positions across the

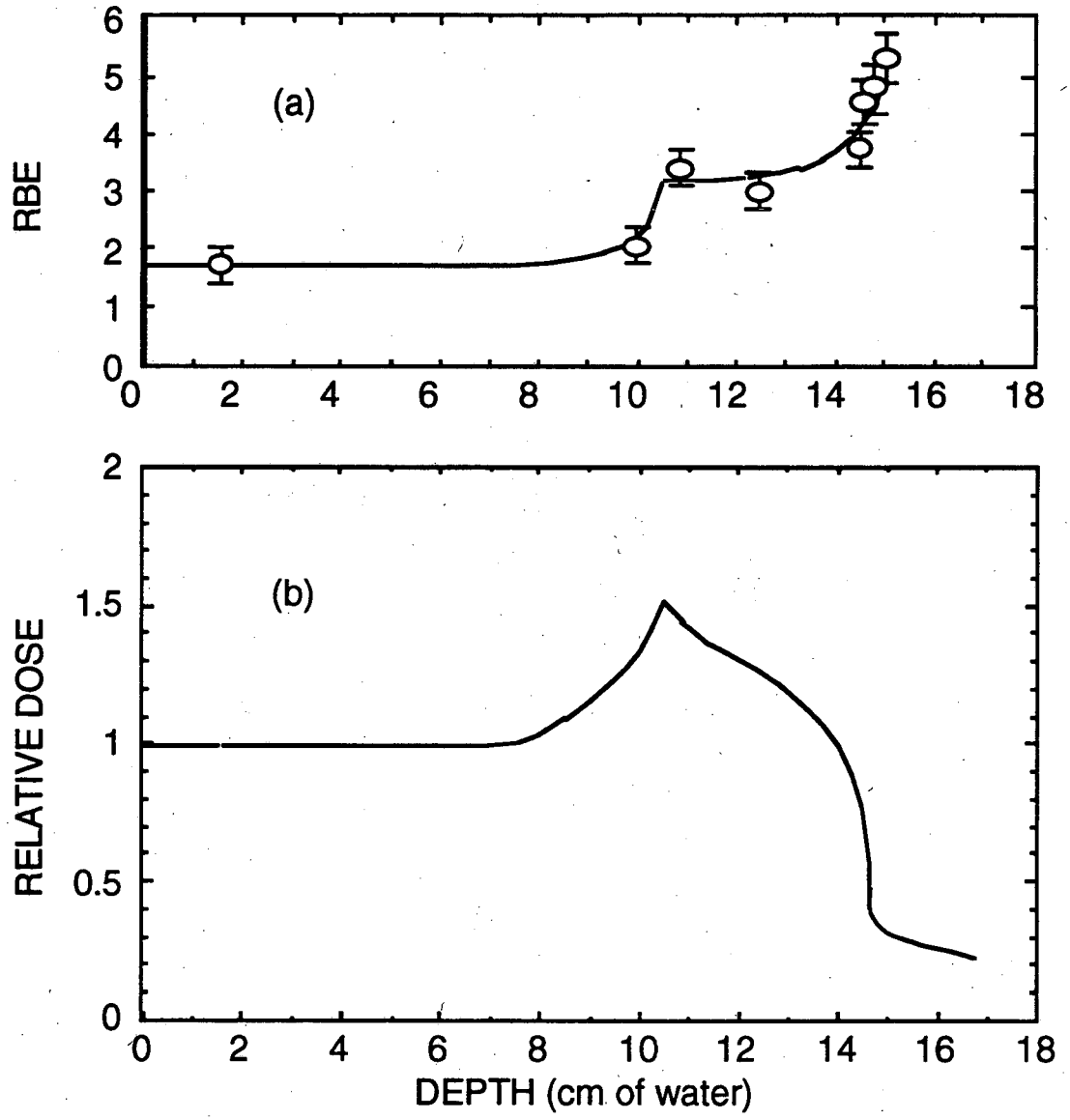

Fig. 13. a) RBE measured at various depths in water of a range-modulated beam. In this plot, RBE is the cell survival fraction as a function of depth for a given dose to the proximal peak of the SOBP. The solid line is to guide the eye. b) The associated dose distribution is also shown.

target allow evaluation of uniformity of cell killing in the target volume.[246] Measurements of the dose-averaged LET[247] (see III.E.4.b), while not a direct measure, are easier to make and serve as indicators of RBE. In particular, measurements as a function of depth and lateral position can be used to monitor changes in the radiation quality.

The iso-effectiveness, *i.e.*, the uniformity of cell killing across the target volume, of the radiation can be measured in two ways. Cell survival curves which describe the effective killing of a cell as a

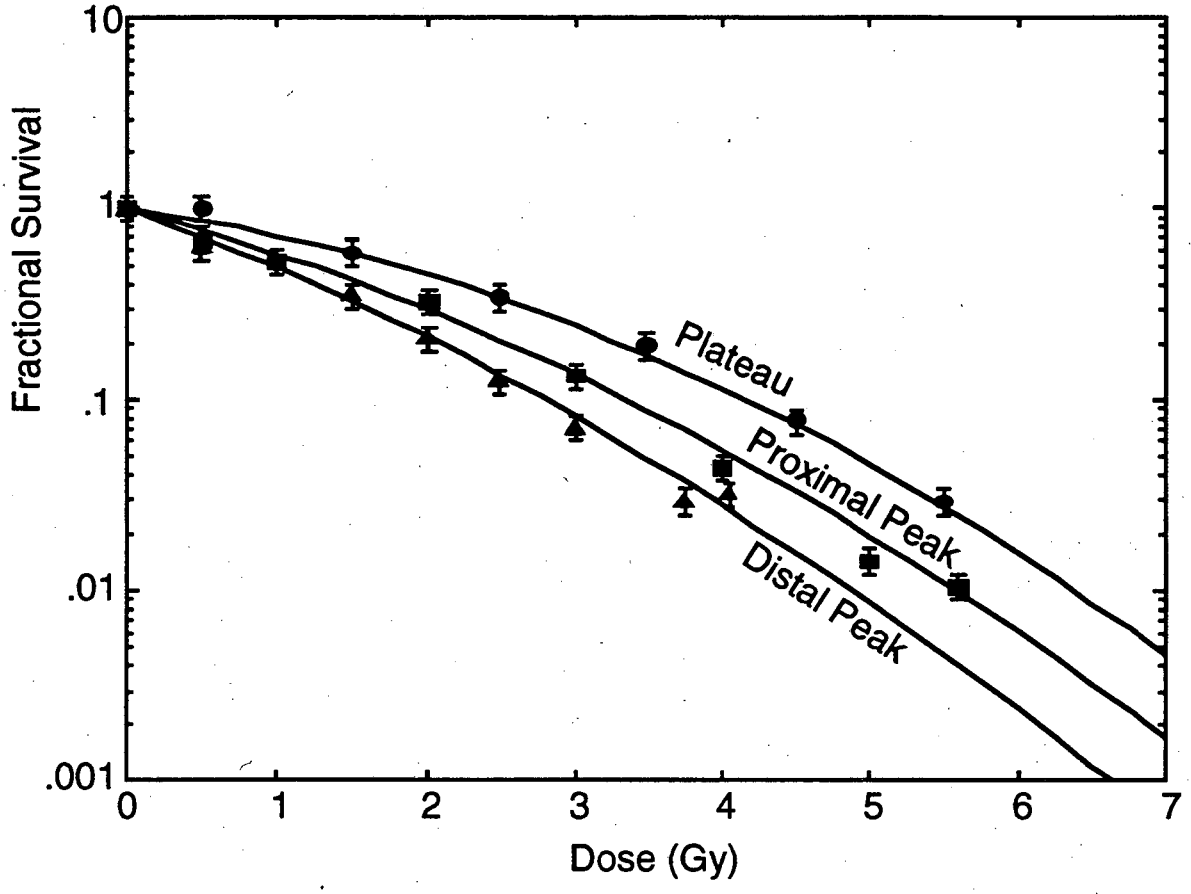

Fig.14. Cell survival curves are shown for three positions in a 12-cm SOBP of a neon-ion beam with an energy per nucleon of 585 MeV. A given cell survival occurs at lower radiation dosages in the distal region than in the proximal peak; hence the need for the slope in the SOBP in Fig. 2.

function of the dose it absorbs can be measured point by point. An example of cell survival curves are shown in Fig. 14 for three positions in a 12-cm SOBP of a neon-ion beam of an energy per nucleon of 585 MeV. Such a graph can be used to check the uniformity of killing as a function of depth. A second, faster but less accurate, method is to simultaneously irradiate a set of cells either deposited on glass cover slips[37] or suspended inside flat-walled flasks,[248, 249] which are stacked in the beam direction to form what is called a "submarine" as shown in Fig. 15. Exposing the submarine to a clinical radiation field and then measuring the cell survival in each flask yields in one irradiation a complete cell survival measurement as a function of depth.

The tail region of the depth-dose curve is a complex mix of particles; its RBE is important in predicting the response of tissue beyond the Bragg peak where critical structures might be found. Tail doses are typically one tenth of the dose in the proximal peak, and biological measurements in the tail region are difficult due to the large dose need at the proximal peak in order to measure

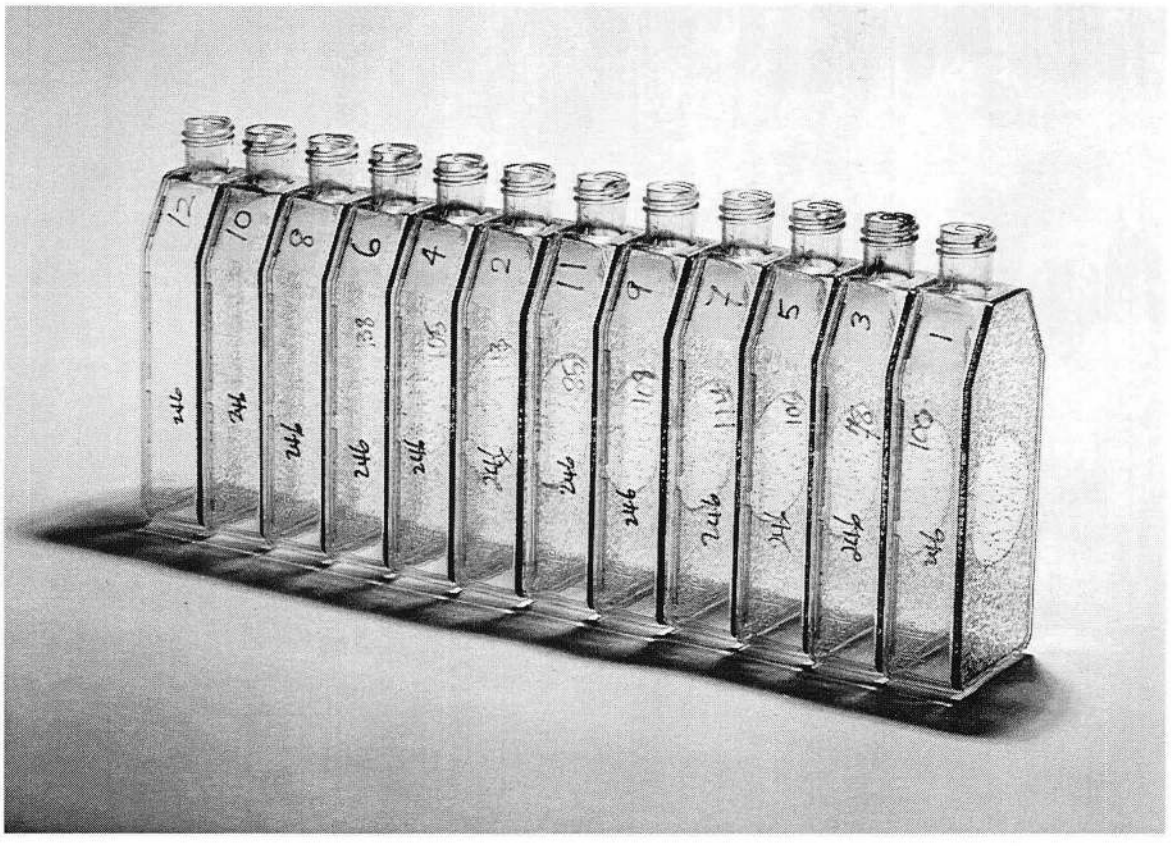

Fig. 15. A submarine, consisting of a stack of chambers containing cells plated on one side of each chamber which is filled with growth medium, is used to measure cell survival as a function of depth after irradiation. A circularly collimated heavy charged-particle beam entered from the left and stopped in the middle of the stack. The cells were incubated subsequent to the irradiation and surviving colonies were made visible by staining; sparse populations in the circles represent cell killing. (CBB 812-1850)

reliably cell responses in the tail. Measurements of dose-averaged LET in this region are simpler to make, but not very straightforward in predicting the biological effects.

II. BEAM PREPARATION FOR CLINICAL USE

The transverse dimension of a particle beam stopping at the patient position is primarily determined by the incident beam spot size, the divergence of the beam, the length of drift spaces, and the multiple scattering of the beam in intervening materials. The longitudinal extent of the distal edge of a stopping beam is primarily determined by the initial energy spread of the incident beam particles and the range straggling in the material. Penetration of energetic heavy charged particles in matter

has been analyzed considering Coulomb, nuclear, and other stochastic processes.[250] For example, for a pencil beam of monoenergetic carbon ions of a range of 20 cm in water, the variance of the longitudinal spread due to the straggling is $\sigma_x \approx 0.06$ g/cm^2, and that of the mean deflection due to multiple scattering is $\sigma_y \approx 0.11$ g/cm^2. Therefore, unless the beam is modified, the concentrated energy of the Bragg peak would be deposited in a small volume given by these variances. To cover an extended target volume with the Bragg-peak dose, the range of the beam must be modulated to spread out the Bragg peak, and the beam profile must be transversely broadened to cover the cross-sectional area of the target volume. This section discusses the instrumentation developed for such beam modifications.

II.A. Variable Range Shifters

A heavy charged-particle beam extracted from an accelerator and transported to the patient treatment area usually has a small diameter (rms radius ~1 cm) and a small spread in energy. The beams from synchrotrons have the typical value $\Delta E/E \approx 10^{-4}$ for a given extraction pulse; and $\Delta E/E \approx 10^{-3}$ when averaged over many pulses. If a monoenergetic beam is introduced into an absorbing medium, such as soft tissue, it will stop in a narrow region at the end of its range, R, which is given by the integral over the stopping power, S, of the medium[251-253]:

$$R = \int_0^E \frac{dE}{S} \tag{9}$$

The stopping power, S (or $\frac{dE}{dx}$), of the particle, measured in MeV/cm is given by[254-257]:

$$S = 0.307 \frac{z^2}{b^2} \frac{Zr}{A} L(b) \tag{10}$$

where z is the projectile-particle charge number and β is its velocity divided by the speed of light. Z is the nuclear charge, A the atomic weight, ρ the density, and L, the stopping number per unit mass of the medium. For certain energy regions there are various approximations for the value of L. It is noted that the range of completely ionized particles traveling with the same velocity scales with a/z^2, where a is the mass of the projectile. This explains the longer ranges of secondary particles created in a nuclear fragmentation since they have practically the same velocity as the primary particle before it fragmented. The range, energy and energy loss for different heavy charged particles in various absorbing media are tabulated elsewhere.[253, 258-260]

As already pointed out in Sec. I.C.3.b above, range straggling is a result of statistical fluctuations in the energy loss processes.[221, 222] For a particle of initial energy E and mean range R, proceeding in the direction of x, the range distribution, s, is shown to be Gaussian,[223, 224] as in Eq. (3). Eq. (3) has corrections at high and low kinetic energies, but its accuracy suffices for the heavy charged-particle beams of clinical interest. The value of the variance in the range distribution, σ_x, for

water is given by Eq. (4).[219] As the density and the atomic composition of soft tissues are similar to those of water, the formula in Eq. (4) may be used for estimating the straggling inside soft tissues.

Heavy charged particles can be accelerated to an energy where their range is sufficient to penetrate the tissues and stop at the desired depth in the patient body. In other words, the residual range of the incident particles can be adjusted to be equal to the skin-to-target distance. Because the target volumes of clinical interests are usually thicker than the width of the Bragg peaks, the energy of the incident beam has to be modulated so that the Bragg-peak dose is deposited throughout the target volume from its proximal edge to the distal edge. This "stacking" of the Bragg peaks at different depth may be accomplished by changing the energy of the extracted particle beams from an accelerator. This requires energy changes every 1~10 seconds and over a ten-fold change in particle flux. This energy modulation is more easily accomplished with synchrotrons than with cyclotrons. Not only is it necessary to change the extraction energy from the accelerator, but also the entire beam transport system must also be changed in such a way that the tune and the positioning accuracy of the beam in the target volume remain constant. Although some accelerators easily allow accelerating and extracting particles at various energies, successively switching all parameters of the accelerator and the beam transport system for several different energies during a given treatment has not yet been achieved. At LLUMC such an ability was envisioned[145] and has been demonstrated on an experimental basis.[261] The current clinical practice is to extract a particle beam at one energy and to adjust its range by having it traverse a medium of variable thickness, called an energy degrader, and a shaped medium for range modulation as discussed in Sec. II.B. This process degrades the beam quality due to fragmentation (Sec. I.C.3.c) and the physical dose distribution due to its detrimental effect on the penumbra, but it is easier accomplished than changing the beam energy by changing the parameters of the accelerator and the beam transport system.

II.A.1. Variable water column

Variable thickness energy degraders may be made using various materials, such as water, oil, plastic plates, or metal plates. A "variable-thickness water column" is a device used to modify the range of the beam by placing a variable thickness of water in the beam path. When the range of the incident beam is known, adjusting the range of the beam to an individual patient's prescription can be done simply and efficiently with such a device. This adjusted range is often called the residual range of the beam to distinguish it from the full range of the beam extracted from the accelerator. Water is often chosen as the medium for degrading the beam energy because of the similarity of its physical characteristics to soft-tissue characteristics of the multiple scattering, range straggling, and for

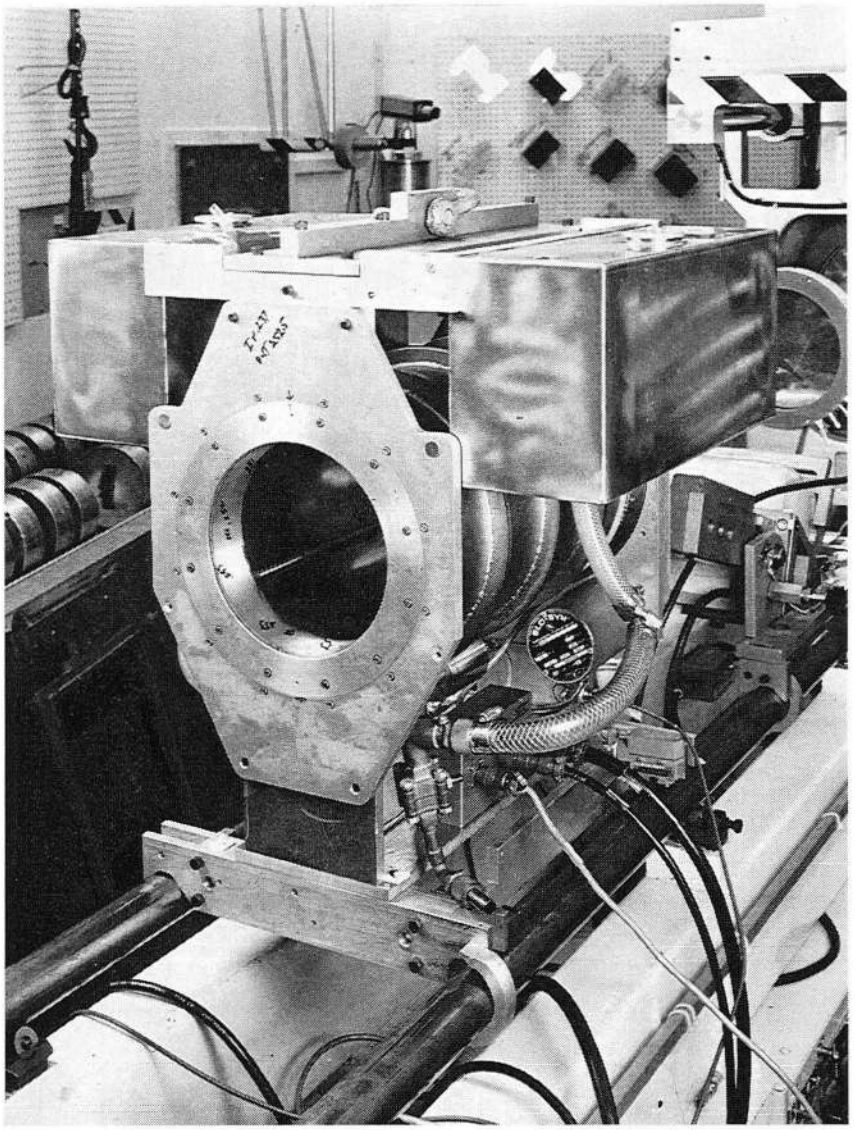

Fig. 16. A water column as shown in this picture is a standard device used for changing the range of the clinical beams and for measuring their radiation field characteristics. (CBB 925-3234)

heavier ions, the fragmentation of the beam particles. However, other considerations may dictate the use of a different absorbing medium.

A typical water column is depicted in Fig. 16. The water occupies the volume between the closed end of a cylinder and a movable piston. The motor-driven piston is sealed against the cylinder wall with O-rings, and, when operated, moves water in and out of a reservoir. This seal limits the rate at which the piston can be driven and hence the speed at which the water thickness can be changed. A rate of approximately 1 cm/sec serves most radiotherapy needs. The mechanical linkage driving the piston is connected to an encoder for water-thickness control and monitoring. A relative accuracy of 0.1 mm in water thickness is achievable with magnetic resolvers or optical encoders. Since the two cylinder ends remain in the beam path, they introduce an additional range shift. Thin windows are therefore preferable, but must be sufficiently stiff, *e.g.*, 5-mm thick Lucite, that their surfaces remain parallel to one another under the pressure of the water.

Variable water columns have been developed at many laboratories to operate in both horizontal and vertical (down) beam configurations.[28, 262-264] The variable thickness is typically 30 to 40 cm which satisfies most clinical needs. Clinical requirements are that the absolute accuracy of the thickness of the column of water is ≈0.5 mm over the entire range. For transmitting a beam with a Gaussian-like beam-spot profile, the cross-sectional area of the water column must be approximately three times the σ of the beam spot to include 95% of the beam particles, plus an additional beam width to allow for beam motion while beam line tuning. Piston diameters of 10 to 30 cm are typical, where the larger diameters are for transmitting transversely spread-out beams (see Sec. II.C).

As a variation of the water column, range shifters using oil as a moderating medium have also been developed. For a vertical pion beam, a tank unit of the range shifter with a moving window powered by a piston was developed at Los Alamos.[265, 266] Another device, an "atmospheric shuttle bath" was developed at NIRS for their vertical-beam geometry.[267] It was filled with 1.05 g/cm^3 density oil, which can vary the proton range in soft tissue within 1 mm accuracy. In an early design, in which the oil was simply pumped in and out, problems arose due to air bubbles in the oil. A piston-type range modulator is now used to eliminate this problem. As discussed in section II.A.5.a below, the variable water column is also used for dosimetric purposes. A Bragg curve can be generated by varying the water column in steps and measuring the beam before and after the water column at each step.[268]

II.A.2. Binary filter

A device called a "binary filter" adjusts the range of the beam by means of a set of metal or plastic plates. The thicknesses of the series of plates double with each successive plate. The name "binary filter" derives from this power-of-two relationship among the plate thicknesses. Based on a set of ten plates, with the thinnest plate of 0.5 mm in water-equivalent thickness, any thickness from 0 to 511.5 mm can be achieved in steps of 0.5 mm. Because each plate is independently moved in or out of the beam, the time to setup the desired range change is independent of the incremental change in the thickness. This feature permits range modulation with minimum loss of time (Sec. II.B). Fig. 17 shows the binary filter developed at LBL, in which twelve metal plates are driven by air pistons that can move the plates in and out of the beam path within 0.5 second.[269]

Several physical and biological factors must be considered when choosing the material used for plates in the binary filter. For protons and helium ions low-Z materials for the plates, such as Lucite or Plexiglas ($C_5H_8O_2$), reduce multiple scattering for a given stopping power. For heavier ions high-Z materials, such as copper, reduce the fragmentation with little increase in multiple scattering. The use of copper plates also reduces the physical thickness compared to water or plastics since

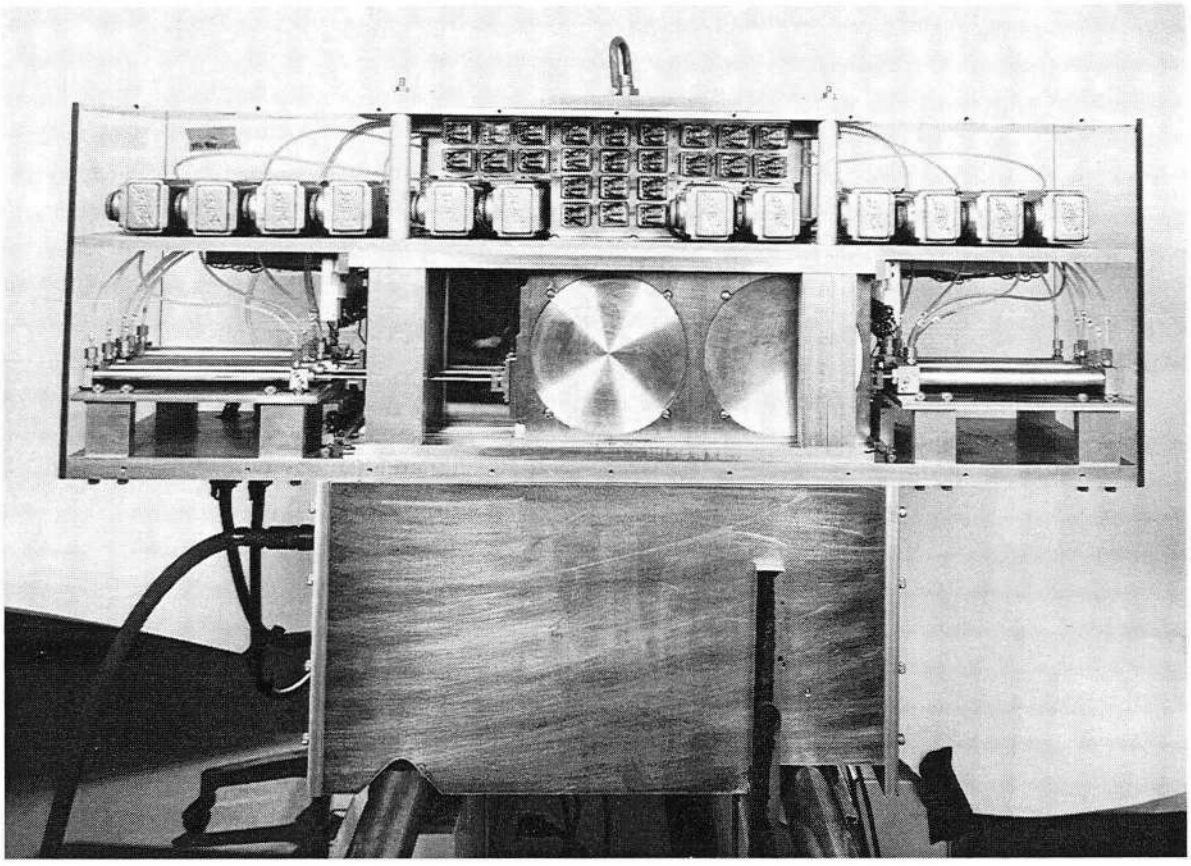

Fig. 17. An example of a binary filter, which changes the range of the beam by means of solid metal plates placed in the path of the beam. (CBB 8211-10042)

copper provides the comparable stopping power as water of ~6 times the thickness. The reduction of the physical thickness of the degrader assembly can be important when the beam-line space is limited. Copper is a preferred metal because it is ductile and can easily be rolled to the desired thickness with close tolerance on density and surface uniformity. In some applications, such as in lateral spreading methods discussed in Sec II.C, it is important that the beam profile remain constant for any residual range. To achieve this a combination of materials may be used to produce equivalent multiple scattering for different energy degradation (see Sec. II.C.1.c).[270]

II.A.3. Double-wedge variable absorber

Alternatively, the thickness of absorbing material can be varied by using an absorber formed in a wedge shape. For a finite beam-spot size, not all particles would traverse the same thickness of the wedge, and therefore the range shifting would not be uniform. This problem can be corrected by using two wedges placed in opposing directions and moved in such a way that the particles in the

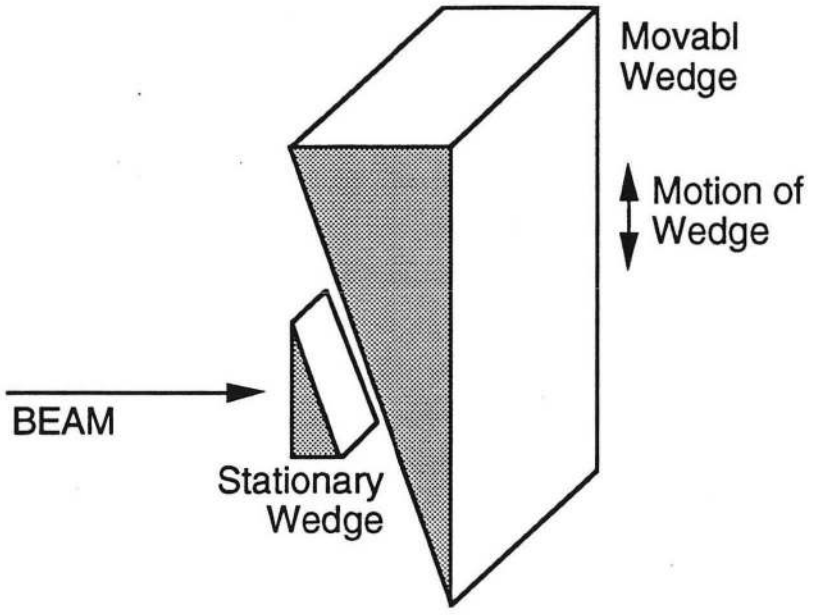

Fig. 18. Schematics of a double wedge system which is used to shift the range of the beam.

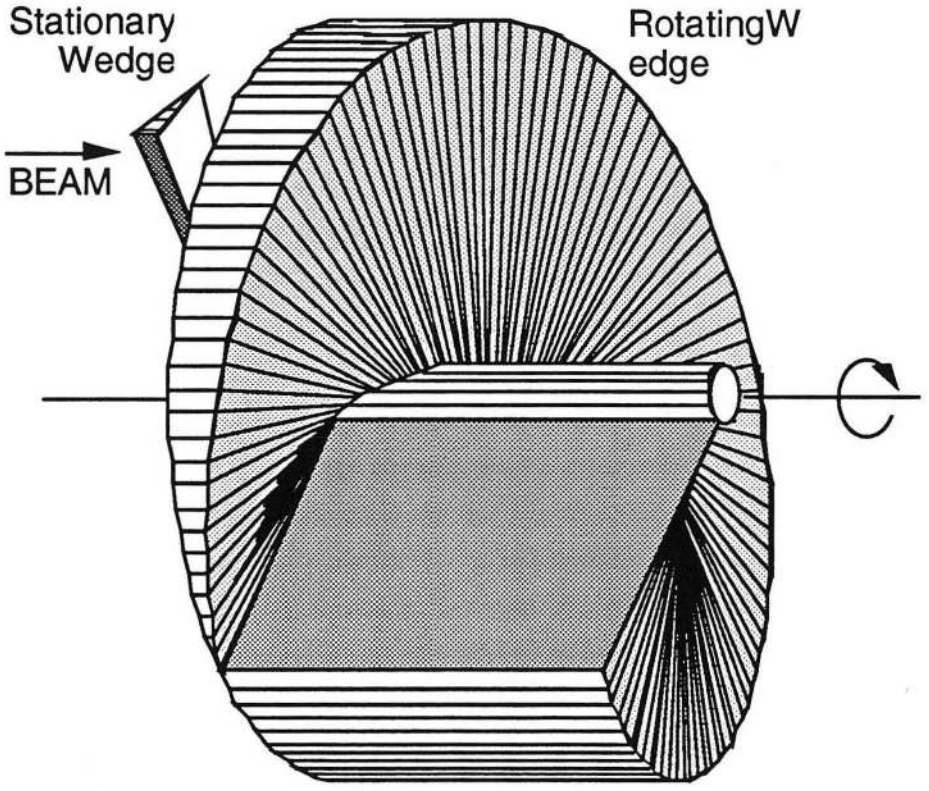

Fig. 19. Schematic drawing of a circular wedge used to reduce the size of the double wedge system. The thickness of the absorber is a function of angular displacement. The beam penetrates off-axis of the device.

finite beam spot traverse a constant thickness[16, 271] as shown in Fig. 18. The overlapping area of the two wedges, which presents a constant thickness surface to the entire beam, must be larger than the beam spot. Consequently there is a minimum absorber thickness, greater than zero, attainable in such a system. Drawbacks are that for a small wedge angle the wedge becomes too large, and for a large wedge angle the minimum thickness attainable for a finite beam-spot size becomes large.

As a variation, the wedge may be circularly shaped; each radius has a constant thickness, and its magnitude varies linearly with the angular displacement. In the example depicted in Fig. 19, the beam goes through the circular wedge at an off-axis spot, and the range change is made uniform by a small compensating wedge placed in the beam path.[272] The thickness of the absorbing material is varied by rotating the circular wedge on its axis, and its thickness is monitored by measuring its angular displacement. Again the minimum attainable thickness is finite as in case of the linear wedge system. The beam traverses parallel to the diameter of the circle in the axial wedge (Fig. 20), in which the thickness of the wedges varies as function of the angular displacement.[174]. In this setup, the off-axis beam traverses different thickness from that traversed by the central ray along the diameter of the circle. The finite size of the circle and multiple scattering effects degrade the sharpness of the *distal* dose falloff of the transmitted beam.

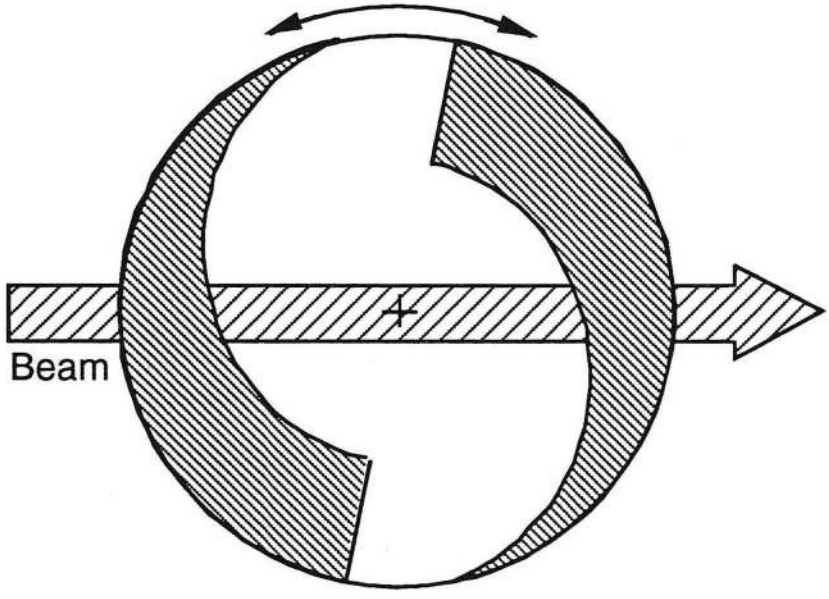

Fig. 20. An example of another type of circular wedge is drawn. The beam penetrates both sides the device to produce a uniform range change across the radiation field.

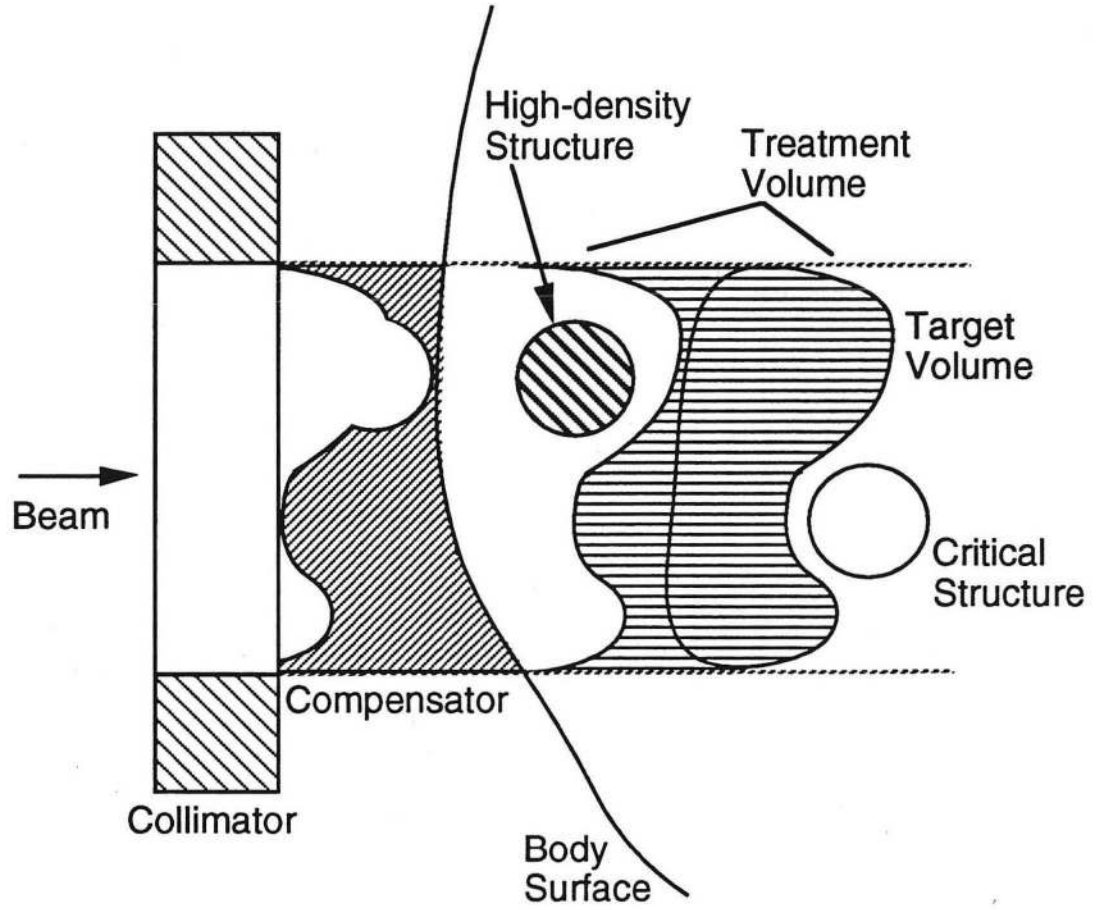

Fig. 21. Schematic representation of the compensator that conforms the distal surface of the radiation field with the distal surface of the target. The total water equivalent thickness of the compensator, intervening tissue, and tumor is constant across the tumor.

II.A.4. Compensator (Bolus)

While many beam-line devices are generic in their use, a few are specific to a particular treatment prescription. A patient-specific device for modifying the beam range according to the patient anatomy is a compensator or bolus. Its function is to adjust the range of the beam across the target to conform the distal edge of the Bragg peak to the distal geometry of the target volume.[273] Fig. 21 shows schematically the function of a compensator in two dimensions, and Fig. 22 shows a photograph of an actual compensator made from Lucite. The details in the bolus structure are computed by considering the effects of tissue inhomogeneities due to bones and air cavities.[274] Compensators may be constructed out of Lucite sheets cut to a pattern specified by the treatment plan, and then assembled together. This process is inherently labor intensive. An alternative method is to mill the 3-dimensional surface out of a hard wax material as shown in Fig. 23. The entire

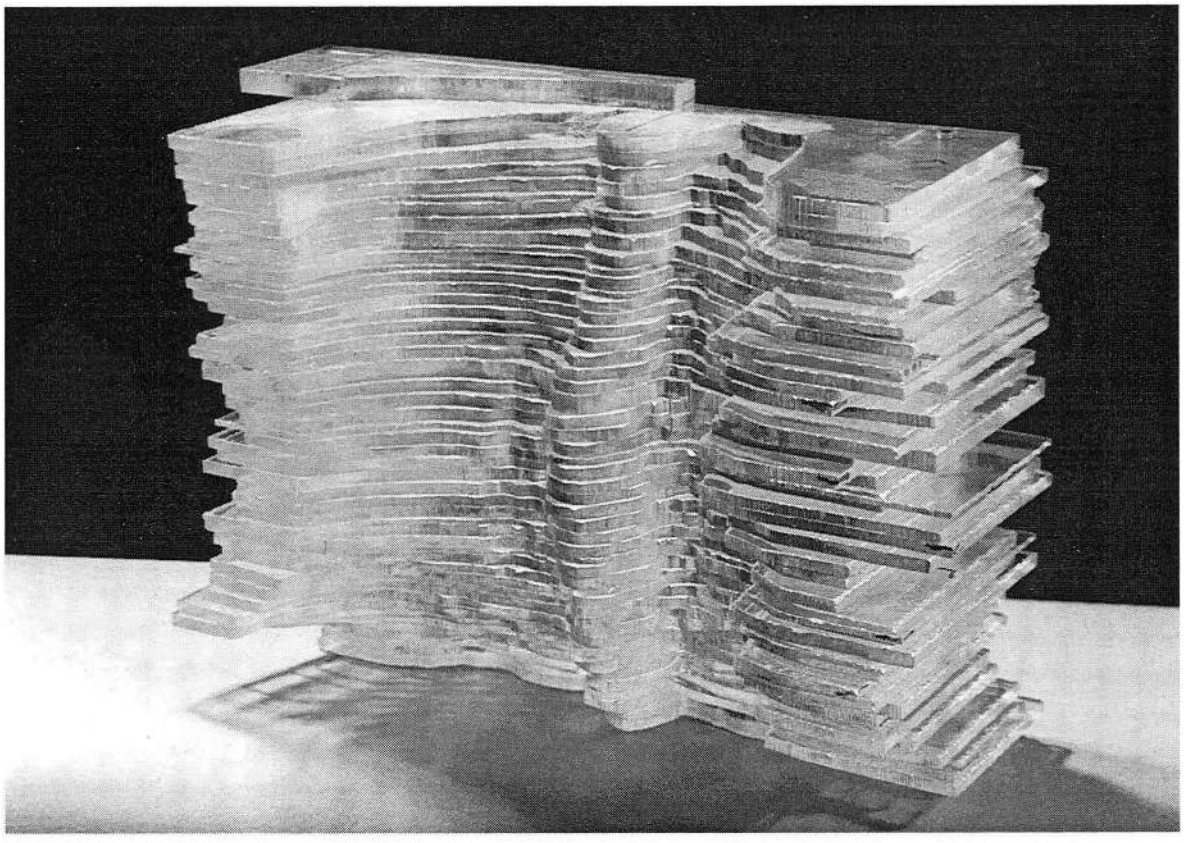

Fig. 22. An example of a Lucite compensator made to conform the distal surface of the Bragg-peak dose to that of the target of an individual patient. (CBB 875-3746)

process, from obtaining the compensator contours based on the treatment plan to cutting the material on a numerically-controlled milling machine, can be automated.[275, 276]

II.A.5. Range verification

Verification of the actual residual range placed inside the patient body is the primary safety issue. An off-line measurement can be done before a patient is treated with the assumption that the range remains constant during the treatment. Radioactive beam imaging (Sec. V.A.1) is an example of range verification methods. The beam range can also be monitored on-line, *i.e.*, during a patient treatment.

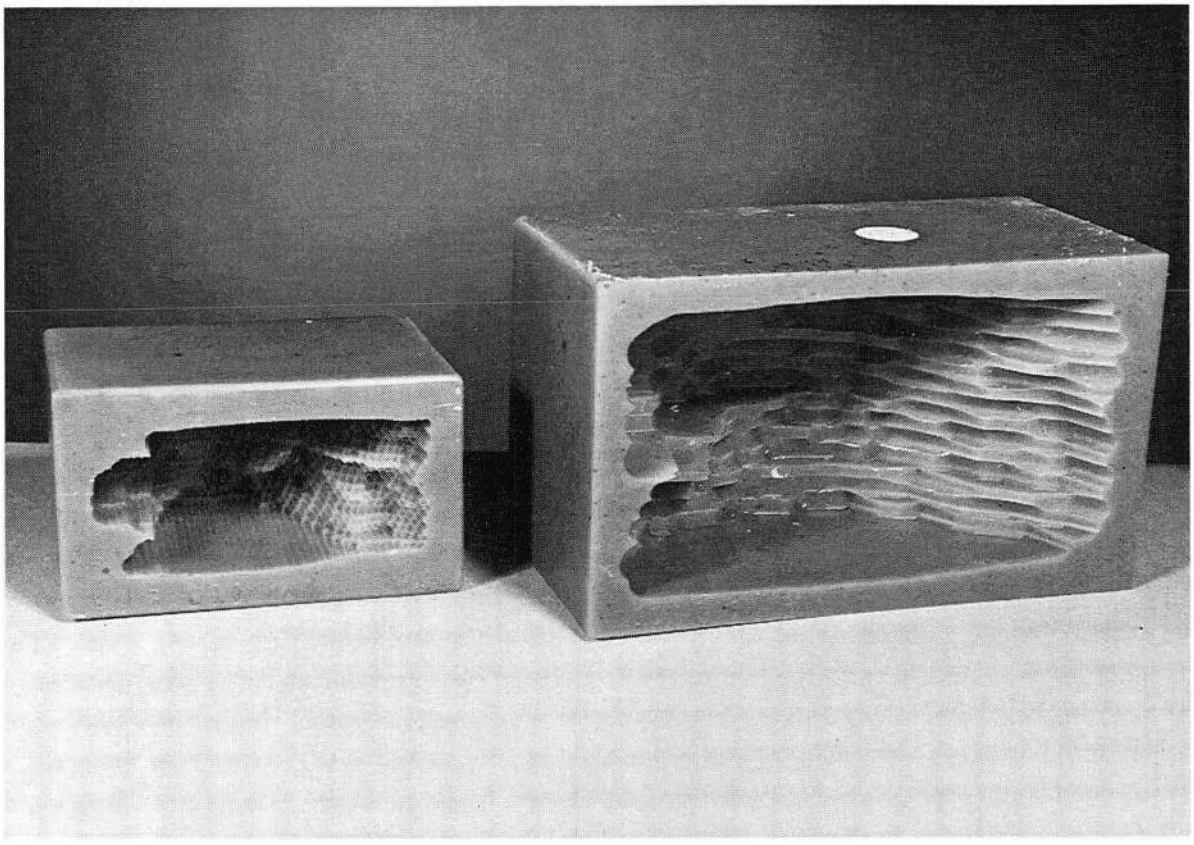

Fig. 23. Picture of compensators cut out of a hard wax block. (CBB 875-3748)

II.A.5.a. Off-line beam-range measurements

A measurement of the range of a beam can be made using a water column or binary filter along with two dose detectors, such as transmission ionization chambers. One detector placed upstream of the degrader measures the incoming beam. The second detector placed immediately downstream of the degrader measures the ionization of the exiting beam. The ratio of the two measurements as a function of the degrader thickness yields the relative ionization of the exiting beam. A Bragg ionization curve is measured if the beam is monoenergetic. The beam range can be deduced from the absorber thickness where the Bragg peak occurs. For a modulated beam, the range, usually in water, may be defined for clinical purposes as the depth of the distal line of 90% of the isoeffect contour. Alternatively, it may be defined operationally as the water depth of the position in the distal dose falloff where the relative ionization is 50% of that of the peak, *i.e.*, the peak position plus a portion of the width of the distal falloff due to the range straggling. If there are other absorbing material, including the air space, between the water column and the patient, their range-modifying characteristics must be included in the computation of the residual range in the patient.

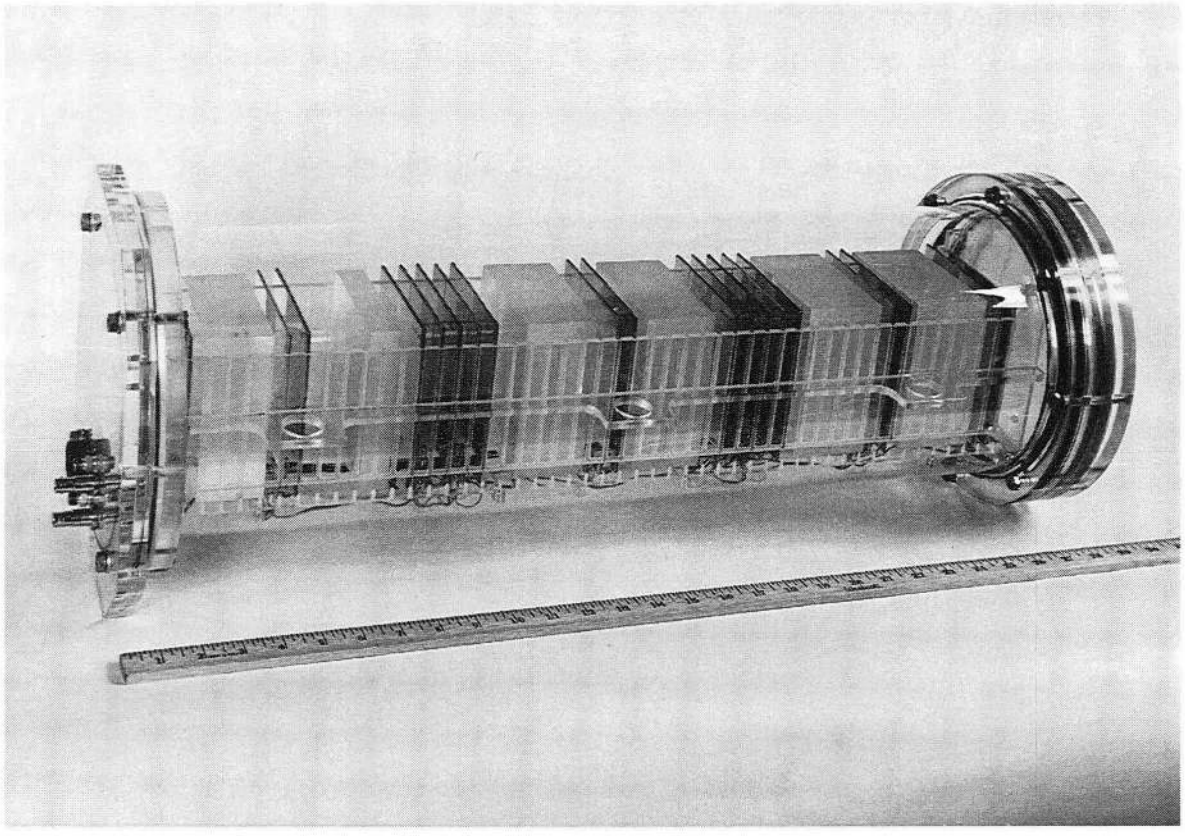

Fig. 24. The Bragg curve telescope measures a Bragg curve at several points using a series of ionization chambers, which are interspersed by pieces of material of known water-equivalent thickness. (CBB 874-5230)

An alternative method for obtaining the range is to measure a depth-dose distribution in a water phantom. Here a small detector, either an ionization chamber or a diode, is moved in a volume of water and its readings are normalized to the incoming beam. It is important that the size of the detector be small compared with the field so that the change in dose as a function of depth is not dominated by the effect of the beam divergence.

A plastic scintillator can also be used as a range detector. In a device developed at LLUMC, the beam is stopped in a scintillator block and the output of light as a function of depth is viewed by a CCD camera.[143] The light output is related to the energy loss of the beam, but is not exactly proportional to dose. Therefore, a calibration procedure is required to map the light output into a dose distribution. Its main advantage is that the entire range measurement can be done at once; however, the drawback is that such a device can be large, since the scintillation in the block must be optically imaged

Another device, developed at LBL (Fig. 24) is a series of ionization chambers sandwiched between degraders of predetermined thicknesses, which can be used to verify the range and the shape of the Bragg ionization curve using only a few beam spills from the accelerator. This method is as fast as that of the scintillators camera, but can take measurements only at predetermined depths. Thick absorbers are placed in the region where the dose changes gradually, and thin absorbers where the dose change rapidly. The overall length of the device, a sum of the thicknesses of absorbers and ionization chambers, is significant. The effects of beam divergence and beam size must be taken into account in the design. This device is further described in Sec. III.A.2.d.

Similarly, a stack of films with intervening materials of known thicknesses can also measure the Bragg ionization curve, but this method is extremely time consuming and requires knowing the dose response of the film. Nevertheless, a relative measurement can be useful even without such calibrations.

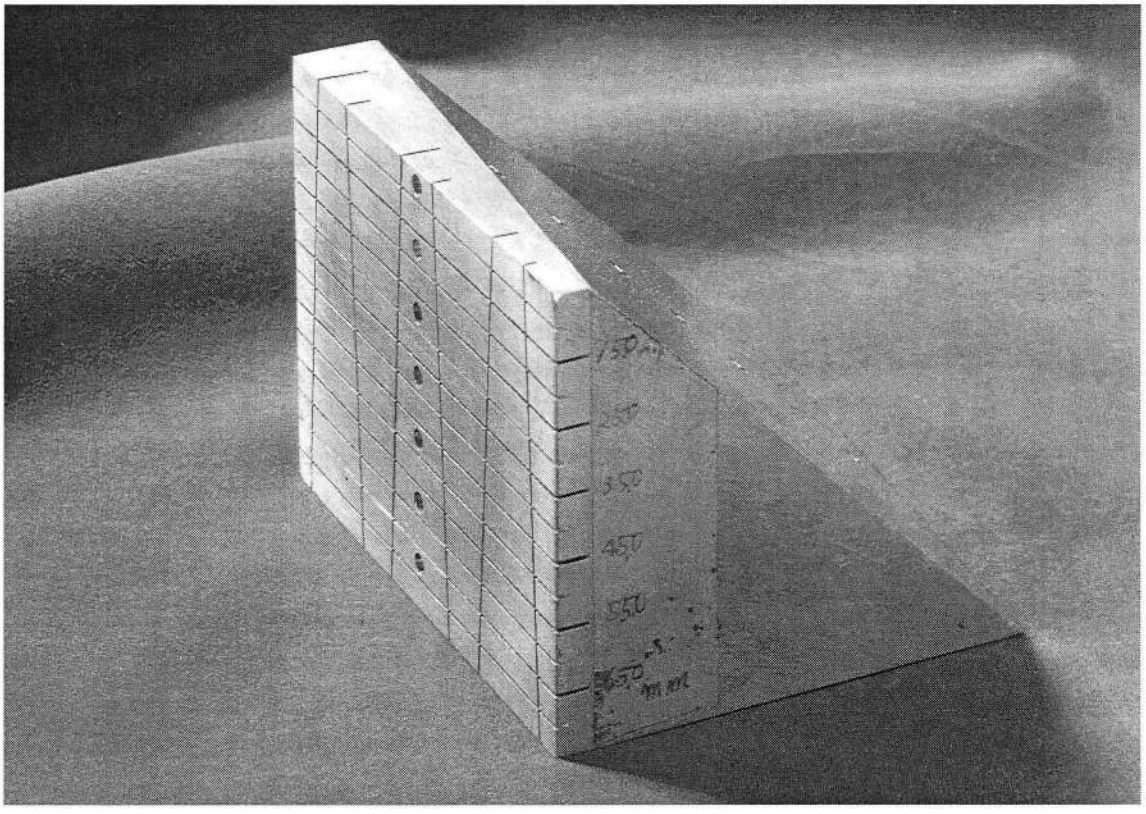

Fig. 25. A simple system for measuring the range of the beam consists of a complex wedge in front of a piece of film. The sharp distal falloff in dose at the end of the Bragg curve is imaged on the film for range verification of the beam. (CBB 7910-14624)

Film behind a wedge absorber with a complex wedge angle, as shown in Fig. 25, can also serve to locate the distal edge of the beam.[277] The range measured in the wedge material is converted into the water-equivalent range by applying the ratio of the integrated stopping powers of the wedge and water.

II.A.5.b. On-line measurement of the beam range

Since patient treatment must not be perturbed by a range measurement, an on-line range verification is difficult. The periphery of the beam, *i.e.*, the area outside the collimated radiation field, may be used for a range measurement, provided the range is uniform across the entire field. A device located on the outside and upstream of the patient collimator aperture can make such measurements. A series of detectors, such as diodes, downstream of a metal wedge can be used to verify the range. Each detector in effect measures the energy loss of the beam at a different depth. The number of detectors determines the number of data points and the wedge shape determines the spatial resolution of the measurement. A variation of this is a rotating wedge with a detector behind it. The response of the detector and the position of the wedge can be correlated to give a depth-dose measurement. Both these methods require a normalization detector upstream of the wedge.

A recent idea to measure range[278] is to use the acoustic pulse generated by particles traversing a medium.[279] By using a pulsed particle beam and knowing the speed of sound, the location of the sound pulse can be determined by measuring the propagation time. The intensity of the acoustic pulse is shown to be proportional to absorbed dose, and therefore the detected acoustic pulse has the same shape as the depth-dose distribution.[280] This method has been experimentally tested; however, is has not yet been clinically implemented.

II.A.6. Effects of range shifting on the lateral and distal dose falloff

In order to take full advantage of the dose localization properties of the heavy charged-particle beams, great care must be taken to minimize the width of the lateral dose falloff. The apparent source size of the radiation field causes a penumbra, which contributes to broadening of the width of the lateral dose falloff. In order to minimize the apparent source size, the diameter of the beam has to be small where the beam traverses material.[281] This can be accomplished by placing any scattering and range-shifting material upstream of where the beam begins to spread transversely. However, any amount of material in the beam introduces an additional beam divergence due to multiple scattering. Positioning the material far upstream of isocenter may lead to an intolerable increase in beam spot size at the target, which, if collimated, results in a reduction in the dose rate. On the other hand, placing the scattering material close to the target volume reduces the scattering effect on the low-velocity particles and preserves the modulated Bragg peak shape. For this reason the patient compensator is usually placed against the patient body. The unavoidable multiple scattering inside

the patient body and other material in the beam path, especially those near the patient such as the compensator, also contributes to the broadening of the width.

The amount of material used for scattering or energy degradation also affects neutron production[282] and projectile fragmentation,[230] which in turn affects the peak-to-plateau ratio of the SOBP. The placement of this material also affects the peak-to-plateau ratio. The ratio is enhanced when the material is placed far upstream of the target as a large portion of the neutrons and fragments diverge out of the main beam. The sharpness of the Bragg peak and the width of the distal falloff is largely determined by the amount of range straggling introduced by the material in the beam path. The width of the distal falloff of the SOBP also depends on the details of the range modulation, as discussed in Sec. II.B. All of these effects must be considered in optimizing the design of a beam-delivery system.

II.B. Range Modulation

Neither monoenergetic photon nor electron beams exhibit sharp distal dose falloff in an absorbing material. The doses deposited by high-energy photon beams decrease approximately exponentially as a function of the depth of penetration. In absorbing material, monoenergetic electrons do not have a well-defined range because of their small mass results in large multiple scattering. On the other hand, monoenergetic heavy charged-particle beams have well defined ranges.

As shown in Fig. 2, the Bragg peaks of heavy charged-particle beams are quite narrow. Its width in the target volume is primarily due to the energy spread in the beam and the straggling of the incident particles in the absorbing material, including the part of patient body itself, located along the beam path up to the stopping region. The resulting Bragg peak is still narrower than the target thicknesses usually encountered in the clinic, typically from 0.5 cm to 16 cm, and the beam range must be modulated in order to cover the extent of the target thickness with the Bragg-peak doses.

Modulation of the residual range in order to spread out the width of the Bragg-peak dose region, as schematically shown in Fig. 26, can be accomplished in two ways. In the first method, called dynamic modulation, the residual range of the beam is changed in a stepwise fashion during the treatment and the resulting Bragg peaks are sequentially stacked throughout the depth of the target volume. The second method employs a passive system that modulates the residual range by means of a bar ridge filters. Use of range-modulating propellers or rotating spiral ridge filters falls in between these two methods.

For clinical use a biologically uniform dose distribution within the entire target volume is required. A biologically uniform dose distribution may or may not result from a uniform physical dose distribution. In the example shown in Fig. 26, the implicit assumption is that the cell killing capability per unit dose remains the same for the radiation over the entire width of the SOBP. Such

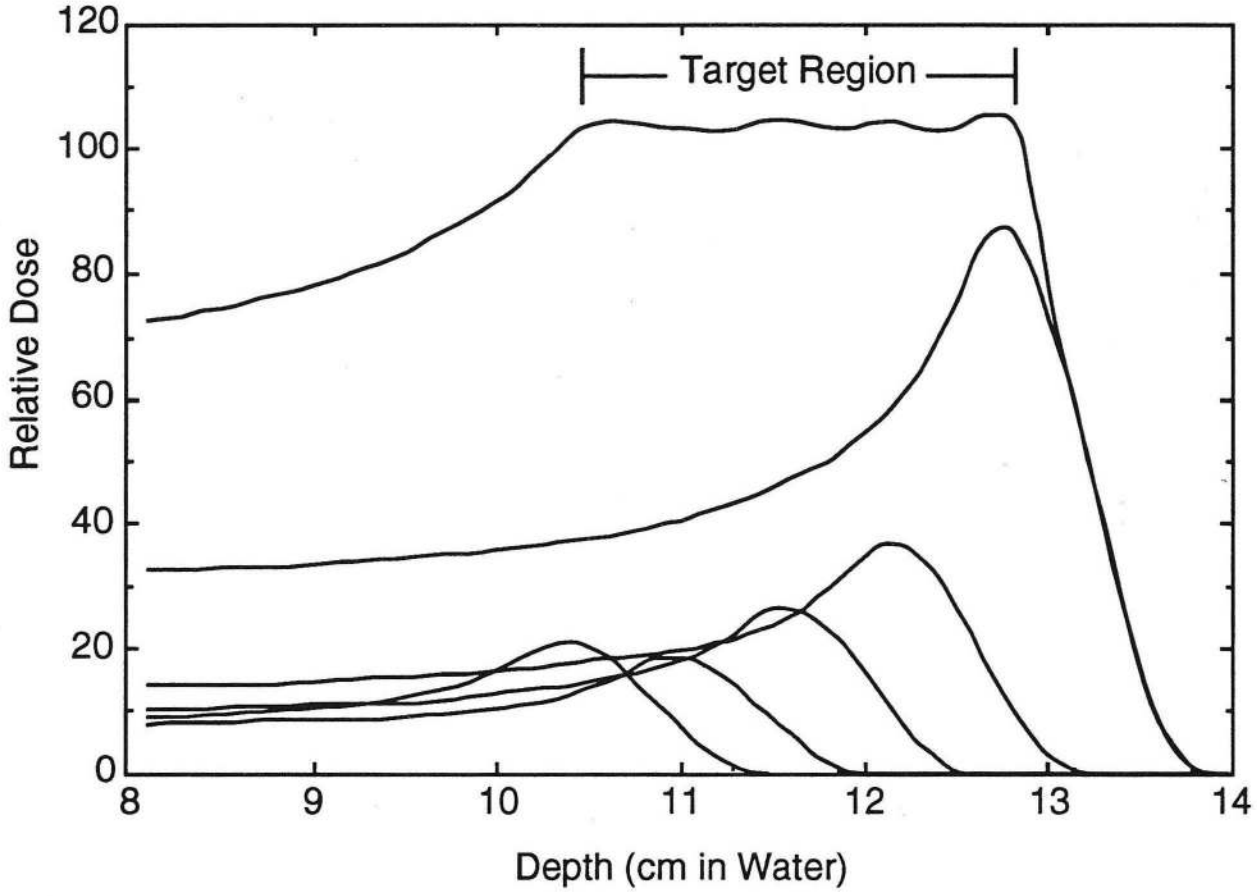

Fig. 26. Bragg curves of different range beams are stacked to create an appropriate spread-out Bragg curve.

cell killing capability is characterized by the RBE of the radiation, which is defined as a ratio of the radiation dose required to arrive at specific biological endpoints over that of the reference radiation that achieve those same endpoints. The value of RBE for the accelerated proton beams remains close to 1.0 from the plateau region to the peak region, *i.e.*, 1.0 ~1.1, although some data show RBE values of 1.7 and higher.[283-292] Therefore the proton beam whose Bragg peak is spread out according to Fig. 26 will exhibit a biologically uniform dose throughout the width of the SOBP.

As can be observed in Fig. 26, the distal part of the SOBP is almost entirely made up by the Bragg peak; whereas, as one moves toward the proximal peak of the SOBP, the contribution of the plateau dose increases and that of the Bragg peak diminishes. If the RBE values are different in the plateau and peak regions of the Bragg ionization curve, the physical dose distribution must be adjusted to achieve a biologically uniform dose across the SOBP. In fact, the value of RBE for heavier-ion beams is a function of the penetration depth, and rises very rapidly to a maximum at the Bragg peak. Since the objective is to achieve a biologically uniform dose throughout the width of the

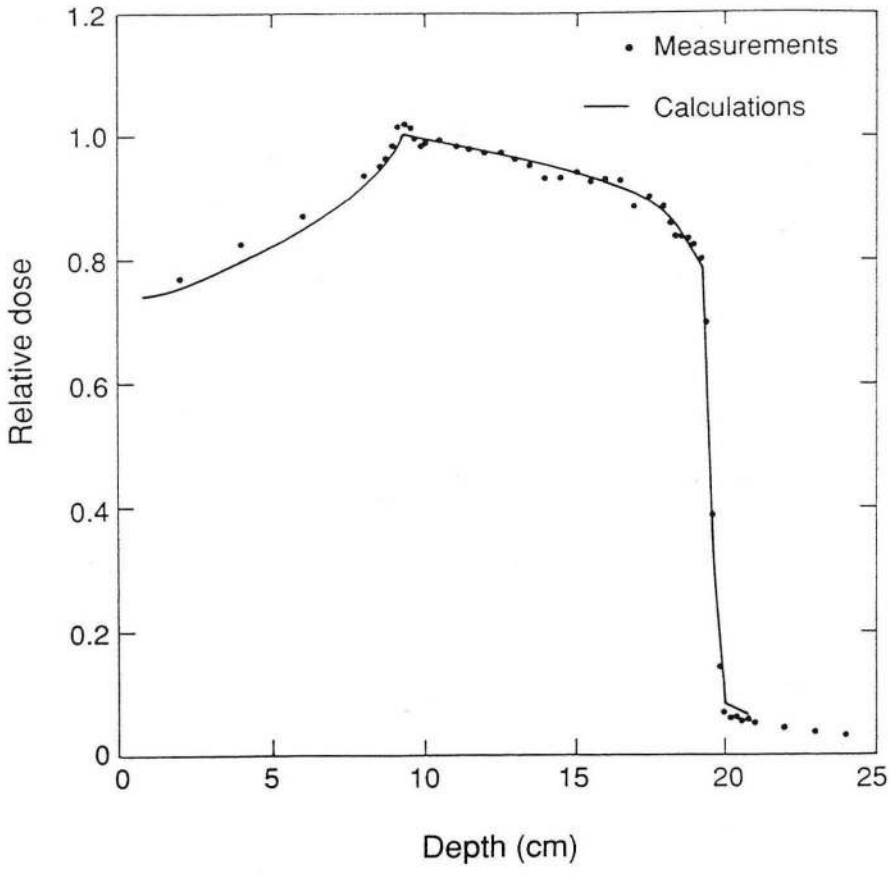

Fig. 27. Shown is a physical dose distribution of the SOBP that provides a constant biological effect across the entire width of the SOBP for a helium-ion beam. If the varying RBE as a function of depth is multiplied by the physical dose, the resulting biological dose becomes constant across the width of the SOBP. A comparison between data (dots) and calculation (solid line) show good agreement. (XBL 902-6270)

SOBP, the physical dose distribution is made to slope down as one moves from the proximal to the distal part of the SOBP, as shown in Fig. 27.

There are other complications in the design of an appropriate physical dose distribution for obtaining a biologically uniform dose throughout the width of the SOBP. Since the scattering increases with the beam penetration, the peak-to-plateau ratio for small beams decreases as the residual range increases. This effect must be taken into consideration even for proton beams. For the heavier-ion beams, the primary nuclei may fragment in the absorbing material and turn into lighter nuclei, which have longer ranges and lower RBE, and create a "tail" dose beyond the distal fall-off of the SOBP (see Sec. I.D.3.) The fragment dose is not confined to only the tail region. The

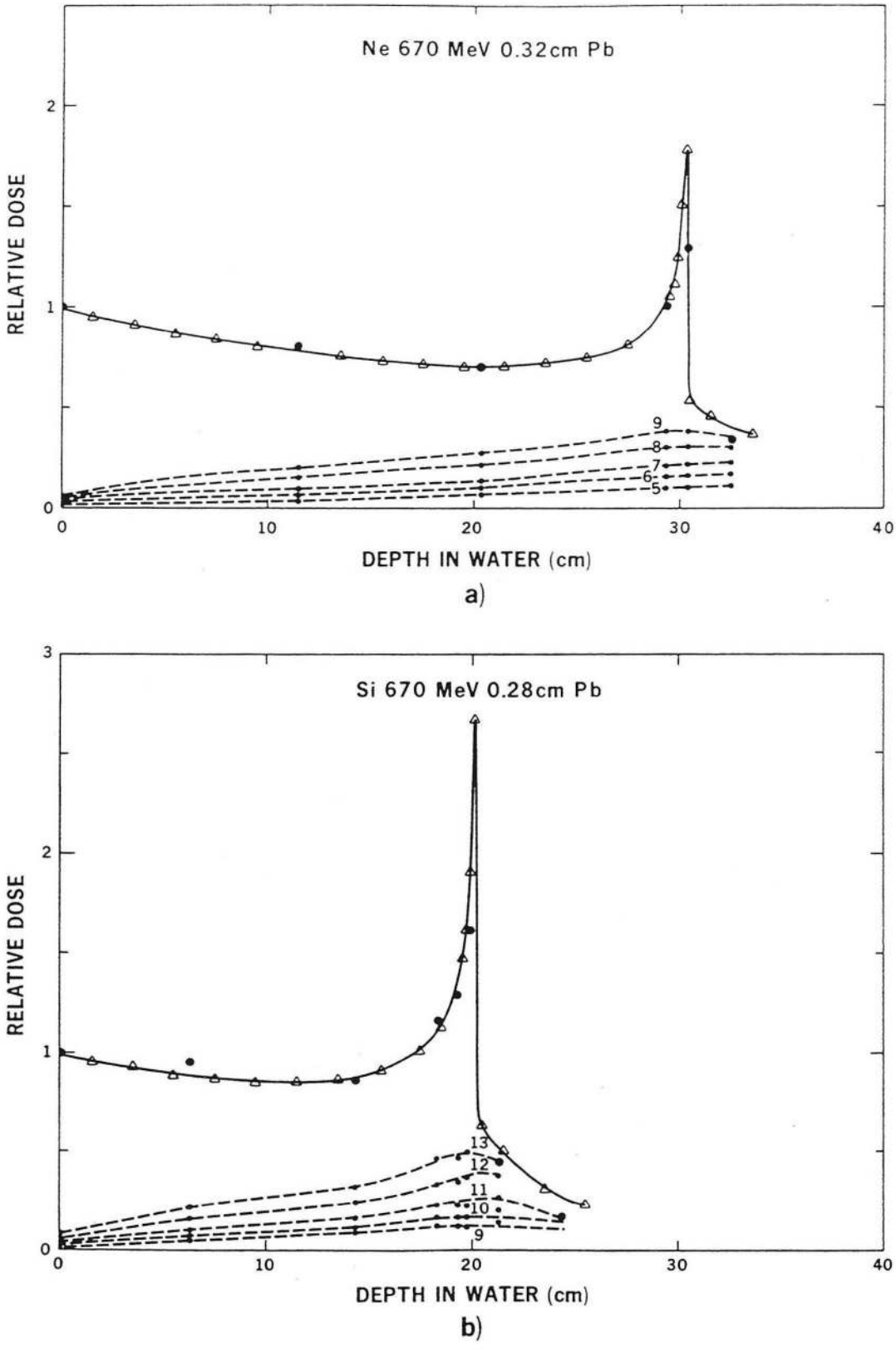

Fig. 28. The heavier-ion beam dose distribution consists of the dose due to the primary particles (triangles) and fragments of different charge as

projectile particles fragment throughout the medium, and therefore the fragment dose is also embedded throughout the beam path upstream of the distal edge of the dose distribution, as shown in Fig. 28.[229]

In all methods of modulating the range to spread the Bragg peak over the target volume, the fraction of the total number of particles used to irradiate a particular depth of the target volume must be determined as a function of particle range. In practice, a set of fractions at discrete range steps, called "beam weights," is determined. These beam weights are determined by: (1) measuring the unmodulated Bragg peaks at different residual ranges in the appropriate beam-line geometry, (2) calculating or measuring the LET of the beam as a function of depth, and (3) using a cell survival model along with the dose distributions and LET values. These can then be used, as discussed below, to create a spread-out Bragg peak that gives the desired (usually uniform) cell survival distribution over the target volume.[293]

In the absence of fragmentation with only the primary beam particles contributing significantly to the cell killing, the beam weights can be found by the following procedure. The dose at d_i in a SOBP is the sum of the doses of the individual Bragg ionization curves at d_i,

$$D(d_i) = \sum_{j=1}^{m} W_j D_j(d_i) \tag{11}$$

where $D_j(d_i)$ is the dose at depth, d_i, for a Bragg ionization curve with residual range R_j for $j = 1,...,m$. R_m is the maximum range of the spread out Bragg ionization curve and W_j are the j-th beam weights. If $Q_j(d_i)$ is the calculated LET of the $j-th$ Bragg ionization curve at depth d_i then the dose-averaged LET, $\overline{Q}$ at depth d_i is:

$$\overline{Q}(d_i) = \frac{\sum_{j=1}^{m} W_j D_j(d_i) Q_j(d_i)}{D(d_i)} \tag{12}$$

---

indicated by the numbers. The curve labeled z corresponds to a cumulative dose distribution for fragments from the lowest charge detected to the given z. The data are from (a) Ne-ions with an energy per nucleon of 670 MeV penetrating 0.32 cm of lead, and (b) Si-ions with an energy per nucleon of 670 MeV penetrating 0.28 cm of lead. The lead is placed far upstream in the beam to enlarge the radiation field and account for the beam fragmentation. The Bragg curves are measured with ionization chambers and the fragment data are based on BERKLET measurements. (XBL 837-10785) (The authors thank Dr. J. Llacer for the permission to use the unpublished data.)

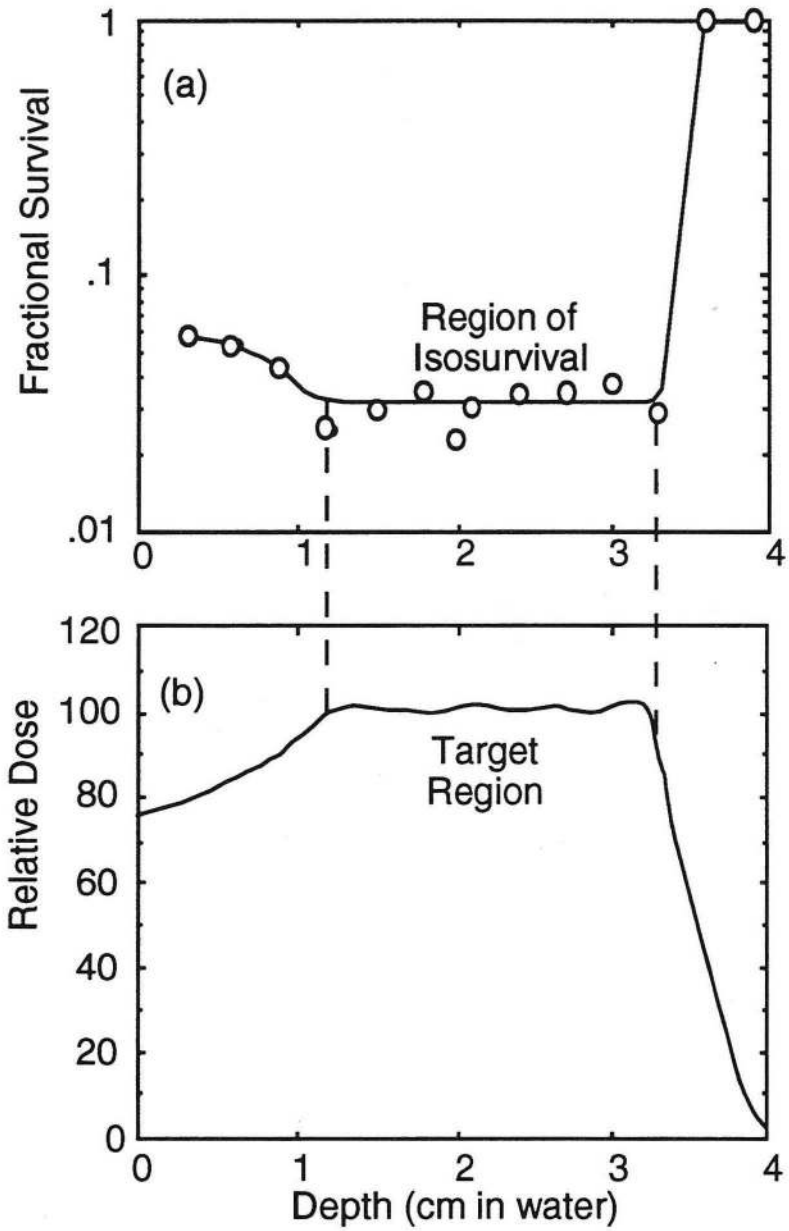

Fig. 29. (a) Fractional survivals as a function of depth is shown for the case where 3% of the cells survive after one irradiation. The open circles are data, and the solid line is a guide for the eye. (b) The spread Bragg curve which produces this survival is also shown.

The cell survival S can then be calculated using a cell survival model such as the alpha-beta model[294-297] with $\alpha(\overline{Q})$ and $\beta(\overline{Q})$ parameters determined from fits[19, 298, 299] to experimental cell survival data:[249, 300, 301]

$$S(d_i) = e^{-\alpha D(d_i) - \beta (D(d_i))^2}, \tag{13}$$

where α and β are functions of $Q(d_i)$. The beam weights are determined by minimizing the function

$$\min\left[\sum_{i=a}^{b}\left(S_0 - S(d_i)\right)\right]^2 \tag{14}$$

where $i = a,...,b$ stands for the intervals in the region of isosurvival and S_0 is the desired cell survival in this region.

The validity of a set of computed beam weights, W_j, may be checked using a real beam and measuring the resulting dose distribution along the central ray. Fig. 27 shows a set of Bragg ionization curves with the appropriate beam weights applied and their sum. Fig. 29 shows the calculated and measured fractional survivals as a function of depth for 3% survival after one irradiation in the region of the spread out Bragg ionization curve. A different biological endpoint, such as a different survival fraction or a fractionation scheme, gives a different set of beam weights, and therefore, a different slope in the SOBP dose.[298]

For low-LET radiation, such as a proton or helium-ion beam, the beam quality is less complicated than with heavier ion beams. Nuclear fragmentation plays a smaller role for helium ions and the variation in LETs is smaller than for heavier ions. A calculation of LET values for helium ions along with a simple model of beam quality and the alpha-beta model of cell killing provides satisfactory results as verified with measured cell survival data.[19, 298] For heavier ions, beam fragmentation must be taken into account since α and β depend not only on the dose-averaged LET but also on the charge and mass of the incoming particles. Model calculations or measured data of beam fragmentation are needed as input.

II.B.1. Dynamic range modulation

In a dynamic method a desired SOBP is obtained by accumulating the Bragg peaks with different residual ranges as shown in Fig. 26. Each Bragg ionization curve range is adjusted by means of either an a change in absorber thickness or an accelerator energy change. Because the width of the Bragg peak is only a few mm wide and the target thickness may be as large as 16 cm, many steps must be used to create a smooth SOBP. To simplify this process, a special filter may be used to spread out the Bragg peak to a width between 5 mm and 10 mm. A smaller and more manageable number of these "minipeaks" of different ranges are then used to create the desired SOBP.

Dynamically modulated beams for the helium-ion beams are used at LBL for the treatment of ocular melanomas and for stereotactic radiosurgery of intracranial disorders.[299, 302] Widths from 1 cm to 4 cm are generated using 5-mm wide minipeaks. In this method, at the distal end of the SOBP, a Bragg peak, not a minipeak, is stacked to sharpen its distal dose falloff. The range modulation is accomplished by using a variable thickness water column described in Sec II.A.1. A discrete step range shifter using plexiglass plates was constructed at the Batho Biomedical Facility of TRIUMF in Vancouver to spread out the negative pion beams whose Bragg peak is approximately 0.7 cm.[303]

The dynamic range modulation would become very advantageous if it were accomplished by accelerating and extracting particle beams at different energies. Absorbers in the beam path, and

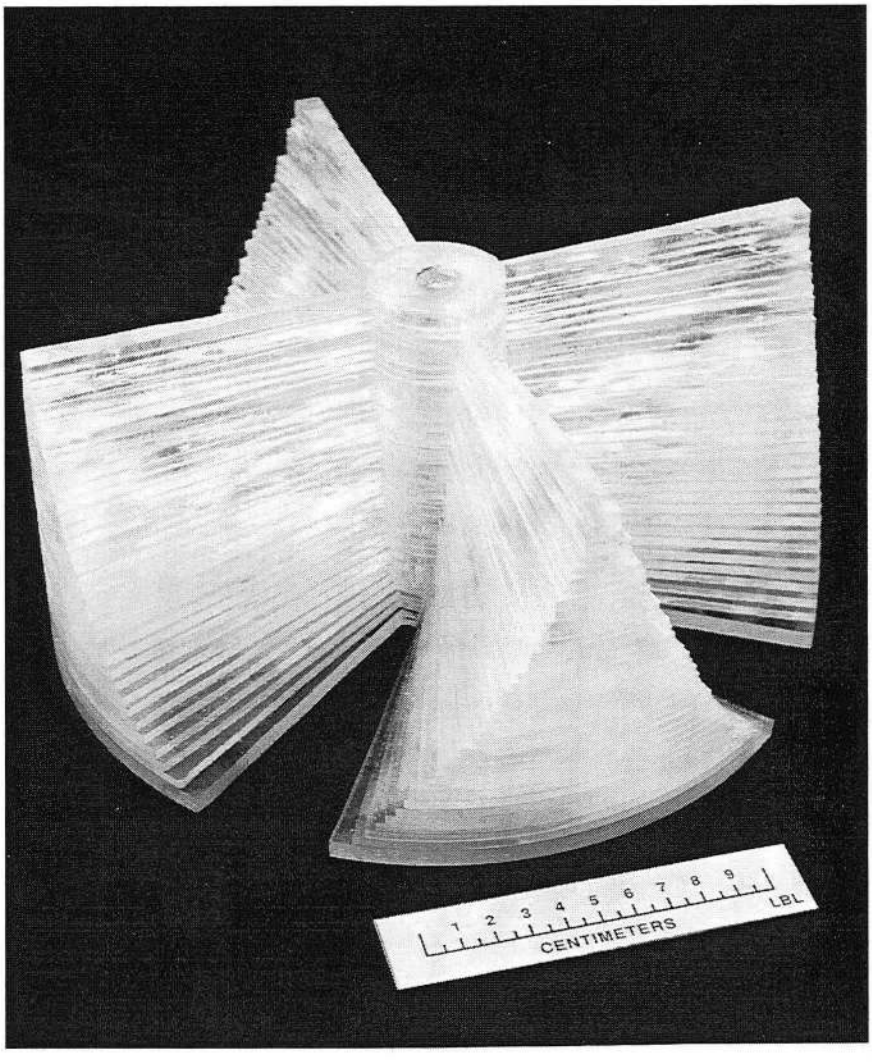

Fig. 30. Shown is a picture of a propeller used with He ions at the LBL Bevatron. It is used to extend the Bragg peak over the target volume. (CBB 901-261)

therefore multiple scattering and straggling in the absorber which reduce the sharpnesses of both the lateral and distal dose falloffs, could largely be avoided. However, it involves not only accelerating and extracting particle beams at different energies, but also transporting beams of different energies while maintaining the correct beam optics. To prevent an incorrect irradiation of the patient, the dynamic range modulation requires more stringent safeguards than in the passive method. However, this method can be readily adapted to deliver 3-dimensional conformal treatments when coupled with a variable collimator as discussed in Sec. II.C.3.c.

II.B.2. Range-modulating propellers

The function of range modulation may also be accomplished by designing a "propeller," or fan-shaped stepped absorber, which is made to rotate rapidly in the beam so that the appropriate thickness of the propeller "blades" intercept the beam. The propeller used at LBL with helium-ion beams is shown in Fig. 30. The beam passes through the propeller off axis in such a way that it

traverses the blades and avoids the propeller drive mechanism. The blades are made of Lucite, or Plexiglass, which are "water-like" in their absorbing and scattering characteristics for the helium ions, and of various thicknesses, whose angular widths are made according to the appropriate beam weights, W_j, as determined in Eqs. (11) - (14). If the beam intensity and beam profile are held constant over the beam-spill time and the blade intercepts the beam at a constant angular velocity, the desired spreading of the Bragg peak is obtained when integrated over the time of an integer period of the propeller structure.

For balancing of the rapidly rotating blades, the propeller is usually made of two or four blades. In the examples shown in the figure, each blade, in passing through a beam, modulates the beam range twice across the width of the SOBP, namely from the distal part of the SOBP to the proximal part, then back to the distal part. Therefore each revolution of the four-blade propeller modulates the beam range across the SOBP eight times. Propellers used at cyclotrons can rotate at a moderate angular speed, slower than a few hundred rpms since the beam current, with the rapid cyclotron pulsing structure, may be regarded as constant for range modulation purposes. Since the propellers are bulky, even at these low rotational speeds, the patient and clinical staff must be protected from the rotating blades and from their possible break-up projectiles.

The stepped rotating absorber was first proposed by R. R. Wilson.[20, 304] This type of propeller has been used at the HCL with proton beams,[18, 305] for helium ions at LBL,[299] and recently at LLUMC for proton beams.[143] A small propeller for beams less than 2 cm in diameter was produced,[306] and used for ocular treatments. In an application outside of radiotherapy, a range-modulating propeller was developed to deposit primary particles in a predetermined fashion in order to produce a constant yield of radioisotopes with depth.[307] A propeller to produce a depth dose for constant cell killing was also described by Katz and Sharma.[308]

Using a propeller to modulate the range of the beam from a synchrotron requires several refinements. First, the extracted beam from the accelerator must be of long duration and maintained at a constant level, *i.e.*, flat-top extraction. Next, since it is not practical to have each spill intercept an exact integer number of blades, the propeller is made to rotate rapidly, and the blade structure is repeated in the construction (an 8-fold repetition in the example shown in Fig. 30) to increase the number of interceptions of the beam by the blades. The effect of the uneven starts and stops of the beam spill must statistically be reduced to an acceptable variation in the dose distribution. If f is the rotation frequency, τ is the spill time and the propeller has n-fold repetition of structure, then:

$$\varepsilon = \frac{1}{nf\tau} \tag{15}$$

where ε is the fractional dose variation. A propeller used with the wobbled helium-ion beams at the LBL Bevatron rotates at 900 rpm and has 8-fold repetition of structures per revolution; therefore, $\varepsilon \approx 0.4\%$. The propellers are placed in a sealed cylindrical body, so that the blades and the air in the body rotate together, to reduce the noise. Actual construction of the propellers is done by making a set of layers cut to the desired shape and then glued together. A water equivalent thickness of 4 mm of water is a practical Lucite thickness. Again Lucite is chosen because it is a low-Z material thereby reducing multiple scattering and the associated increase in beam divergence. At LLUMC the propellers are machined out of plastic blocks.[309] The useful radial size of the blades must be approximately three times the beam diameter.

Because of the required high speed of rotation, a system for quickly accelerating and braking the propeller rotation is necessary. The propeller must be balanced to avoid unnecessary vibration and wear on the drive mechanism. If the propeller fails to rotate, the resulting depth-dose distribution will be incorrect. A means of verifying that the propeller is spinning at a correct speed is important for successful clinical use. For each target thickness, an appropriate propeller is needed; verification must be performed that the correct propeller is being used.

II.B.3. Ridge filters

The above-mentioned plastic propellers have been used for proton or helium-ion beams. The main objections to them are their bulky size and the high rotational speeds. To overcome these shortcomings, several types of "ridge filters" have been made — stationary ridge filters, linearly oscillating bar ridge filters, and rotating spiral ridge filters.

II.B.3.a. Bar ridge filters

An example of a bar ridge filter machined out of brass is shown in Fig. 31. The cross-sectional shape is calculated according to the beam weights given by Eqs. (11)-(14) above, so that when the ridges are uniformly illuminated by a particle beam, the transmitted beam exhibits a relative abundance of penetrating particles of appropriate residual ranges. If they are mixed appropriately, an acceptable SOBP results throughout the target volume. The mixing is accomplished by the multiple scattering of the particles including in the ridge filter itself.

Another practical way of designing the ridge filter is developing an analytical form of the ridge shape. An example is a bi-exponential form.[310] Let $F(t)$ represent the fraction of the width of the ridge at which the thickness is t, and $F'(t)$ the fraction of the beam traversing the filter where the thickness is t, which is normalized by

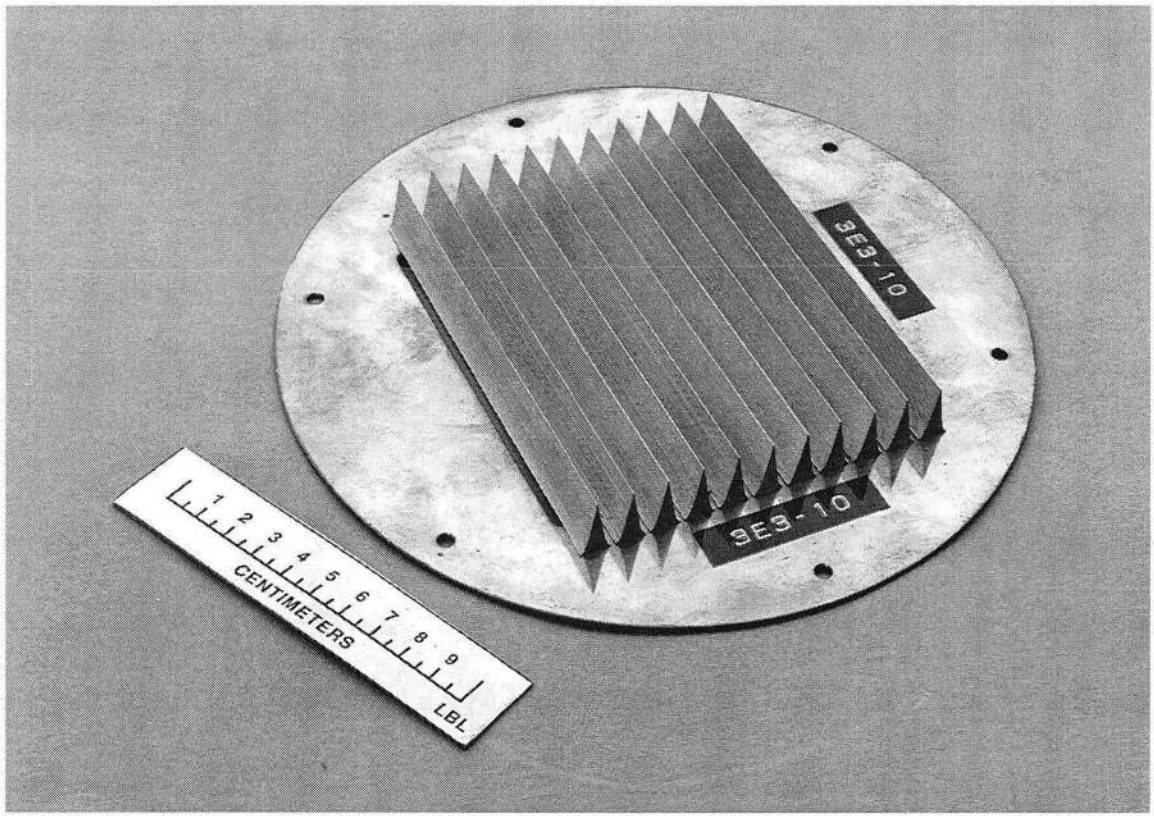

Fig. 31. A brass bar ridge filter for modulating the range of the Bragg curve is shown. This device is primarily used with the heavier ions where multiple scattering in the brass is less than for protons. Multiple scattering accounts for the lateral spreading of the different range particles over the target volume. (CBB 901-257)

$$\int_0^T F'(t)\,dt = 1 \tag{16}$$

where T is the maximum filter thickness. For $F'(t)$, a bi-exponential form is assumed, viz.,

$$F'(t) = A\left(Be^{-cT} + e^{-dT}\right) \tag{17}$$

The ridge shape is given by:

$$F(t) = -A\left(\frac{B}{c}e^{-cT} + \frac{1}{d}e^{-dT}\right) \tag{18}$$

For a neon-ion beam of an energy per nucleon of 585 MeV, the parameters used at LBL for the filter design were: B = 4, c = 0.4 (cm water equivalent)$^{-1}$, and d = 0.008 (cm water equivalent)$^{-1}$. A set of bar ridge filters of bi-exponential form for SOBP width of from 4 cm to 15 cm at a step size of

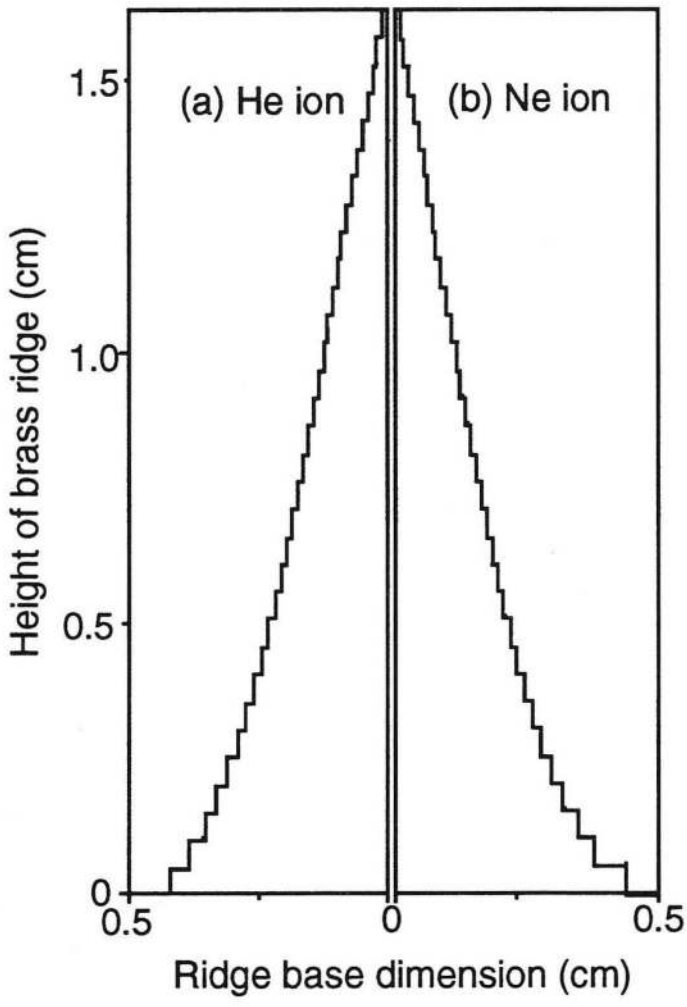

Fig. 32. The cross-sectional shapes of the ridge filters designed according to a bi-exponential form (a) for a helium-ion beam and (b) for a neon-ion beam.

1 cm has been fabricated for wobbled neon-ion beams at LBL, as illustrated in Fig. 32. The physical and biological characteristics of the wobbled beams modified by the bar ridge filters have been experimentally measured and the biologically uniform dose across the SOBP verified.[311]

Because the particles traversing the thickest part of the ridge arrive at the proximal part of the SOBP and those traversing the thinnest part (zero metal thickness) reach the distal part, the height of the ridges, in water-equivalent thickness, represents the width of the resulting SOBP. The half-base distance of the ridges, usually ≈5 mm wide, is made comparable to but smaller than the transverse scattered distance suffered by the heavy charged particles at the target volume. This ensures that the particles of different ranges mix thoroughly so that particles arriving in the treatment volume produce the proper SOBP everywhere without imaging the ridges. If the ridge bases were too large so that the mixing by scattering is not complete, the ridges may be linearly oscillated in orthogonal direction to the lines of the ridges and the beam axis to ensure the mixing.

When expressed in terms of water-equivalent thicknesses, the cross-sectional shape of the ridges is similar to that of the plastic propeller. For example, if plastics are used to make a ridge filter for a SOBP of a 14-cm width, the cross-section of the ridges will have a base of 1 cm and a height of 14 cm. Such ridges are too sharp to machine out of plastics, but by using a high density material the heights of the ridges are made manageable. For heavier ions, such as neon or silicon nuclei, the ridge filters are typically made from a metal. Because heavier ions suffer less multiple scattering than do protons and helium ions, high-Z materials can be used and, in fact, are preferred. For the same absorbing power, the higher-Z material fragments the beam less than the lower-Z material. Furthermore, the metal filters can be machined easily and are more compact. Metal bar ridge filters have been used with the proton beams at the Theodore Svedberg Laboratory in Uppsala (Tungsten-alloy),[28, 312] at ITEP,[313] and at PARMS (aluminum).[267]

II.B.3.b. Spiral ridge filters

Another method to move the ridges across the beam is rotating a spiral ridge. Many types of spiral ridge filters have been developed.[314] An example developed at LBL and used for the double-scattered beams is shown in Fig. 33. Many such filters for double-scattered beams of carbon, neon, silicon and argon ions have been used with water equivalent widths from 4 to 12 cm.[315]

The spiral ridges are cut on a brass plate using a specially shaped tool bit. One difficulty of machining this type of spiral ridges is encountered near the central axis, where the radius of the spiral becomes very small and the machining necessarily produces an imperfection, a dead spot. This problem was circumvented for the double scattering system by placing the central post of the occluding-ring assembly at the axis, which covers the imperfection. For biology experiment which do not require very large beam spots, the spiral ridge filter is simply positioned off-axis so that the beam spot does not go through the imperfect center.

II.C. Transverse (Lateral) Spreading of Particle Beams

The accelerated heavy charged-particle beams extracted from the accelerators are usually transported in well-focused fashion toward the treatment areas. The size of the beam spot is determined by the emittance of the beam, ε, which is a product of its size, x, and divergence, x', namely, $\varepsilon = x\,x'$. If the drift distance from the final focusing quadrupole magnets to the isocenter is L and the spot diameter, D, then $\varepsilon = (\pi\, D/2)\,(D/2L)$. The emittance of a modern synchrotron for medical use is typically $\varepsilon = 10\pi\ 10^{-6}$ m-radians. This results in a spot size of 40-mm diameter for a drift distance of 5 meters.

Many patient treatments require large uniform radiation fields, often as large as 30 cm x 30 cm, and occasionally even larger. This does not imply that such large areas are routinely irradiated in the clinic; the large-area capacity allows accommodation of target areas of various irregular shapes,

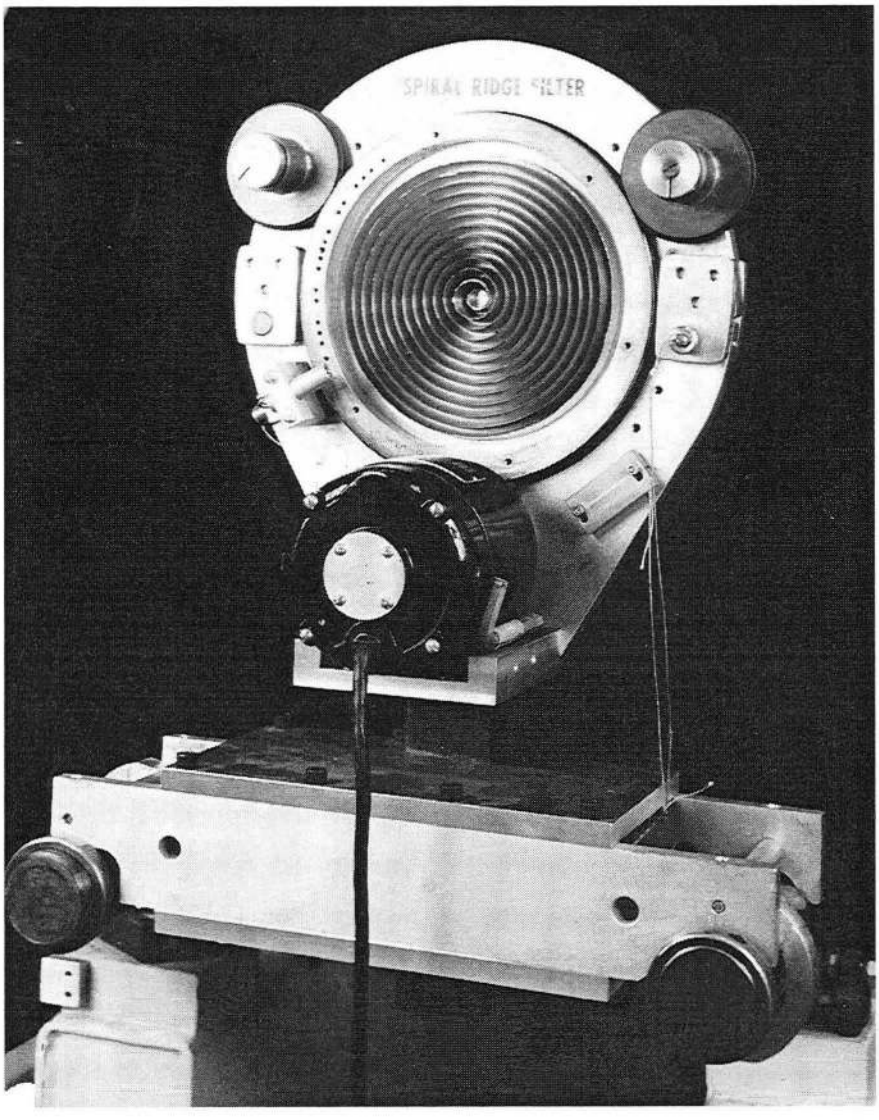

Fig. 33. A spiral ridge filter with its drive motor, as shown, is used in a similar fashion to the bar ridge filter and propeller as discussed in the text. (XBB 8412-9512)

sizes, and orientations. To obtain such large fields, the beam must be laterally spread out, in the direction perpendicular to its central ray, since the beam transported into the treatment area has a relatively small spot size. The aim is to produce a large field that covers the target area with a uniform dose with a variation of less than ±2.5%. The tolerable dose variation depends on the particular clinical application for which the beam is used. Other important considerations are: optimization of such beam characteristics as the sharpness of the lateral dose falloff, the sharp falloff of the distal-peak dose, the beam utilization efficiency, dose rate, neutron production, beam fragmentation in case of heavier ions, the ease of beam tuning, repeatability and stability of the delivered dose distributions, and patient safety.

Many different methods for lateral spreading of the beam have been investigated. In the following discussions, these methods are divided into *static* (or *passive*) and *dynamic* (or *active*) beam delivery systems. A passive system, such as the scattering system, spreads the beam into a uniform dose across the entire treatment volume at all times. On the other hand, a dynamic system, such as the raster-scanning beam delivery system, moves a beam spot in a predetermined way across the treatment area and delivers the dose to only a part of the treatment volume at a time. A desired dose distribution results with such a system only after completing an entire treatment.

II.C.1. Passive beam delivery systems

Several passive methods have been developed at various laboratories. Discussed below are scattering systems and multipole magnet systems.

II.C.1.a. Single-foil scattering method

The simplest beam delivery method uses a single scattering foil or plate. When a particle beam traverses a medium, each particle is deflected by many small-angle elastic scatterings mainly due to elastic Coulomb scattering from the nuclei within the medium, and its intensity profile is broadened to a 2-dimensional Gaussian-like distribution for small scattering angles, θ[316]:

$$\frac{d^2N}{N} = \frac{1}{2\pi\theta_0^{\,2}} e^{-\theta^2/2\theta_0^2} \sin\theta d\theta d\phi, \qquad (19)$$

where the standard deviation, θ_0, is defined as the half-width of the Gaussian distribution where the magnitude is $1/\sqrt{e} = 0.61$ of the maximum. An approximate value of θ_0 for thin scatterers is parameterized as[317, 318]

$$\theta_0 = \frac{14.1 \cdot Z_{inc}}{p\beta}\sqrt{\frac{L}{L_R}}\left\{1+\frac{1}{9}\log\left(\frac{L}{L_R}\right)\right\} \text{ radians}, \qquad (20)$$

where Z_{inc} is the charge number of the incident particle, p is its momentum in MeV/c, $\beta = v/c$, L is the thickness of the scatterer, and L_R is the radiation length characteristic of the scattering material in g/cm^2. The radiation lengths of particles in various materials are tabulated in standard reference publications.[319] For beams of heavier ions, as mentioned in Sec. I.C., a higher-Z material is preferred for the scatterer, since it introduces more scattering and produces fewer nuclear fragments compared to a low-Z absorber of the same absorbing power. It has recently been shown that Molière theory has an average error of no more that 1% and a *maximum* error no more that ±5% for protons,

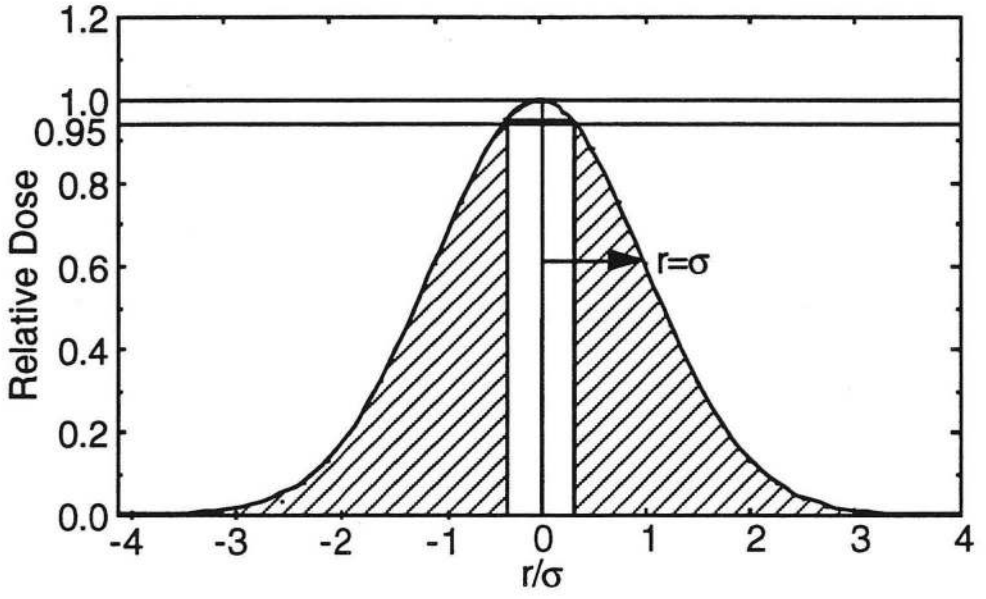

Fig. 34. A pencil beam passing through a thin scatterer results in a Gaussian-like dose distribution. A dose accuracy of ±2.5% is obtained if the beam outside of $r \geq 0.32\ \sigma$ is collimated out as shown in the hatched areas in the figure.

and also that, contrary to widely held views, Molière theory is valid for mixtures, compounds and thick targets (up to thickness of ≈97% of the mean proton range).[320]

A narrow pencil beam scattered by a thin scatterer produces an approximately 2-dimensional Gaussian dose distribution at isocenter.[321] Here a scatterer is called thin when the kinetic energy of the particle does not change significantly by traversing it. The dose distribution as a function of the radial distance, r, from the central axis is

$$D(r) = \frac{1}{\pi \tilde{r}^2} e^{-\left(r^2/\tilde{r}^2\right)}, \tag{21}$$

where $\tilde{r}$ is the rms radius of multiple scattering, and is related to θ_0 above as

$$\tilde{r} = T\left\langle \theta^2 \right\rangle^{1/2} = T\theta_0/\sqrt{2}, \tag{22}$$

where T is the drift-space distance from the scatterer to the isocenter. If the dose profile D is assumed to be strictly a Gaussian with a standard deviation σ, and the clinical requirements limit a dose variation to ±2.5%, only those particles near the central ray within the radius where the dose is ≈95% of the peak dose can be used. These particles provide a dose distribution of 97.5 ± 2.5% as

shown in Fig. 34. This implies that those particles outside the radius of 0.32σ are discarded, and the beam utilization is not quite 5%. Conversely, for example, if a radiation field with a 3-cm radius and the dose accuracy of ±2% is desired, the beam must be spread out to a Gaussian with $\sigma > 10.5$ cm.

An excessively thick scatterer is required to produce such a wide beam; hence only small radiation fields can be generated in this way. Small beams with radii <2 cm prepared in this way are used in clinical applications in treating small targets, such as tumors in the eye or some small-size intracranial disorders, *e.g.*, arteriovenous malformations (AVMs).[299]

II.C.1.b. Double-scattering beam delivery method

As described above, the single-foil scattering method can provide the dose distributions of acceptable variations only in relatively narrow fields. If one tries to widen the circle of utilization by using a larger portion of the scattered beam, an excess dose would result around the central ray. To obtain a broader uniform dose distribution at the isocenter, some of these excess particles near the central ray must be removed. One of the methods developed for this purpose is the double-scattering method. Such scattering systems were developed for proton beams at HCL,[322, 323] and at LBL to spread helium-ion beams at the 184-Inch Synchrocyclotron.[324] A similar beam spreading system has also been used for electron beams.[325]

The example shown in Fig. 35 uses an occluding post of sufficient thickness to stop the beam particles which is placed in such a way that it blocks the central portion of the Gaussian distribution. Past the occluder, the transmitted beam intensity distribution is shaped as an annulus with a null in the middle. Its profile in a plane through the central ray exhibits two peaks as shown in the figure. The second scatterer, of an appropriate thickness and placed strategically, diffuses the particles in these two peaks filling the dose void in the middle, and produces at the isocenter a larger flat-dose area. The dose distribution as a function of the radial distance from the central axis at the isocenter is[322]

$$D(r) = \sqrt{\frac{2}{\pi R_1^2 R_2^2}}\, e^{-r^2/R_2^2} \int e^{-(R_1^2+R_2^2)r^2/(R_1^2 R_2^2)}\, I_0\left(\frac{2r\rho^2}{R_2^3}\right) \rho\, d\rho, \qquad (23)$$

where R_1 and R_2 are the rms radius due to multiple scattering in the first and second scatterer, respectively, as shown in Fig. 35, $\rho = r/R_2$, and $I_0(t)$ is a Bessel function,

$$I_0(t) = \frac{1}{\pi}\int_0^{\pi} e^{t\cdot\cos\theta} d\theta. \qquad (24)$$

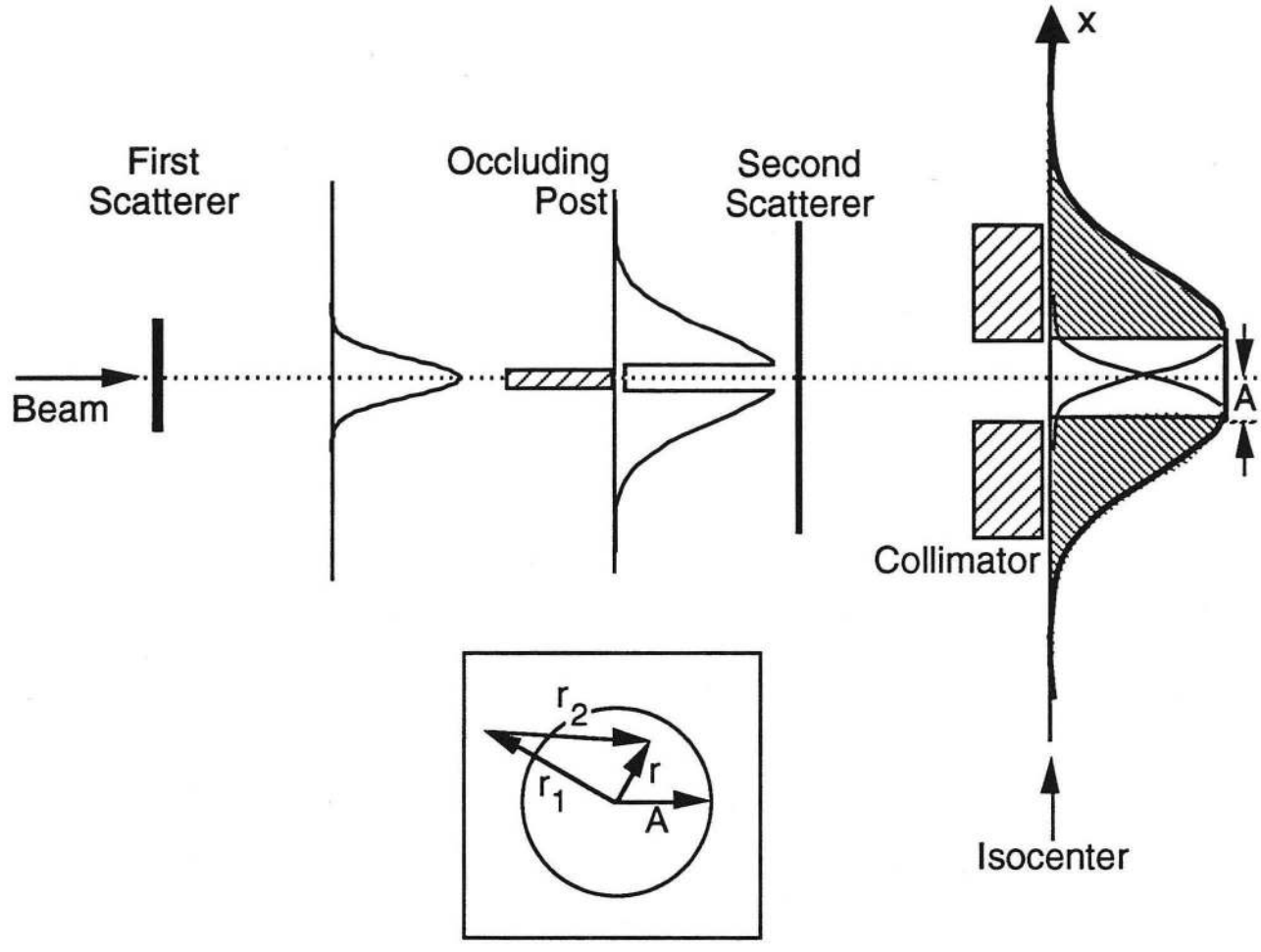

Fig. 35. Schematics of a double-scattering method using a central post occluder. The beam profiles downstream of the first scatterer, passed the occluding post, and at the isocenter are shown. The relationship between the size of the flat field at the isocenter (A), and the two scatterers is discussed in the text. In the lower figure, projected field at the isocenter is shown: the projected radius of the occluder is A, the beam enters at the center axis, the first scatterer scatters it by r_1 if there were no second scatterer, the second scatterer scatters it by r_2, and the net displacement is r.

For an occluding post, whose projected radius is A at the isocenter, the integration of Eq. (23) is for $\rho > A/R_2$. In one such system developed at HCL for the 180-MeV proton beam, the choice of two scatterers with $R_1 = 1.7A$ and $R_2 = 1.3A$ produced a flat proton field of a radius out to 1.5×A with a ±2.5% dose deviation.[322]

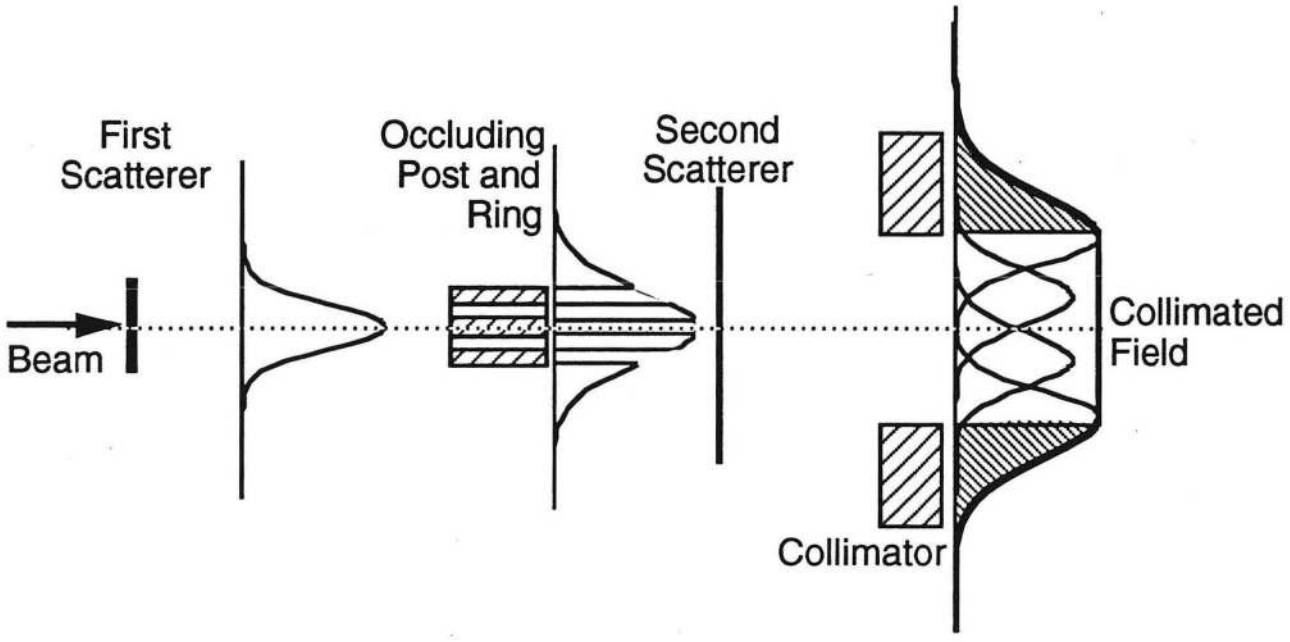

Fig. 36. Shown is the uniform field created using an annular ring plus a post occluder assembly.

For a broader beam, a simple annulus occluder can be used. The beam through the central opening and that outside the occluder will be transmitted. The dose profile in a plane through the central ray exhibits three peaks. When scattered by the second scatterer, the broadened three peaks fill the annular dose void and produce a large flat-dose area at the isocenter. For example, such a double-scattering system designed at HCL for 250 MeV proton beams, with a distance of 3 m from the first scatterer to the isocenter, produced ±2.5% flatness in a circular treatment area of ≈25 cm useful radius with ≈23 cm water-equivalent residual range.[323] PARMS at Tsukuba has also used a single annulus system to spread their 250-MeV vertical proton beam.[267]

A flat dose of even larger area can be obtained by using a set of annuli and/or post occluder system as shown in Fig. 36. Such a system was used at LBL to broaden a neon-ion beam of an energy per nucleon of 670 MeV to a flat field of a diameter of 20 cm. Successively larger-area dose fields could be obtained by increasing the number of annular rings of increasing radii. A practical limit is reached when the beam utilization efficiency drops too low to perform a treatment in a reasonable time, *i.e.*, several minutes.

In making large flat fields, a large portion of beam particles is stopped in the occluder as well as scattered into the collimators. Suppose the beam intensity profile at the isocenter in the absence of the occluder is $\Phi(r)$, where r is the radial distance from the central axis; $\Phi(r)$ is typically a Gaussian as shown in Fig. 37(a). Making a flat field of radius R, using the occluders is approximately

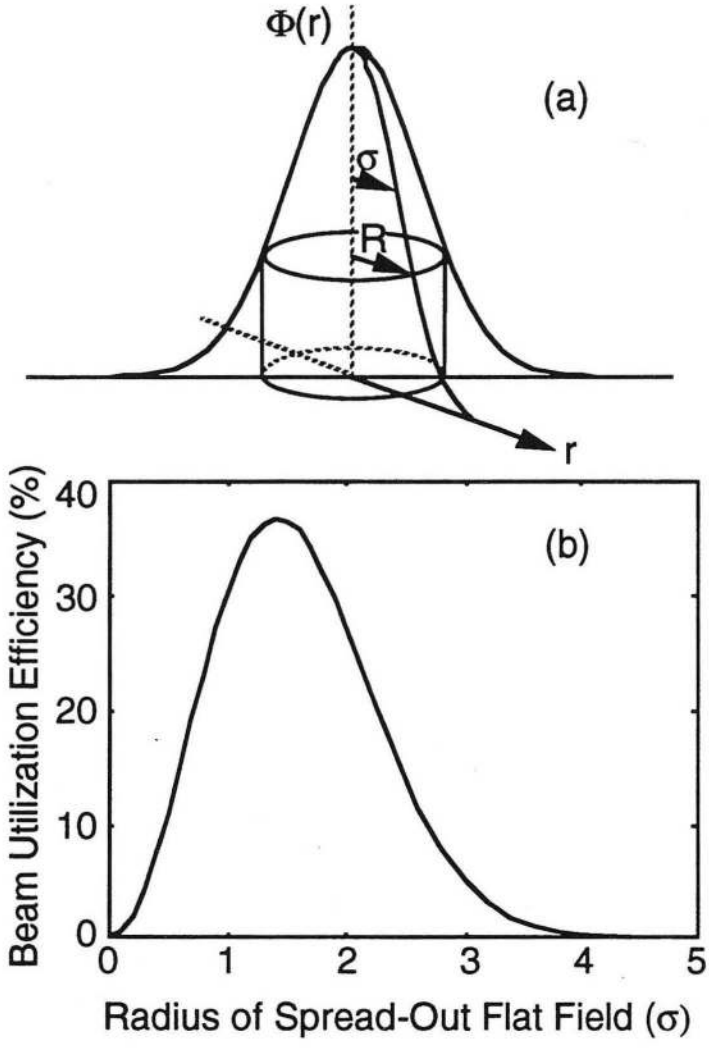

Fig. 37 (a) Two-dimensional Gaussian intensity distribution at the isocenter as a function of r, the radial distance from the central axis. The fractional radiation used in a flat dose field is proportional to the cylindrical volume, if the total radiation is assumed to be proportional to the total integrated volume of F(r). (b) Beam utilization efficiency as a function of the radius of the flat field in units of σ.

equivalent to modifying the intensity distribution $\Phi(r) = F(R)$ for $r \leq R$, and $\Phi(r) = 0$ for $r > R$ where the beam is discarded through collimation. The beam utilization efficiency is then simply the ratio of the cylindrical volume and the total integral volume of $\Phi(r)$ in the figure. If $\Phi(r)$ is a Gaussian with a standard deviation σ, the beam utilization efficiency E for obtaining a flat field of a radius R is approximately

$$E(R) = \frac{R^2}{2\sigma^2}\, e^{-R^2/2\sigma^2} \qquad (25)$$

The beam utilization efficiency E(R) is shown in Fig. 37(b). In making clinical beams, R is usually larger than σ and the beam utilization efficiency is at best 37%. For an individual patient treatment, the flat field is further collimated and the resulting efficiency is even lower. This result agrees substantially with the calculation of Koehler, Schneider, and Sisterson.[322]

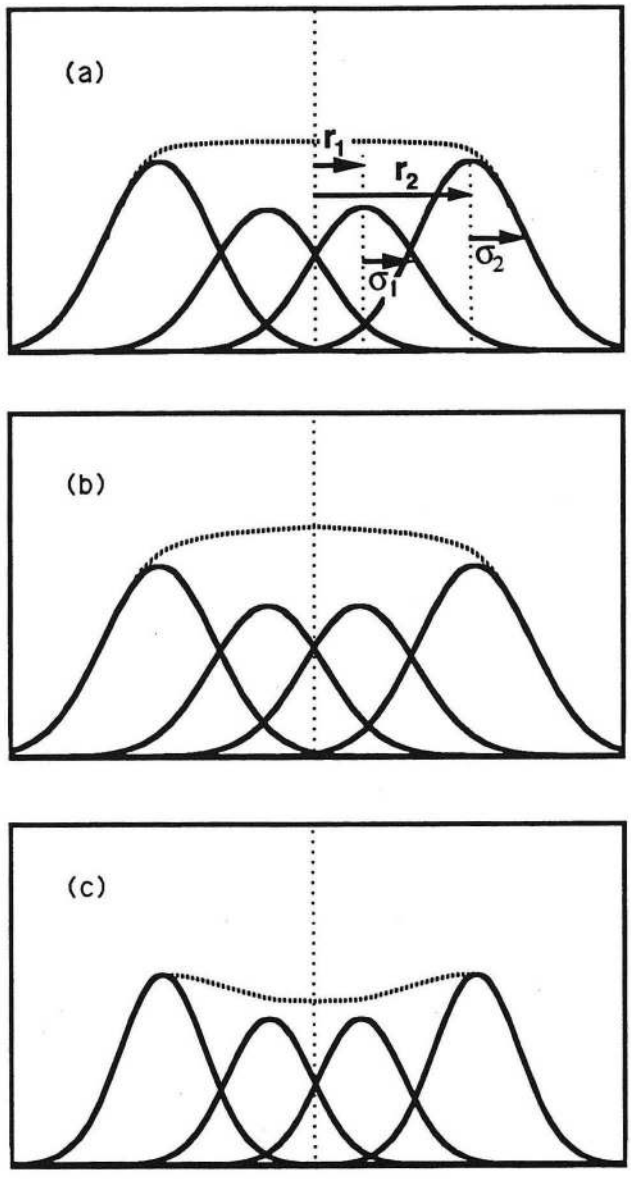

Fig. 38. The importance of matching the radii and half-widths of annular beams in obtaining a flat dose distribution is illustrated. (a) Two annular shaped beams, with radii, r_1 , r_2 , and half-widths, σ_1, σ_2, add up to a uniform dose distribution of a radius approximately equal to r_2. (b) If σ_1 and σ_2 are increased without changing radii, the resulting dose distribution exhibits a central bulge. (c) If σ_1 and σ_2 are decreased without changing radii, the resulting dose distribution exhibits a central depression.

Given the particle species, the beam energy, the beam spot size, and beam divergence, a suitable double-scattering system can be designed by specifying thicknesses and throws (drift distances to the isocenter) of the two scatterers, and the physical dimensions of the occluder assembly and its location. To ensure the proper workings of a double-scattering system, the beam profile broadened by the first scatterer must have a correct σ at the occluder, and its central ray must be very precisely aligned with the axis of the occluder assembly. The dose uniformity produced by this method critically depends on the cylindrical symmetry. The axis of the beam and that of the double-scattering system must be accurately aligned. In the LBL system described above, a misalignment of

the beam by 1 mm at the occluder assembly produced ±7% tilt in the dose distribution at the isocenter.

Shown in Fig. 38(a) is how the doses transmitted through the occluder assembly and broadened by the first scatterer as shown in Fig. 36 add up to a flat dose distribution at the isocenter. The transported radiation fields are two annuli, one with a radius r_1 and a half-width of σ_1, and the other with r_2 and σ_2. All quantities r_1, r_2, σ_1, σ_2, as well as the beam fractions of the two annular fields are adjusted so that they add up to a flat field inside the radius $\approx r_2$. Such a situation is violated if the incident beam energy is modulated by additional material in the beam path, or by mistuning the quadrupole magnets that focus the beam. What would happen if the widths of the transmitted annular doses were broadened, while their radii remained the same? The resulting dose distribution will not be uniform but will have too much dose near the central ray as shown in Fig. 38(b). To remedy the situation, either the radii of the occluding rings must be enlarged or the widths of the transmitted annular doses reduced. Conversely, making the values of the widths smaller without changing the radii would make the resulting dose distribution too high near the edge and too low near the central axis as depicted in Fig. 38(c).

The radii and widths must scale together to maintain the field flatness. This implies that, after developing an appropriate double-scattering system, the beam tuning must be done carefully to ensure not only the cylindrical symmetry but also the correct size of the beam spot at the occluder assembly. In the LBL system discussed above, by tuning the beam carefully, *i.e.*, centering the beam to the occluder axis with an accuracy of better than 1 mm, it was possible to achieve a dose uniformity of ±2% at the isocenter.

Scattering characteristics of a given scatterer depend on the incident particle species (charge, Z, and atomic mass, M) and the beam energy. Therefore a double-scattering system developed for a certain beam must be modified if any of these beam parameters are changed. Providing a different occluder system for each particle species and energy used is costly, and changing the systems each time the beam is changed is not practical in clinical operations. One way to resolve this problem is to vary the locations of the occluder assembly and the second scatterer. When the energy of the beam is modulated by an absorber, and consequently the values of the beam widths are made larger, the occluder assembly may be moved upstream nearer to the first scatterer so that the projected radii at the isocenter are proportionally increased. This process compensates the parameters in such a way that the resulting dose distribution again exhibits an acceptable deviation from the average.[323] Another method is to devise an absorber system which will provide varying absorbing power while maintaining constant scattering characteristics. Such a system has been constructed with two

different materials of very different atomic numbers, for example, plastic and lead (see Sec. II.C.1.c below).[326, 327]

Another practical point to note is that the double scattering method requires thick scattering foils, which produces secondary particles for beam particles with Z>1, which lowers the peak-to-plateau ratio and raises the dose beyond the Bragg peak. These fragments also lower the RBE and raise the OER values, thereby lowering the biological advantage.[328] As discussed above, the beam utilization efficiency is low, typically 20%. The low efficiency implies that a large portion of radiation is absorbed in the occluder, as well as in collimators and scatterers, resulting in increased background radiation in the treatment room. This becomes a serious problem when a double-scattering system must be placed near the patient, such as in the case of mounting it on a rotating gantry. Shielding needed to block unwanted radiation may become unacceptably heavy.

II.C.1.c. Bi-material scattering

The different scattering characteristics of heavy charged particles for different atomic-mass scatterers may be exploited in the preparation of therapy beams. A high atomic-mass material scatters more with little range loss; whereas, a comparable low atomic-mass material scatters little while modulating the range more. A pencil beam is laterally spread out to a Gaussian-like beam spot and is made to impinge upon the second scatterer. In order to flatten the field, the rays near the

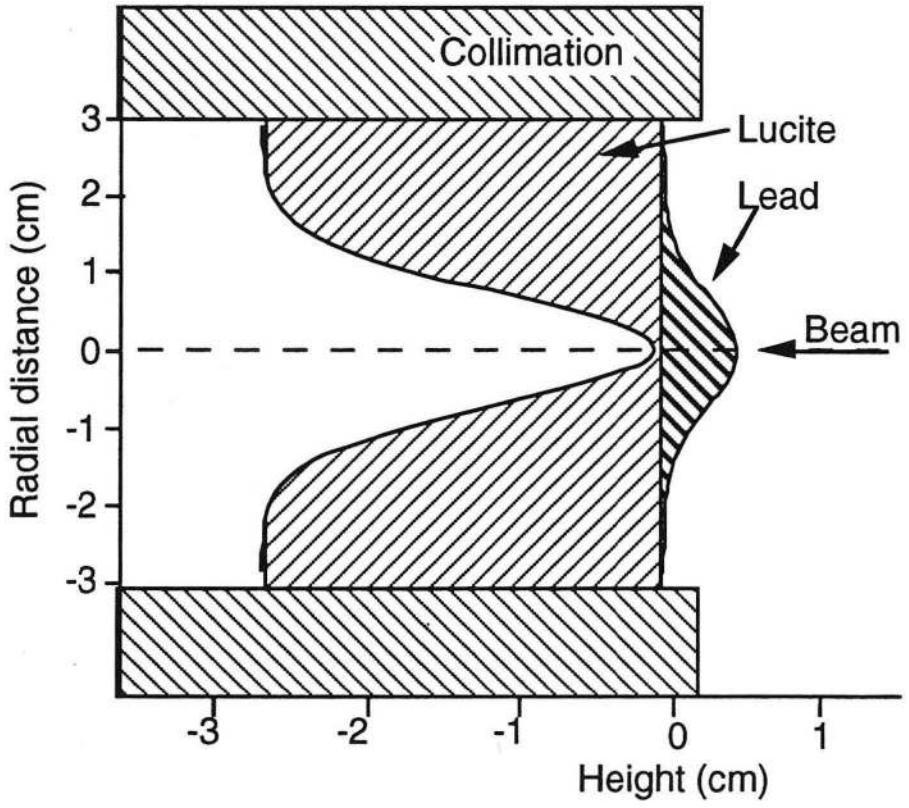

Fig. 39. Shown is a schematic representation of the cross-section of a bi-material filter for beam spreading. (Courtesy of Dr. B. Gottschalk, HCL.)

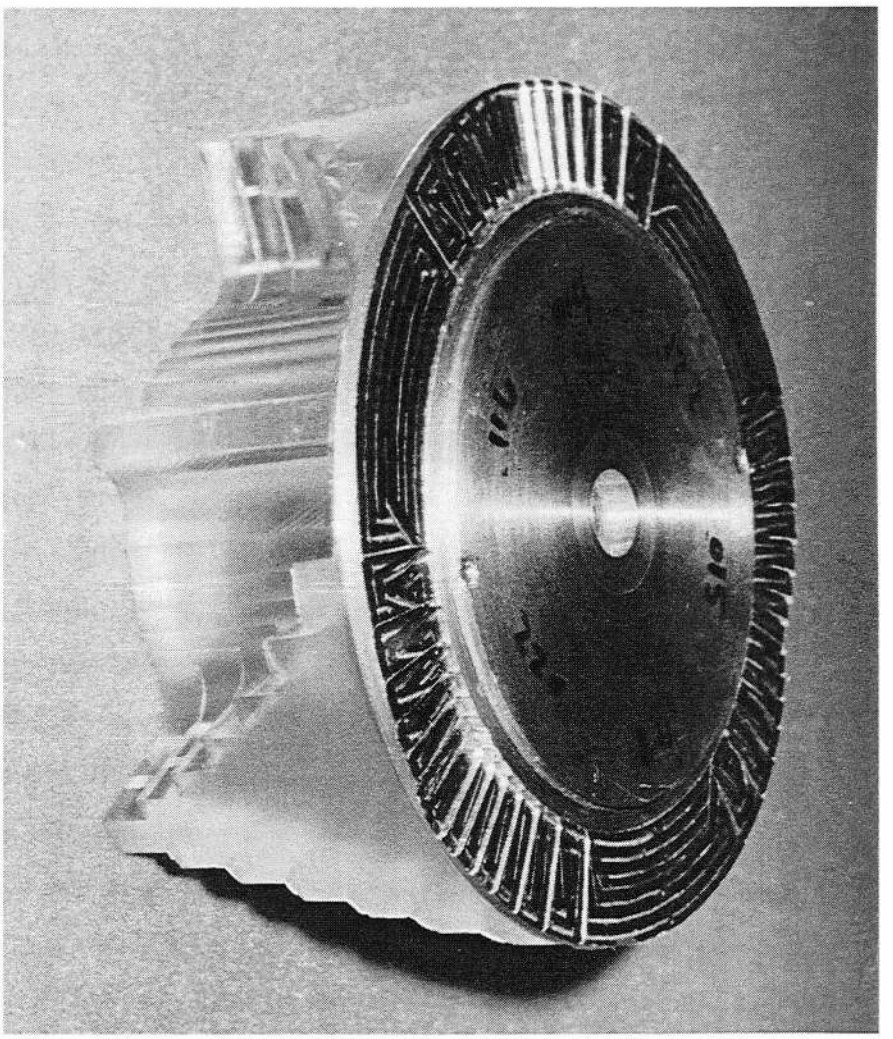

Fig. 40. Picture of a compensated modulator, which provides approximately constant scattering at all thicknesses of the filter. (Courtesy of Miles Wagner, HCL.) (CBB 925-3798)

central ray must be scattered out more than the rays further away from it. This differential scattering must be achieved while keeping the range modulation of the beam constant at all radial distances of the second scatterer. An elegant solution is a bi-material (*e.g.*, beryllium and lead, or copper and plastic) scatterers, as illustrated in Fig. 39, which havesuccessfully been produced and used at HCL,[270, 327] and adapated at LLUMC. The particles suffer the same energy loss throughout the scatterer, but their scattering characteristics are a function of radial distance from the axis of the scatterer.

Another application of a bi-material filter is to modulate the range of the particle beam while keeping its scattering characteristics constant at all residual ranges. A compensated modulator, as illustrated in Fig. 40, has been fabricated to achieve this goal for modulating the range of a 156-MeV proton beams at HCL.[329] Because this type of modulator can be placed further upstream from the patient than a simple propeller the lateral dose falloff can be significantly improved.

II.C.1.d. Multipole magnet beam delivery method

The intensity distribution of a typical beam extracted from an accelerator is in many cases adequately approximated by a Gaussian distribution. The Gaussian beam profile may be transformed into a larger uniform field by transporting the beam through multipole magnets. A system of controlled third-order aberrations produced by a pair of octupole magnets placed at certain locations along the beam line was shown to produce uniform dose distributions over a larger area by spreading the central excess and folding in the diffuse edges of the beam.[330-333] More recently, experimental measurements were obtained for spreading 200 MeV H^- beams using a pair of octupoles and three quadrupole magnets.[334] This method utilizes more than 97% (theoretically 99.7%) of the beam, and provides a ±7.5% field uniformity. The drawback is that the required drift space is quite large, ≈100 m, with small prospects for reduction.

II.C.1.e. Lithium lens

A novel method of using lithium lens with an axial magnetic field to spread the charged particle beams has been developed at Novosibirsk.[335] The beams spread out by this device is still too small to be useful in the clinic.

II.C.2. Dynamic Beam Delivery Systems

A dynamic beam delivery system produces a desired radiation field when a controlled extraction of the beam from an accelerator is coupled with strictly prescribed patterns of the motion of the beam spot. For example, two dipole magnets, placed in tandem so that their magnetic fields and the incident beam form three orthogonal directions, can move a beam spot in a predetermined way to produce a desired dose distribution. It is also possible to devise a magnet with compound coils, a rotating set of permanent magnets, or electrostatic deflectors to accomplish similar functions. Discussed below are many different schemes devised for clinical use. These dynamic systems have a distinct advantage over the scattering systems in minimizing the material in the beam path, maintaining the beam range, reducing fragmentation of the beam particles, and decreasing the background radiation for the patients.

II.C.2.a. Rotating dipole

The simplest form of the dynamic beam delivery systems uses one rotating dipole. A beam incident along the central axis of a dipole is deflected in a certain angle, and if the dipole is rotated around the central axis of the incident beam, the exiting beam will wobble around the initial direction and produce an annular-shaped dose distribution at the isocenter. The resulting dose field is similar to that produced by the double scattering method using a post occluder as shown in Fig. 35. A system

studied at HCL[322] uses a 160-MeV proton beam, focused down to a 4-mm spot at the entrance of the magnet, and a dipole magnet with a 0.16-T magnetic field, rotated at 100 rpm. The emerging beam is scattered by a 0.75-mm lead foil to produce a rms scattering angle of about 18 milliradians. It results in a uniform dose distribution within ±5% over a 15-cm diameter field. Actually, this method was considered by Koehler *et al.*[322] before the double-scattering method.

II.C.2.b. Lissajous pattern maker

If two dipole magnets are placed in tandem with their magnetic field directions orthogonal to one another and to the beam direction, and energized sinusoidally with two different frequencies, which are related to each other in a ratio of integers, a beam going through the system will draw a rectilinear Lissajous pattern at the isocenter. If the beam spill level is held constant, a limited regions at the middle part of the Lissajous pattern would exhibit a dose distribution of an acceptable uniformity since the rectilinear speed of the beam spot is approximately constant there. A system fabricated at Uppsala for 185-MeV proton beams produced a 2 cm × 2 cm field.[27, 28, 336] In this system, the beam-spot structures were smeared out by a thin scatterer. Two-dimensional beam spreading using a toroidal magnet was also considered.[100]

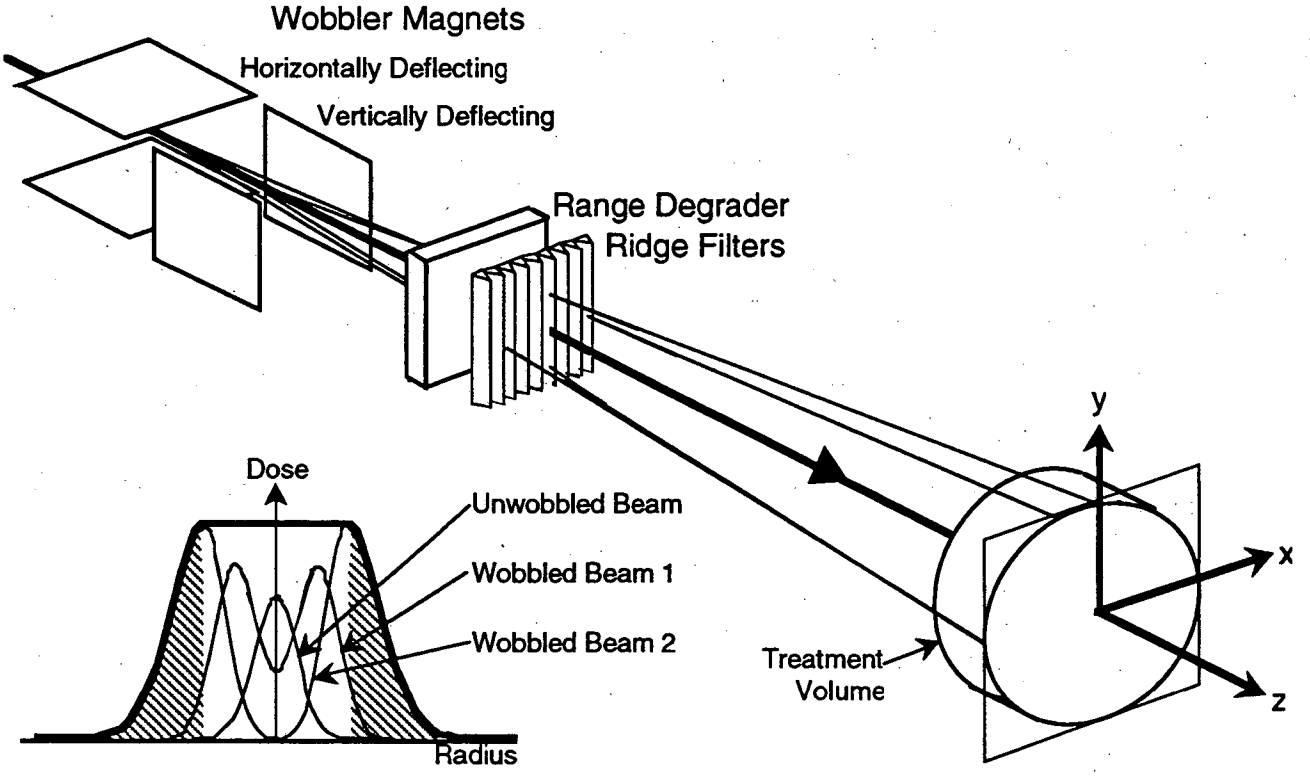

Fig. 41. A wobbler beam delivery system is depicted schematically.

II.C.2.c. Wobbler systems using two electromagnetic dipoles

A wobbler system consists of two dipole magnets placed in tandem with their magnetic field directions orthogonal to one another and to the beam direction. The magnets are energized sinusoidally with the same frequency but with a 90 degree phase shift between them. If the amplitudes of the

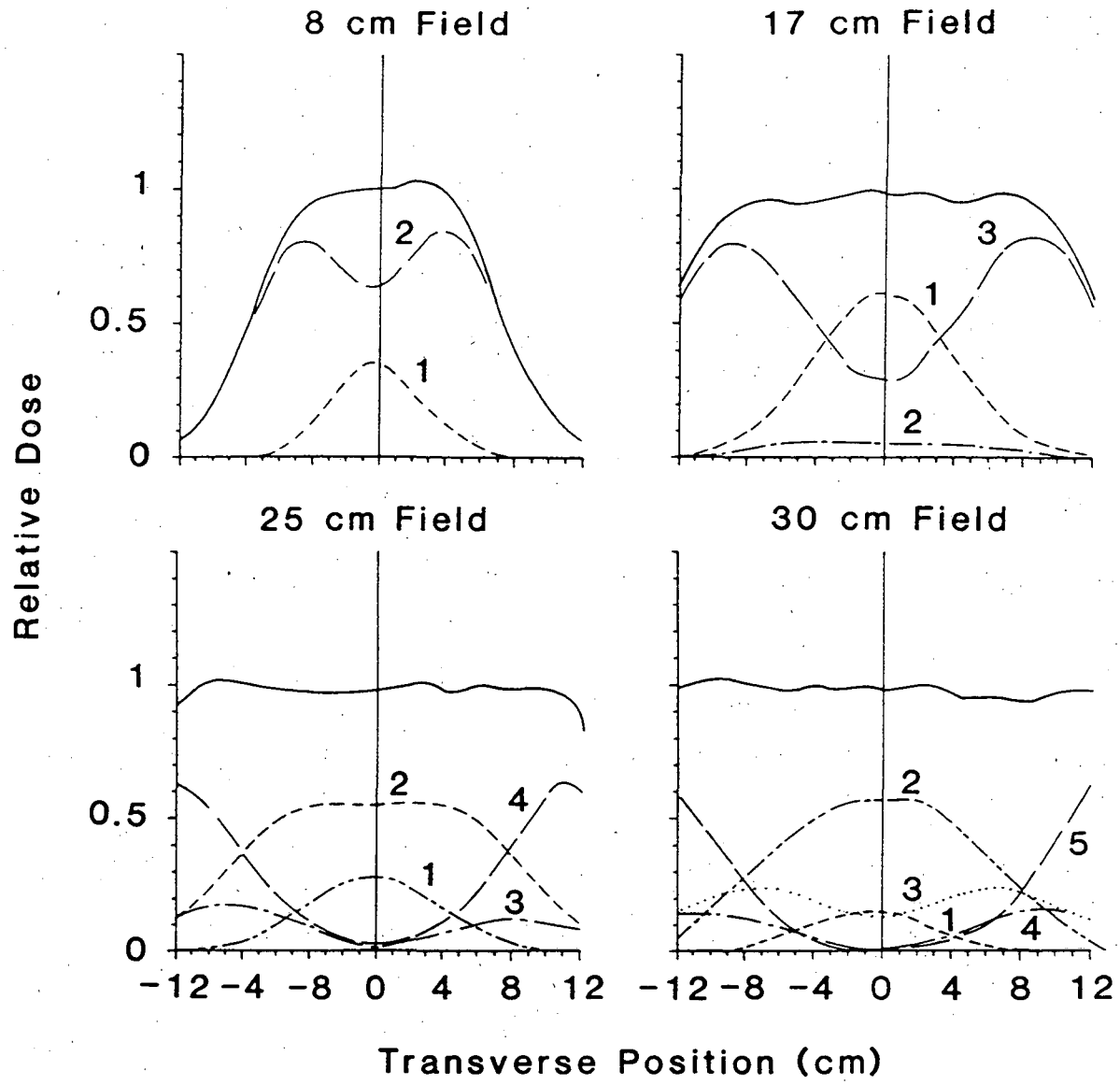

Fig. 42. A large-area flat dose is produced by appropriately summing several Gaussian-like profiles of different wobble radii with appropriate flux fractions. The doses at various wobble radii and their sum are shown for four different sizes of the flat fields. (XBL 868-2852)

magnetic fields are properly controlled, a beam entering the system along its axis emerges from it with the beam direction wobbling around the original beam direction, and "paints" an annular-shaped dose distribution as shown in Fig. 41. The diameter of the dose annulus is changed by adjusting the amplitudes of the currents in the wobbler magnets. A large area of uniform dose is obtained by painting the treatment area in several concentric annuli with different diameters, each with a certain predetermined particle-number fraction, as schematically depicted in Fig. 42. The wobbler magnet power supplies, which provide sinusoidal currents, are easy to construct and reliable.[337] The pertinent parameters to obtain flat fields are constant spill intensity, precise wobble radii and correct particle-number fractions at various radii.

A wobbler system was developed at the NIRS in Chiba for their 70 MeV proton beams,[338] and a similar system has been used at the Riken Ring Cyclotron facility in Tokyo for carbon-ion beams of an energy per nucleon of 135 MeV.[183] A bigger wobbler system was developed at the Bevatron at LBL to spread the neon-ion beams of an energy per nucleon up to 580 MeV for clinical use.[337, 339-342] Wobbler systems are selected as the beam-delivery system of choice at HIMAC, under construction at the NIRS.[179] Two sizes are contemplated: a larger version for spreading the horizontal heavy-ion beams of an energy per nucleon of 800 MeV, and the other for the vertical beams at an energy per nucleon of 600 MeV.

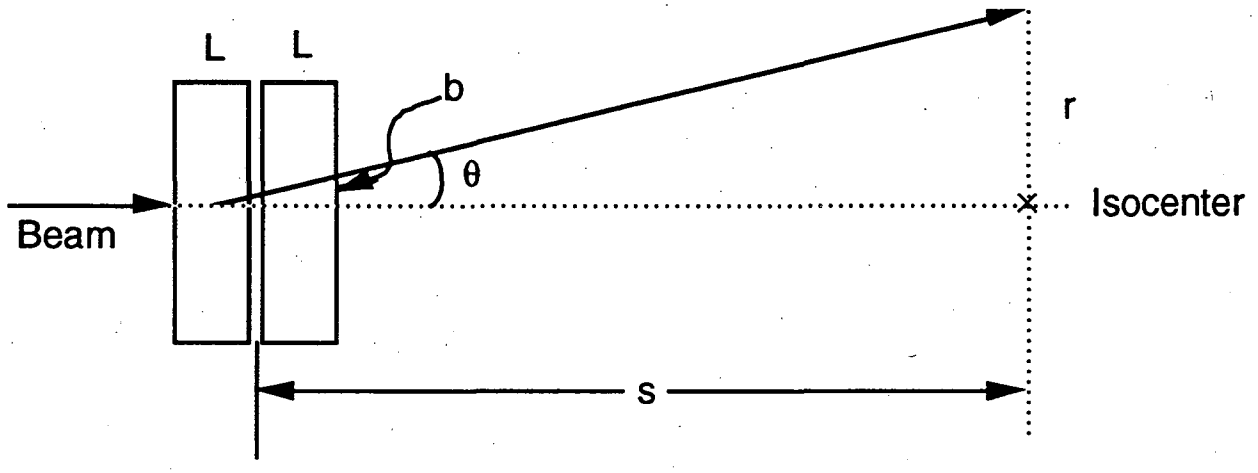

Fig. 43. The figure shows the relationship between the lengths of wobbler magnets (L), magnet-to-isocenter distance taken from the midpoint of two wobbler magnets (s), deflection angle (θ), the radius of the flat radiation field at the isocenter (r), and distance of the beam exiting the wobbler system (b).

As an example, the wobbler parameters are calculated below for a 250 MeV proton beam, whose particle rigidity, $B\rho = 2.43$ Tesla-meter, where ρ is the radius of curvature of the proton beam. The maximum magnetic field is decided by the value of ρ. Referring Fig. 43, one can show that

$$BL = B\rho\theta, \tag{26}$$

and

$$\theta = \tan\theta = \frac{r}{s + L/2} = \frac{2b}{3L}, \tag{27}$$

where b is the deflection distance of the beam when it leaves the downstream magnet, s is a wobbler-to-isocenter distance, L is the length of each wobbler magnet, and r is the radius of a desired flat radiation field at isocenter. For example, if s = 3 m, L=0.5 m, and r = 0.2 m, Eqs. (26) and (27) give b=0.046 and $\rho = 9.38$ m. For the exiting beam spots to clear the pole tips, the magnet pole face must be separated from the central plane by a distance of a sum of b and the radius of the beam spot, which is about 6 cm. The amplitude of the magnetic field in the wobbler magnets is 0.26 Tesla. One can lower the value of B by increasing the magnet lengths, which also increases the aperture, and results in an increase in stored energy in the magnets. Or B can be lowered by increasing the magnet to isocenter distance, which is usually limited by practical reasons.

If the beam extraction level and the circular speed of the wobbled beam spot were kept constant, an annular dose distribution produced by the wobbler would have no dependence on the azimuthal angle, provided that the beam on and off points are exactly overlapped to obtain the same number of wobbles at all azimuthal angles for a given beam pulse. If the overlap is uneven, for an average of n wobbles per beam pulse, there will be a region painted over either n+1 or n–1 times, which would end up with a fractional dose deviation of $\pm 1/2n$ from an average. The effect of this dose deviation may be reduced to an acceptable level in two ways. First, increasing the number of wobbles per beam spill, n, decreases the dose deviation per spill. Next, by making the phases of the wobbling and the beam extraction proceed asynchronously, and by painting a given annulus over many beam pulses, the effect may be statistically diluted on the overall dose distribution since the regions of the uneven overlap will happen randomly in azimuthal angles. If the number of beam pulses used for a given wobble radius is M, then the overall fractional dose nonuniformity expected is $\sim 1/2n\sqrt{M}$. If one assumes the treatment time of 2 minutes and wobbling at 5 different radii, wobbling at each radius lasts on the average about 20 seconds. Suppose that the accelerator beam extraction operates at 1 Hz, then M=20 on the average. If the dose deviation due to this cause is to be limited to less than 1%, $1/2n\sqrt{M} < 0.01$, or $n > 100/2\sqrt{20} = 11.2$ Hz. If the spill length is 0.5 second, i.e., the duty factor is 2, then the required wobbler frequency is twice of the above n, or 22.4 Hz. For

example, the LBL wobbler discussed above operates with ~60 Hz at the Bevatron, which provides 1-second long spills every 4 seconds. If the wobbling for a given radius lasts for 5 pulses, the fractional dose deviation is $1/2n\sqrt{M} = 1/120\sqrt{5} = 0.38\%$.

A large area of flat dose is produced by summing several wobbles of different radii. If, for example, five radii are used, the largest wobble covers about 100 times the area of the smallest wobble. To complete all the different wobbles on comparable numbers of beam spills, a control of the spilled beam intensity over a dynamic range of ~100 is necessary, which may increase treatment time.

There are tradeoffs for the wobbler beam delivery system compared to the double-scattering system. First, no scatterers are needed in the beam path and the same available beam range can be achieved at a lower accelerator energy than that required for scattered beams. No beam is lost in scatterers and occluders. As the size of the flat field is readily varied according to the port size, less beam is lost in collimation, and therefore, the beam utilization is higher than that for a scattered system. Beam alignment is not as critical as in the case of the scattering system; however, the high stability of the beam entering the wobbler magnets throughout a treatment time is critical to provide concentric annular dose distributions. Since the effective source size, *i.e.*, the beam spot size is small, the wobbler produces sharper lateral dose falloffs than those attainable with the scattering system. The neutron production in absorbers and collimators is curtailed, and, therefore, the shielding requirement is lower than that for the double-scattering method. This becomes an important consideration when one tries to place a beam delivery system on a rotating gantry. As a dynamic mode of beam delivery, the wobbler system requires active monitoring of the wobbler magnetic fields. Furthermore, the time structures in the extracted beams, which are translated into a spatial variation in the dose distribution, must be reduced to a tolerable level.[343]

II.C.2.d. Wobbler systems using two rotating permanent dipoles

A wobbler system using two rotating permanent magnet dipoles has been proposed[344] as schematically shown in Fig. 44. In this proposed system, the rotating dipole magnets produce the circular sweep while the radius of a wobble is controlled by a change in the phase angle $\theta_1 - \theta_2$. A null deflection is obtained at 180-degree out of phase of the two magnets. The magnets are mounted on bearings, and rotated by electromagnetic drives using 3-phase coils (stators) acting on an external dipole field. The magnets require uniform dipole fields in a large bore area: a 16-segment permanent magnet dipole has been designed using rare-earth permanent magnets as shown in the figure. Compared with the electromagnet systems, a permanent magnet system would be relatively light and compact, and have a low electrical power requirement. The mechanical control and monitoring of the rotating magnets, as well as preventing mechanical failures for ensuring patient safety may require bigger effort than those required with the electromagnet system.

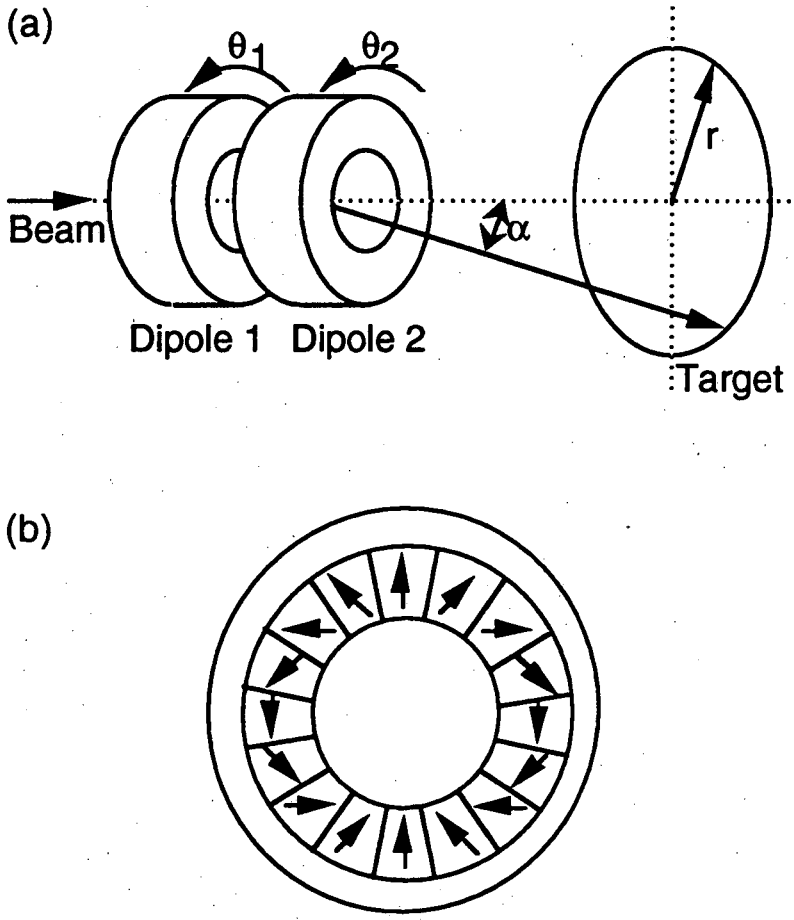

Fig. 44. Schematics of (a) a wobbler system using two rotating dipoles and (b) a 16-segment permanent magnet dipole designed for the purpose.

II.C.2.e. Specifications for scanning

A large field of a specified dose distribution may be produced by scanning a beam across a treatment area. In principle, scan speed and beam intensity can be varied as a function of the spot location in the treatment volume to generate the desired dose distribution. A schematic diagram of scanning is shown in Fig. 45. In general, a scanner consists of one or two dipole magnets, one for the fast scan in the x-direction and the other for the slow scan in the y-direction. (Here the x and y represent arbitrary orthogonal directions.) Range modulation moves the stopping region of the beam spot, the Bragg peak of the beam, in the z-direction.

Spatial characteristics of scanning have been analyzed by Leemann et al. in terms of its scanning speed and power requirement.[345, 346] In a homogeneous medium, if a scanning pattern is described by a distribution function of relative spot weights S(x, y, z), and the contribution to the dose at (x, y,

z) from a beam spot with its centroid at (x', y', z') by a function g(x–x', y–y', z–z'), the dose D(x, y, z) is then expressed as a Fredholm integral equation of the first kind:

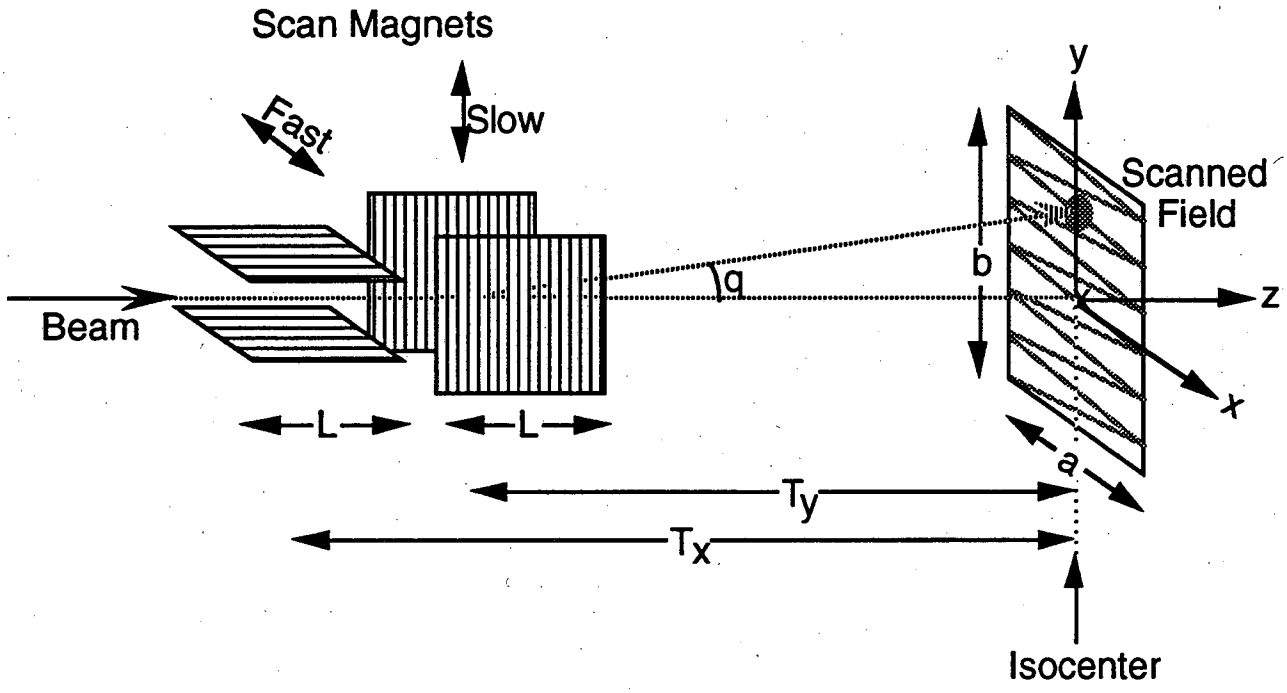

Fig. 45. A geometry of beam scanning for evaluating the requirements in scan speeds, stored energy in the magnets, and magnet peak power. The length of each raster-scanning magnet is L, the magnets are placed at distances T_x and T_y from the isocenter, and the scanned field is a rectangle with sides a and b.

$$D(x,y,z) = \int_{-\infty}^{+\infty}\int_{-\infty}^{+\infty}\int_{-\infty}^{+\infty} S(x',y',z')\,g(x-x',y-y',z-z')\,dx'\,dy'\,dz'. \qquad (28)$$

If the desired dose distribution D is specified and the function g is known, the exact solution for the scanning pattern S(x', y' z') is obtained by deconvolution of Eq. (28).[347] If one assumes a homogeneous medium, with negligible secondary components resulting from nuclear interactions, and the three coordinates of the g function are independent thus g may be written as following

$$g(x-x',y-y',z-z') = g_x(x-x')\,g_y(y-y')\,g_z(z-z'), \qquad (29)$$

a simple solution of Eq. (28) is obtained in terms of Fourier transforms:

$$\mathcal{D}(l,m,n) = S(l,m,n)\,g_x(l)\,g_y(m)\,g_z(n), \qquad (30)$$

where $\mathcal{D}$, $\mathcal{S}$, and $\mathcal{g}_i$ are the Fourier transforms of D, S, and g_i, respectively. The (spatial) frequency range of $\mathcal{D}$, and therefore attainable resolution, is obviously limited by the finite beam spot size and the Bragg peak width of the beam spot. The sharpness of field edges, or the smallest size of inhomogeneities which can be compensated for, is determined by this resolution. Conversely, a discrete scanning pattern, resulting in a function S(x, y, z) which is a collection of δ-function-like spots, yields smooth dose distributions if the step size is kept under one half of the spot size. This is the case for the spot scanning method adopted by PSI as described in Sec. II.C.2.g below. The LBL raster scanner described below scans continuously in the x direction in order to obtain a dose uniformity along the raster lines in the x-direction, and the y-scan is specified in such a way that the adjacent scan lines overlap at least one-half of the spot size. Lower limits for beam spot sizes are given by multiple scattering (see Sec. I.C.) and are of the order of 2 ~ 3 mm for carbon or neon ions and 5 ~ 7 mm for protons for ranges in tissue between 20 cm to 30 cm. The spot sizes used in actual beam scanning are generally bigger.

Given a desired dose distribution D(x, y, z), obtaining a *practical* solution of a scanning pattern function S(x, y, z) in Eq. (28) necessitates the use of techniques, mathematical inversion methods, developed for *inverse treatment planning*,[348-353] which are generally developed for photon treatments. Important attributes in the inverse treatment planning are to find a fast and deterministic procedure which determines the optimal density function (relative spot weights) for narrow pencil beams, with the known Bragg-peak depth-dose profile and a Gaussian transverse dose cross-section, which generate a three-dimensional dose distribution as close as practically possible to a specified D(x, y, z). The requirement of practicability implies an optimization, which is done under some general conditions, such as that the beams come from specified directions and that no underdosing in the target volume is permitted. The general requirements for the solution are: (i) optimization of the dose uniformity inside the target volume and the sharp dose falloffs at the boundaries of the target for normal tissue sparing, (ii) optimization of the number of ports, their directions and shapes, shapes of the port at each range, and (iii) the solution amenable to precise control of the beam delivery system and consideration of its compliance and limitation. The beam delivery based on the inverse therapy planning using the raster scanner and light-ion beams will be attempted in the near future.[354, 355]

The scan sweep velocity requirements are analyzed as follows. A treatment volume V is subdivided into cubical voxels with their sides L_c corresponding to the characteristic dimensions. If the beam-spot dimensions are L_x, L_y, and L_z, the treatment time τ, and the accelerator duty cycle η, then the scanning speed in x-direction, v_x, and the corresponding time to scan across the spot, Δt_x, are:

$$v_x = \frac{V}{\eta \tau L_c^2} \tag{31}$$

and

$$\Delta t_x = \frac{L_x}{v_x} = \frac{\eta \tau L_x L_c^2}{V} \tag{32}$$

In a fixed horizontal beam line as shown in Fig. 45, both magnets may be placed in the last drift space, which can be fairly long. However, in a vertical beam line or on a rotating gantry, the final drift space would be severely limited and may not provide enough space to mount both magnets. In such a case, placing one of the scan magnets upstream of the final bending magnet may be considered; in other words, the drift space from the center of the fast-scan magnet to the isocenter, T_x, may be much longer than that for the slow-scan magnet, T_y, in the figure. Referring to the figure, the flat-dose field at the isocenter is a rectangle of a×b, and if bipolar operation of the magnet is assumed, *i.e.*, $-\theta_{max} \le \theta(t) \le +\theta_{max}$, the corresponding field in the magnet is given by:

$$\int B_{max}\, dL = B_{max}\, L = \theta_{max}\, B\rho \tag{33}$$

where

$$\theta_{max} = \frac{b}{2T_y} \tag{34}$$

and

$$B_{max} = \frac{b\, B\rho}{2L\, T_y} \tag{35}$$

The stored energy, U, in the scan magnet is given by:

$$U = f \frac{10^7}{2\pi} \frac{\varepsilon^2 (B\rho)^2}{L} \left(\frac{a}{2s}\right)^2 \frac{T_y^2}{T_x^2}\,, \tag{36}$$

where ε is the beam emittance, and s the spot size.[345, 346] The factor f accounts for that the actual magnet field volume is somewhat larger than the beam aperture. For $f \approx 1.5$, $\varepsilon = 10^{-5}$ m-rad, s = 3 mm, b = 30 cm, L= 1 m, and Bρ = 6.5 T-m (carbon-ion beam of 30-cm range in water), the stored energy becomes:

$$U \approx 25 \frac{T_y}{T_x} \text{ Joules} \tag{37}$$

and with a rise time of 1.5 msec from B = 0 to B_{max}, the required peak power is:

$$P \approx 35 \frac{T_y}{T_x} \text{ kW} \tag{38}$$

If the magnets are placed together in the last drift space, i.e., $T_y / T_x \approx 1$, the stored energy $U \approx 25$ J and the peak power $P \approx 35$ kW.

In the following two Sections, two scanning methods for producing large fields of uniform dose distribution are discussed. Scanning beam delivery systems are classified according to the ways in which the beam spot is moved: namely, raster scanning, spot scanning, and pixel scanning, which are discussed in Sec. II.C.2.f, g, and h, respectively. Raster scanning employs a smooth motion of the beam spot while keeping a constant beam extraction. The last two scanning methods involve a more discrete spot motion; the spot is moved to the next position when the prescribed dose is deposited at a given position. In spot scanning, the spots overlap at least a half-width of the spot; whereas, in the pixel scanning, each pixel is individually irradiated and the adjacent spots overlaps only at their edges. This choice of terminology is not always followed in the literature. Making large fields of arbitrary dose distributions is discussed in Sec. II.C.2.h and II.C.3

II.C.2.f. Raster scanning

A raster-scanning beam delivery system has been developed at LBL to broaden light-ion beams into large flat radiation fields.[356, 357] It is designed to scan an entire port area during one Bevatron spill which is approximately 1 second long and repeated every 4 seconds. The magnets are designed to deflect a beam with a magnetic rigidity of 8.0 T-m up to ±20 cm in the horizontal and vertical directions at the isocenter, which is ~6 m from the raster magnets. The fast-scan magnet is placed upstream of the slow-scan magnet. The apertures of the magnets are designed to permit the transport of the beam without interference during the largest deflections of the beam. In the first magnet the beam is deflected parallel to its pole faces, and the gap of the fast-scan magnet has to be barely wide enough to pass through the beam spot. The beams deflected by the first magnet continue to diverge through the second magnet, and therefore the gap of the second magnet has to be wide. The gaps of the fast and the slow magnets are 5.7 cm and 15.2 cm, respectively. Laminated iron cores of the magnets minimize the induced eddy currents during their operation.[358]

The slow scan sweeps the vertical extent of the field, up to 40 cm at the isocenter, in slightly shorter than the Bevatron spill time. The fast scan is fast enough to paint the raster lines close enough with a 2-cm FWHM beam spot, whose profile is approximately Gaussian, to ensure a dose distribution without peaks and valleys between the adjacent scan lines. An analysis showed that the accuracy of this edge matching depends on an accurate control of the magnetic fields and the gradual slope of the edges of the beam spots.[359] Beam spots with sharp edges are hard to align to produce a uniform dose distribution; at least ~4 mm edge fall-off width is required, and typically $\pm 5 \times 10^{-4}$ accuracy in the control of the magnetic field is needed.

The fast x-scan speed is set at a constant 2400 cm/sec in the scan plane at the isocenter, which is equivalent to a frequency of 30 Hz over a ±20 cm field. The fast-scan speed is maintained constant for all sizes of fields; therefore, the scan frequency is higher for smaller fields. To allow the beam

to dwell at a certain vertical position before the y-scan starts, the slow-scan power supply runs with a d.c. current offset. In order to achieve a dose uniformity of ±2.5% and minimize the introduction of non-uniformity by the magnet power supplies, the regulation of the magnet currents (which determine the rates of change in the magnetic field) is controlled to approximately ±0.25%.[360] The required dose uniformity sets the specifications of the circuit control parameters: a closed loop d.c. feedback gain for both systems of at least 60 db and a unity gain bandwidth of 10 kHz for the fast-scan system and 1 kHz for the slow-scan system.[361]

For an alternative method of constructing a power supply of the raster scanner, a recent evolution in high power servo controller technology may present an attractive cost and size alternative to commercially-available linear actuator systems.[362] These controllers are essentially high frequency (82 kHz) pulse-width-modulation amplifiers which operate at efficiencies of 95% and have controlled bandwidths of 15-20 kHz. This design has been adapted to drive inductive loads in both polarities. The fast scanning magnet designed for spot scanning at PSI, discussed in the next section, uses this type of controller. The raster scanner magnets fabricated at LLUMC will also employ these controllers.

An integrated system for delivering clinical beams using the LBL raster scanner is schematically shown in Fig. 46. The incident beam before the raster scan magnets is measured by an ionization chamber and a secondary emission monitor. The radiation dose over the entire radiation field is

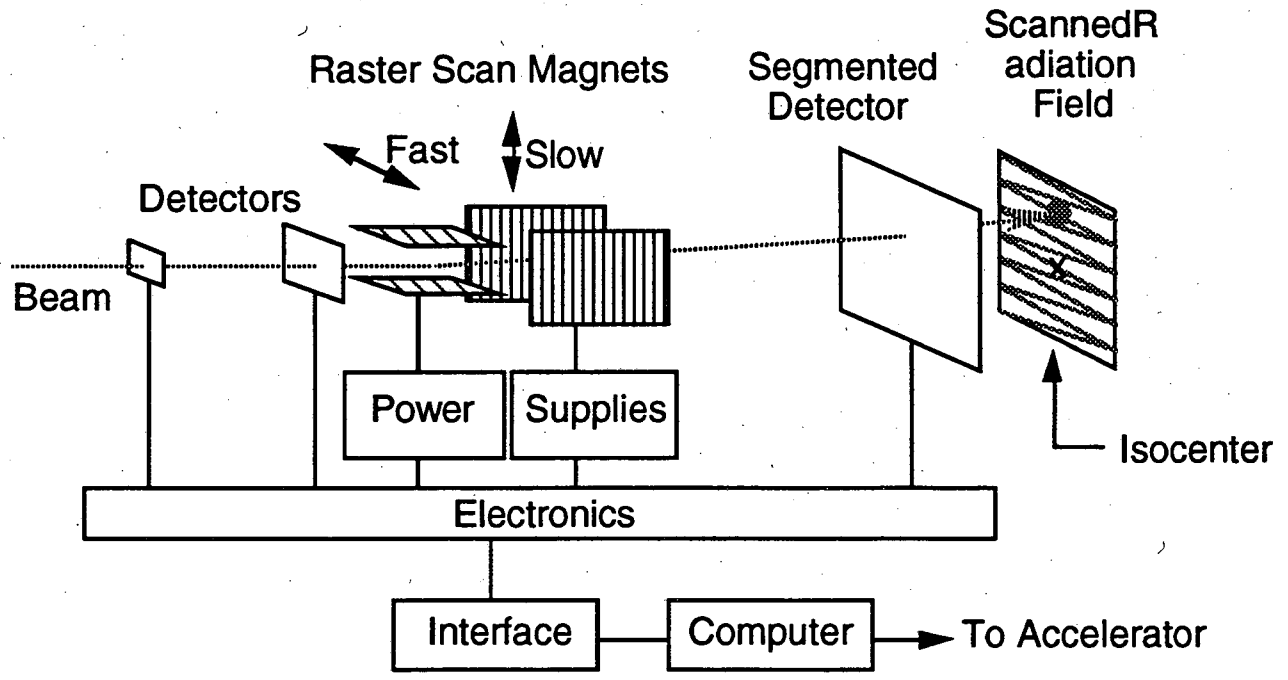

Fig. 46. A general schematic of the LBL raster scanning beam delivery system is shown. The individual components are magnets, power supplies, detectors, electronics, computer interface, and a computer system.

measured near the isocenter by a multi-segmented ionization chamber (See III.B.3).[363] Using CAMAC hardware, a VAX 780 computer controls the scanned beam, and records and displays the measured results. The control system establishes the size of the field to be irradiated, its displacement from the central ray, the scan initiation point, the scan speeds, and the beam level to be extracted on a pulse-by-pulse basis. Rectangular radiation fields of any desired aspect ratio with scan dimensions ranging from 5 cm to 40 cm can be produced.[364] Very uniform dose distributions, measured with films showing a uniformity of ±3%, were obtained over a useful area of up to 30 cm x 30 cm with neon and helium-ion beams. An important point to note is that the dose uniformity obtainable through the raster scanner is very insensitive to the beam tuning. This is because the entire field is scanned once during one beam spill, and therefore a small beam misalignment simply displaces the entire scanned field by the amount of the misalignment, which is insignificant. This is in contrast to a scattering or wobbling method in which a large dose nonuniformity could result.

A raster scanner producing clinically acceptable flat fields places strict requirements on the accelerator performance. (1) The temporal structure in the beam spills, the beam flux as a function of time, translates into spatial structures in the scanned radiation field. Coarse structure in the beam spill on the order of 1 Hz can lead to a gradual dose variation of the radiation field, whereas a high-frequency structure leads to localized hot/cold spots in the radiation field. Therefore, a uniform beam spill is required. (2) For a requested dose to be uniformly delivered over the entire scanned field, the beam spill should not be interrupted in the middle of a pulse. (3) The beam intensity must also be controlled so that each pulse delivers a specified fraction of the total dose. In order to reach the prescribed dose within the specified accuracy without overshooting it, an ability to step down in beam intensity is required. This implies a need to control the number of particles extracted on a pulse-to-pulse basis to an accuracy of ~50% over a wide dynamic range. (4) The extraction optics must not change while the beam is extracted at different flux levels. (5) The duty factor of the accelerator can become an issue if the number of scans increases to produce an acceptable clinical field.

The raster scanning system has several advantages over the scattering system as well as the wobbler system. The raster scanning system uses no absorbing material in the beam path. Rectangular fields of various aspect ratios produced by a raster scanner conform better with many irregularly-shaped ports than circular fields produced by a wobbler. Going beyond the simple rectangular scans, by varying the extents of each fast scan, irregularly shaped fields may be produced, and provide better conformations of the radiation fields to irregular target volumes. (See II.C.3 below.)

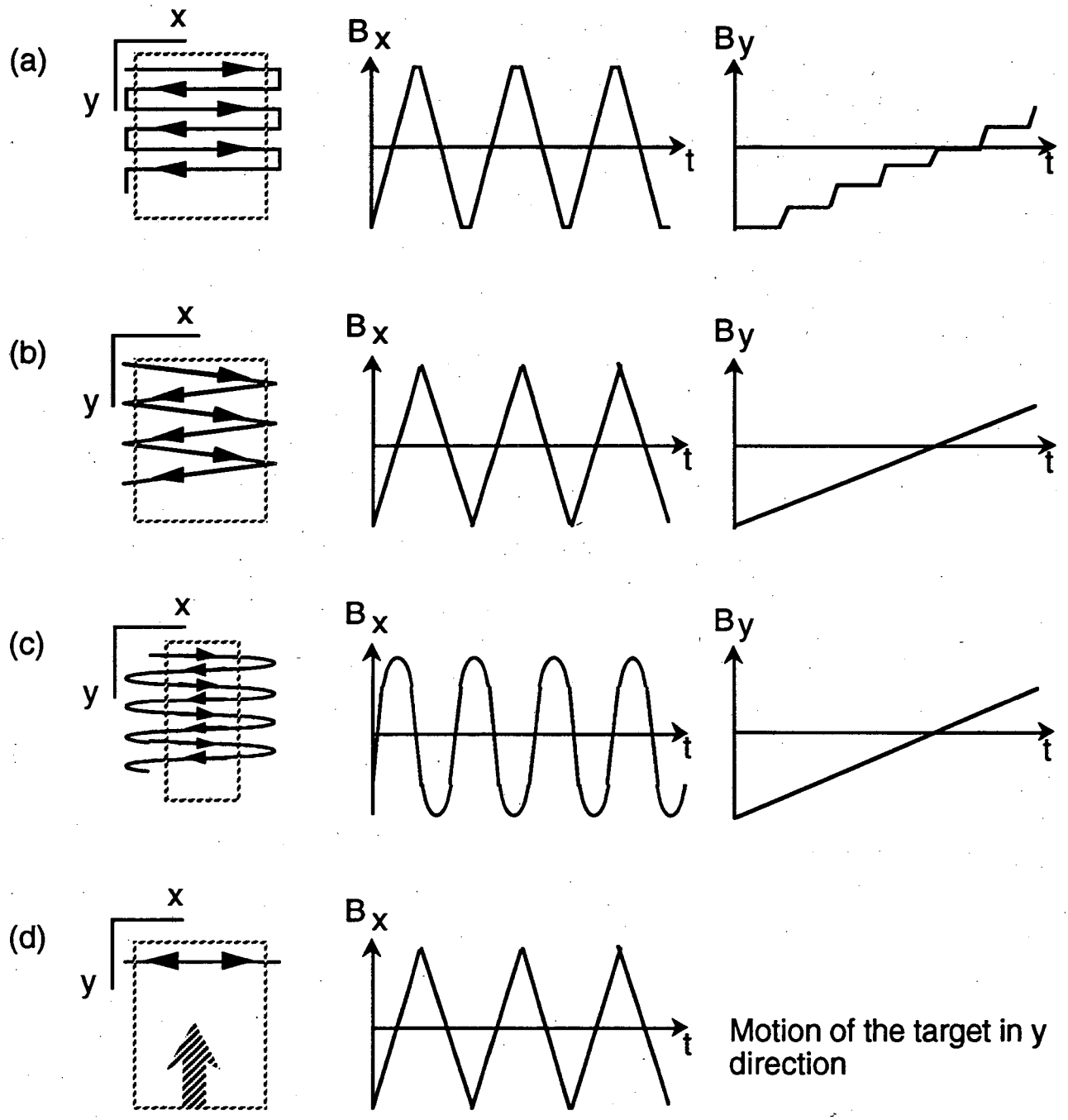

Fig. 47. Schematics of various raster-scanning techniques. For each method, the scan pattern is shown in the left diagram, and the magnetic field wave forms are shown in the right two diagrams. Shown are (a) Parallel rasters, (b) zigzag rasters, (c) sinusoidal scan, and (d) fast line scan plus the target motion.

A large flat-dose field may be produced by moving the beam spot in rasters with a constant sweep speed while holding the beam extraction level constant. This can be achieved in two ways: in

parallel rasters as shown in Fig. 47(a) or in zigzag rasters as in (b) of the figure. The latter can be considered as two sets of parallel rasters, one set moving in the +x direction and the other in the –x direction. These methods require a fast-scan in x-direction and a slow scan in y-direction. If the scans are accomplished with two magnets, their magnetic fields are varied as shown in the figure. The LBL raster scanner described above falls into this category. Sinusoidal variation of the fast-scan field can be considered as in (c) of the figure. Only a small central part of the scanned field would exhibit an approximately flat dose area; a large portion of the beam outside of the area will be discarded. A scheme may be devised to enlarge the useful flat-dose area by modulating the beam-spill intensity according to the scan speed. Clamping the beam off while it is outside the constant scan-speed area could also increase the beam utilization efficiency. A two-dimensional scan can be accomplished with only a fast-scan magnet performing line scans while moving the target in an orthogonal direction as shown in (d) of the figure.

The raster scanner proposed at Uppsala[28] consists of two narrow-gap magnets: an upstream slow-scan magnet is fixed and a downstream magnet pivots around the virtual scanning center of the first, so that its median plane coincides with the direction of the proton beam as it leaves the first scanning magnet. Through this arrangement, the gap size of the downstream magnet can be reduced. Because the downstream magnet has to move mechanically, it is chosen to be the fast-scan magnet, so that it has to move only slowly with the slow scan. This pivoting raster scanner is planned to be on a rotating gantry, and would be able to deliver a large field up to 30 cm × 30 cm with an 1-m effective distance from the magnets to the isocenter.

ACCTEK Associates has produced a raster scanner for proton therapy.[365] The horizontal-sweep magnet is the fast scanner and is powered at 240 Hz sinusoidally; where as, the slow magnet scans vertically at 4 Hz in linear ramps in both polarities, as shown in Fig. 47(c). To reduce the cost of the fast-magnet power supply, an AC power supply is used and the magnet is resonated. At a scanner-to-isocenter distance of 1.5 m, the system scans a 200-MeV proton beam into a rectangular field of 18 cm horizontal and 13 cm vertical dimensions in 0.12 second. An aberration in the system causes flaring near the edges of the scanned rectangular field. Modulating the accelerator intensity is contemplated to achieve the dose uniformity in the scanned field.

Another fast-cycling raster scanning system is developed for medical application in Novosibirsk.[335] It is reported that the fast scan is operated at 1 kHz.

It is interesting to note that applications other that radiotherapy requires spreading high energy heavy charged-particle beams into a large uniform field. One example is in the production of nuclear fuel, to minimize peak-power density and radiation damage to fuel cells, 450 MW of 1500 MeV proton beam is first defocused into thin vertical ellipse, then rastered horizontally across the target at ~1 kHz.[366]

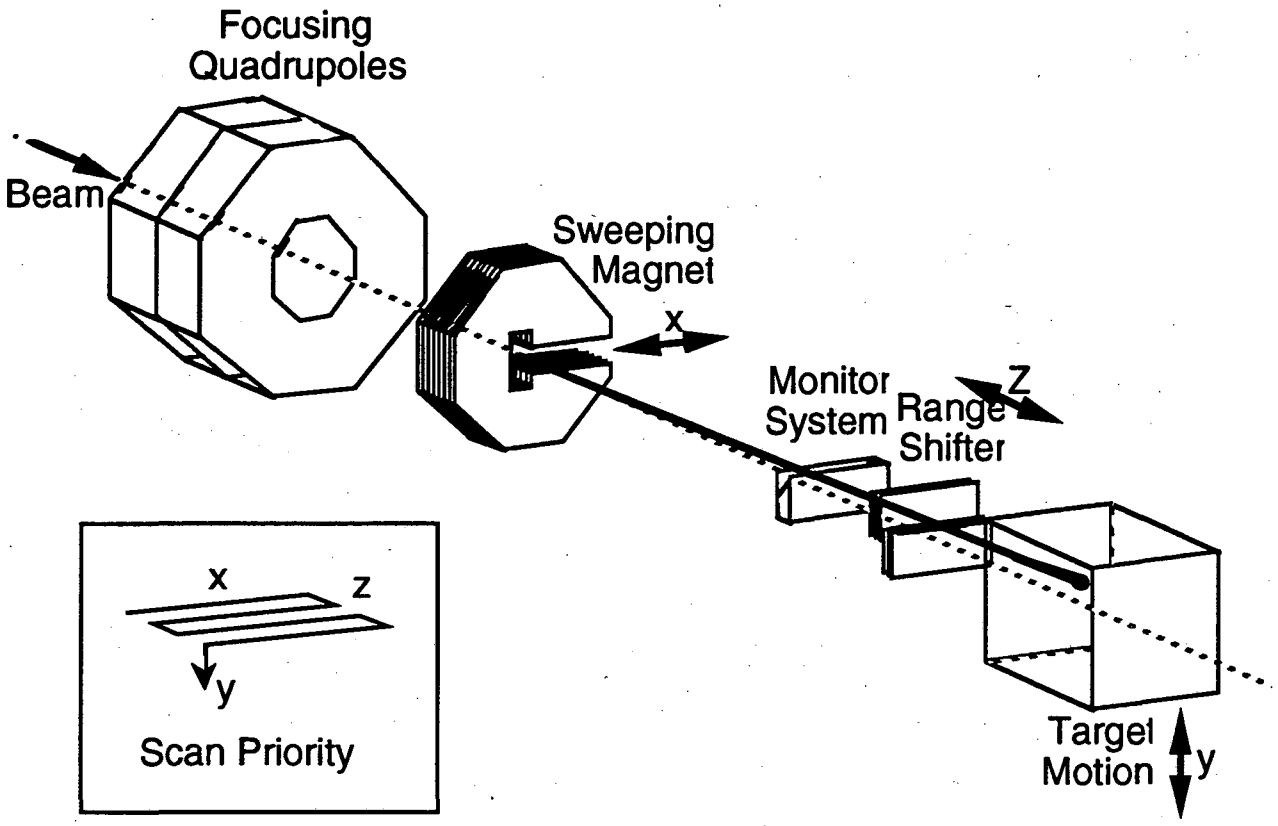

Fig. 48. Schematic of spot scanning developed at PSI.

II.C.2.g. Spot scanning

A large field of flat dose can also be obtained by moving a beam spot across the field in discrete steps; after positioning a beam spot at a given location in the field, a predetermined amount of radiation is deposited. The spot is then move to the next position, and the process is repeated. This approach adopted at PSI to perform spot scanning of high-energy protons[133, 354, 367, 368] is schematically shown in Fig. 48. To achieve an acceptable dose uniformity across a scan line, the step size is kept under one-half of the spot size as discussed in Sec. II.C.2.e. The spot size at the isocenter is about 1 ~ 2 cm FWHM in all three directions, and the grid size chosen is 5 mm. An 1-liter (10 cm × 10 cm × 10 cm) treatment volume would be filled with 20 × 20 × 20 spots, or about 10^4 spots. If an entire treatment were to be completed in 2 minutes, irradiation at a given spot must be accomplished within 12 msec on an average. The beam at a given spot must be switched on and off with a reaction time of 120 μsec if the dose were to be controlled at a 1% level. The fast beam switching is accomplished with a fast kicker magnet. The proton beam spot is moved in ±x direction by a sweep magnet, and the movement of the spot in the y-direction is accomplished by moving the target. The spot position in the x- and y-direction as well as the delivered dose are monitored by a position-sensitive ionization chamber. The fast kicker magnet is placed upstream of the sweep magnet, and when it is de-energized the proton beam is let through a narrow slit and the gap of the

sweep magnet. When the predetermined amount of protons are delivered, the fast kicker magnet is energized to deflect the beam away from the slit and into a slit plate, which acts as a beam stop, with a response time of 50 μsec. While the beam is blocked, the beam spot is moved to the next x position, and the irradiation is allowed to resume by de-energizing the fast kicker magnet. Upon completion of a line scan, the target (the patient) is moved in the y-direction for the subsequent line scan. Upon finishing the irradiation of a plane, the penetration depth (in the z-direction) of the proton beam is shifted by the range shifter and the entire process is repeated. An actual treatment will take longer than 2 minutes as the movement of the target between the line scans must be tolerated by the human patients. The maximum speed proposed for the patient movement is 2 cm/sec with an acceleration not greater than 0.05g. Typically 20 steps of y-motion, each on the order of 1 second, are required for an irradiation in each z step; these add up to additional 20 seconds in the treatment time.

II.C.2.h. Pixel scanning

A large uniform field can be made by subdividing the treatment area into a large number of pixels and delivering a predetermined dose to each pixel. To achieve efficient pixel scanning, very fast magnets and fast monitoring systems are required. Considerations of multiple scattering of protons in the treatment volume and the edge matching of neighboring pixels make the smallest acceptable size of the pixel bigger than 1 cm by 1 cm.

The first two-dimensional pixel scanning system for proton radiotherapy was developed at NIRS to spread the 70 MeV proton beams.[369-371] The system was called "spot scanning," but under our classification scheme (see Sec. II.C.2.e.), here it will be called a "pixel scanning" system. It employs two dipole magnets which deflect the beam either horizontally or vertically, four sets of beam defining slits, a quick beam shutter, and three monitoring chambers. The power supplies of the dipole magnets are digitally controlled by a computer, which direct the 1-cm square beam spot to any desired position in the treatment field. A highly collimated proton beam is prepared through four slits to produce a 1-cm square beam spot at the isocenter and the grid size used for the spot movement is the same as the spot size. Using the maximum field of the scanning magnet of 0.1-Tesla, they achieved a flat dose within 18-cm square fields with dose deviation of ±2.5%. A parallel-plate transmission ionization chamber is used to monitor the delivered dose at each spot location. The spot speed at the isocenter is ~1 cm/msec. It is possible to irradiate a field of any irregular shape with an arbitrary dose distribution, and to correct any fluctuation in the beam extraction intensity. The beam-spot position stability is achieved through severe collimation paying a great penalty in the beam utilization efficiency. The dose rate within the 1-cm square beam spot is ~1 Gy/s, and the system takes about 3 minutes to scan a 10-cm square field, *i.e.,* 100 pixels. The system is also used to deliver a large radiation field of a complex dose distribution by varying the

dose at each spot. It is also used in a 3-dimensional dose delivery as described in Sec. II.C.3.c) below.

II.C.3. Conformal Therapy Delivery Using Variable Modulation

II.C.3.a. Fixed vs. variable modulation

Heavy charged-particle beams with Bragg peaks and their favorable peak-to-plateau ratios[372] have been successfully used to treat tumors at a number of different sites in the body with less morbidity than with conventional radiation. In the systems described so far, passive range modulation was used to create fixed-width spread-out Bragg peaks (SOBPs) as depicted in Fig. 49(a). The width of the Bragg peak is determined by the thickest part of the target volume along the direction of the beam, and the Bragg peak is spread out to the same width for all rays in the beam (*fixed modulation*). The treatment volume, the region so irradiated with the fixed SOBP, is a cylinder, whose length is equal to the width of the SOBP. The distal envelop of the treatment volume is usually shaped by a compensator to conform it with the distal surface of the target. Generally, the longitudinal thickness of the target volume is not uniform and this method delivers a Bragg-peak dose to tissues upstream of the target, where some critical normal tissues, such as the skin as depicted in the figure, receive the same high dose as the target. In spite of this limitation, successes in treatments using charged-particle beams are the result of reductions of the high-dose volume and the dose to structures in the remaining irradiated volume when compared to external photon therapy.[3, 55, 71, 72, 373]

In realizing the full clinical advantage of heavy charged-particle beams, one of the important future developments in dose localization is to develop a beam delivery system that allows modulation of the spread Bragg peak over the target volume (*variable modulation*). The shape of the high-dose volume, in other words the treatment volume, can be made to conform more closely to that of the target volume, as shown in Fig. 49(b). Such a system will not only improve the therapeutic efficacy of the delivered,[374] but also increase the versatility of the beam spreading system for varied clinical situations.

II.C.3.b. Clinical advantages of variable modulation

Many investigators have studied the gains that could be anticipated from the implementation of a variable modulation beam delivery system.[375, 376] The parameters considered are the type of charged-particle beams and the size and depth of the target region. The gains depend very much on the circumstances of each case, but one may expect reductions in the "integral dose" in the range of 8% to 18%, and even larger gains if one restricted the integral dose calculation to regions outside the target volume. Here, the integral dose means the dose integrated over a volume in question; it is a

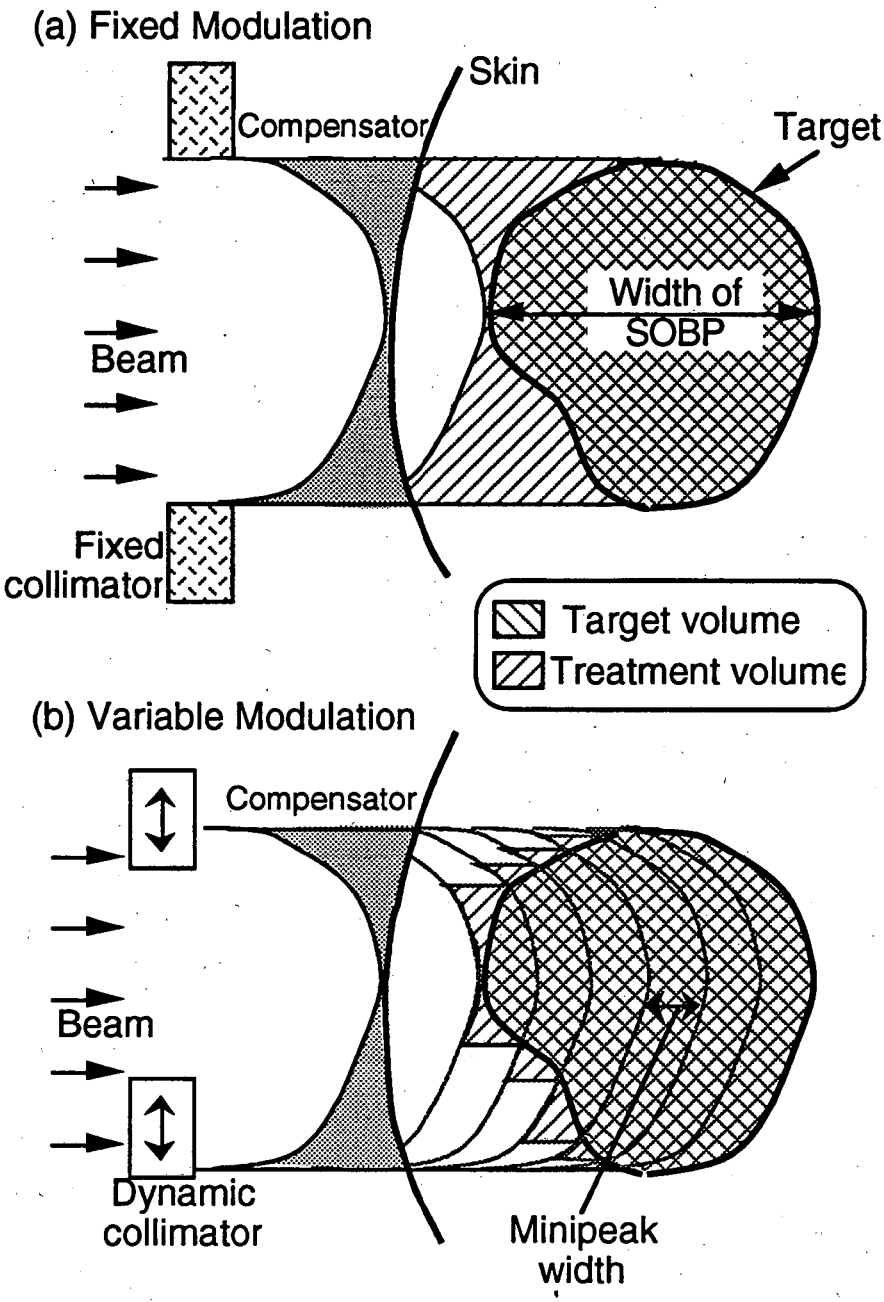

Fig. 49. (a) The *fixed-modulation* method using a compensator produces a cylindrical treatment volume whose length is equal to the thickest part of the target volume. Normal tissues upstream of the target volume are irradiated unnecessarily. (b) The unwanted radiation may be trimmed by the use of the *variable modulation* method. The treatment volume is made to conform more closely to the target volume than in (a).

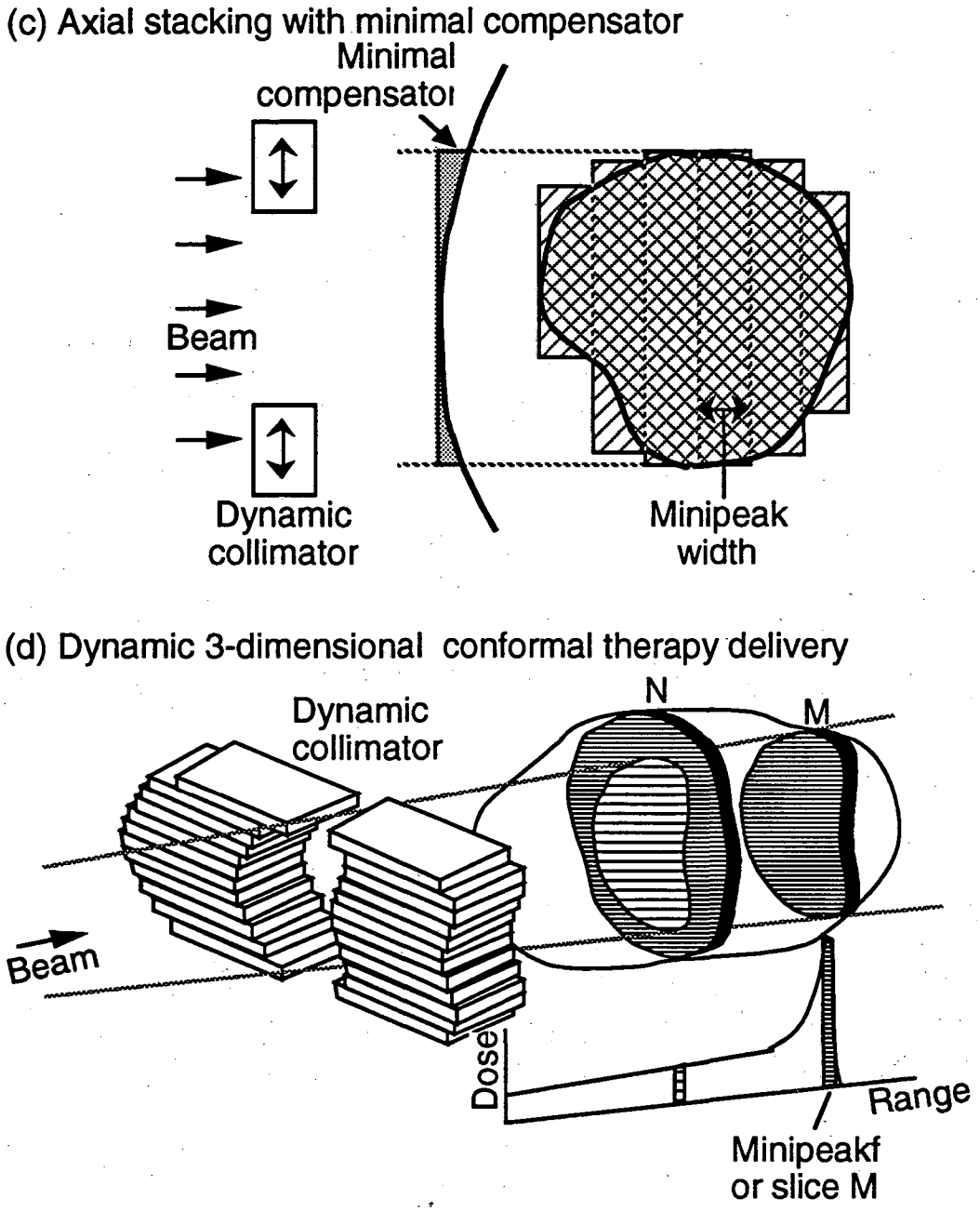

Fig. 49. (c) Axial stacking with a variable-speed raster scanning technique. (d) Schematic illustration of a 3-dimensional conformal therapy delivery.

non-physical quantity used as a descriptive clinical parameter and has a dimension of dose-volume. Improvements to the dose distributions offer improved tolerance to treatment and may allow an increase in the effective tumor dose with a resulting increase in the probability of tumor control. Lyman and Petti have performed treatment planning comparisons of the fixed versus variable Bragg-peak modulations in targets involving the prostate.[377] Based on the analysis of dose-volume

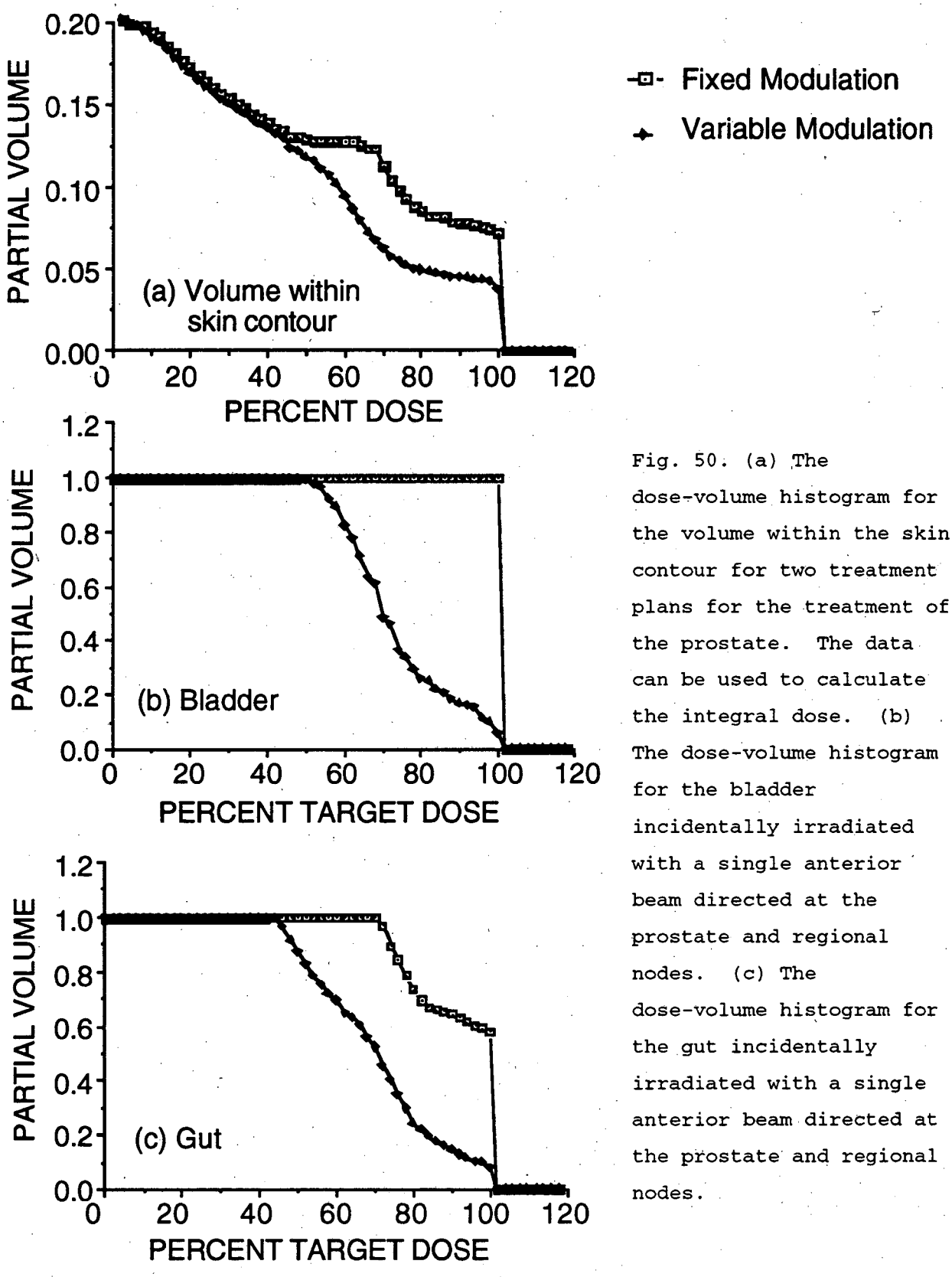

Fig. 50. (a) The dose-volume histogram for the volume within the skin contour for two treatment plans for the treatment of the prostate. The data can be used to calculate the integral dose. (b) The dose-volume histogram for the bladder incidentally irradiated with a single anterior beam directed at the prostate and regional nodes. (c) The dose-volume histogram for the gut incidentally irradiated with a single anterior beam directed at the prostate and regional nodes.

histograms (DVH is a plot of the dose, expressed in units of the target dose, versus the integrated volume that receives a dose greater than a given dose.[378, 379]), the total integral dose by variable modulation was 14.5% and the reduction of the integral dose outside the target volume was 16.8%. In this example the target volume is small relative to the irradiated volume as indicated by the modest increase in the integral dose reduction seen with the exclusion of the target volume. The reduction for the total integral dose is within the range predicted based on simplified assumptions.[376] A similar analysis was reported for proton beams in pelvic and head tumors.[380]

Daftari et al. studied the fixed versus variable modulation beam delivery techniques for tumors in the gastrointestinal tract using protons and neon ions.[381] Their study revealed that with variable modulation, the localization of the dose to the target volume can be improved significantly. The dose to the critical structures can be reduced as observed in Fig. 50. This figure shows the dose-volume histogram for liver for a patient with tumor in the biliary tract and was treated with five fields. Their study indicates the reduction of average integral dose for variable as opposed to fixed modulation of 17% with neon ion beams and 18% reduction with proton beams. If the tumor volume is excluded, the reduction in the integral dose to normal tissues ranged from 15% to 32% for neon ions and between 18% to 34% for proton beams. Their study also suggests that variable modulation will permit the use of simpler two and three-field charged-particle treatment plans as opposed to more complicated multi-field plans.

II.C.3.c. Conformal therapy delivery in three dimensions

Several methods are proposed to reduce the dose in the surrounding healthy tissues. Fig. 49(b) schematically depicts one of these methods. The treatment volume may be divided into many layers, as shown in the figure, and scanned layer by layer by changing the residual range of the beam. In order to reduce the number of layers, the Bragg peak is spread out to a 'minipeak' of approximately 1-cm width, and these minipeaks are axially stacked by changing the range. The accuracy of obtaining correct SOBP using the range stacking depends on the slope of the minipeak. Analogous to the edge-matching problem in beam scanning, the gradual rise and fall of the minipeak facilitates correct stacking when the pulse-to-pulse energy variation of the beam is taken into consideration. The distal dose falloff of the SOBP is decided by the most distal minipeak. A pristine Bragg peak with the steepest possible distal dose fall-off should be used at the deepest penetration.[359]

The contours of the proximal and distal surfaces of the target volume are usually smaller than the widest lateral extent and, as the axial stacking proceeds, the aperture of the variable collimator is reduced in such a way that healthy tissues adjacent to the target volume, especially those upstream of it, are protected from the unwanted Bragg-peak radiation. It is especially important to spare the skin and critical organs from unnecessary radiation. For example, the skin surface in Fig. 49(a) would

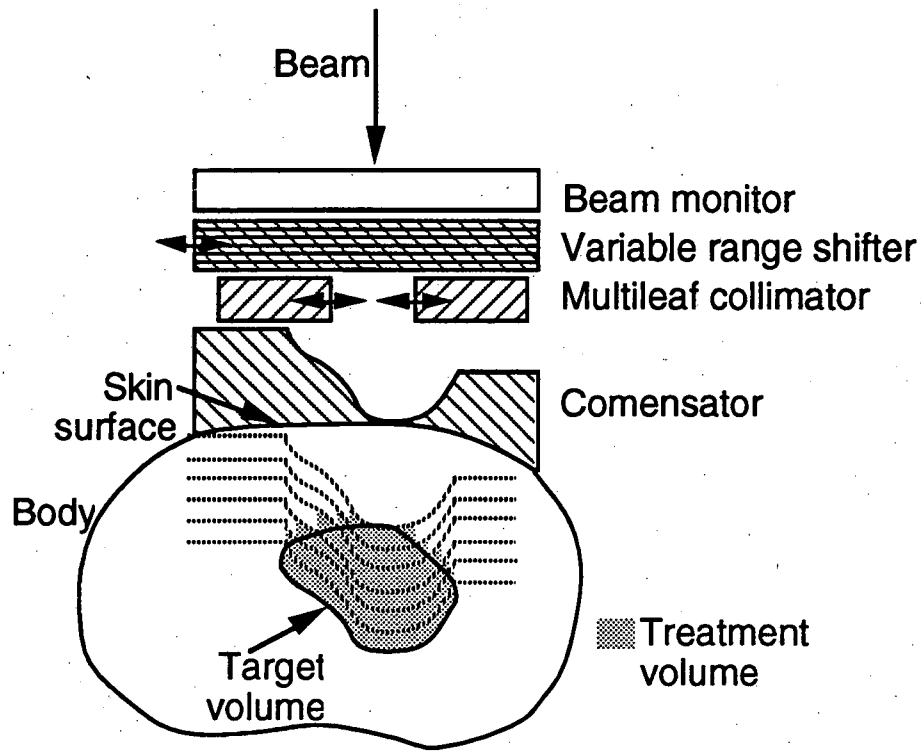

Fig. 51. A three-dimensional irradiation system using a scattering system for lateral spreading of proton beams as developed at NIRS.

receive the full Bragg-peak dose in a fixed modulation method; whereas, it will receive only the plateau dose, lower in magnitude and LET, in a variable modulation method as indicated in Fig. 49(b).

A three-dimensional irradiation system using scatterers for lateral spreading was proposed at NIRS.[382] As shown in Fig. 51, the treatment volume is layered according to the shape of the distal surface of the target, and the dose is built up using a variable range modulator and a fixed bolus. As the range is shortened, the irradiation field is changed using a variable aperture, such as a multileaf collimator.

A prototype three-dimensional pixel scanning methods for proton beams developed at NIRS[383, 384] is depicted in Fig. 52. The two-dimensional pixel scanning technique, developed at the same laboratory and described earlier in Sec. II.C.2.h above, is used. The scanning in three dimensions is accomplished by stacking the ranges of two-dimensionally scanned fields using a Lucite degrader of variable thickness from 0 to 48 mm in steps of 1 mm. A spot size of 6 mm × 6 mm is used. This method demonstrates the reduction of the integral normal-tissue dose, i.e., the unwanted radiation in the surrounding tissues.

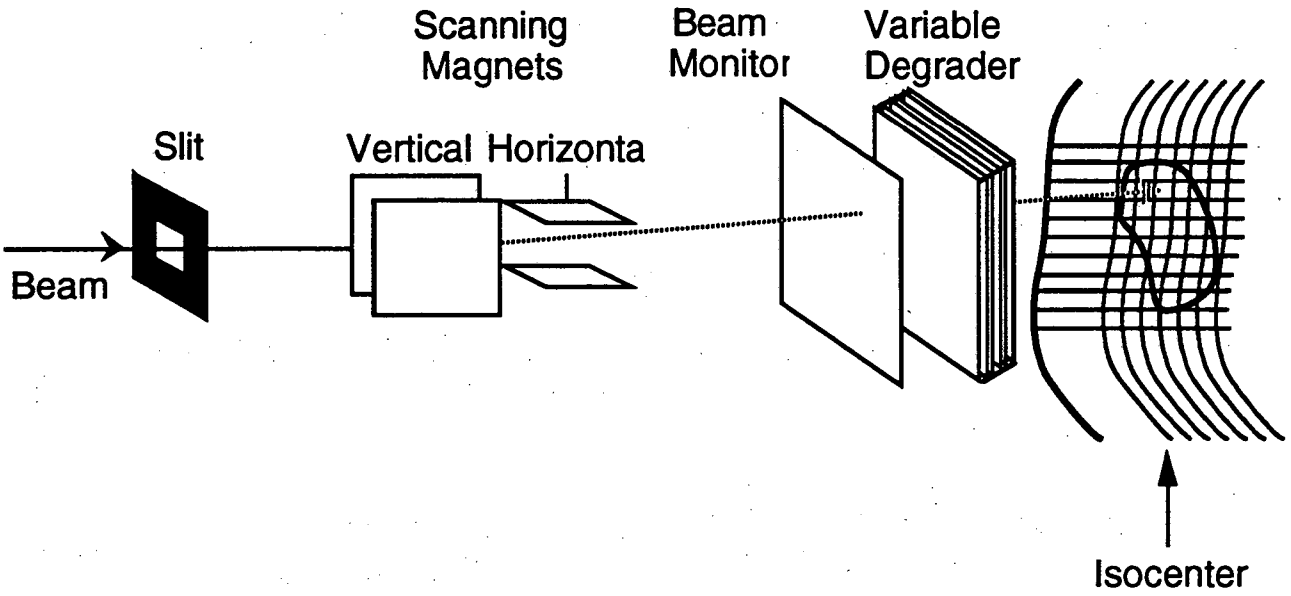

Fig. 52. Three-dimensional irradiation system using pixel scanning technique for lateral spreading of proton beams as developed at NIRS.

For the proton and helium-ion beams which produce no or few fragments, and therefore have no 'tail' dose (the dose due to the fragments beyond the distal edge of the Bragg peak), the method in Fig. 49(b) produces satisfactory dose distributions. However, the necessarily thick compensator ends up broadening the lateral dose falloff through multiple scattering of the projectile particles. For heavier ions, multiple scattering is less; however, the tail dose is significant. Blocking the proximal part of the spread Bragg peak with the variable collimator deprives the occluded area of the tail doses. The beam delivery method schematically illustrated in Fig. 49(d) overcomes these shortcomings. First, the most distal part of the target, slice M in the figure, is shaped by the aperture of a variable collimator and scanned with a uniform scan speed to produce a uniform dose distribution. While the slice M is 'painted,' a part of the slice N and all other parts upstream of slice M traversed by the beam receive the plateau dose, whereas the periphery of the area receives no dose. Thus, to deliver a uniform dose to the slice N, a smaller dose should be delivered to the area upstream of M than to its periphery. One way of achieving this, for example, is to vary the speed of the raster scanning — faster in the areas upstream of M, and slower outside of it — while keeping the level of extracted beam constant. When combined with the already deposited plateau dose, the resultant dose in N becomes uniform. This process is repeated for all subsequent slices to produce a uniform dose distribution in the target volume while imparting minimal radiation outside of it. This result could also be achieved by keeping the raster speed constant while varying the extraction level of the beam with time. This method, however, is technically much more difficult to apply.

One way of delivering conformal therapy with variable-modulation SOBPs is to employ a raster scanner with controllable scan speed and a variable collimator. Requirements for accuracy and stability of the scan magnets are stringent.[359] To ensure patient safety, the spatial distribution of the delivered dose must be monitored in real-time using a large-area high-resolution dose detector. The system requires an automated control along with a means of very fast and fail-safe irradiation termination. Fast on-line monitoring is required of various system parameters, such as scanning magnet currents, extraction levels of the particle beams, aperture of the multileaf collimator, width of the spread-out Bragg peaks and the residual range of the beam. Constancy of the beam extraction level is required over a large dynamic range in the extracted beam intensity.

II.C.4. Dose rate effects

II.C.4.a. High dose rate effect in beam scanning

Compared to a passive beam delivery system which irradiates the entire treatment area at the same time, a dynamic beam delivery system covers only a part of the treatment area at any given time. If the treatment time remains the same, the dose to a given area is delivered in a shorter time; the dose rate for the dynamic mode is higher. In general, the dose rate will be increased by the ratio of beam spot area to the entire treatment area that is subdivided in the irradiation. For example, if a treatment volume of 20 cm × 20 cm × 10 cm is irradiated to 2.5 Gy in 2 minutes using the double-scattering method, the average dose rate is R_{scatt} = 2.5 Gy × (duty factor) / 2 minutes ≈ 0.1 Gy/sec if a duty factor were 5. In a scanning method, if the treatment volume is subdivided into 1 cm × 1 cm × 1 cm cubes, i.e., into 4,000 equal voxels, $R_{scanning}$ ≈ 400 Gy/sec if a duty factor of 5 is again assumed. If there are time structures in the extracted beam, the instantaneous dose rate can be sometimes even higher. Therefore clinical effects of the elevated dose rates in dynamic modes of beam delivery must be given careful consideration.

The potential effect of very high dose rates on survival of mammalian cells has been studied independently by some investigators, and interesting results have been found and reported. Berry and Hall[385] reported an apparent lower effectiveness of radiation exposure when x rays were delivered at extremely high dose-rates. Using a single very short duration (7 nsec) pulse and varying the dose received by the cells within this brief pulse, they found that the corresponding log-survival curve at first showed a slope similar to that obtained under normal irradiation conditions but then broke away at some particular dose level to give a line of lower slope, the value of D_0 being similar to that usually obtained under anoxic conditions. The breaks in the survival curves appear at different dose levels (doses greater than 0.5 - 3.0 Gy) for different pulse lengths. A further analysis of their experimental data indicates that at all dose levels, mammalian cells may show greater survival

when irradiated with higher dose-rates (3×10^{10} to 1.2×10^{11} Gy/min)[386]. Using dry eggs of Artemia, Iwasaki et al.[387] observed similar effects for high-energy electrons at ultra-high dose rates ranging from 6×10^{6} to 1.2×10^{8} Gy/min. No comparable high dose-rate study with heavier ions can be found in the literature.

A high dose-rate effect was also found in animal systems. Hornsey and Alper[388] determined that there is increased radiosensitivity of intestinal epithelium as the dose rate is increased from 1 to 60 Gy/min. This tissue has a large capacity for repair of sublethal damage, some of which takes place in as short a time as 10 minutes so that there is a marked sparing effect during irradiation at low dose-rates. Ultra high dose rate (5×10^{3} - 10^{9} Gy/min) studies by Field and Bewley using 7 MeV electrons[389] and by Inada et al. using 8 MeV electrons[390] on rat and mouse skin indicate a decrease effectiveness. The effects observed in the skin studies have been attributed to oxygen depletion (see below) since experiments done with the skin under hypoxic conditions did not show any dose-rate effects.

The dose-rate region where the decreased effectiveness is observed is unclear. Field and Bewley observed a decrease in effectiveness at 5×10^{3} Gy/min, and Inada et al. have seen a decrease above 10^{6} Gy/min as has been shown for cells in vitro[385] and Artemia eggs[387]. These differences may reflect species differences in radiosensitivity and in tissue oxygenation. Normal tissue cells that are at low oxygen tension may potentially become anoxic at high doses delivered at high dose rates.

At high dose rates, dissolved gaseous oxygen in cells may be depleted and the cells rendered more radioresistant.[391] If an oxygen depletion state is reached due to the high-dose rate of scanning, it will work against the efficacy of a scanning system. The following analysis suggests that no oxygen depletion is caused by the high dose rate of the scanning method.[392] For a radiation chemical yield, denoted by G and defined as substances produced or destroyed, n, per mean energy E for oxygen-mediated lesions:

$$G_d = \frac{n}{E} = \frac{10^{-3}}{100}\ \text{eV}, \tag{39}$$

Typical tissue contains 0.3 μM of dissolved oxygen, which means the number of O_2 molecules per gram of tissue is

$$N = \frac{N_0\, c}{M} = 5.6 \times 10^{15}, \tag{40}$$

where N_0 is the Avogadro's number, c is the O_2 concentration, and M=32 is the molecular weight of O_2. If we irradiate the tissue with an oxygen concentration at a fraction, f, of the normal concentration, oxygen molecules will be depleted when a dose D is administered:

$$G_d D \geq f N, \tag{41}$$

or

$$\frac{D}{f} = 9 \times 10^4 \text{ Gy} \tag{42}$$

Eq. (42) may be called the oxygen depletion condition by a high dose-rate radiation. Weiss et al.[35] observed a change in the dose-rate of the cell survival at a dose of 200 Gy at 0.9% O_2 concentration, which implies that an experimental value of D/f = 200 / 0.009 = 2.2×10^4 Gy. This experimental result compares well with Eq. (40); they agree with each other within a factor of 4. In a typical treatment, the delivered dose per fraction is 2.5 Gy and the value of f is close to 1 for oxygenated tissue, or D/f = 250, which is too small to deplete the available dissolved oxygen in tissue. In well oxygenated tissue, the oxygen depletion condition will not be reached by a scanner-delivered therapy dose, even if the entire dose were delivered instantaneously. With a therapy dose of 2.5 Gy, the oxygen depletion becomes important if the oxygen concentration drops below $f = 3 \times 10^{-5}$. There is an ongoing attempt to measure the high dose-rate effect in cells and tissue.[246]

II.C.4.b. Dose rate effects in heavy charged-particle therapy

The important parameters of a therapeutic particle beam is the time structure of the extracted beam because it can alter the biological effect of the radiation and impact the ability of the beam delivery systems in delivering desired radiation fields. The biological effects of multiple ionizing-particle tracks placed closely together, in time and space, can interact with one another. Such effects are called the dose-rate effects, which if large enough place constraints on the acceptable radiation dose rate.

An estimate of 10^{11} Gy/min has been made of where an effect might be seen.[393] For various dose rates, Fig. 53 shows the probability for a given track to accompany a second track within a distance r and time t. The lines in the figure represent the probability of 37% (≈1/e) of finding the second track within r and t. Also shown is an estimate of where the dynamic and passive beam delivery systems discussed above are found in the plot.[392] To date, all heavy charged-particle accelerators and beam delivery systems have operated at flux density or fluence rate (number of particles per cm^2 per second) where such effects are not important.

We do not anticipate observing high dose-rate effects with high LET heavy charged-particle irradiation because: 1) the reduced repair for sublethal damage, 2) reduced differences in radiosensitivity due to cell cycle phase, 3) reduced protection due to hypoxia and 4) the doses per fraction used during radiotherapy with heavy charged-particles will be far below the doses at which dose-rate effects have been seen in tissues. Fig. 53 also illustrates graphically the dose-rate regions where effects have been observed and the high dose-rate region where the raster scanner will be operated. The dose rates delivered by the raster scanner will fall within a region where effects have

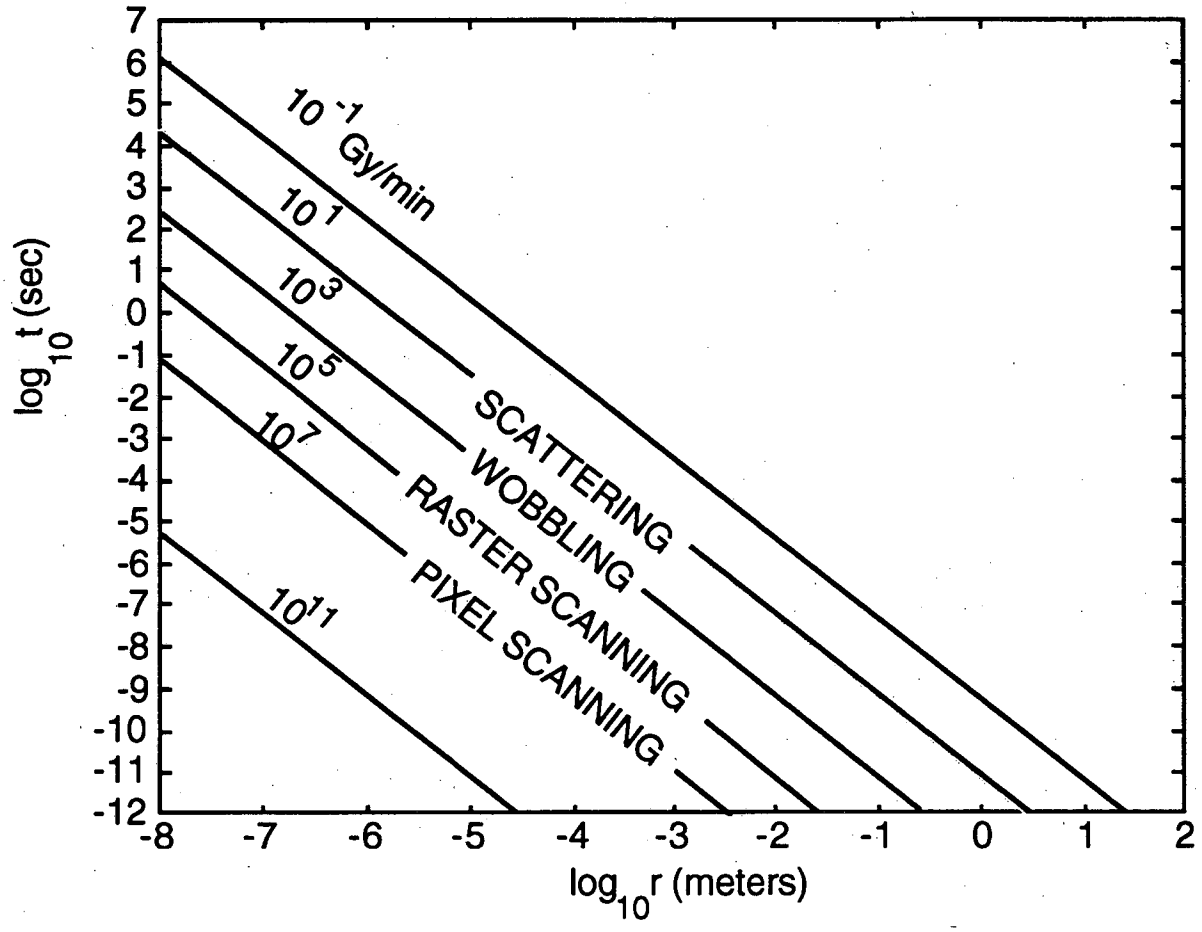

Fig. 53. Temporal and spatial distances of two tracks for various dose rates in Gy/min. Approximate regions of the dose rates for various beam delivery methods are indicated.

been observed in mammalian tissues and cells, and because of this we need to test for dose-rate effects with heavy charged-particles and to assess the relationship with increasing LET. However, it is noted that, based on physical and radiochemical arguments, the dose-rate effect may be appreciable at the dose rate $>10^{11}$ Gy/min, which is at least two to three decades above the expected dose rates encountered in any scanning methods.

II.D. Collimators

Shaping the radiation field to conform to the irregular target volume, while conceptually simple, is one of the more difficult tasks in preparing the beam for a patient treatment. The various methods that have been investigated vary in their complexity and the degree to which they conform the radiation to the target volume. The simplest and earliest method uses a block of material with a fixed

aperture which conforms to the projected area of the target volume as seen from the beam direction. A more refined method involves shaping a mechanically variable aperture to achieve the desired shape at various depths of the target volume. Another method, yet to be implemented clinically, requires no physical collimation of the beam, but relies on precise control of the position and profile of very small beam spots.

II.D.1. Collimator Construction

The thickness of the collimator must be sufficient to stop the beam in the case of protons; but significantly thicker than the range of the primary beam in the case of heavier ions because fragments produced in nuclear interactions of the beam with the collimator material can travel further than the range of the primary particles. The tail dose for a heavier-ion beam is significant (see Sec I.C.3.c). The LET of the fragments delivering this dose, however, is less than that of the radiation in the SOBP. The lower LET here implies a lower RBE, and therefore a decrease in the actual damage done by the particles penetrating the collimator. The collimator thickness is usually chosen to reduce the dose delivered by the penetrating secondaries to ~1% of the SOBP dose of the uncollimated beam. For example, neon ions with an energy per nucleon of 585 MeV stop in ~ 30 cm of water, but the collimators used have a water equivalent thickness > 90 cm.

Collimators can be made from any number of materials. The less dense the material the thicker the collimator will be in the beam direction; however, the weight will be approximately the same (±20%) regardless of the material since the stopping power of a material is approximately proportional to its physical density (±20%). One of the major concerns in the choice of collimator materials is the induced radioactivity from the beam stopping in the collimator. Generally the residual activity created from exposure to a single treatment must be low enough for clinical personnel to work in the vicinity immediately following the exposure. Gamma rays coming from the induced activities are the most important component of the radiation because of their long range. An absorbed dose of 1 Gy in a Cerrobend collimator results in an induced activity of 50 mSv at the surfaces with an initial half-life of about 5 minutes. Heavier materials such as tungsten have higher induced activity levels with longer half-lives and emit photons with higher energies compared with lighter materials such as aluminum.

II.D.2 Fixed aperture collimators

Fixed aperture collimators have an opening designed by clinical personnel based on the projected target shape. See Fig 54. While this method cannot avoid delivering unwanted radiation to some normal tissue surrounding the target volume, the simplicity of these collimators makes them widely used. One method of making such fixed-shape collimators involves casting a low melting-point alloy in a Styrofoam mold. An example is Cerrobend, which is composed of 50% Bi, 26.7% Pb,

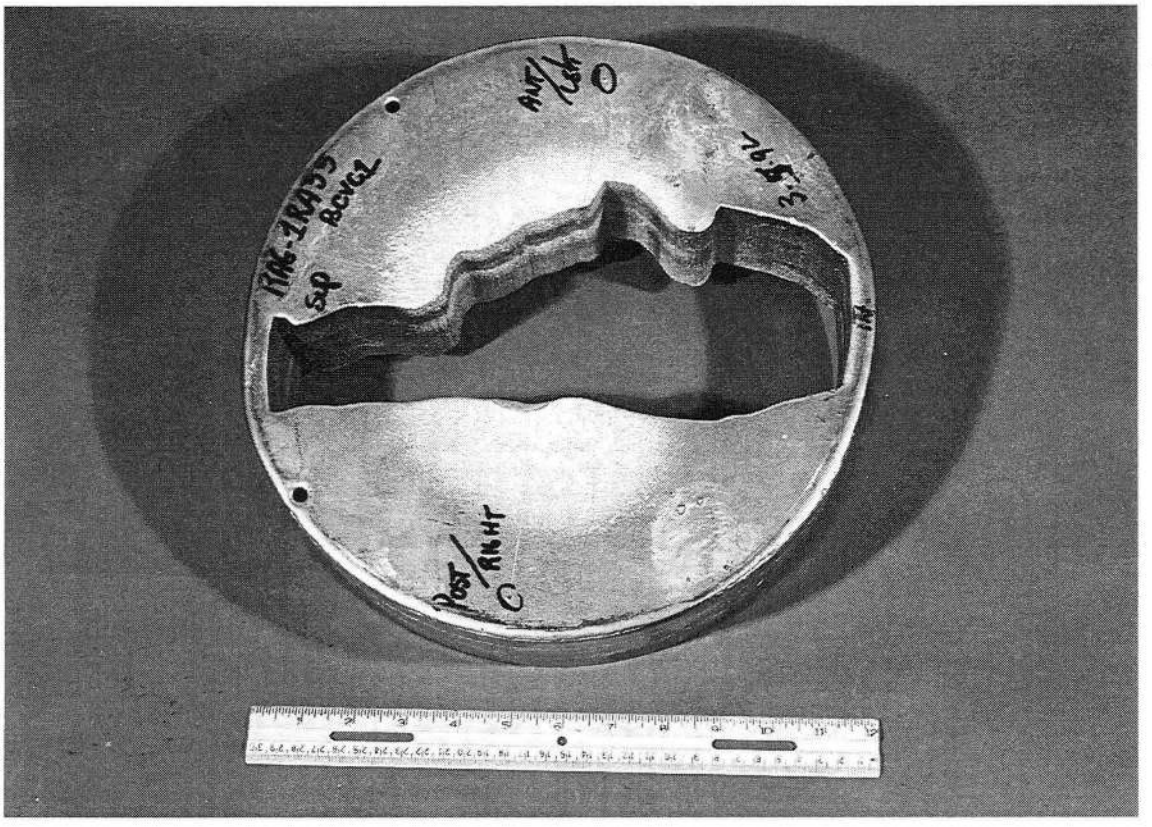

Fig. 54. Collimators made of heavy metal as shown in this picture are used to shape the beam's profile to match the cross section of the patient's tumor from a beam's eye view. (CBB 925-3278)

13.3% Sn and 10.0% Cd with a melting point of 70°C. Such alloys are easy to use and may be reused after induced radioactivity has decayed to an acceptable level. Another method of making collimators is machining an aperture out of a metal such as brass. By automating the design and milling processes, this type of collimators may be fabricated routinely.

The major disadvantage of the fixed-aperture collimator is that a unique collimator must be cast for each patient port, which is a labor-intensive process. A clear need exists for a collimator with a variable aperture, but their mechanical complication has daunted their construction until recently.

II.D.3 Variable aperture collimators

A variable aperture collimator is a device whose aperture can be changed mechanically to a desired profile. The first example to be discussed is a slit collimator consisting of a slit with moveable end blocks. Such a collimator can be used with line-scanning beam delivery systems.

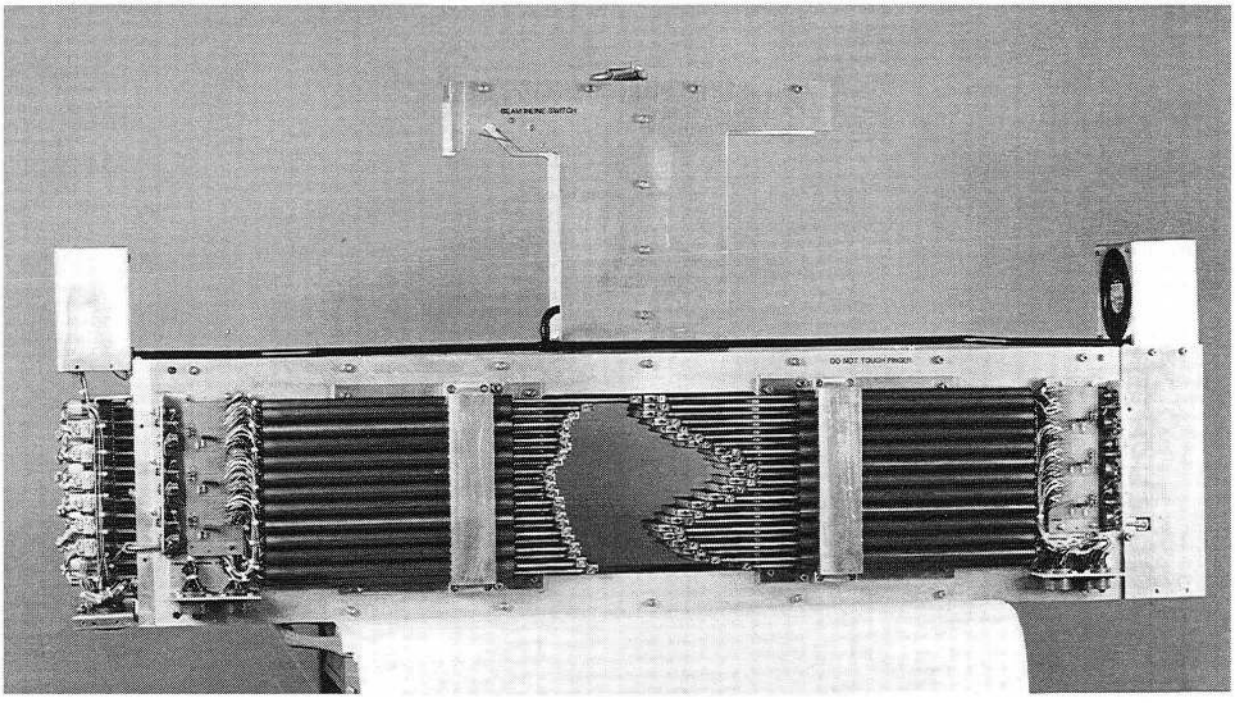

Fig. 55. A multileaf collimator are used with dynamic conformal radiotherapy to allow dynamic shaping of the radiation field to the tumor volume. (CBB 919-7469)

During a line scan, the slit is aligned with the scanning beam, and the radiation field is collimated to a rectangular shape of a specified length by the slit and the end blocks which are moved to the desired positions At the completion of a given line scan, the patient is moved to a position where the next line-scanned beam is aligned with the doses already delivered in preceding line scans. Repetition of this process produces an irregularly shaped radiation field in two dimensions. If the end blocks are made to rotate around pivots in such a way that their collimating edges align with the curved boundaries of the irregular port, the resulting irregular port shape conforms more closely to the target shape. This type of dynamic collimator has three controls: one for the patient motion and two for the linear motions of the end blocks. The pivoted version would require two additional controls for the angular displacements of the end blocks. The system can be adapted to two-dimensional scanning, in which the patient remains stationary and the line scans are moved across the patient.

An example of a variable aperture collimator is the multileaf collimator which defines irregular shapes by means of many movable absorber bars, called leaves or fingers. A multileaf collimator, whose leaves are manually moved, has been developed and used at NIRS.[394] Shown in Fig. 55 is

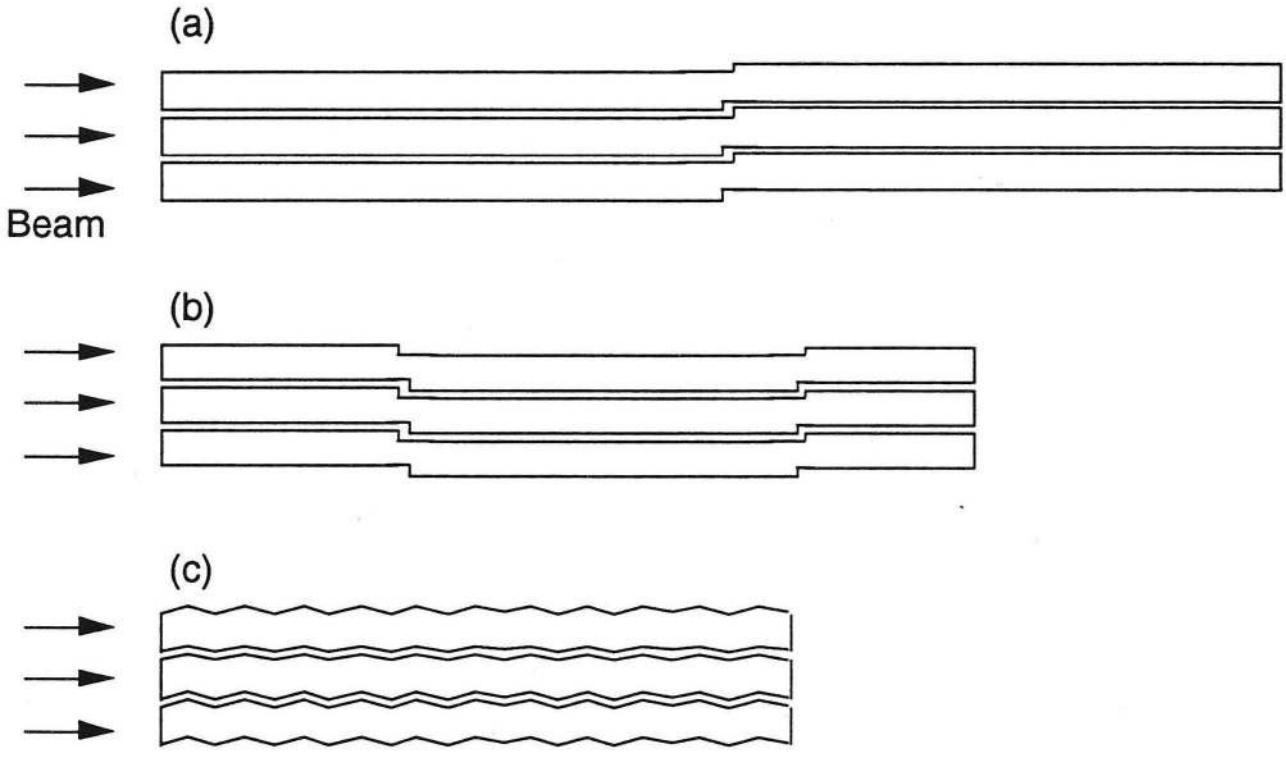

Fig. 56. (a) The finger design with one step in a multileaf collimator is not satisfactory in blocking the heavy charged particles. (b) The fingers with two steps, used at NIRS, stops radiation from reaching the patient. (b) Corrugated fingers can also be used to stop radiation from reaching the patient while reducing the width of the finger.

an example of an automated multileaf collimator developed at LBL, and whose leaves are moved by actuators under computer control.[395] The leaves are stacked together to form what is called a jaw, and two jaws are placed in opposing positions. There are twenty-three 9 mm-thick leaves at each side of the aperture. The maximum opening between two opposite leaves is 22 cm; each leaf has a 20-cm stroke. The leaves are driven by DC motors, not stepping motors, and a feedback loop is required for positioning the leaves and keeping them in place. Commercial units which combine motor, gearbox, and magnetic encoder in one very small housing of about 1.6 cm in diameter and 5 cm in length are used. The motors drive the leaves directly via a ball screw. A sliding potentiometer attached to a leaf is used for measuring its absolute position. The generated signal is compared to a reference and the difference used to drive the motor. The leaf position is monitored by a magnetic encoder attached directly to the motor. Thus the position monitoring is independent of its control. The multileaf collimator is mounted in such a way that it can be rotated 90 degrees around the central ray of the beam, allowing collimation of almost any field shapes encountered in radiotherapy applications. The leaves were made of steel as the best compromise for satisfying the following

parameters: high density, high rigidity, ease of fabrication, durability, low induced radioactivity, and reasonable cost.

Even though the fingers are machined to a high degree of precision, particles leaking through the spaces between the bars can be a problem. Several methods have been investigated to circumvent this leaking radiation problem. In the simplest method, the planes between the fingers are slightly (~2 degrees) tilted so that they are not parallel to the beam direction. Since a significant fraction of primary particles which scatter into the tilted plane readily go through the cracks, this method is unacceptable. To provide a more tortuous path for particles to make it through, the bars must be shaped in such a way that the "cracks" have multiple bends. As shown in Fig. 56(a), the finger design with one step requires that the span (the thickness along the beam direction) of each side of the step to be wide enough to stop the beam particles. Therefore the leaf width is at least twice the range of the particles. Another design developed at NIRS employs two steps in each finger as shown in Fig. 56(b).[396] Each finger width has two short and one long spans. The sum of one long span and the short span must be wide enough to stop the particles; therefore, the width of the fingers of this design is narrower than the one-step design. The other method, as illustrated in Fig. 56(c), employs corrugated surfaces to provide multiple bends in the cracks. This geometry has been adopted in the LBL multileaf collimator. The width of the collimator depends on the machining tolerance of the corrugated surfaces and their mating with the adjacent surfaces, but is less than the widths required in the above two methods.

A multileaf collimator, when used with range modulation, can perform three-dimensional conformal irradiations as discussed in section II.C. The use of dynamic multileaf collimation for shaping of arbitrary dose distribution for photon beams has also been considered,[397] which eliminates the use of wedges for beam shaping.

II.D.4. Dynamic Beam Shaping

Shaping of the treatment port by magnetic control of the beam, without resorting to the use of a collimator, has not been clinically implemented. Pixel scanning with pencil beams without collimation has been done on an experimental basis with proton beams.[367, 369] This method requires the precise control of the beam profile, position and intensity. The lateral dose falloff of the collimated beam is defined by the profile of the beam spot; to achieve a comparable lateral dose falloff to that of a fixed collimator a beam spot size of $\sigma \approx 0.5$ cm must be used. (The beam spot collimator should not to be confused with the port collimator.) Because no physical means of stopping the beam at critical positions is used in this method, proper control of the beam must be guaranteed and an independent means of verifying the beams position and the dose being delivered must be provided.

III. RADIATION DETECTORS

Many of the radiation detectors described in this section have been used in the dosimetry of photon, neutron, and electron radiation. Others have been developed for single particle detection in nuclear physics measurements. How these detectors are used clinically with heavy charged-particle beams will be the subject of this section.[68] Since any detector or detector system has limitations and only measures a subset of the quantities characterizing a particle beam or radiation field, a broad variety of detection methods are needed for measuring all the quantities of interest. These uses include following applications: dose detectors whose signals are proportional to absorbed dose, radiation detectors that can be used to measure dose after being calibrated for a particular type of radiation, detectors for absolute calibration measurements, and specialized detectors which measure properties of individual particles, such as lineal energy transfer, scattering angle or scattering cross section.

Dosimetry systems for radiotherapy and radiosurgery have three main functions: 1) measurement of the dose being delivered to the patient in real time in order to terminate the irradiation at the prescribed dose, 2) measurement of the lateral distribution of the radiation delivered in order to insure that the patient prescription is satisfied, and 3) measurement of radiation field parameters for controlling the beam delivery system.

III.A. Dose Detectors

The purpose of the dosimetry system is to measure precisely the delivered dose to the patient. The detectors used in such systems must measure a quantity proportional to the dose imparted to the patient, must not significantly perturb the radiation field, and must measure the dose independent of the LET distribution in the beam. This is especially important for light-ion beams which contains particles with a wide range of LET values due to fragmentation of the projectile particles. In addition, large radiation detectors with fine spatial resolution are important for comparing the prescribed and delivered radiation distributions over the entire treatment area. A required dose accuracy for clinical purposes of ±2.5%, measured over a large dynamic range (~10^6), adds to the difficulty of monitoring the radiation.

III.A.1. Ionization chambers

Ionization chambers are the primary dose measuring devices.[398] The ionization of the gas contained in the detector is proportional to the energy loss which in turn is approximately proportional to the dose absorbed by the detector.[399] This dose can then be related to the absorbed dose in another medium, such as human tissue, by the ratio of the stopping power of the gas to that

of the medium. The ionization, Q (measured in Coulombs), produced by the beam passing through such a chamber is proportional to the absorbed dose, D (measured in Grey), by what is known as the Bragg-Grey equation[400]:

$$Q = \frac{D\rho V}{W} \tag{43}$$

where ρ is the mass density (kg/m^3), V is the volume (m^3), and W is the ionization energy (eV) per ion pair. The amount of ionization per unit of deposited energy varies for different types of radiation. However, for heavy charged-particles (proton and light-ion beams) at clinically relevant energies there is only a weak dependency of the W-value on particle type and velocity.[43, 401, 402] This is particularly important when using light-ion beams because the beams generally contain a mixture of particles at various energies produced by the beam modifying devices.[403, 404] A value of 34.3 eV for protons in air and 33.7 eV for heavier ions in air are standard W values.[234] Values of W for other gases are recommended by the International Commission on Radiation Units and Measurements[405] and more recent measurements have been made for protons in nitrogen gas.[402, 406]

III.A.2.. Types of ionization chambers

III.A.2.a. Transmission ionization chambers

A transmission ionization chamber consists of two parallel planes with an electric field applied between them.[60, 62, 363, 407-410] Particles traversing the chamber ionize the gas in the volume bounded by the planes. The thickness of the planes and gas are such that they have little effect on scattering or fragmenting the beam. Recombination of these ionization charges at the highest expected dose rates must be taken into account in choosing the type of gas, the gas pressure, the plane separation, and the high voltage at which the chamber is to be operated. Multiplication of the produced charge is undesirable because uncertainties in gas pressure and high voltage in such a proportional mode of operation can lead to unacceptable measurement errors in the dose. The accuracy to which the dose must be measured and the speed at which the radiation must be controlled or terminated dictate the response time of the detector. The drift velocity of the ions and their drift length in the gas govern the detector response time.

The elements of a transmission ionization chamber are the support body, gas windows, signal and high-voltage planes, and the electrical and gas connections as shown in Fig. 57. The body supports the internal elements of the chamber and positions them relative to some reference coordinate system. Thin Kapton foils or nonconducting plates are ideal for use as beam entrance and

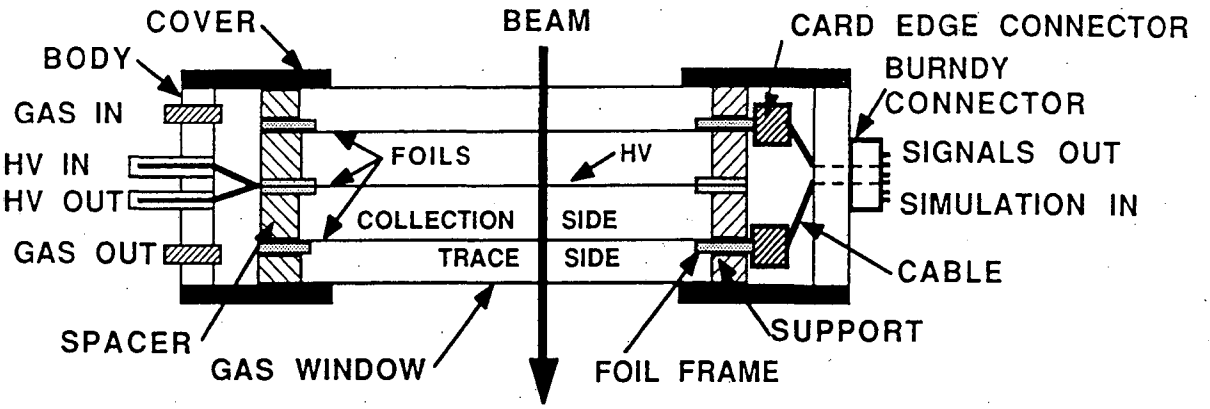

Fig. 57. A cross section of a transmission ionization chamber is depicted in this figure. Various elements of such a detector are labeled. (XBL 892-598)

exit windows and for creating a gas enclosure. Additional foils (or plates) define a pair of parallel planes and create a known ionization volume. One foil is usually connected to a high voltage source and the other, a collecting foil, is connected to appropriate electronics for measuring the ionization charge. Collection of charge on the signal leads is avoided by shielding them from stray electric fields with a ground plane and positioning them outside the primary radiation field. An additional trace to each element can be used to check an element's continuity. Simulation of a beam's ionization can be accomplished by injecting a known amount of charge onto an element via this trace. In addition a test of each channel for its proper working can also be made with a calibrated current source connected to this extra trace.

Recombination effects as well as the chamber's sensitivity increase with increased foil separation, sometimes requiring a careful compromise in chamber designs. Uniformity in the separation of the foils is important since inaccuracies can result if the charge collection is distorted by skewed electric field lines or the ionization volume varies erratically from element to element in the case of segmented foils.[411] Parallel electric field lines at the boundaries of the collecting region are achieved by an extension of the ground and HV planes beyond the collecting area.[411] Calibration of these chambers is usually against a thimble ionization chamber in a phantom.[363, 412, 413]

In contrast to the transmission chambers described above, a *longitudinal* ionization chamber has been constructed at TSL. This parallel-plate ionization chamber is used to measure a narrow proton beam which is introduced between the plates and parallel to them.[64] In this design, the plates do not have to be thin as the particles do not penetrate them, and the electrodes consist of thin layers of silver on plexiglass plates. The chamber measures the total number of particle.

III.A.2.b. Thimble ionization chambers

Thimble ionization chambers are spherical or cylindrical chambers made from conductive plastic with a center stem for charge collection.[408, 410] The plastic walls are typically a few mm thick and the volumes vary from 0.1 to greater than 1.0 cm^3. Such detectors serve as practical calibration devices and are routinely calibrated against an NIST(National Institute of Standards and Technology)-calibrated standard. However, care must be taken in their use to insure an equilibration of the radiation entering and leaving the chamber.[414] Smaller chambers afford better spatial resolution, but are less sensitive. These chambers are primarily used with air or a tissue-equivalent gas as the ionization medium. Their calibration must be corrected for the gas temperature and pressure.

III.A.2.c. Segmented ionization chambers

In the multi-segmented type each segment measures the collected charge independent of the other segments. Such chambers have a variety of uses such as measuring the beam profile and position[65, 324, 415] or measuring the spatial dose distribution.[363] The layouts of such ionization chambers depend on the required spatial resolution or segment size, the total area to be covered, and other properties.

As heavy charged-particle accelerators can have temporal variations in their spilled-beam characteristics, and a dynamic beam delivery system deposits the dose in space as a function of time, real-time information on the location of the dose deposition is required.[395, 407] Segmentation of the collecting planes of the ionization chambers provides a means of obtaining spatial dose information. For example, a plane surface with a set of concentric rings can be used to measure beam profiles with cylindrical symmetry by measuring the intensity distribution along a radius.[415] The azimuthal distribution can be measured by dividing the annular rings.

Segmented ionization chambers have also been constructed to measure the beam profiles that lack cylindrical symmetry. The example in Fig. 58 shows the hexagonal layout used at LBL. The size of the hexagonal electrodes is approximately 5 cm across. In highly segmented chambers the large number of elements makes calibrating each individual element cumbersome. Reliance on the accuracy of an element's construction is then desirable. The volume of each element must be within 1% of a nominal value in order to maintain the clinically required measurement accuracy. Detectors that cover 30 cm by 30 cm with 2.5-cm[363] and 0.5-cm[395] spatial resolutions have been built at LBL for monitoring dynamic beam delivery systems.

The size of a segment can vary form 0.1 to 100 cm^2, and the practical limit on the reduction of the size of the collecting elements is governed by three factors: (1) the element must be large enough so that the charge collected is accurately measurable in its typical application, (2) each electrode requires a lead to bring the charge out for measurement and the achievable packing density of such

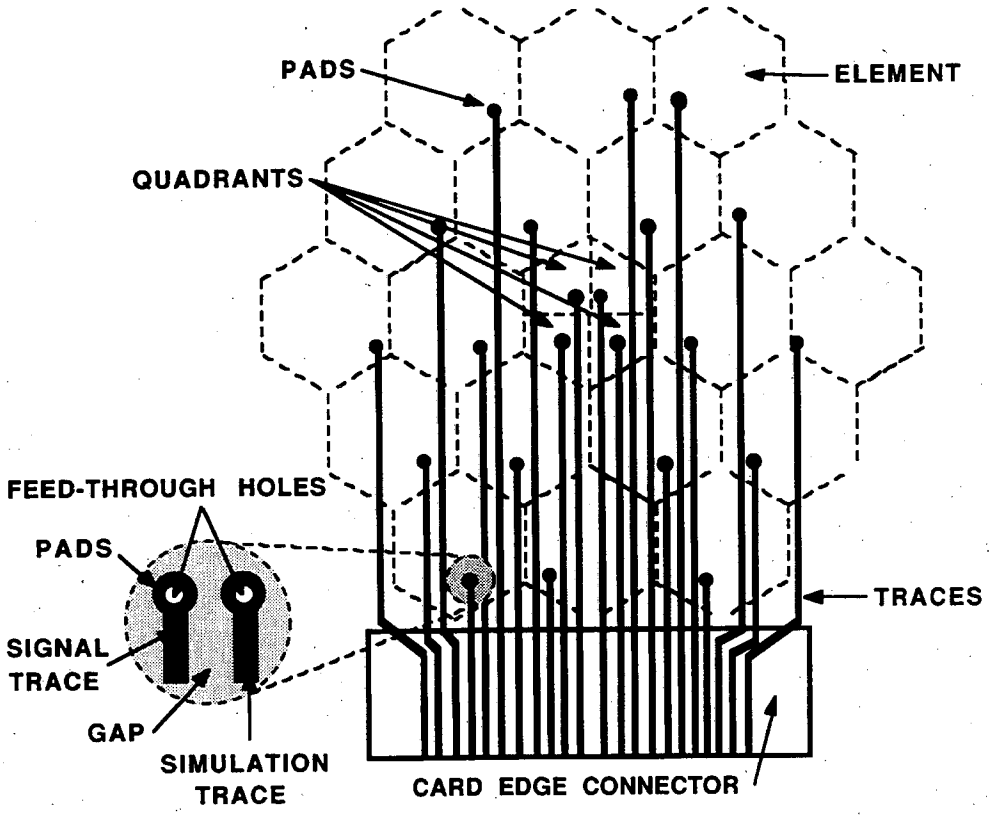

Fig. 58. Multisegmented ionization chambers allow detailed spatial measurements of the dose distribution. A typical layout is shown. (XBL 892-595)

leads on the foil surface places a limit on the number of elements per unit area, and (3) the number of elements increases with the square of the inverse of the linear dimension of the element, and with it the cost of the associated electronics.

One solution to the problem of signal extraction utilizes thin traces located on the opposite side of the foil or plate from the collection elements. Holes drilled through the foil or plate allow a connection between the element and a trace. This method avoids collection of charge on these traces by placing them away from any electric field. More space is available this way for laying out the traces and for collecting elements. For a highly-segmented ionization chamber, where more space is needed to lay the traces, a multilayer construction has been used.[395]

III.A.2.d. Other types of ionization chambers

Another use of ionization chambers is to interleave a set of them with absorbers of known thickness. A series of measurements can then be made at the same time at different water equivalent depths. An ionization chamber telescope produced at LBL to measure a depth-dose distribution is illustrated in Fig. 24. Eleven ionization chambers are stacked, and absorbers of pre-determined thicknesses are placed between them. With this setup a series of measurements at different depths can be made simultaneously. The placement of appropriate absorber thicknesses allow the measurement of the absorbed doses at entrance, plateau, proximal peak, mid peak, distal peak, and tail regions using one accelerator pulse. Sets of thin absorbers are used around the proximal and distal peak regions to assess their locations accurately. The use of such a device reduces the time spent measuring the depth-dose curves in the daily verification of the therapy beams.

A position sensitive ionization detector has been developed at PSI[416] which consists of a high voltage foil tilted with respect to two parallel signal planes. The ratio $Q_1/(Q_1 + Q_2)$ of the charges collected on both sides of the tilted foils measures the mean position of the beam. Resolutions of better than 0.5 mm have been achieved. Since this detector is used in conjunction with a spot scanning beam delivery system as described in Sec. II.C, the collection time is required to be less than the dwell time of the beam to obtain a true position measurement. Measurements show this to be under 1 ms with charge measurement times on the order of 10 μs. To control the dose being delivered the response time of the detector system must be even faster than this or on the order of the minimum dose divided by the dose rate and the required dose accuracy. Less than 100 microseconds is required for the PSI detector.[133]

III.A.3. Ionization-chamber design considerations

The properties of the gas used in these chambers determine ionization yield and recombination probability of the charge carriers before their collection. The produced charges can recombine in two ways resulting in a collected charge which does not reflect the total energy deposited in the chamber. Initial recombination occurs within the track of the incoming particle before the ions and electrons become separated by the applied electric field or diffusion. The proportion of ions removed this way is independent of dose rate. Initial recombination is not significant for ionization chambers at atmospheric pressure except for very heavy or very slow ions. This allows the use of an electric field parallel to the particle track to collect the ionization charge. General recombination takes place while the charges migrate through the gas and is a function of the density of charge carriers throughout the active volume.

The collection efficiency of the ionization chamber depends not only on its design but also on the time structure of the radiation, *i.e.*, whether the radiation is continuous, pulsed, or fluctuating. The collection efficiency is the reciprocal of the ion-recombination correction factor, P_{ion}, whose use was

recommended by the 1983 AAPM protocol for dosimetry of high-energy photon and electron beams.[417] The collection efficiency = $1 / P_{ion} = q / q_{sat}$, where q_{sat} is the generated charge and q is the collected charge in an ionization chamber. Boag and Currant reported on a two-voltage technique for determining the collecting efficiency of a chamber exposed to pulsed radiation.[398, 418] Almond applied this technique to continuous radiation,[419] Boag used it for pulsed-swept electron beams,[420] and Hayakawa *et al.* applied it to compensate for beam intensity fluctuation.[421]

Gases such as nitrogen, air, tissue-equivalent gas, and argon, have been regularly used in ionization chambers. Nitrogen gas or air are most commonly used because their ionization potential, W, and stopping power ratio of gas to tissue, S_m, are well known and their saturation levels are acceptable at beam intensities used for radiotherapy and radiosurgery. Air is also practical because its temperature and pressure variations can be easily measured and corrected for and the humidity of the air has a negligible effect on the detector response.[405] At high beam intensities where saturation effects become important an inert gas which does not form negative ions, such as Ar or He, can be used. For example, recombination effects for Ne ions would not be expected up to 200 Gy/sec for Ar gas as compared to 20 Gy/sec with air. For higher yields Xe can be used with a lower W-value and a higher density. For fast response times He has been used because of its higher ion drift velocity.

The voltage applied between the planes must be high enough to collect the charge before appreciable recombination occurs. A measurement of the charge collection efficiency as a function of the high voltage is necessary to establish the operating range of the chamber. A limiting voltage, V_{min}, at which the collection efficiency falls significantly below unity for transmission ionization chambers is given by:

$$V_{min} = 5.65 \times 10^{10} \rho d^2 \qquad (44)$$

where ρ (C/m^3) is the ionization density and d (m) is the separation between planes.[398, 422] Typically, voltages above 500 V provide better than 98% collection efficiency at treatment dose rates of 1.0 Gy/min for separations of 1.0 cm.

III.A.4 Calibration methods for ionization chambers

The dose absorbed by an ionization chamber and averaged over the sensitive area can be calculated from the charge collected during the irradiation, the charge collecting volume, pressure and temperature of the gas in the active volume, and the W-value.[423] By correcting the ionization chamber reading with the ratio of the stopping power in the gas and that of another material, for example tissue, the dose which would have been received by the other material in place of the ionization chamber can be deduced.

Mainly because of uncertainties in the W-value, it is desirable to calibrate an ionization chamber against some other method before using it in a dosimetry system. For irradiation with monoenergetic particles a Faraday cup can be used as a calibration device (see Sec. III.D.7). In practice, however, Faraday cup measurements exhibit errors of up to ±5% mainly because of uncertainties in the charge collection and, secondly, because light ion beams often contain an added mixture of secondary particles. The most basic and absolute measurement of absorbed dose is done with a calorimeter which measures the deposited energy independently of particle type and energy. Water calorimeters have successfully been used and can serve as a calibration standard.

Because calorimetric measurements are very cumbersome and laborious, ionization chambers whose calibration is traceable to NIST standards are used to calibrate other ionization chambers used in a dosimetry system. Since at NIST the ionization chambers are calibrated with a particular type of radiation, for example Co^{60}, a correction factor has to be applied when the chamber is used in a heavy charged-particle field.[234] Although this method does not result in an absolute calibration, it provides for reliable relative calibrations.

In order to be able to measure on-line the dose received by a patient, a second type of calibration is needed. The ionization chamber and other dosimetric measurements of the radiation field have to be related to the dose absorbed in the target volume at isocenter.[268] This is best done by placing a small calibration detector, usually a NIST-calibrated thimble ionization chamber in a tissue equivalent phantom simulating the treatment geometry and calibrating the dosimeters against it.

III.B. Electronics for dosimetry system

III.B.1. Requirements on dosimetric electronics

Ionization chambers have a charge output proportional to the deposited dose. Because the clinical beams originating from an accelerator have temporal structures, measuring the dose means measuring the total charge as an integral of a fluctuating current. The electronics for these devices are generally some form of charge integrator with a response time fast enough for control purposes. For example a preset scalar, connected to the output of a charge integrator, may be set at the onset of an irradiation to a predetermined number such that when the scaled output of the integrator reaches the preset count the beam is either shut off or moved to another position in the target. In addition, this electronics must be linear over a large dynamic range to allow measurements at different dose rates, accurate to a few percent over the required dynamic range, insensitive to noise, and fast enough to accommodate the unexpected variability of the accelerator output, especially at high instantaneous beam currents.

Typical radiation doses used for heavy charged-particle radiotherapy range from 1 mGy used in exposing diagnostic x-ray films to heavy charged-particle beams for the purpose of patient alignment

to ~10 Gy used for treating ocular melanomas. As an illustration, an ionization chamber using nitrogen gas at atmospheric pressure and room temperature with a 1.0 cm^3 volume exposed to such a radiation source produces between 35 pC to 0.35 μC. Accounting for the variation in volumes that are used in an ionization chamber requires the current integrator to be able to measure as little as 10 pC and as large as 3.5 μC. The rate at which this dose can be delivered can vary from 10^{-3} to 1 Gy/sec and even higher instantaneous dose rates, leading to saturation of the electronics. As saturation leads to an inaccurate count of the charge produced in the detector and results in an incorrect dose measurement, some means of detecting a saturation condition is necessary.

III.B.2. Recycling integrators

A form of charge integrator that is particularly well suited to clinical applications is one which issues a pulse for every fixed increment of input charge. A standard circuit for this purpose is the charge balancing current integrator or recycling integrator,[424-426] whose charge to pulse conversion is sensitive enough that any residual charge smaller than one pulse can be ignored. When used with digital electronics these circuits have following major advantages over conventional integrators: a large dynamic range, exceptional linearity, and excellent noise immunity. A simple integrator designed for use at the highest current levels suffers at low current levels where the small output signal is difficult to discriminate from noise and is difficult to digitize with sufficient resolution. Another alternative is an integrator with variable ranges. Such a system is not suited for dose monitoring since the proper range must be selected before the measurement is made, and in clinical situations the selection must be always correct.

A recycling integrator, as shown in Fig. 59, works in the following manner. A specified input charge, called a unit charge, accumulated on an input capacitor triggers a one-shot circuit. This in turn produces an output pulse and either switches on a current source for a fixed time or charges a second capacitor to a fixed voltage. The combination of precise time and current or discharge of the second capacitor subsequently decreases the input capacitor charge by a unit charge. The unit charge is small, typically between 1 and 10 pC. Discharge of the input capacitor in this manner is independent of its accumulating further charge from the input, preventing any loss of charge during the measuring process. Temperature variation in the discharge circuit must be compensated to maintain an accurate charge to pulse conversion.

If, in the time required to discharge the input capacitor, the incoming charge exceeds a unit charge the recycling integrator is in saturation. The recycling integrator will maintain its maximum output frequency and continue to store charge with some penalty in the linearity of the charge to pulse conversion. At some input current the input will no longer appear as a virtual ground and the charge measured will be incorrect. Current inputs that will saturate the recycling integrator must be

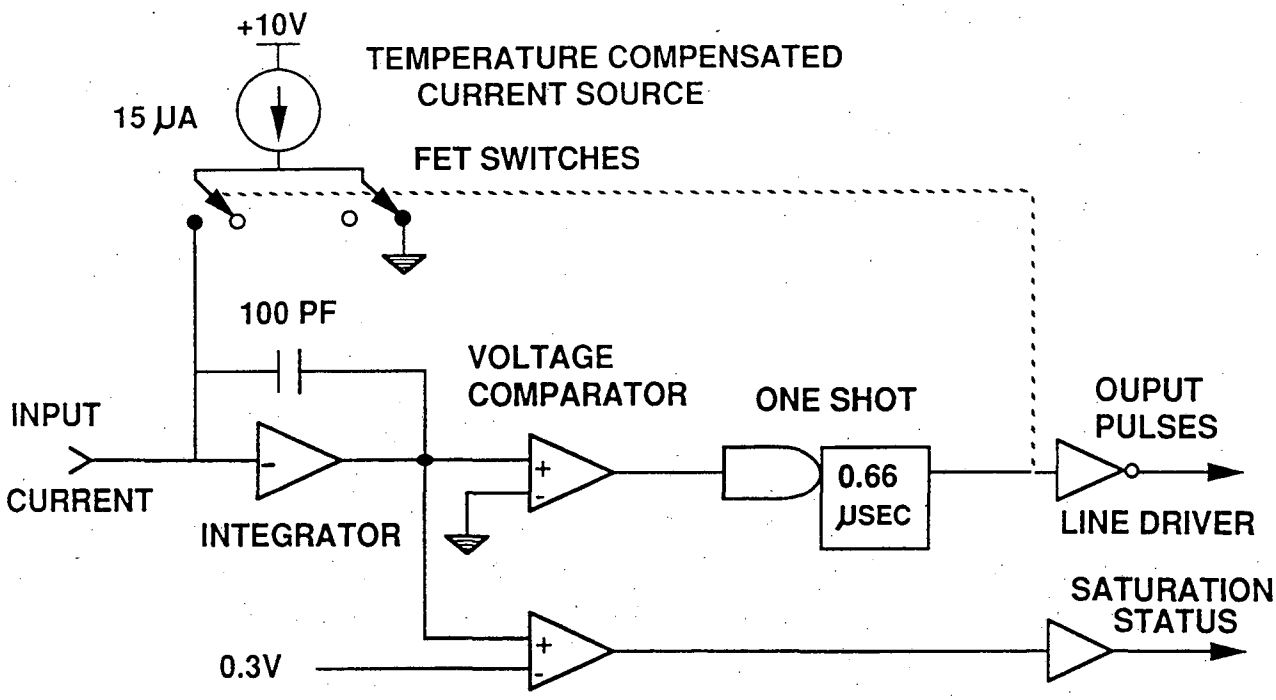

Fig. 59. Schematic of a recycling integrator used to measure the charge output produced by dose detectors for the clinical use of charged particle beams. (XBL 892-592)

detected so that corrective action can be taken. A simple frequency counter can signal the onset of such a condition once it is determined at what output frequency this occurs.

Due to unknown capacitance and charge sources that may occur between detector and recycling integrator, a small bias must be applied to each recycling integrator channel to compensate for the resulting unknown input leakage current. This unknown bias can cause a charge loss from the ionization chamber to the recycling integrator and lead to a dose measurement error. This small intentional bias can also be used to insure that a circuit is working since the small output frequency can be read by the control system for consistency. A background adjustment is made to compensate for this background current source. Calibration of the recycling integrators can be done in a straightforward way by means of a current source and a frequency counter.

III.C. Other Radiation Detectors

Many other kinds of detectors can be used for measuring radiation. Several of the more common types will be discussed here in terms of their medical applications.

III.C.1. Secondary emission monitors

Saturation in ionization chambers can be a major problem in their use as dose-detecting devices. Secondary emission monitors (SEM) can serve as alternative detectors to ionization chambers.[427] Though they can not be used as primary dosimeters, they can be used as beam monitors when calibrated against an ionization chamber for the particular type of radiation to be measured.[268] Saturation in these detectors has not been seen in electron beam current densities of up to tens of mA/cm^2,[428] making their use ideal in situations where there is a concern about ionization chamber saturation. The output of these devices is expected to be linear until space charge effects become important which has been estimated to be above ~10^9 Gy/sec. Another advantage of a SEM detector is its fast response time, which is determined by the travel time of the electrons rather than the slower migration time of ions in an ionization chamber. Responses in the nanosecond time scale are possible. Their major disadvantage is the low yield of secondary electrons per primary particle compared with ionization chambers. This limits their use for low beam particle fluxes.

An SEM consists of a set of parallel foils (as few as 2 to as many as 24) in a vacuum enclosure. The foils alternate between collection foils and bias foils. The more foils that are used, the greater is the signal. The number of secondary electrons depends on the energy deposited in the layer, called the escape zone. The work function of the material and the condition of the surface determine the thickness of this escape zone. The electron production scales linearly with foil thickness up to the point where electrons do not escape the foil. The efficiency of SEMs can vary from 10^{-2} to 1 where the efficiency is defined to be the secondary current divided by the primary current.

Aluminum foils of 6-μm thickness are commonly used to minimize the material in the beam and still retain enough strength and durability for easy handling and extended operation. The foils are typically separated by 3 mm and are made large enough to encompass the entire beam. Good vacuum in the chamber is important for keeping the foil surfaces free of absorbed material which can affect the electron emission. Pressure below 1 mP reduces the ionization of the residual gas to an acceptable level; however, the better the vacuum the more consistent the performance. A vacuum of 1 μP is used for radiotherapy purposes and beam line monitoring. A bias voltage of approximately -50 V is applied to the bias foil to insure nearly complete collection of the electrons which have energies less than 25 eV. Bias voltages above this value begin to collect the higher energy component of the electron spectrum coming from delta electrons, whose production is more dependent on the primary particle species and energies used.

Accuracy of an SEM detector can be better than 1.0% and the long term stability of its output is excellent, making it ideal for radiotherapy use. An absolute calibration of the SEM can be done against a calibrated ionization chamber. A fluence calibration can also be made by using the foil activation technique, a calorimeter, or a Faraday cup, as discussed below.

III.C.2. Wire chambers

In radiotherapy with heavy charged particles, wire chambers are primarily used for beam monitoring during beam line tuning. The beam characteristics of interest are: locating the centroid of the beam spot within 1 mm, and monitoring the beam shape, which is generally Gaussian-like with σ varying between 1 cm and 15 cm. The fact that good spatial resolution is obtained with a small number of signals and variable sensitivity make these devices extremely practical for this purpose. The principles of construction and operations of wire chambers have been discussed widely,[429] and here only the pertinent information related to their clinical applications is presented.

In the simplest form, a wire chamber consists of two planes of evenly spaced parallel wires separated by a given distance, and the intervening volume filled with gas. One wire plane is used as the signal plane, and the other as the high voltage plane. The high voltage plane can also be a solid foil conductor instead of parallel wires. While the common application of wire chambers in particle physics is to count traversing particles on a particle-by-particle basis, in medical applications wire chambers are more often used as integrating devices that integrate spatially along a wire as well as temporally during an irradiation procedure. Beam intensities from 0.1 pA to 0.1 mA are used for experiments ranging from microdosimetry to radioactive beam imaging.

Wire chambers are typically operated in a proportional mode where a multiplication of the initial ionization occurs, but can be operated in an ionization mode where the gain is unity. In the former mode multiplication of the initial ionization occurs when the ionized electrons, accelerated by the strong potential gradient around a wire, cause further ionization. The gain is dependent on the gas used, its pressure, and the wire spacing, and is an exponential function of the high voltage. By decreasing the wire spacing, increased spatial resolution can be achieved at the price of decreased gain due to the decrease in potential gradient around the wires.[429, 430] Wire spacing as coarse as 6 mm and as fine as 0.2 mm are practical. Gold coated beryllium/copper wires of 50 μm diameter are a good choice because of their longevity and mechanical stability in the beam. Common gases used in such devices are air, argon, or gas mixtures such as 10% argon and 90% CO_2. Atmospheric pressure is a convenient gas pressure; however, lower as well as higher pressures have been used. For example, at NIRS, to avoid the recombination effect due to the high instantaneous rate of 2 X 10^6 Gy/min of the pulsed beam, wire chambers have been operated at 0.2 Torr.[267] With the use of very thin entrance and exit windows, a water equivalent thickness for the chamber of a fraction of 1 mm can be achieved. With thicker windows the wire chambers have operated at atmospheric pressure in a beam pipe under vacuum.

III.C.2.a. On-line monitoring of beam profile and centroid position

Two planes of orthogonal sense wires can show the horizontal and vertical projections of the beam profile. The centroid and the width of the beam can be computed in each plane for beam-

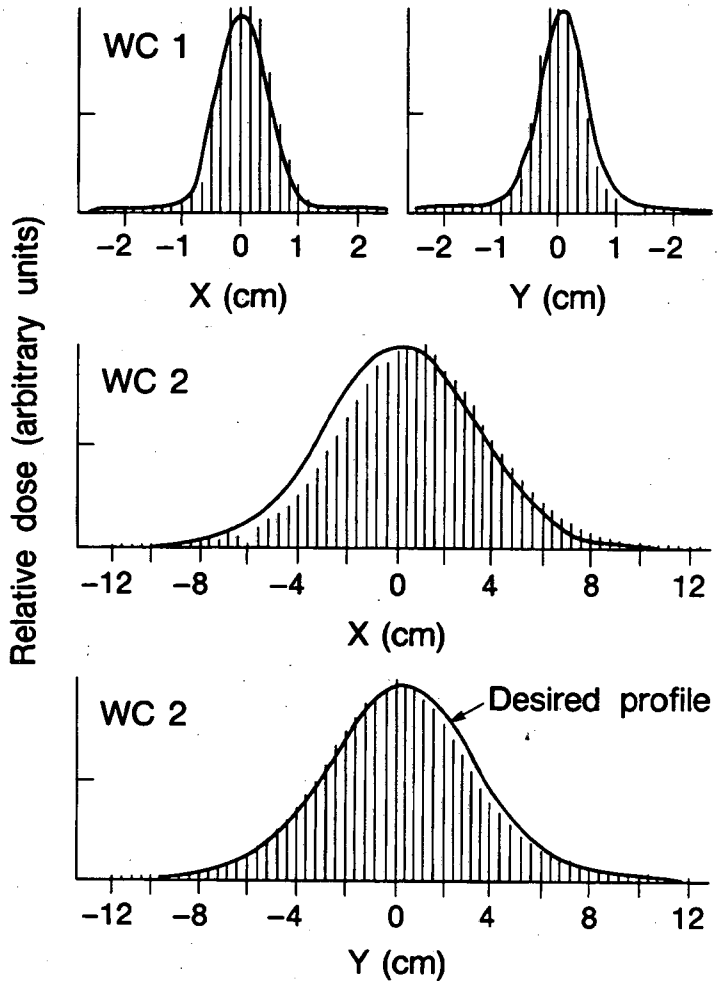

Fig. 60. Comparison between a measured beam profile and a standard expedites beam line tuning and facilitates beam line monitoring. Two detector outputs are shown. (XBL 854-9823A)

stability information. A comparison between the beam profile and a desired profile, as shown in Fig. 60, is a useful guide to the operator for tuning the beam delivery system. Monitoring beam profiles is important for efficiently transporting the beam and obtaining the correct dose distributions with the beam delivery system. Typically a wire chamber is positioned upstream of the beam delivery system and a second wire chamber is located downstream of the delivery system, near the patient. The active area of the second chamber is typically large to accommodate the large radiation fields.

III.C.2.b. Dose-profile monitoring

At NIRS, a multiwire ionization chamber (MWIC) was developed to monitor the beam profile of the dose delivered by spot-scanning methods. The chamber is operated in an ionization mode. The chamber has one hundred 0.18-mm diameter, tin-plated copper collector wires, 12 mm long and spaced 1 mm apart. Two high-voltage planes are placed on either side of the collector-wire plane at a distance of 2.5 mm. Each wire is surrounded by a sensitive volume of 1 mm by 12 mm by 5 mm. The chamber has 1.5-mm thick Lucite windows.[383] A similar multiwire ionization profile monitor has been used at PARMS[267] and LLU.[143]

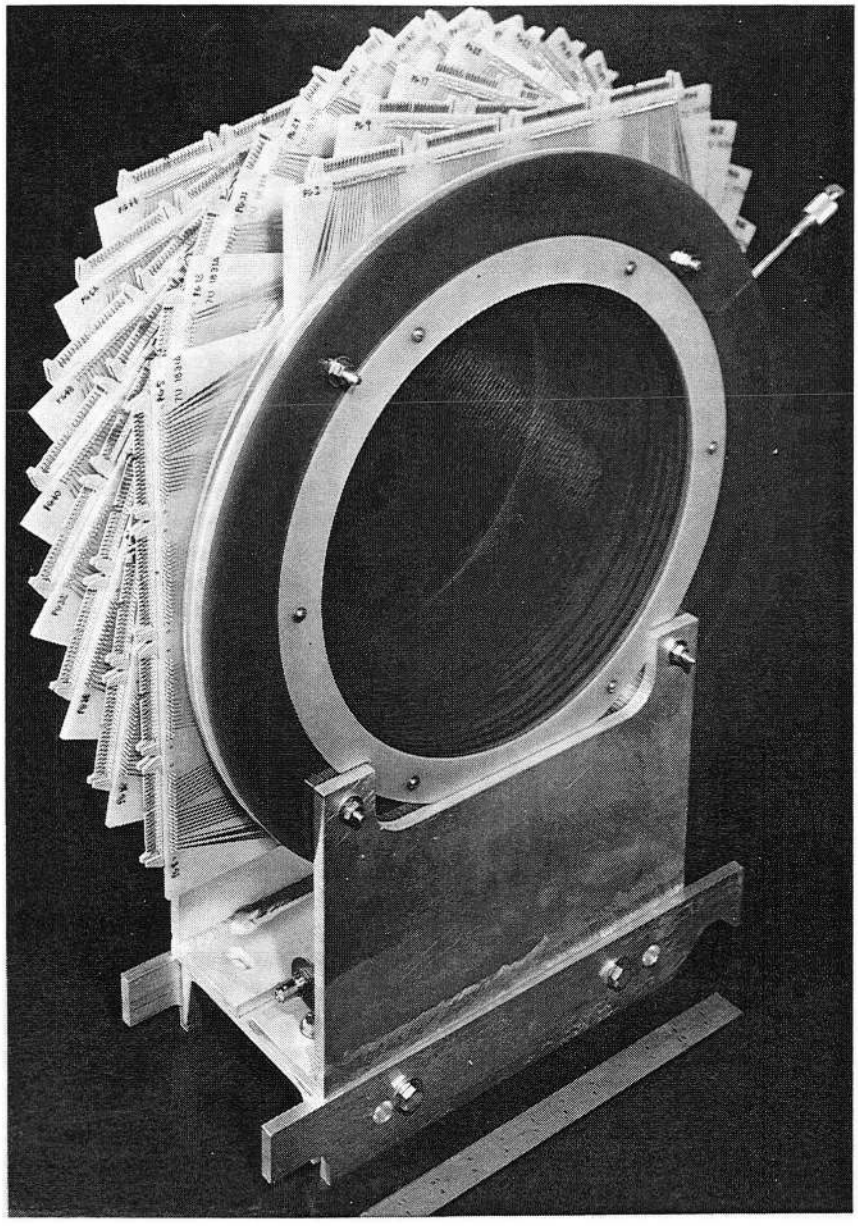

Fig. 61. This multiplane, multiwire chamber, called MEDUSA, is used to reconstruct dose distributions in two dimensions with 2 mm spatial resolution. (CBB 783-3335)

III.C.2.c. MEDUSA (Medical Dose Uniformity Sampler)

A multi-wire, multi-plane wire chamber, called MEDUSA, was developed at LBL to reconstruct the two-dimensional dose profile of a beam.[431-433] The device is illustrated in Fig. 61. It has 16 wire planes, each of which has 64 wires separated by 4 mm. Each plane samples the beam profile projected into the particular wire direction, which is offset by 11.25 degrees (180 degrees divided into 16 equal angles) from adjacent planes. Based on the 16 projected profile data sets, MEDUSA reconstructs the 2-dimensional dose profile within a circular area of 256-mm diameter. The reconstruction of the two dimensional image relies on the "filtered back projection" algorithm.[434]

To increase the spatial resolution of MEDUSA without constructing more data channels, another wire chamber has been constructed and the MEDUSA electronics reconfigured. In this configuration, there are three sense wire planes, each containing 300 wires with a wire spacing of 1 mm. The three planes have been mounted in separate chambers on a circular bearing, centered on the

beam axis. Relative angular displacements of the three chambers can be varied; for example, the three chambers can be placed at 60 degrees from each other. A simultaneous exposure of these chambers in an ionization mode gives information on the circular symmetry of the beam.

For a more detailed representation, the triple chamber can be rotated to predetermined angular positions between sequential exposures to obtain a larger number of projections of the beam profile in various directions. For example, the three chambers can be mounted with their wire directions at 0, 60, and 120 degrees, and the entire triple chamber system rotated by an angular increment of 5 degrees between exposures. Twelve sequential exposures provide 36 projections of the beam profile sampled every 5 degrees covering the entire 180-degree space. The 12 sequential sets of data are then normalized and used for reconstruction of the dose distribution of the beam. If a single beam pulse is used for each angular position, then one would obtain a cross-sectional image of the radiation field with good resolution after 12 pulses.

III.C.2.d. Wire chambers for measurement of LET distributions

Characterizing the heavy charged-particle beam profiles used for therapy, the distribution of LET is important in the understanding of the clinical efficacy of the beam. Detectors such as the BERKLET, time-of-flight spectrometers, or microdosimetry detectors, have been designed to measure the LET distribution at a given point in the radiation field. To obtain a 2-dimensional LET profile, such devices have to be moved to various points in the radiation field and independent measurements must made. Because of their counting rate limitations, characterization of the LET profile of the radiation field by such devices is prohibitively time consuming.

A high resolution wire chamber has been constructed at LBL to measure such 2-dimensional LET distribution. Two wire chambers, each equipped with 100 wires, spaced 1 mm apart, are placed with their wire orientations orthogonal to each other. Adjustable thresholds for the signal from each wire allow the selection of a minimum LET. A particle with a LET value above this threshold is detected and its x and y coordinates determined. Even though this device counts single particles, by counting for a period of time a two-dimensional profile of particles above the threshold is measured. By repeating the measurements with different thresholds, a two-dimensional differential-LET map of the radiation field can be made.[435]

III.D. Other Types of Dosimeters

Several types of devices other than ionization chambers, SEMs, and wire chambers have been successfully used to measure the dose deposited by heavy charged-particle beams. Each has its special application. Several of these detectors have also been integrated into systems for measuring

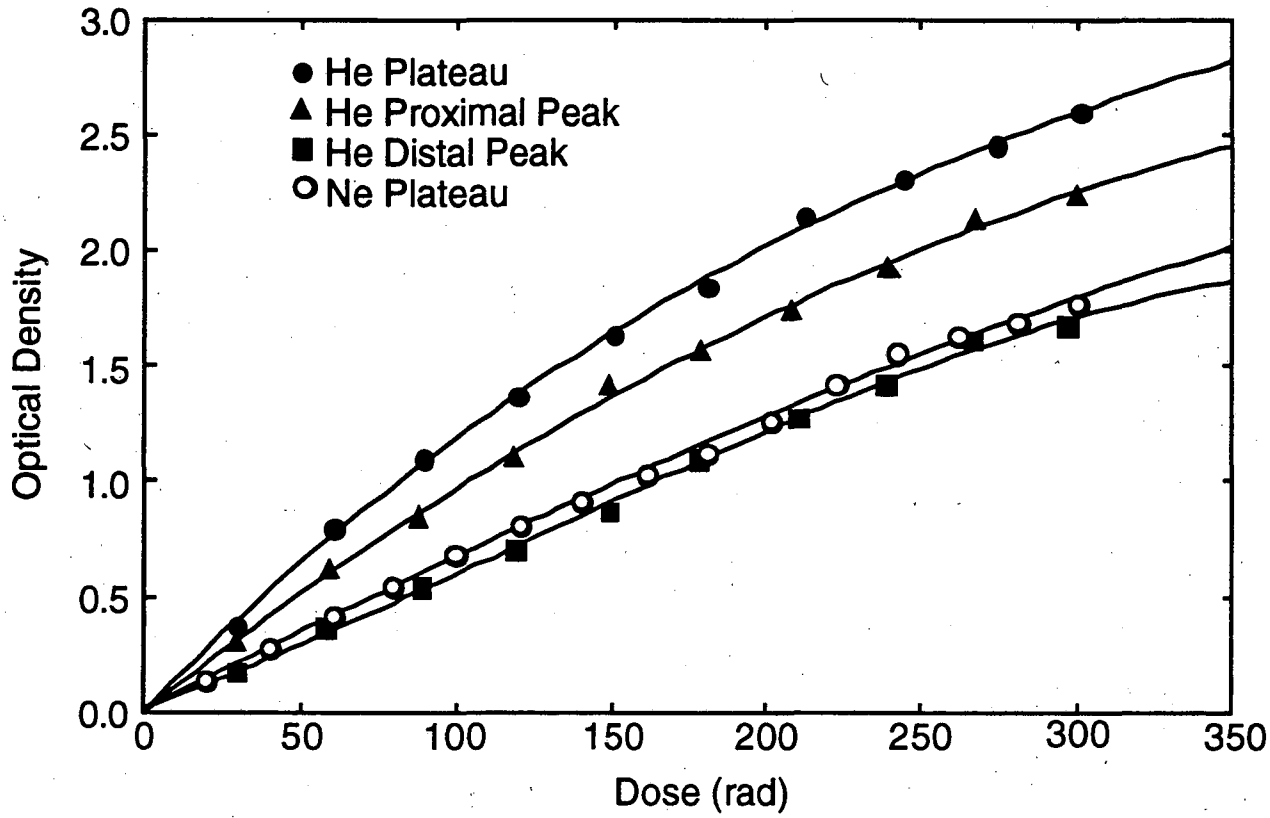

Fig. 62. Plot of optical density versus dose for He and Neon ions exposing Kodak XV film. The response is nonlinear with dose and is dependent on ion and the LET of the beam. The lines are to guide the eye.

the composition of the beam under various conditions. The resulting characterizations have been used both for clinical purposes and to compute cell response predictions based on biological models.

III.D.1. Diodes

The usefulness of diodes as dose detectors derives from their small size.[436] Measuring dose distributions with fine spatial resolution is difficult with ionization chambers, but simple with diodes which intrinsically have small active areas. As a solid, they absorb a lot more dose in a small volume. A calibration of the diode must be done before use since they suffer radiation damage over extended exposure. They are however excellent for relative measurements over short time periods. Arrays of diodes have successfully been used for measuring profiles of radiation fields and Bragg ionization curves.[437]

III.D.2. Film

Film has been used since the discovery of x rays (actually the x ray was discovered by observing the blackening of film) and is still the most economical method for measuring spatial dose

distributions with fine spatial resolution. Clinical dosimetry of complex dose distribution associated with charged-particle radiotherapy requires a rapid and convenient technique with good spatial resolution. The spatial resolution achievable with film is better than that of any other method. It is limited by the resolution of the digitizing procedure which, in turn, is limited by the time required for digitization and data reduction. The darkening of the film, *i.e.*, optical density, after exposure to a heavy charged-particle beam depends more on the particle fluence than the dose deposited. In other words, it depends on the LET of the particles.[438] For this reason film is primarily a relative dose detector and is used for measuring lateral dose distributions rather than depth-dose distributions. Fig. 62 shows the response of Kodak XV film in terms of optical density verses dose for two different ions. The measurements were made at the plateau, proximal peak and distal peak of a He ion beam of an energy of 215 MeV, and the plateau of a Ne ion beam of an energy of 585 MeV.

The use of cellulose triacetate (CTA) film dosimeters have been also investigated with proton beams. The optical density change per unit absorbed dose is measured. The CTA dosimeter was found to be useful to obtain dose distributions with high spatial resolution in samples exposed to proton beams.[439]

III.D.3. Thermoluminescent dosimeters

Thermoluminescent dosimeters (TLDs) are inorganic materials, such as LiF or CaF_2, that do not scintillate promptly, but rather trap electron-hole pairs created from the exposure to ionizing radiation. Upon heating the exposed material, the trapped electrons can escape, leading to light emission which can be detected. The light output is a function of temperature, often called a glow curve; the total light output is then related to radiation exposure. The light output is a function of the LET and the particle species composition of the heavy charged-particle beams.[440] Thermoluminescent LiF dosimetry has been used to characterize the therapeutic heavy charged-particle beams.[438, 441, 442] These methods are not amenable to real-time analysis, but are useful for treatment verification purposes.

III.D.4. Chemical dosimeters

In chemical dosimetry, radiation dose is determined by measuring the chemical change produced in an irradiated medium.[443] The most well-known chemical dosimeter is the Fricke dosimeter, which is an aerated solution of ferrous sulfate in diluted sulfuric-acid medium. Measuring the ferric-ion yield from the oxidation of Fe^{+2} to Fe^{+3} by the interaction of the ionization and the ferrous ion is a measure of the deposited energy. The measurement of optical density of the irradiated solution at a specific wave length can be interpreted in terms of the ferric-ion density, which is in turn related to dose.[444, 445] An early example of measuring high-LET radiation by the chemical dosimeter was the measurements of the G value, the ratio of the number of Fe^{+3} over the energy deposited, of the

stopping nitrogen nuclei with the ferrous sulfate system at the Princeton Particle Accelerator by Schimmerling et al.[60]

III.D.5. Nuclear activation

Another method for determining the number of particles in an irradiation involves measuring the induced radioactivity by the beam in a thin foil. Foil activation utilizes the beam undergoing a nuclear reaction of known cross section in a foil of known thickness. The radioactive yield can then be measured by means of its decay over time and an calculation of the initial beam intensity can be made.[268] For example, the reaction $^{12}C+p \rightarrow ^{11}C+p+n$ has been used to determine absolute fluence and absorbed dose of heavy charged-particle beam for therapy.[64] Again this method is used more for verification than on-line analysis.

As a variation of the above method, *in vivo* dosimetry for assessing the integral dose of a proton irradiation have been studied by detecting the decay products of ^{11}C, ^{13}N and ^{15}O from tissue activation.[446]

III.D.6. Calorimeter

Calorimeters have been established as the absolute method for the calibration of dose.[69, 447-449] The rise in temperature of a material from the energy deposited in it by the beam is used for dose measurement. For water a temperature increase of $2.4 \times 10^{-4} K$ occurs per Grey of deposited dose, making accurate measurements difficult. Calorimeters are not practical means of measuring dose for on-line clinical dosimetry, but rather serve as calibration standards.[422]

III.D.7. Faraday Cup

These devices can be used to measure the number of particles by measuring the charges collected on an electrically isolated and evacuated container which stops the beam. Typical Faraday cup designs, which are discussed in literature,[403, 450] maximize their collection efficiency by considering the thickness of the cup, the guard-ring bias voltage, the uniformity of the bias field, the vacuum, and the effects of nuclear interactions.[403, 451] When monoenergetic heavy charged particles impinge upon the Faraday cup, the dose is calculated from the measured number of particles per unit area and the mass stopping power of the particle at the given energy in tissue.[253]

III.E. Specialized Detectors and Detector Systems

Several types of detector systems have been developed to measure the characteristics of heavy charged particle beams. Energy loss detectors such as silicon detectors or gas proportional counters have been used to measure the LET of the beam particles. Other detector types such as solid state Ge detectors or time-of-flight detectors have been used to measure the total energy of the particle.

Several of these detectors also have been integrated into systems for measuring the properties of the radiation under various conditions. The resulting characterizations have been used for clinical purposes and for biological modeling of the response of cells to radiation.

III.E.1. Semiconductor detectors

Semiconductor detectors such as Si surface barrier detectors or thin Ge detectors are excellent for measuring the energy loss of a particle since they have high sensitivity,[452, 453] and their response is independent of the particle type and proportional to the energy deposited. A much smaller amount of energy is required to produce an electron-hole pair compared to approximately 30 eV needed in a gas ionization chamber to produce an ion pair.[405] However, they do suffer from a pulse height defect associated with large energy depositions leading to recombination of electron-hole pairs.[229] A Ge crystal of sufficient thickness to stop an incoming particle can serve as a total energy detector. Ge detectors have excellent particle energy resolution, typically dE/E ~ 0.1%, but radiation damage can lead to a degradation in their energy resolution. These detectors are used primarily for single particle detection and are not suitable for measurements at normal clinical beam intensities.

III.E.2. Scintillators

Scintillators have been used extensively in high-energy and nuclear physics experiments for single particle detection.[454-456] In medical accelerators they have been used primarily for beam control because of their fast response time and large dynamic range of operation when used in conjunction with phototubes. When used to measure large beam currents, radiation damage to the solid scintillator can limit their lifetime and effect their response. A Xe gas scintillator has been used to control the beam at LLUMC.[457] Because light production in the scintillator is not simply proportional to the energy loss of the particle due to quenching,[458] their use as a dose detector requires special calibration.[459] Recently they have been used in conjunction with charged coupled devices (CCD cameras) to measure the lateral uniformity of a radiation field and to measure the scintillation light as a function of depth for range verification.[460]

III.E.3. Solid-state nuclear track detectors

The passage of heavy charged particles through most insulators lead to the formation of narrow regions of radiation damages, called latent tracks.[461] In crystals, such a track may be detected by viewing with an electron microscope; and in polymers by means of special coloring of the track.[462] A more practical method is to etch the latent tracks selectively, and view the etched tracks with an optical microscope.[463] The use of solid-state nuclear track detectors in experimental nuclear physics has been reviewed recently by Tret'yakova.[464] Lists of commercial sources of most commonly used

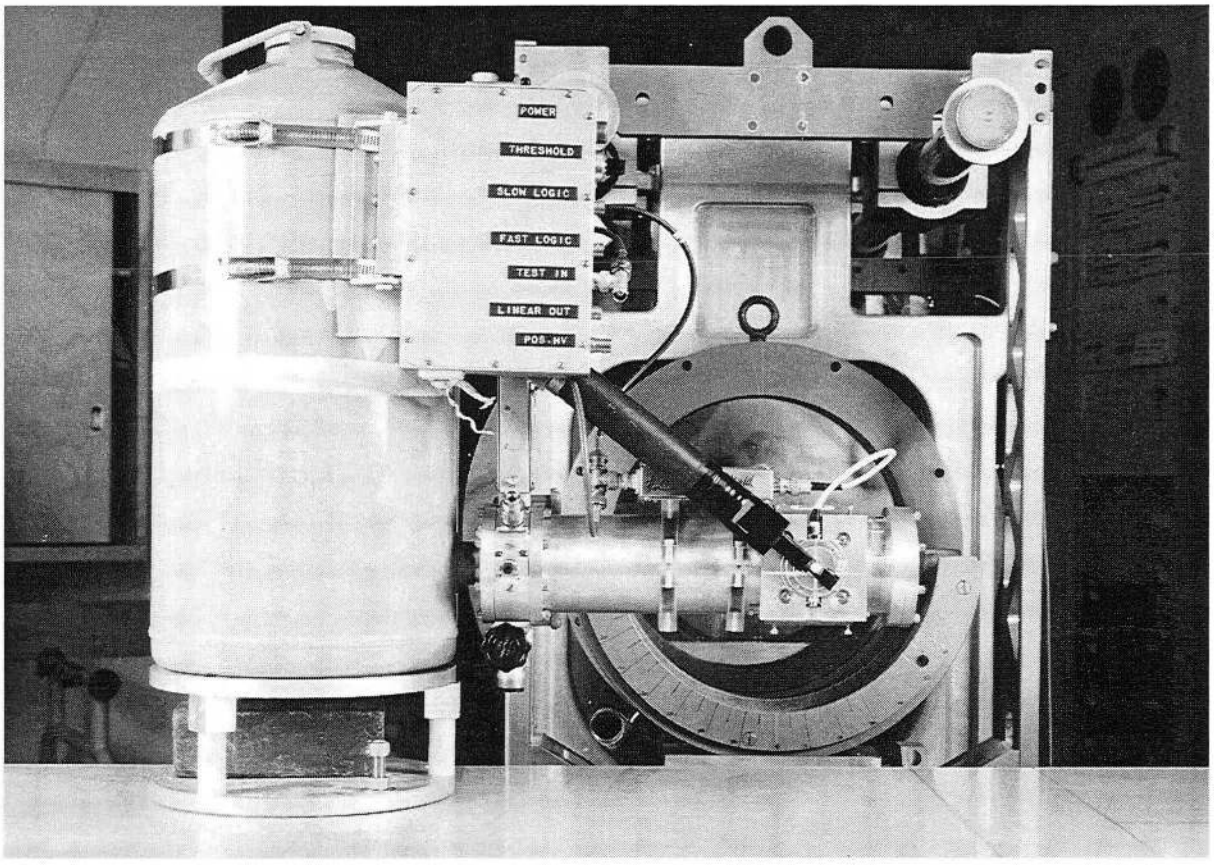

Fig. 63. The detector system, known as the BERKLET, is used to measure characteristics of radiation fields produced by heavy, charged-particle beams. (CBB 875-4111)

material for solid-state nuclear track detectors are found in a publication by Fleischer, Price and Walker.[465]

When a plastic sheet, exposed to heavy charged-particle beams, is etched, the radiation damage to the plastic sheet is made visible. The beam characteristics can be determined by examining individual etched tracks. This can be done under a microscope, by scanning optically and digitizing individual tracks or by measuring the area-density of scattered lights, or even by measuring the gas permeability through the etched plastics. Plastics such as CR39 have been extensively used to measure the LET distribution of heavy charged-particle beams.[466, 467] Measurements of an individual track left by traversing or stopping heavy charged particle in plastic detectors render information about their dE/dx, A, Z, and sometimes velocity.[468-472] Using a stack of plastics, heavy-ion beams can be characterized in terms of LET and particle fluence distribution as a function of depth of penetration. Their use requires low fluences to allow resolution of individual particle

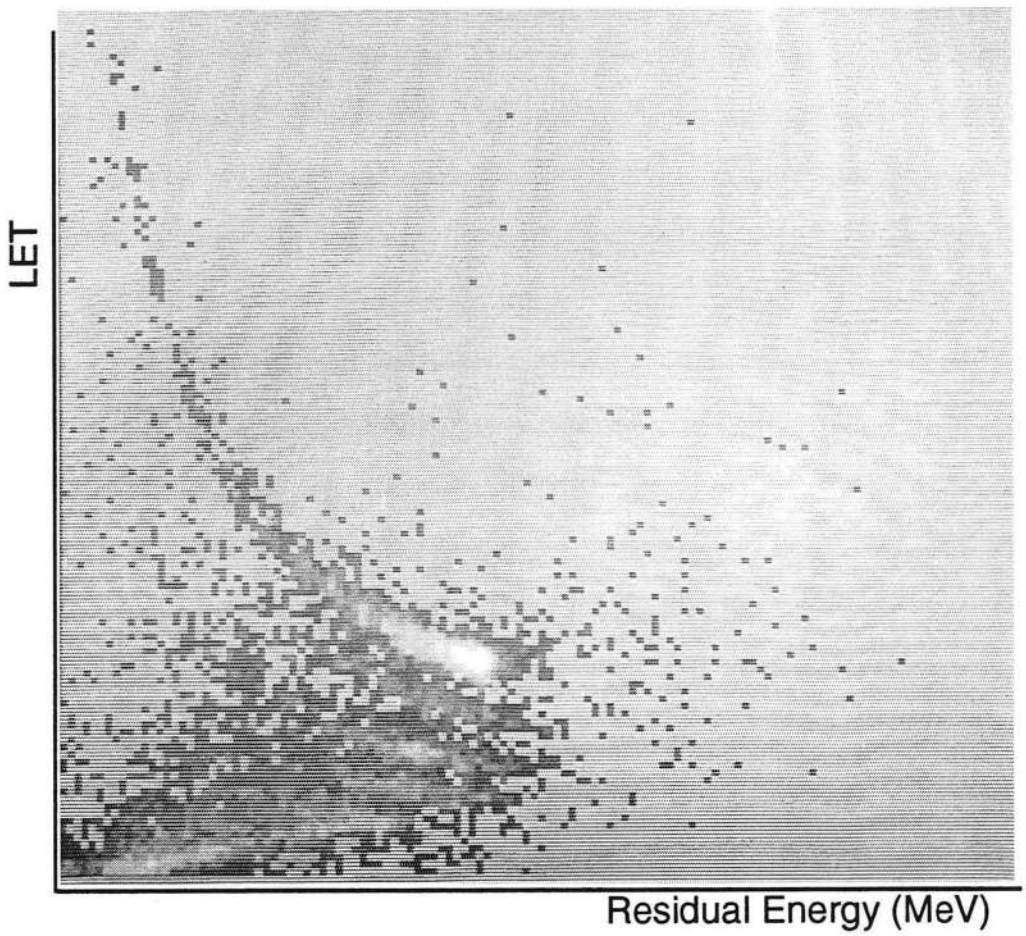

Fig. 64. A plot of residual energy of versus LET (or dE/dx) obtained with the BERKLET. The brightest spot is the primary beam particles. The bands are particles of a given charge that are produced in fragmentation reactions of the primary beam particles with the target nuclei. (CBB 875-4105)

rracks. While real-time measurements are not possible with these detectors, beam characterizations similar to those performed with solid state detector systems are possible.

III.E.4. Detector Systems

Because the biological damages due to high-LET radiation can not completely be described by the two parameters, namely dose and average LET, it has been recognized that there is a need to measure the actual composition of the beam in terms of the particles contained in it and their relative contributions to the biological damages. Studies of nuclear fragmentation and multiple scattering of heavy charged particle in various materials such as water, plastic, aluminum, brass, and lead have also been of clinical interest. These type of measurements however require more sophisticated detection systems which are described in the following Sections.

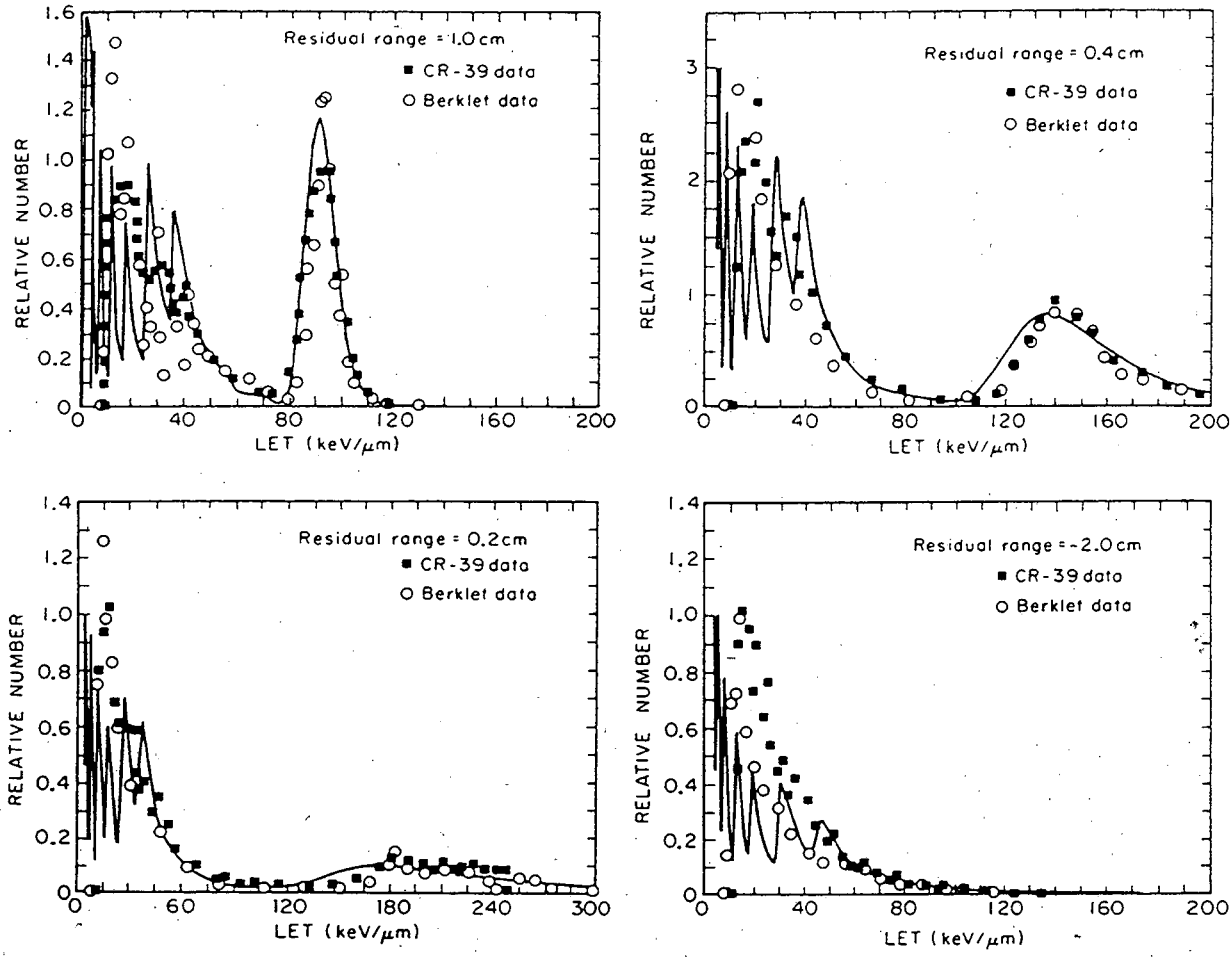

Fig. 65. A plot of LET versus residual energy as measured by the BERKLET and CR39 plastic. The four graphs represent different locations in the Bragg curve as indicated by the residual range. Good agreement is observed between the two types of detectors and calculations. (XBL 8311-4137)

III.E.5. BERKLET

A particle detector system known as the BERKLET, shown in Fig. 63, has been developed at LBL in order to identify the particle charge, but not mass, along with its residual energy and LET as shown in Fig. 64.[229, 247, 473, 474] Knowledge of the fluence of each particle species, or nuclear charge, as a function of LET can then be used as input for biological models to calculate the effects of the beam. This becomes especially important when the primary beam has traversed enough material to cause significant fragmentation of the primary beam, as previously indicated in Fig. 28.

The system consists of a 300-μm thick Si detector and a 5.5-cm thick Ge detector. The two detectors, operated in coincidence, measure the dE/dx and the total energy of the particle, respectively. The total energy that can be measured in the Ge detector corresponds to a particle with an 18.7-cm penetration in water. Particles with very low velocities or ranges in water less than 600 μm stop in the Si detector, and consequently cannot be identified. Because the system detects individual particles, its usefulness is limited to particle intensities much smaller than clinically used intensities. This prohibits its use under actual treatment conditions; however, conditions identical to treatment conditions at a reduced beam intensity can be measured. Furthermore damage to the detectors can occur with sufficient radiation exposure.[475]

The data from these measurements have been used with cell survival models to assist establishing the RBE of light ion beams in various clinical setups.[232] For example, studies of the LET of the tail region of spread Bragg ionization curves have been made to assess their biological significance. Fig. 65 shows LET spectra at several depths in water around the distal edge of a spread-out Bragg peak, measured in a ^{20}Ne beam of an energy per nucleon of 670 MeV, degraded by a 0.8-mm thick lead foil upstream, and approximately 32-cm water absorber.

III.E.6. Time-of-flight detectors

Time-of-flight systems using solid state detectors for velocity and for energy loss measurements have also been developed to analyze the particle composition of the beam in terms of mass, charge, energy loss, and velocity of the particle. These data have been analyzed to study the beam composition in similar fashion to the BERKLET data. The time-of-flight measurements give more detailed results since a direct velocity measurement is made along with energy and energy loss. A spectrometer for relativistic heavy ions has been developed and used to characterize the heavy ion beams at the Bevalac.[476-479] This device combines gas ionization chambers, solid state silicon detectors, NaI scintillation detectors, and a channel plate time-of-flight system.[480] The energy loss and total energy of a particle with mass, A, and charge, Z, were measured as a function of depth of penetration in water. The spectrometer was also used to measure the quantity W, the average energy to produce an ion pair in the medium.

III.E.7. Multiple scattering measurements

Another experiment utilizing position sensitive Si detectors at LBL measured multiple Coulomb scattering and compared the data against several scattering formulas. The results corroborated the accuracy of the formulas for Uranium ions with energy per nucleon of 650 MeV, thus validating their use for particles heavier than protons.[481] Multiple scattering measurements have also been done at HCL for protons on various targets with good agreement with theory.[320]

III.E.8. Microdosimetry

Microdosimetry measurements utilize gas proportional counters to study energy losses on the microscopic scale of a cell. Dose, being defined as a macroscopic quantity, does not account for the fluctuations, inhomogeneities and stochastic nature of the effect of radiation on matter,[482] even though these effects are important in understanding radiation biology of cells and smaller structures. To understand the effects of the inherently statistical nature of the energy deposition in a cell, a detector comparable in size to a cell is required.[483-489] Gas proportional counters are used with sizes and at gas pressures that replicate the energy deposition in a cell and which have enough gain for reasonable signal processing.[490-494]

IIV. Control System and Safety

The treatment of humans with radiation requires an accurate, reliable, and safe method for controlling the heavy charged-particle beam. The accurate delivery of the prescribed dose is essential for achieving the desired cure and preventing an overdose of radiation. The fact that humans are purposefully being exposed to radiation with a potential to harm, as well as help, makes the design and construction of control systems of critical importance, especially in the case of dynamic beam delivery systems.

IV.A. Control System

The beam produced by the accelerator and channeled through the beam line into the treatment room consists of monoenergetic particles focused in a narrow beam spot. Beam modifying devices as previously discussed (Sec. II) are needed for the generation of useful treatment fields. These devices combined with beam monitors and dosimeters (Sec. III) comprise what is called the beam delivery system. Conceptually and practically the beam delivery system is best separated from the accelerator by having two independent but communicating control systems.

The beam delivery control system requests beam with a specified energy, intensity, spot size and position from the accelerator, controls beam modifying devices, reads the beam monitors and dosimeters, and terminates the irradiation when required during the course of a treatment.[495] It may also control the positioning of the patient during the treatment. The system must operate at all times with a response time sufficient to provide monitoring systems and human operators information on the status of the radiation.[496] At the heart of the beam delivery control system is the beam monitoring or dosimetry system which ensures precise treatment delivery and patient safety.

IV.A.1. Dosimetry control system

The beam delivery system as shown in Fig. 66 is controlled by a central computer which receives the required input data from medical personnel or directly from a treatment planning computer. The

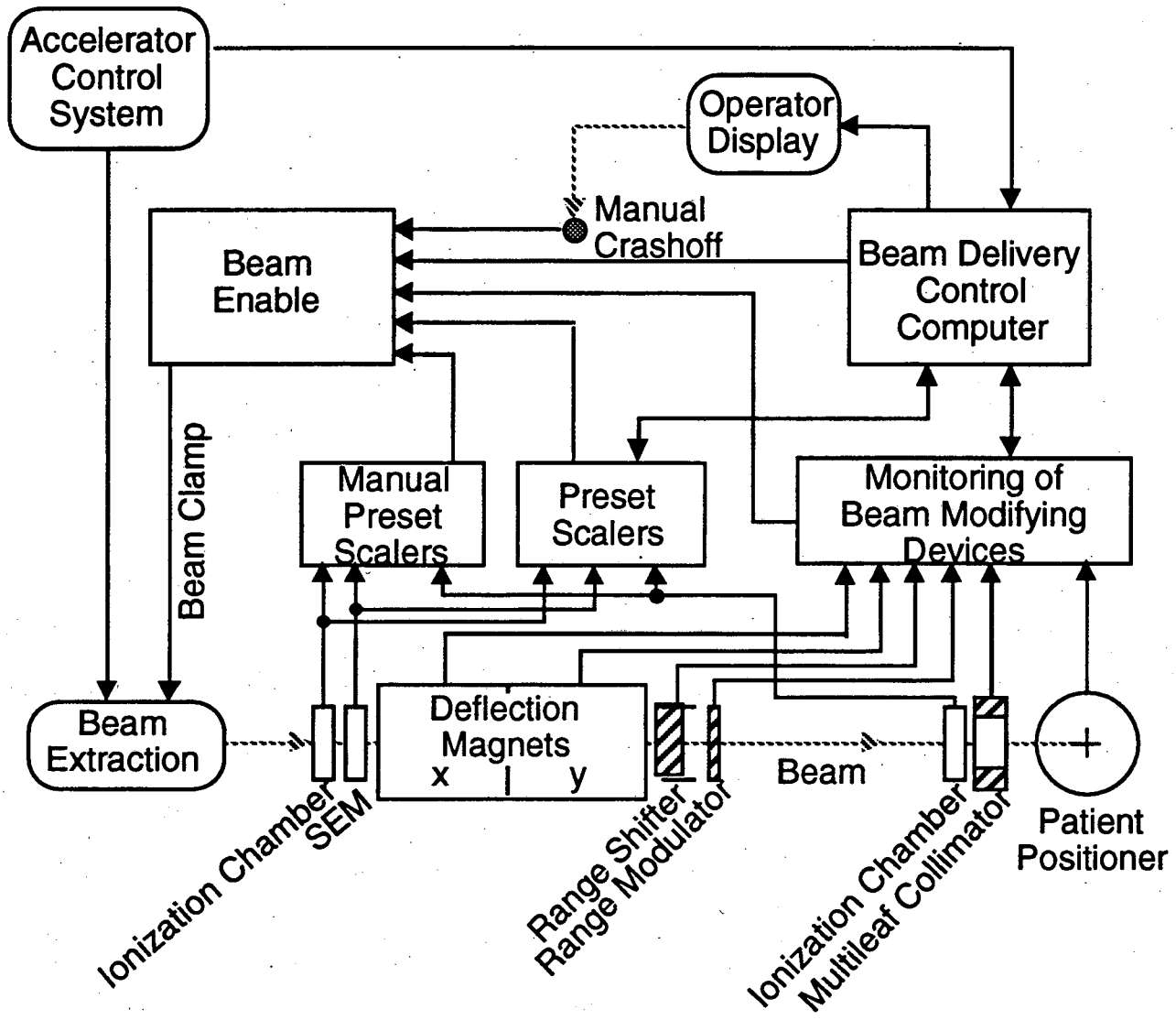

Fig. 66. A schematic of a control system for heavy charged-particle radiotherapy is shown.

physical devices and detectors are interfaced to the computer. Before beginning a treatment all beam-line devices are set to their initial values and checked by independently reading their status. During the treatment the beam modifying devices are set to new values whenever required and the dosimeters are read at fixed time intervals, which in the case of synchrotrons is after each beam pulse. Information on the status of the treatment is displayed for operator monitoring. On-line monitoring of critical parameters is done by the computer or by dedicated hardware where timing is critical. After the treatment has been finished a treatment summary is produced and archived.

IV.A.2. Dosimeters

Dosimeters for clinical use have three main functions: 1) the measurement of the dose delivered to the patient in real time, 2) the measurement of the spatial distribution of the radiation and 3) the monitoring of the radiation for control of the beam-delivery system. The first one allows termination of the treatment when appropriate. The second one insures the beam delivery system is modifying the beam properly. Heavy charged-particle beams from the accelerator undergo range changes, spatial deflections, and nuclear interactions before reaching the patient. The third one is required for dynamic beam-delivery systems for which it measures the distributions of the dose already delivered to determine the subsequent course of the irradiation.

In principle, if the beam is properly tuned and the beam delivery is functioning correctly, one calibrated detector is sufficient for measuring the delivered dose. In practice, however, depending on the complexity of the beam delivery system, several detectors, with possibly many elements, are needed for achieving the required level of accuracy and safety. The sensitivity of beam spreading systems to beam position, entrance angle, divergence, and intensity fluctuation makes beam monitoring extremely important. For redundancy a minimum of two dosimeters are required which can terminate the treatment independently of one another. Three dosimeters improve the overall reliability and safety of the control system. Three detectors also make determining which one is malfunctioning easier. The dosimetry systems used at LBL are based on transmission ionization chambers since they are the most basic and practical dose monitors (See Sec. III.A.2.a). Due to recombination effects in the gas of these chambers, there can be a saturation effect for high beam intensities. In order to guard against such saturation a SEM (Sec. III.C.1) is usually used as a third device to monitor the beam.

IV.A.3. Beam-line setup

Since a direct measurement of dose in the patient can not be easily done, the dosimeters must be calibrated against a reference ionization detector, typically a thimble ionization chamber, placed inside a phantom target volume in conditions similar to an actual treatment. For an actual treatment the detector response for a prescribed dose can be deduced from this calibration. Placing a monitoring detector as near the patient as possible, downstream of all beam modifying devices, helps to insure that the reading is closely related to the delivered dose.

A second ionization chamber is often located upstream of the beam-delivery system (Fig. 7) providing a normalization measurement of the unmodified beam. By monitoring the ratio of upstream and downstream detectors a malfunction of beam spreading and beam modulating devices located between them can be detected. When fields larger than a few centimeters in diameter are used, it is necessary to pay close attention to the field uniformity in passive as well as dynamic beam-spreading systems. A highly-segmented ionization chamber located as close as possible to the

patient collimator is best suited to provide the desired on-line information. The number of elements can range from several to a few thousand and their geometric arrangement can be tailored to the beam spreading system.

IV.B. Safety Systems

The way the beam and the dose delivery are monitored are largely dictated by safety considerations. Special care has to be taken in order to ensure safe operation of the beam modifying devices. To safeguard the patient, the system design must adhere to the following principles:

- For all devices, monitoring and control functions are performed independently.
- The hardware which can terminate the irradiation is independent of the control system.
- The beam parameters such as position, size, intensity, etc., are continuously monitored independently of the accelerator control system.
- The functioning of the beam spreading device is monitored by measuring on-line the dose distribution of the radiation field.
- At fixed intervals detector readings are compared with standard values to verify the correct function of the beam modulation and beam spreading devices.
- Absolute dose measurements are continuously monitored and displayed for operator surveillance.
- Any detected inconsistency or "out-of-tolerance" value initiates a termination of the irradiation.

It is preferable to provide a simulation capability in the control system. A method for assuring the systems reliability and safety without the use of radiation should be provided. The detectors, their electronics, the dosimetry system and the entire treatment control system may be tested by means of this simulation capability. Pretreatment testing of new software and hardware saves time and increases the user confidence in the treatment system performance.

V. IMAGING

Heavy charged-particle imaging, such as heavy charged-particle computed tomography (CT), is of interest because it provides information of patient anatomy different from the information provided by x-ray computed tomography (xCT) or magnetic resonance imaging (MRI) techniques.[497] In particular, it provides information on the stopping power in the patient body. This information is needed in precision radiotherapy to align the depth of the Bragg peak accurately with the target volume. Three topics are discussed: (A) detection of the stopping region of energetic radioactive beams brought to rest inside the patient body; (B) detection of induced radioactivities at the end of the range of therapy beams; and (C) obtaining 2- and 3-dimensional distributions of stopping power inside the patient body through heavy charged-particle CT.

V.A. Accelerated Radioactive Beams

Two clinical applications of energetic radioactive nuclei beams have been explored at LBL.[498-500] The first use, as discussed below, is to determine the integrated stopping power of the patient body by measuring the range of the stopping radioactive beam. The second application is to measure the blood flow by depositing radioactive particles in a small blood volume at a specific location and measure the diffusion of the isotopes as a function of time by monitoring its decay.[501] This application is not discussed further in this article.

V.A.1. Radioactive beam ranging

One of the limiting factors in the attainable accuracy of placing the Bragg peak at a planned position in the target volume is the uncertainty in the knowledge of the stopping power of traversed heterogeneous medium, which may include irregularly shaped soft tissues, bone, lung tissues, or liquid and air passages. A therapy plan may be inaccurate if it is based on xCT data, which is a representation of various tissues in terms of their x-ray mass absorption coefficients. Since the x-ray absorption coefficients largely depend on electron densities, while the stopping power of the heavy charged particles depend on physical densities and atomic numbers (Z) of traversed media, substantial errors may occur if the xCT data are used in therapy planning for heavy charged particles. This is especially true when the beam traverses hydrogenous materials which have relatively high ratio of electron density over physical density. Although the xCT numbers for various tissues are calibrated for stopping powers before they are used in therapy planning,[241] such plans are found to render errors as large as ±5 mm in a 10 cm range.[502, 503] Some preliminary work has been done at LBL to verify the placement of the stopping region of the beam at the distal edge of the target volume in phantoms[504] and in real patients.[505] By substituting a radioactive beam to deliver a dose according to a therapy plan, and imaging the actual treatment volume, the conformation of the delivered dose with the target volume can be verified.[473] While a great deal more work is required to bring these uses to complete fruition in the clinic they have already been established as an important future application of heavy charged-particle beams.

V.A.1.a. Production and collection of accelerated radioactive beams

The basic mechanism for producing radioactive beams is nuclear fragmentation. When a beam of stable nuclei is aimed at a target, some of the projectile nuclei collide with the nuclei of the target material in what are known as peripheral collisions. In such peripheral collisions, the two nuclei knock off pieces (nucleons) of one another. In the process, new nuclei are created, some of which are radioactive and decay via particle emissions into daughter nuclei. The new radioactive nuclei produced from the projectile nuclei are of interest here. Such projectile fragments have momentum close to the original projectile nuclei and, as a consequence, are kinematically focused into a small,

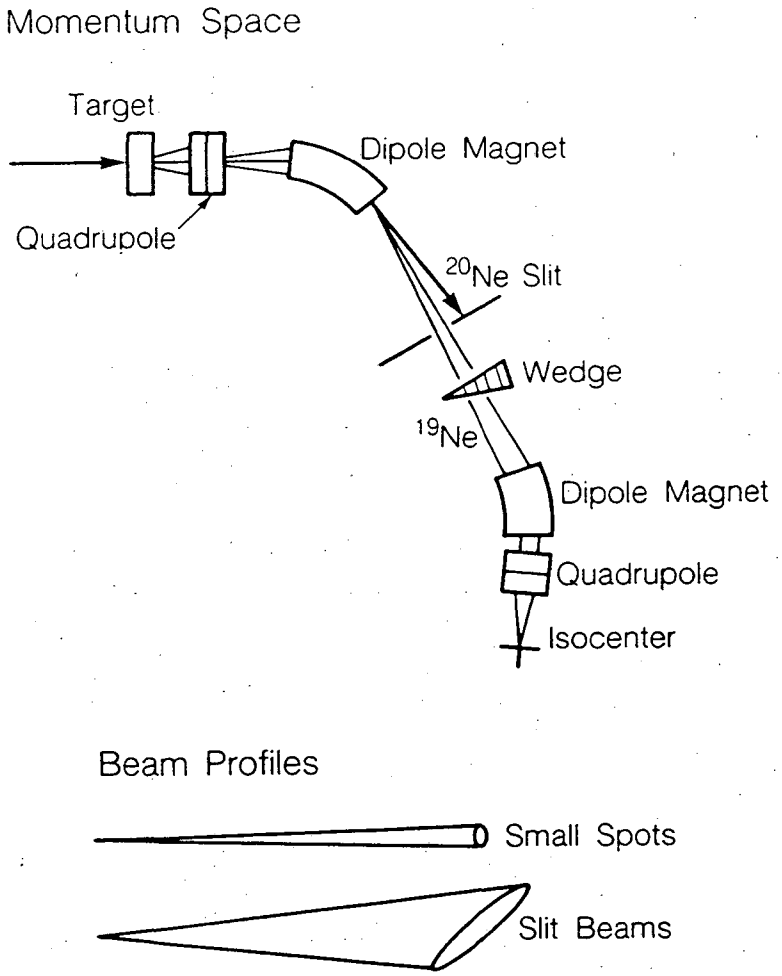

Fig. 67. A schematic of radioactive beam production. After production of the desired secondary beam in a target, the primary and secondary beams are separated by means of a spectrometer.

forward-directed cone. At clinically relevant energies, this cone has an angular opening on the order of a degree. The angular opening originates from the ratio of the transverse component of the Fermi momentum of the nucleons inside the spectator nucleus, ~200 MeV/c, over the projectile momentum. The secondaries can be separated from the primary beam by magnetic momentum analysis and collected, and transported from the production target to the treatment room.

The production cross-section of the radioactive nuclei and the target thickness determines the yield of radioactive nuclei. The momentum spread of the radioactive beam, the divergence of the primary and secondary beams, and the momentum difference of the desired nuclei from the primary beam and other radioactive nuclei determine the separation and collection efficiency. The momentum spread of the secondary beams and its divergence are larger than the primary beam after emerging from the thick production target. Production and collection of radioactive beams such as ^{19}Ne produced form ^{20}Ne and ^{11}C and ^{10}C from ^{12}C have been investigated at LBL.[506, 507]

One method of producing radioactive beams is to focus a primary beam onto a suitable (usually beryllium) target and to transport the mixed primary beam and secondary beams to an analyzing system for separation of the desired radioactive beam. The analyzing system consists of a analyzing (bending) magnet and a pair of slit collimators to define the momentum of the selected beam and to remove the unwanted beam. As an example, in the system for ^{19}Ne production at the Bevalac, a secondary to primary yield ratio of 1 to 300 is obtainable. After momentum analysis and separation the on-target yield is only 1 to 1000. The secondary beam is then passed through a wedge such that the higher momentum particles pass through the thicker part of the wedge so that the energy spread of the secondary beam is reduced.[508] The radioactive beam emerging from its production target has a large momentum spread ($\Delta p/p \approx 1\%$) which is reduced to $\Delta p/p \approx 0.1\%$ through this remonochromatization process. Finally the beam is refocused with electromagnetic quadrupole lenses to produce a circular or elliptical beam spot for imaging. A depiction of this production method is shown in Fig. 67.

An alternative production method recently proposed uses a 15-30 MeV proton or deuteron beam of high intensity on a suitable target to make radioactive ions. The radioactive ions are then extracted and transported to an electron cyclotron resonance (ECR) ion source where they are highly ionized and injected into a larger cyclotron for acceleration. This method potentially can provide more species of radioactive beams at much higher intensities.[509, 510]

V.A.1.b. Imaging of the radioactive beams by PEBA

The use of radioactive beams that decay via positron emission relies on the detection of the two nearly back-to-back gamma rays, each with an energy of ~511 keV, emitted after annihilation of the positron, *i.e.*, $e^+ + e^- = 2\gamma$. The positron emission for all practical purposes occurs after the radioactive nuclei come to rest in a stopping medium. The small range straggling and energy spread of the incident radioactive beam, the small recoil of the emitting nucleus, the low kinetic energy of the positron (hence a short travel distance, ~0.5 mm, between emission and annihilation of the positron), and the nearly 180-degree emission of the annihilation gamma rays allow placement of the line joining the two photons to the stopping point of the radioactive nucleus to within a few millimeters. Determination of the stopping point on the line is done in two ways. The first way is based on the time difference in the arrival of the two photons at the detectors.[511] This method is limited by the rise times of the detectors and the electronics, and the time resolution of these signals. The second method relies on the knowledge of the trajectory of the incident radioactive nuclei. If the trajectory is known, the stopping point can be determined within a few millimeters. The accuracy is limited by the multiple scattering of the incident particle in the medium before coming to a rest.

^{19}Ne beams with a half-life of approximately 18 seconds have been used clinically at the Bevalac to measure the stopping region of the beam in patients. A detector, called PEBA, that is similar to

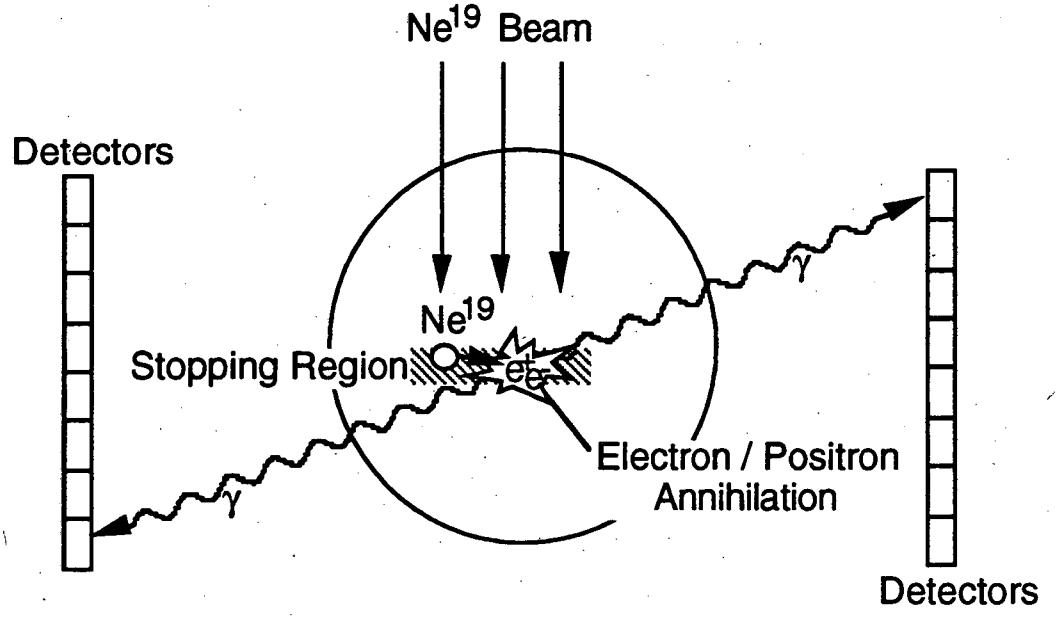

Fig. 68. A schematic showing how PEBA localizes a stopping radioactive (positron-emitting) nucleus by measuring the annihilation photons of the positron emitted by the decay of the nucleus. The transverse dimension of the stopping region of the Ne^{19} nuclei and distance between the stopping nucleus and the point of annihilation are greatly exaggerated in the figure.

PET (positron emission tomography), has been developed for imaging the gamma rays from the positron annihilation.[512, 513] PEBA consists of two arrays of 64 bismuth germinate (BiGe) scintillators in a 8×8 matrix arrangement, which are separated by a distance of ~1 meter. A target (patient) is positioned between the two arrays of detectors and the radioactive beam is stopped in the target. Each pair of gamma rays from the positron annihilation is detected in coincidence and a line following the trajectories of the two photons established. The trajectory of the incident radioactive beam and this line define the stopping region, as schematically shown in Fig. 68. It has been shown that, by accumulating many events, the centroid of the stopping region can be established with an accuracy of ~1 mm.

Because the BiGe scintillators are activated, largely by neutrons, if left near the patient during a treatment using full intensity beams, the PEBA must be removed from the irradiation room. Placement of the detectors must be done quickly and accurately before each use. To overcome this difficulty, replacement of the solid state detectors with more radiation resistant ones is considered, and a design based on multiwire proportional chambers has been suggested.[514]

In clinical use, range verification at a single point requires a tightly focused circular beam, while imaging along a line requires an elliptically-shaped beam. Such line imaging can be used to measure

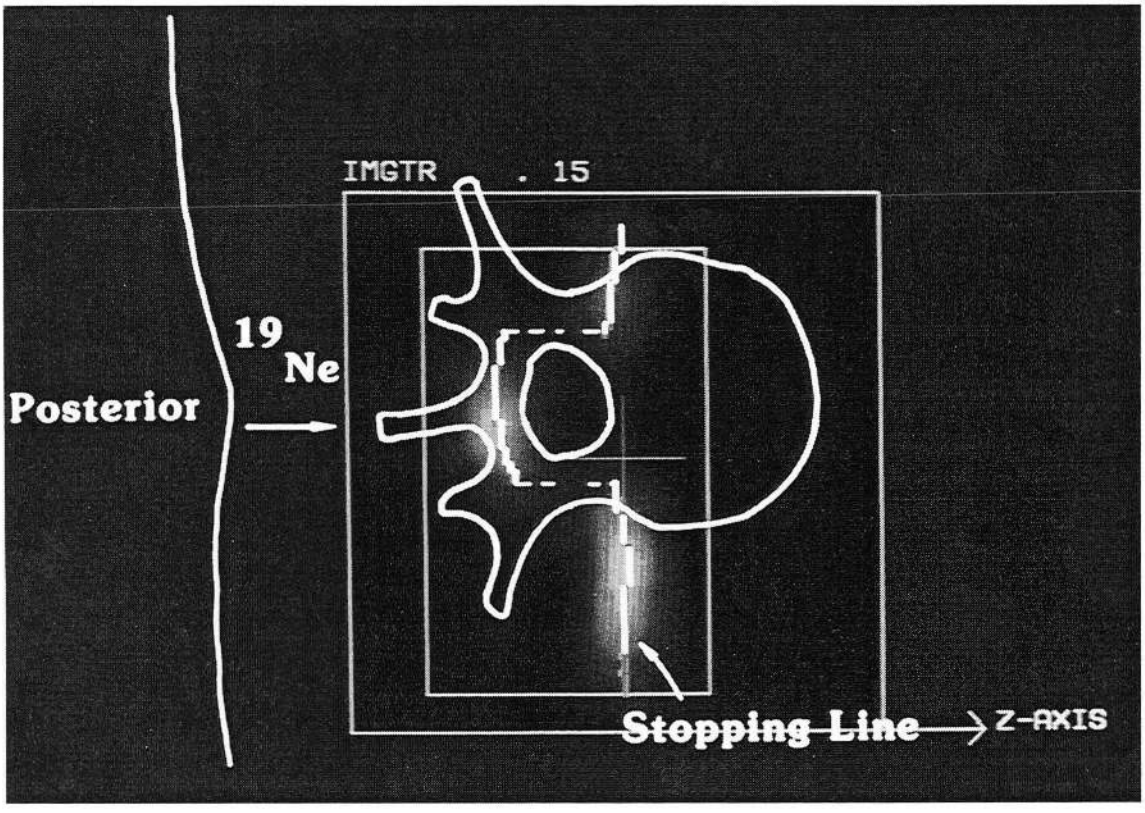

Fig. 69. An image of the stopping region of Ne^{19} created by a compensator to exclude the spinal cord region of a patient from the Bragg peak radiation. (XBC 865-4162)

the range modification created by a compensator or to verify that the range in fact conforms to the geometry of the anatomy being spared. See Fig. 69 for an example of a compensator modifying the stopping region to exclude the spinal cord region of a patient from the unwanted radiation. Three dimensional imaging is a future goal of this development.

V.B. In Vivo Activation of ^{15}O with Protons

When an energetic proton penetrates a tissue-like medium, it can produce ^{15}O by displacing a neutron from ^{16}O in the medium.[515-518] This phenomenon can also be utilized to localize the stopping region of the proton beam used in Bragg peak therapy. There are, however, several factors which affect the accuracy of this technique. The cross-section for the reaction ^{16}O (p, pn) ^{15}O has a broad peak at the proton energy of 50 MeV and a threshold energy of 20 MeV. The 20 MeV threshold energy implies that the last 4 mm of the range in soft tissue is not detectable. Next, the

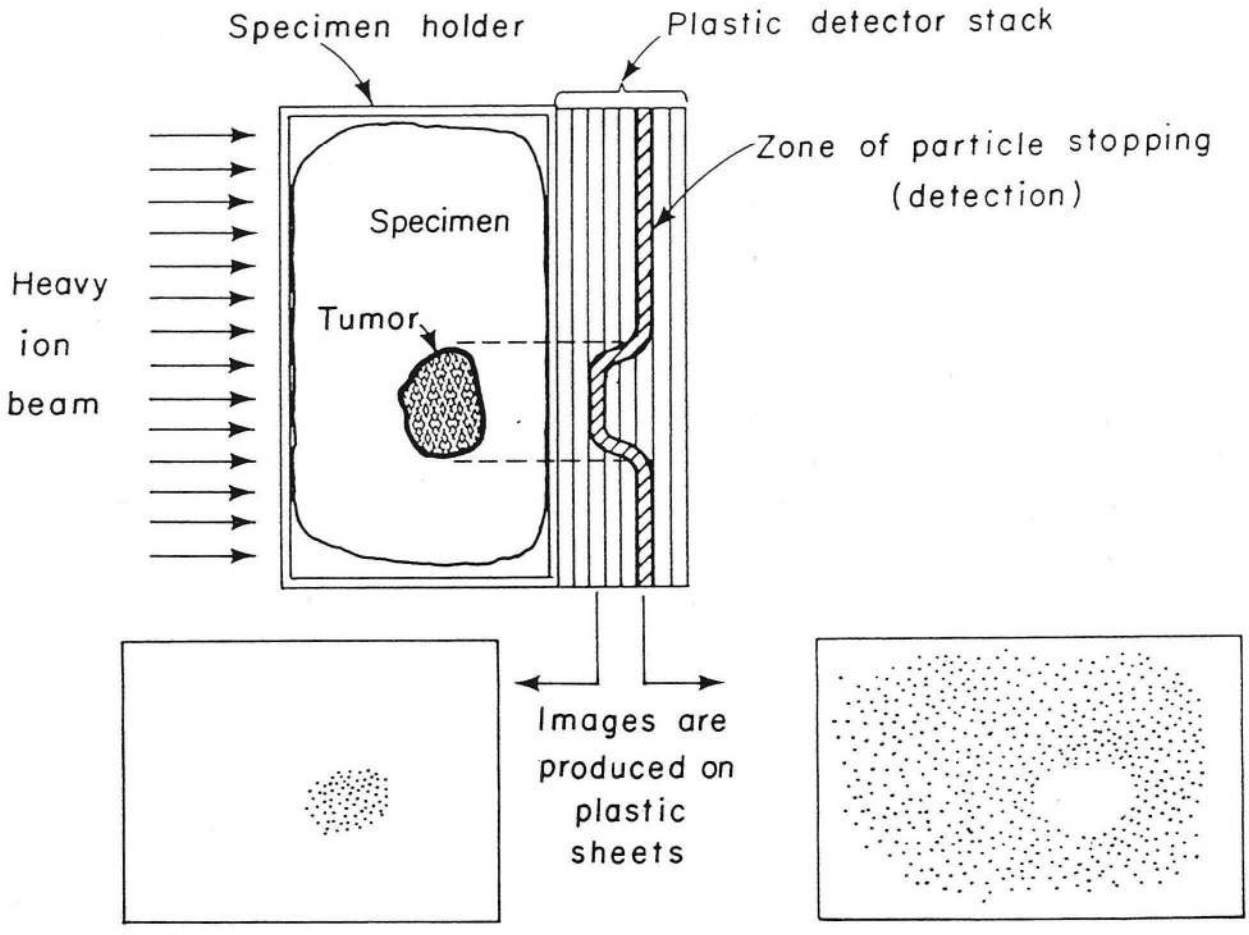

Fig. 70. Schematic drawing of the principles of heavy charged-particle imaging. (XBL 774-811)

kinetic energy of the emitted positron is large (1.7 MeV) that it could travel up to 8 mm from the original excited nucleus before suffering annihilation. However, the mean energy in beta decay is about one third the maximum, and the mean positron range is about 2.8 mm in tissue. The uncertainty in any three mutually orthogonal directions further reduces this uncertainty to about $2.8\text{mm}/\sqrt{3} \approx 1.6\text{mm}$. On top of these uncertainties, the error introduced in the detector, largely due to the inherent resolution of the detector elements, must be added. The combined error in this method is comparable to the errors encountered in the therapy planning based on x-ray CT data, which are estimated to be ~5 mm in 10 cm range.

V.C. Heavy Charged-Particle Imaging

The sharpness of stopping regions of monoenergetic particles may be utilized for imaging purposes. The residual range of monoenergetic particle beams traversing the patient body will render

Fig. 71. Heavy charged-particle images of human leg. The image is a composite image obtained by analyzing images on plastic sheets exposed in a stack. Note the delineation of the soft tissues which are invisible in x-ray images. (XBB 7810-13076)

the map of integrated stopping power of the body.[37, 519] A narrow pencil beam of charged particles may be used to scan the body and the residual ranges of transmitted particles can be determined using a scintillator stack. Alternatively, a laterally-broadened beam, *e.g.*, a fan beam, may be used and individual particle trajectories and ranges are measured using detectors such as multiplane wire chambers.[520] CR39 plastic stacks may also be used to determine the track locations and their ranges.[433] The data so obtained represent a two-dimensional projection of the integrated stopping power of the intervening tissues.[521] A method of making a heavy charged-particle radiograph is schematically shown in Fig. 70. Heavy charged-particle radiographs distinguish small differences in the integrated stopping power, and thereby image the soft tissue. Fig. 71 shows a radiograph of a human leg taken using a carbon-ion beam.[433] The image is a composite image

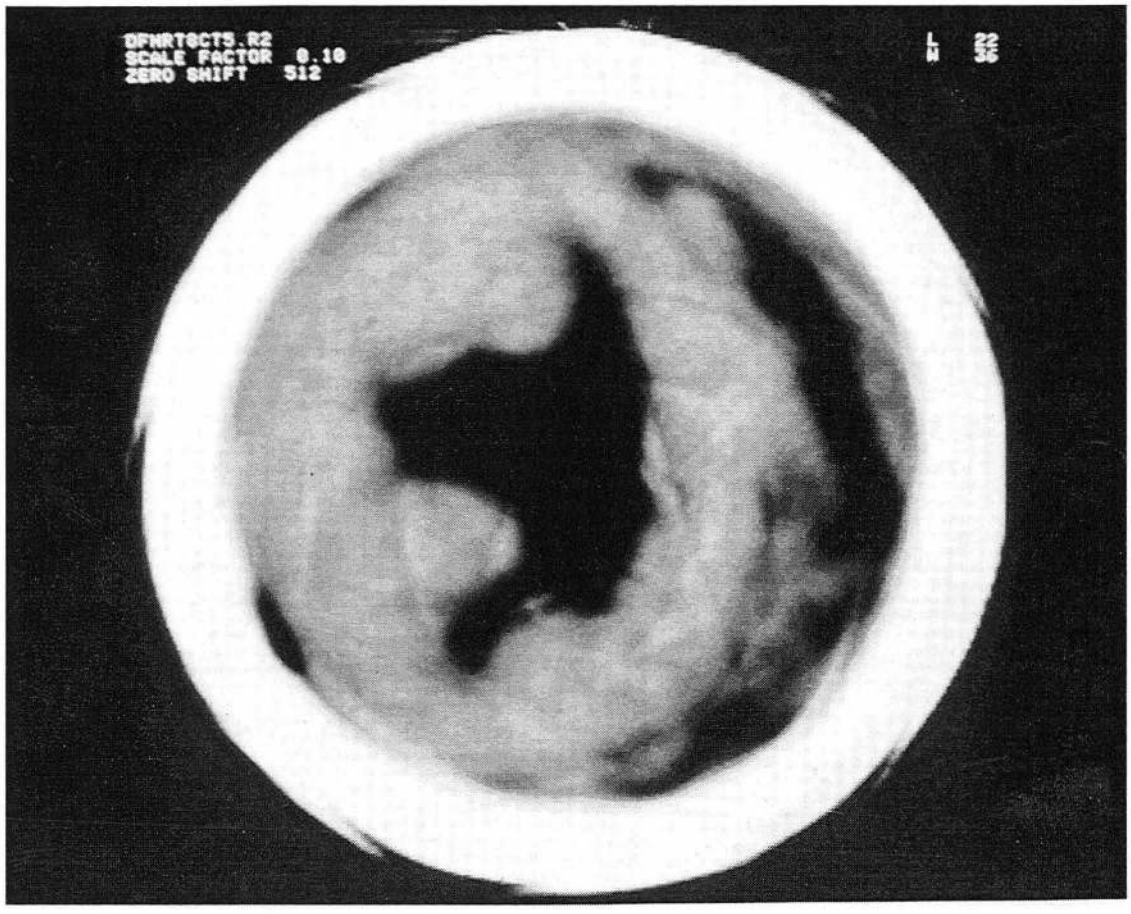

Fig. 72. A cross-section of the canine heart obtained through computed tomographic (CT) reconstruction using heavy charged-particle beams. (XBB 809-10851)

obtained by analyzing images on plastic sheets exposed in a stack. Note the delineation of the soft tissues which are invisible in x-ray images.

The technique may be extended to produce a CT (computed tomography) with heavy charged-particle beams, which represents the patient anatomy in terms of mass stopping power values. By rotating the patient, analogous to rotating the x-ray sources around the patient in xCT, and repeating the procedure, projections of the body in many different directions are made. Reconstruction algorithms applied to this data produces a three-dimensional map of the anatomic slice in terms of its stopping power. Such data may be viewed in cross-sectional slices as in xCT. For such a CT procedure, particle beams of range sufficient to penetrate the patient body are needed. For many parts of the body, such as head and neck, 30 cm range will suffice; however, to utilize the method for all parts of the body, 40 cm range beams are necessary.

Heavy charged-particle CT has been studied using proton,[522, 523] carbon-ion and neon-ion beams.[433, 497, 521, 524-528] Sheets of plastic (CR39 and others) nuclear track detectors in a stack

were used to record the stopping position of a nearly parallel stream of heavy charged particles after they traversed a patient. It is possible to reveal only the stopping tracks, and not the plateau tracks, through an appropriate etching technique. The thickness of the stack upstream of each of these stopping tracks determines the integrated stopping power of the patient body along the track. The reconstructed tomograms were capable of resolving structures as small as 0.7 mm and density differences as small as 0.005 g/cm^3. Fig. 72 shows an example of the heavy charged-particle CT, a cross-sectional image of a canine heart. Multiplane, multiwire ionization chambers and solid state detectors were investigated as replacements for the plastic stack to provide an on-line heavy charged particle tomography system. Also position-sensitive solid-state detectors have been used, together with a total energy absorber, as in BERKLET described above, to reconstruct a heavy charged-particle CT images.[529, 530] MEDUSA described above may also be used to reconstruct the projection images, and by combining several projections, a three-dimensional image of an object in terms of the stopping power can be obtained.[531, 532]

ACKNOWLEDGMENTS

We would like to express our admiration for the continued effort by the following LBL personnel who have invented, designed, or produced many instrument reviewed in this article: Cornelius A. Tobias, Mark A. Nyman, R. P. Singh, Ronald Stradtner, Jose R. Alonso, Moises O. Balagot, John H. Bercovitz, Aloke Chatterjee, J. Michael Collier, Inder K. Daftari, Tony T. Freeman, J. B. Halliwel, Lloyd H. Harmon, William R. Holley, Jorge Llacer, Ivan C. Lutz, John T. Lyman, Krista Marks, Maurice B. McEvoy, Essie Mitchell, Paula L. Petti, Richard M. Reimers, Robert W. Sorensen, Gregory D. Stover, and others. We would like to thank Dr. John T. Lyman and Dr. Paula L. Petti of LBL for critically reading the manuscript. We also would like to extend our thanks to those who supplied us with information used in this review article: Professor Eugene V. Benton of University of San Francisco, Dr. George Coutrakon of the Loma Linda University Medical Center, Professor John F. Dicello, Jr., of Clarkson University, Professor Peter Fessenden of Stanford University, Professor Tetsuo Inada of the University of Tsukuba, Dr. Kiyomitsu Kawachi and Dr. Tatsuaki Kanai of the National Institute of Radiological Sciences, Chiba, Professor Börje Larsson of Uppsala (now at Geneva), Dr. Jorge Llacer of LBL, and Dr. Janet M. Sisterson and Dr. Bernard Gottschalk of the Harvard Cyclotron Laboratory. Also, we would like to thank Ronald Stradtner for helping to assemble the illustrations. This work is supported by the Director, Office of Energy Research, Office of High Energy and Nuclear Physics, of the U.S. Department of Energy under Contract No. DE-AC03-76SF00098 and in part by the National Institute of Health under Grant No. CA49562.

References

1. C. A. Tobias, H. O. Anger and J. H. Lawrence, Am. J. Roentgenol. 67, 1-27 (1952).
2. M. L. Boone, J. H. Lawrence, W. G. Connor, R. Morgado, J. A. Hicks and R. C. Brown, Int. J. Radiat. Oncol. Biol. Phys. 3, 65-69 (1977).
3. J. R. Castro, G. T. Y. Chen and E. A. Blakely, Radiat. Res. 104, S263-S271 (1985).
4. J. R. Castro, *Treatment of Cancer with Heavy Charged Particles*, Lawrence Berkeley Laboratory, February 1991, PUB-5301 (1991).
5. P. H. Fowler and D. H. Perkins, Nature 189, 524 (1961).
6. A. B. Perris, F. A. Smith and D. R. Perry, Phys. Med. Biol. 23, 217-234 (1978).
7. C. Richman, Med. Phys. 8, 273-291 (1981).
8. B. J. Mijnheer and J. J. Broerse, "Dose distributions of clinical fast neutron beams," in *High LET Radiations in Clinical Radiotherapy* (ed. by G. W. Barendsen, J. J. Broerse and K. Breur), Pergamon, Oxford, 109-115 (1979).
9. R. S. Stone, J. H. Lawrence and P. C. Aebersold, Radiology 35, 322-337 (1940).
10. S. B. Field, Curr. Top. Radiat. Res. Q. 11, 1-86 (1976).
11. M. Catterall, H. J. G. Bloom, D. V. Ash, L. Walsh, A. Richardson, D. Uttley, N. F. C. Gowing, P. Lewis and B. Chancer, Int. J. Radiat. Oncol. Biol. Phys. 6, 261-266 (1980).
12. P. D. Kurup, T. F. Pajak, J. S. Nelson, J. Mansell, F. R. Henerickson, L. Cohen and T. W. Griffin, J. Neuro-Oncology 4, 123-129 (1986).
13. A. Wambersie, "Fast Neutron Therapy (Clinical Data and Research Programmes)," *Proc. of the 17th Int. Congress of Radiology* (ed. by *Paris*, Paris (1989).
14. L. Gray and T. E. Kalogeropoulos, Radiat. Res. 97, 246-252 (1984).
15. W. H. Bragg and R. Kleeman, Phil. Mag. 8, 726-738 (1904).
16. B. Larsson, T. Svedberg and H. Tyrén, *Årsbok för Riskföreningen för kräftsjukdomarnas bekämpande*, Yearbook for the Swedish Cancer Society, Stockholm, 41 (1956).
17. S. D. Warshaw and D. G. Oldfield, Am. J. Roentgenol. 78, 876 (1957).
18. A. M. Koehler, R. J. Schneider and J. M. Sisterson, Nucl. Instrum. Methhods 131, 437-440 (1975).
19. J. T. Lyman, "Computer modeling of heavy charged particle beams," in *Pion and Heavy Ion Radiotherapy: Pre-Clinical and Clinical Studies* (ed. by L. Skarsgard), Elsevier, North Holland, 139-147 (1983).
20. R. R. Wilson, Radiology 47, 487-491 (1946).
21. M. R. Raju, *Proton Radiobiology and Radiotherapy*, Int. J. Radiat. Oncol. Biol. Phys., to be published (1993).

22. W. M. Brobeck, E. O. Lawrence, K. R. McKenzie, R. S. E. M. McMillan, D. C. Sewell and R. L. Thornton, Phys. Rev. 71, 449 (1947).
23. C. A. Tobias, J. E. Roberts, J. H. Lawrence, B. V. A. Low-Beer, H. O. Anger, J. L. Born, R. McCombs and C. Huggins, "Irradiation hypophysectomy and related studies using 340-MeV protons and 190-MeV deutrons," *Proc. of the International Conference on Peaceful Use of Atomic Energy* (ed. by *Geneva*, 10: 95-106 (1955).
24. C. A. Tobias, J. H. Lawrence, J. L. Born, R. K. McComb, J. E. Roberts, H. O. Anger, B. V. A. Low-Beer and C. B. Huggins, Cancer Res. 18, 121-134 (1958).
25. H. D. Suit, M. Goitein, J. Tepper, A. M. Koehler, R. A. Schmidt and R. Schneider, Cancer 35, 1646-1657 (1975).
26. J. Lawrence, C. Tobias et al., J. Am. Med. Assoc. 186, 156 (1963).
27. S. Graffman and B. Larsson, Atomkernenergie 27, 148 (1976).
28. B. Larsson, Brit. J. Radiol. 34, 143-151 (1961).
29. L. L. Goldin, V. P. Dzhelepov et al., Sov. Phys. Usp. 16, 402 (1973).
30. J. R. Castro, J. M. Quivey, J. T. Lyman, G. T. Y. Chen, T. L. Phillips and C. A. Tobias, Cancer 46, 633-641 (1980).
31. J. R. Castro, J. M. Quivey, J. T. Lyman, G. T. Y. Chen, T. L. Phillips and C. A. Tobias, J. Assoc. Canad. Radiol. 31, 30-34 (1980).
32. L. G. Gray, Am. J. Roentgenol. 85, 803 (1961).
33. C. A. Tobias and P. W. Todd, Radiobiology and Radiotherapy, Natl. Cancer Inst. Monogr. 24, 1-21 (1967).
34. H. A. Grunder, W. D. Hartsough and E. J. Lofgren, Science 174, 1128-1129 (1971).
35. M. G. White, M. Isaila, K. Predec and H. L. Allen, Science 174, 1121-1123 (1971).
36. M. V. Isaila, W. Schimmerling, K. G. Vosburgh, M. G. White, R. C. Fritz and P. J. McNulty, Science 117, 424-425 (1972).
37. C. A. Tobias, Radiology 108, 145-158 (1973).
38. E. J. Hall and S. Lehnert, Radiat. Res. 55, 431-436 (1973).
39. A. G. Underbrink, L. A. Schairer and A. H. Sparrow, Tradescantia Radiat. Res. 55, 437-446 (1973).
40. G. W. Barendsen, Radiol. Clin. (Basel) 46, 380-389 (1977).
41. M. R. Raju, *Heavy Particle Radiotherapy*, Academic Press, New York (1980).
42. *PART III. Particles and Radiation Therapy, Third International Conference*, Int. J. Radiat. Oncol. Biol. Phys., **8** (1982).
43. ICRU, *Quantitative Concepts and Dosimetry in Radiobiology*, Int. Comm. Radiat. Units Meas., Washington, DC, Report No. 30 (1979).

44. M. R. Raju, H. I. Amols, J. F. Dicello, J. Howard, J. T. Lyman, A. M. Koehler, R. Graves and J. B. Smathers, Br. J. Radiol. 51, 699-713 (1978).
45. M. R. Raju, E. Bain, S. G. Carpenter, R. A. Cox and J. B. Robertson, Brit. J. Radiol. 51, 704-711 (1978).
46. M. R. Raju, H. I. Amols, E. Bain, S. G. Carpenter, R. A. Cox and J. B. Robertson, Br. J. Radiol. 51, 712-719 (1978).
47. T. S. Tenforde, S. D. Tenforde, K. E. Crabtree, D. L. Parks, W. A. Schilling, S. S. Parr, M. J. Flynn, J. Howard, J. T. Lyman and S. B. Curtis, Int. J. Radiat. Oncol. Biol. Phys. 7, 217-222 (1981).
48. E. A. Blakely, F. Q. H. Ngo, S. B. Curtis and C. A. Tobias, Adv. Radiat. Biol. 11, 295- 389 (1984).
49. S. B. Curtis, W. A. Schilling, T. S. Tenforde, K. A. Crabtree, S. D. Tenforde, J. Howard and J. T. Lyman, Radiat. Res. 90, 292-309 (1982).
50. G. W. Barendsen, Eur. J. Cancer 7, 181-190 (1971).
51. J. F. Fowler, *Nuclear Particles in Cancer Treatment*, Medical Physics Handbook, No. 8, Adam Higler Press, Bristol, England (1981).
52. E. J. Hall, Int. J. Radiat. Oncol. Biol. Phys. 8, 2137-2140 (1982).
53. M. P. Richter, G. E. Laramore, T. W. Griffin and R. L. Goodman, Cancer (1984).
54. J. F. Fowler, "Scientific rationale for the European light ion medical accelerator (EULIMA) project," *Proc. of the Fifth PTCOG Meeting and the International Workshop on Biomedical Accelerators, December 1-2, 1986* (ed. by W. T. Chu), *Lawrence Berkeley Laboratory, Berkeley, CA*, LBL-22962, 5-17 (1987).
55. H. D. Suit, M. Goitein, J. E. Munzenrider, L. Verhey, P. Blitzer, E. Gragoudas, A. M. Koehler, M. Urie, R. Gentry, W. Shipley, M. Urano, J. Duttenhaver and M. Wagner, Int. J. Radiat. Oncol. Biol. Phys. 8, 2199-2205 (1982).
56. J. F. Fowler, Int. J. Radiat. Biol. 47, 115-117 (1985).
57. S. B. Curtis, Radia. Res. 106, 252-270 (1986).
58. A. Ghiorso, H. A. Grunder, W. Hartsough, G. Lambertson, E. Lofgren, K. Lou, R. Main, R. Mobley, R. Morgado, W. Salsig and F. Selph, IEEE Trans. Nucl. Sci. NS-20, 155 (1973).
59. P. W. Todd, J. T. Lyman, R. A. Armer, L. D. Skarsgard and R. A. Deering, Radiat. Res. 34, 1-23 (1968).
60. W. Schimmerling, K. G. Vosburgh, P. W. Todd and A. Appleby, Radiat. Res. 65, 389-413 (1976).

61. J. T. Lyman, G. Chen, L. Kanstein and J. Howard, *Heavy particle facilities at the Lawrence Berkeley Laboratory*, First International Seminar on the Use of Proton Beams in Radiation Therapy; Moscow. Atomistadt, 122-135 (1979).
62. W. Schimmerling, "Heavy-ion dosimetry," in *Advances in Radiation Protection and Dosimetry in Medicine* (ed. by R. H. Thomas and V. Perez-Mendez), Plenum Publishing Corporation, New York, NY, 479-516 (1980).
63. *Part II. Radiological Physics and Chemistry Research*, Biological and Medical Research with Accelerated Heavy Ions at the Bevalac, 1977-1980, ed. M. C. Pirruccello and C. A. Tobias, Lawrence Berkeley Laboratory, LBL-11220, 19-69 (1980).
64. B. Larsson and B. Sarby, Acta Oncologica 26, 143-158 (1987).
65. J. T. Lyman and J. Howard, Int. J. Radiat. Biol. Phys. 3, 81-85 (1977).
66. A. R. Smith, Int. J. Radiat. Oncol. Biol. Phys. 8, 2061-2063 (1982).
67. J. T. Lyman, *Heavy charged particle beam dosimetry*, Advances in Dosimetry for Fast Neutrons and Heavy Charged Particles for Therapy Applications, International Atomic Energy Agency, Vienna, 267-280 (1984).
68. J. J. Broerse, J. T. Lyman and J. Zoetelief, "Dosimetry of External Beams of Nuclear Particles," in *The Dosimetry of Ionizing Radiation* (ed. by K. R. Kase, B. E. Bjärngard and F. H. Attix), Academic Press, Orlando, FL, Vol. I, 230-290 (1985).
69. J. T. Lyman, M. Awschalom, P. Berardo, H. Bichsel, G. T. Y. Chen, J. DiCello, P. Fessenden, M. Goitein, G. Lam, J. C. McDonald, A. R. Smith, R. Ten-Haken, L. Verhey and S. Zink, *Protocol for heavy charged-particle beam dosimetry*, American Association of Physicists in Medicine (AAPM), Report No 16 (1986).
70. J. M. Sisterson, Nucl. Instrum. Methods in Phys. Res. B40/41, 1350-1353 (1989).
71. W. Saunders, J. R. Castro, G. T. Y. Chen, J. M. Collie, S. Zink, S. Pitluck, T. L. Phillips, D. Char, P. Gutin, G. Gauge, C. A. Tobias and E. L. Alpen, Radiat. Res. 104, S227-S234 (1985).
72. W. M. Saunders, G. T. Y. Chen, M. M. Austin-Seymou, J. R. Castro, J. M. Collier, G. Gauger, P.Gutin, T. L. Phillips, S. Pitluck, R. E. Walton and S. R. Zink, Int. J. Radiat. Oncol. Biol. Phys. 11, 1339-1347 (1985).
73. J. R. Castro, J. M. Collier, P. L. Petti, V. Nowakowski, G. T. Chen, J. T. Lyman, D. Linstadt, G. Gauger, P. Gutin, M. Decker, T. L. Phillips and K. Baken, Int. J. Radiat. Oncol. Biol. Phys. 17, 477-484 (1989).
74. W. M. Saunders, D. H. Char, J. M. Quivey, J. R. Castro, G. T. Y. Chen, J. M. Collier, A. Cartigny, E. A. Blakely, J. T. Lyman, S. R. Zink and C. A. Tobias, Int. J. Radiat. Oncol. Biol. Phys. 11, 227-283 (1985).
75. D. H. Char, Trans. Ophthalmol. Soc. U.K. 105, 252-256 (1986).

76. L. W. Brady, J. A. Shields, J. J. Augsburger, J. L. Day, A. M. Markoe and J. R. Castro, "Radiation therapy for malignant ocular tumors," in *Diagnostic Imaging in Ophthalmology* (ed. by C. F. Gonzales, M. H. Becker and J. C. Flanagan), Springer Verlag, New York (1986).
77. D. Linstadt, D. H. Char, J. R. Castro, T. L. Phillips, J. M. Quivey, M. Reimers, J. Hannigan and J. M. Collier, Int. J. Radiat. Oncol. Biol. Phys. 15, 347-352 (1988).
78. D. H. Char, J. R. Castro, S. M. Kroll, A. R. Irvine, J. M. Quivey and R. D. Stone, Archives of Ophthalmology 108, 209-214 (1990).
79. J. I. Fabrikant, J. T. Lyman and Y. Hosobuchi, Brit. J. Radiol. 57, 479-490 (1984).
80. J. H. Lawrence, C. A. Tobias, J. A. Linfoot, J. R. Castro, W. M. Saunders, G. T. Chen, J. M. Collier, D. Char and G. Gauger, "Heavy particle irradiation of intracranial lesions," in *Neurosurgery* (ed. by R. H. Wilkins and S. S. Rengachary), McGraw-Hill, New York, 1, 1113-1127 (1985).
81. J. I. Fabrikant, J. T. Lyman and K. A. Frankel, Radiat. Res. Suppl. 8, S244-S258 (1985).
82. J. T. Lyman, J. I. Fabrikant and K. A. Frankel, Nucl. Instrum. Methods in Phys. Res. B10/11, 1107-1110 (1985).
83. J. I. Fabrikant, J. T. Lyman and Y. Hosobuch, "Stereotactic heavy ion Bragg peak radiosurgery for intracranial vascular disorder: Methods for treatment of deep arteriovenous malformations," in *Neurosurgery* (ed. by R. H. Wilkins and S. S. Rengachary), McGraw-Hill, New York, 1, 1128-1132 (1985).
84. J. R. Alonso, J. Bercovitz, W. T. Chu, B. Ludewigt, M. Nyman, S. R. P, R. Stradtner, R. Tefalski and R. Walton, "Relocation of the Helium Ion Radiotherapy Program from the 184" Synchrocyclotron to the Bevalac," *Proc. of the 1989 IEEE Particle Accelerator Conference, Accelerator and Technology, March 1989* (ed. by *Chicago*, 669-671 (1989).
85. J. H. Lawrence, Cancer 10, 795-798 (1957).
86. C. Y. Chong, J. A. Linfoot and J. H. Lawrence, Radiol. Clin. North Am. 7, 3319-343 (1969).
87. J. H. Lawrence, C. A. Tobias, J. A. Linfoot, J. L. Born, C. Y. Chong, J. T. Lyman, E. Manougian and W. C. Wei, J. Clin. Endocrinol. Metabol. 31, 180-198 (1970).
88. J. H. Lawrence, C. Y. Chong, J. L. Born, J. T. Lyman, M. D. Okerlund, J. F. Garcia, J. A. Linfoot, C. A. Tobias and E. Manougian, *Heavy particles in acromegaly and Cushing's disease*, Endocrine and Norendocrine Hormone producing Tumors, 1973, Year Book Medical Publishers, Chicago, 29-61 (1973).
89. J. H. Lawrence, C. Y. Chong, J. T. Lyman, C. A. Tobias, J. L. Born, J. F. Garcia, E. Manougian, J. A. Linfoot and G. M. Connell, "Treatment of pituitary tumors with heavy particles," in *Diagnosis and Treatment of Pituitary Tumors* (ed. by P. O. Kohler and G. T.

Ross), Excerpta Medica Amsterdam/American Elsevier Publishing Co, New York, 1973, 253-262 (1973).

90. J. A. Linfoot, C. Y. Chong, J. H. Lawrence, J. L. Born, C. A. Tobias and J. T. Lyman, "Acromegaly," in *Hormonal Proteins and Peptides* (ed. by C. H. Li), 191-246 (1975).
91. J. M. Sisterson, K. N. Johnson, A. M. Koehler and B. Gottschalk, Nucl. Instr. Methods in Phys. Res. B 10, 1083-1085 (1985).
92. J. E. Munzenrider, S. M. Austin, P. J. Blitzer, R. Gentry, M. Goitein, E. S. Gragoudas, K. Johnson, A. M. Koehler, P. McNulty, G. Moulton et al., Strahlentherapie 161, 756-763 (1985).
93. J. E. Munzenrider, E. S. Gragoudas, J. M. Seddon, J. Sisterson, P. McNulty, S. Birnbaum, K. Johnson, M. Austin-Seymou, J. Slater, M. Goitein, L. J. Verhey, M. Urie, D. M. Ruotolo, K. Egan and F. Osuna, Int. J. Radiat. Oncol. Biol. Phys. 15, 553-558 (1988).
94. H. Suit, T. Griffin, J. Castro and L. Verhey, A. J. Clinical Oncology 11, 330 (1988).
95. R. N. Kjellberg and M. Abe, in *Modern Stereotactic Neurosurgery* (ed. by L. D. Lunsford), Martinus Nijhoff, 41 (1988).
96. E. S. Gragoudas, J. M. Seddon, K. M. Egan, R. J. Glynn, M. Goitein, J. Munzenrider, L. Verhey, M. Urie and A. Koehler, Ophthalmology 95, 992-999 (1988).
97. H. D. Suit, M. Goitein, J. Munzenrider, L. Verhey, M. Urie, E. Gragoudas, A. Koehler, B. Gottschalk, J. Sisterson, H. Tatsuzaki et al., Strahlentherapie und Onkologie 166, 40-44 (1990).
98. B. Larsson, L. Leksell, B. Rexed, P. Sourander, W. Mair and B. Andersson, Nature 182, 1222 (1958).
99. S. Graffman and B. Jung, Acta Radiol. Therapy Phys. Biol. 9, 1-23 (1970).
100. S. Graffman, B. Jung and B. Larsson, *Design studies for a 200 MeV proton clinic for radiotherapy*, Sixth International Cyclotron Conference, 1972, 9, Am. Inst. Phys., Vancouver, 603-615 (1973).
101. S. Graffman, A. Brahme and B. Larsson, Strahlentherapie 161, 764-770 (1985).
102. B. Larsson and S. Graffman, *Experience with the Uppsala 230 cm cyclotron and preparations for future use in radiotherapy*, Medical Workshop on Accelerators for Charged-Particle Beam Therapy, January 24-25, 1985, Fermi National Accelerator Laboratory, 7-39 (1985).
103. E. Grusell, A. Montelius, A. Brahme, G. Rikner, B. Jung, E. Blomquis, P. Jakobsson, K. Russell, M. Blom and J. Medin, "Present status and future plans for proton therapy at the Gustaf Werner Cyclotron in Uppsala," *Proc. of the NIRS International Workshop on Heavy Charged Particle Therapy and Related Subjects* (ed. by A. Itano and T. Kanai), *July 1991, Chiba, Japan*, 173-175 (1991).

104. Y. I. Minakova, *Review of Twenty Years Proton Therapy Clinical Experience in Moscow*, 2nd International Charged Particle Therapy Workshop, October 1987, Loma Linda, CA, 1-23 (1987).
105. V. S. Khoroshkov, L. Z. Barabash, A. V. Barkhudarian, L. L. Goldin, M. F. Lomanov, L. N. Pliashkevich and K. K. Onosovskii, Med. Radiol. (Moscow) 14, 58-62 (1969).
106. M. F. Lomanov, L. N. Pliashkevich and K. K. Onosovskii, Med. Radiol. (Moscow) 14, 58-62 (1969).
107. I. V. Chuvilo, L. L. Goldin, V. S. Khoroshkov, S. I. Blokhin and V. M. Breev, Med. Radiol. (Moscow) 32, 30-36 (1987).
108. I. V. Chuvilo, L. L. Goldin, V. S. Khoroshkov, S. I. Blokhin, V. M. Breyev, I. A. Vorontsov, V. V. Ermolayev, Y. L. Kleinbock, M. I. Lomakin, M. F. Lomanov, V. Y. Medved', N. A. Miliokhin, V. M. Narinsky, L. M. Pavlonsky, G. G. Shimchuck, A. I. Ruderman, G. D. Monzu, E. L. Shuvalov, V. N. Kiseliova, E. I. Marova, L. E. Kirpatovskaya, E. I. Minakova, V. A. Krymsky, A. F. Brovkina, G. D. Zarubey, I. M. Reshetnikova and A. V. Kaplina, Int. J. Radiat. Oncol., Biol., Phys. 10, 185-195 (1984).
109. V. S. Khoroshkov and L. L. Goldin, Int. J. Radiat. Oncology Biol. Phys. 15 (1988).
110. A. F. Brovkina and G. D. Zarubei, Med. Radiol. (Moscow) 32, 61-66 (1987).
111. E. I. Marova, N. T. Starkova, L. E. Kirpatovskaya, G. S. Kolesnikova, A. I. Bukhman, L. Rozhinskaya and L. V. Belchenko, Med. Radiol. (Moscow) 32, 42-49 (1987).
112. G. V. Makarova, B. P. Matveev, N. S. Leonova, T. G. Ratner and G. V. Molchanov, Med. Radiol. (Moscow) 32, 66-70 (1987).
113. Y. I. Minakova, "Twenty Years Clinical Experience of Narrow Proton Beam Therapy in Moscow," *Proc. of the International Heavy Particle Therapy Workshop, Paul Scherrer Institute, Villigen, Switzerland, September, 1989* (ed. by H. Blattmann),, PSI-Bericht, Nr. 69: 158-162 (1990).
114. V. M. Abazov, S. A. Gustov, V. P. Zorin, S. A. Kutuzov and I. V. Mirokhin, Med. Radiol. (Moscow) 33, 67-70 (1988).
115. V. P. Dzhelepov, O. V. Savchenko, B. V. Astrakhan and A. I. Ruderman, Med. Radiol. (Moscow) 32, 81-84 (1987).
116. D. L. Karlin, B. A. Konnov, B. V. Vinogradov, V. B. Nizkovolos and E. A. Kuznetsov, Med. Radiol. (Moscow) 28, 13-19 (1983).
117. D. L. Karlin, B. A. Konnov, V. B. Nizkovolos, N. K. Abrosimov and A. A. Vorobeev, Med. Radiol. (Moscow) 28, 28-32 (1983).
118. N. K. Abrosimov, A. A. Vorobev, E. A. Zherbin and B. A. Konnov, Proc. Acad. Sci. USSR 5, 84-91 (1985).

119. I. K. Abrosimov, A. A. Vorobev, V. A. Eliseev, E. M. Ivanov and G. F. Mikheev, Med. Radiol. (Moscow) 32, 10-16 (1987).
120. E. A. Zherbin, B. A. Konnov, L. A. Mel'nikov, O. P. Zargarova and V. P. Miagkov, Meditsinskaia Radiologiia 32, 17-22 (1987).
121. Y. Y. Minakova, L. L. Goldin, V. S. Khoroshkov, G. V. Makarova, G. D. Monzul and K. K. Onosovskii, "Proton Therapy at ITEP," *Proc. of the International Heavy Particle Therapy Workshop, Paul Scherrer Institute, September, 1989* (ed. by H. Blattmann), *Villigen, Switzerland*, PSI-Bericht, Nr. 69: 154-157 (1990).
122. H. Tsunemoto, S. Morita, T. Ishikawa, S. Furukawa, K. Kawachi, T. Kanai, H. Ohara, T. Kitagawa and T. Inada, Radiat. Res. Suppl. 8, S235-S243 (1985).
123. T. Nakano, S. Morita, S. Sato, K. Shibayama, S. Hurukawa, T. Kanai, M. Endo, T. Hiraoka and H. Tsunemoto, "Proton beam therapy for ocular disease," *Proc. of the NIRS International Workshop on Heavy Charged Particle Therapy and Related Subjects* (ed. by A. Itano and T. Kanai), *July 1991, Chiba, Japan*, 52-71 (1991).
124. D. Kunihara, S. Suwa, A. Tachikawa, Y. Takada and K. Takikawa, Jpn. J. Appl. Phys. 22, 1599-1605 (1983).
125. S. Fukumoto, *Proton beam therapy at Tsukuba*, Medical Workshop on Accelerators for Charged-Particle Beam Therapy, January 24-25, 1985, Fermi National Accelerator Laboratory, 1-5 (1985).
126. T. Kitagawa, T. Inada, T. Arimoto, A. Maruhashi, Y. Takada, Y. Hayakawa, K. Kobayashi, M. Sato, S. Suwa, Y. Iwasaki et al., Gan No Rinsho 32, 729-739 (1986).
127. H. Tsujii, T. Inada, A. Maruhashi, Y. Hayakawa, Y. Takada, J. Tada, K. Ohara and M. Akisada, "Clinical Results of High Energy Proton Radiotherapy at Tsukuba," *Proc. of the International Heavy Particle Therapy Workshop, Paul Scherrer Institute, Villigen, Switzerland, September, 1989* (ed. by H. Blattmann),, PSI-Bericht, Nr. 69: 90-94 (1990).
128. H. Tsujii, H. Tsuji, H. Inada, A. Maruhashi, Y. Hayakawa, J. Tada and S. Fukumoto, "Clinical results of proton therapy at Tsukuba," *Proc. of the NIRS International Workshop on Heavy Charged Particle Therapy and Related Subjects* (ed. by A. Itano and T. Kanai), *July 1991, Chiba, Japan*, 73-81 (1991).
129. C. Markovits, S. Jaccard and C. Perret, "The Proton Beam Facility OPTIS for the Therapy of Ocular Tumors," *Proc. of the International Heavy Particle Therapy Workshop, Paul Scherrer Institute, September, 1989* (ed. by H. Blattmann), *Villigen, Switzerland*, PSI-Bericht, Nr. 69: 134-139 (1990).
130. H. Blattmann, *Experience with conformation radiotherapy with pions and its relevance to the proton therapy project at SIN*, Fourth Proton Therapy Cooperative Group Meeting, June 26, 1986., Fermi National Accelerator Laboratory, unpublished (1986).

131. E. Egger, L. Zografos, L. Bercher and C. Perret, "Proton Therapy of Uveal Melanomas at PSI," *Proc. of the International Heavy Particle Therapy Workshop, Paul Scherrer Institute, September, 1989* (ed. by H. Blattmann), *Villigen, Switzerland*, PSI-Bericht, Nr. 69: 140-142 (1989).
132. L. Zografos, C. Perret, E. Egger, C. Gailloud and R. Greiner, Strahlentherapie und Onkologie 166, 1 (1990).
133. E. Pedroni, R. Bacher, H. Blattmann, T. Boehringer, A. Coray, E. Egger, M. Phillips and S. Scheib, "The 200 MeV Proton Therapy Project at PSI: A Status Report," *Proc. of the International Heavy Particle Therapy Workshop, Paul Scherrer Institute, September, 1989* (ed. by H. Blattmann), *Villigen, Switzerland*, PSI-Bericht, Nr. 69: 1-8 (1989).
134. P. Mandrillon and C. M. Lalanne, Bull. Cancer (Paris) 73, 596-599 (1986).
135. P. Chauvel, P. Mandrillon, N. Brassart, J. Tuyn, J. Hérault, A. Courd, J. L. Lagrange, M. Héry and F. Demard, "Status report on the installation of proton and neutron therapy in Centre Antoine-Lacassagne," *Proc. of the 2nd European Accelerator Conference, Medical Satellite Meeting, June 1990* (ed. by P. Chauvel, A. Wambersie and P. Mandrillon), *Nice, France*, 2: S85-S87 (1990).
136. P. Chauvel, J. L. Achard, J. J. Bard, M. Bolla, N. Brassart, C. Carrie, J. L. Chassard, R. Clément, A. Costa, G. Coste, A. Courdi, R. Delard, C. Dionet, J. B. Dubois, A. Dussere, R. Garcia, J. Gary-Bobo, S. Gely, J. P. Gérard, C. Ginestet, J. P. Guillet, H. Hay-Meng, J. Hérault, M. Héry, P. Juin, C. Kerr-Picard, J. L. Lagrange, S. Marcié, P. Mèré, P. Ollier, T. Pignon, D. Porcheron, H. Pourquier, G. Puel, M. Reme-Saumon, M. Resbeut, P. Romestaing, R. Rozan, T. Schmitt, I. Sentenac, P. Verrelle, J. Veyssière, C. Vrousos and S. Waultier, "A cooperative group and communication network for proton and neutron therapy in southeast of France," *Proc. of the 2nd European Accelerator Conference, Medical Satellite Meeting, June 1990* (ed. by P. Chauvel, A. Wambersie and P. Mandrillon), *Nice, France*, 2: S88-S90 (1990).
137. D. E. Bonnett, A. Kacperek and M. A. Sheen, "Characteristics of a new 62 MeV proton therapy beam," *Proc. of the 2nd European Accelerator Conference, Medical Satellite Meeting, June 1990* (ed. by P. Chauvel, A. Wambersie and P. Mandrillon), *Nice, France*, 2: S12-S14 (1990).
138. D. E. Bonnett, A. Kacperek and M. Sheen, "The Clatterbridge Proton Therapy Facility," *Proc. of the International Heavy Particle Therapy Workshop, Paul Scherrer Institute, Villigen, Switzerland, September, 1989* (ed. by H. Blattmann),, PSI-Bericht, Nr. 69: 143-144 (1990).
139. N. Griffiths, G. Proudfoot, M. Nightingale, D. Bonnet and T. Saxton, *A Novel Accelerator System for Proton Therapy*, Fourth Workshop on Heavy Charged Particles in Biology and Medicine and XV PTCOG Meeting, Gesellschaft für Schwerionenforschung (GSI), September

23-25, 1991, Extended Abstract, Report GSI-91-29, ISSN 0171-4546, Darmstadt, paper F3 (1991).

140. J. M. Slater, D. W. Miller and J. O. Archambeau, Int. J. Radiat. Oncol. Biol. Phys. 14, 761-775 (1988).
141. J. M. Slater, J. O. Archambeau, J. D. Slater, I. Neilsen and W. Preston, "An integrated hospital-based facility for proton beam radiation therapy," *Proc. of the NIRS International Workshop on Heavy Charged Particle Therapy and Related Subjects* (ed. by A. Itano and T. Kanai), *July 1991, Chiba, Japan*, 82-91 (1991).
142. R. Little, Nucl. Instrum. & Methods in Phys. Res. B56/57, 1192-1196 (1991).
143. G. Coutrakon, M. Bauman, D. Lesyna, D. Miller, J. Nusbaum, J. Slater, J. Johanning, J. Miranda, P. M. DeLuca Jr., J. Siebers and B. Ludewigt, Med. Phys. 18, 1093-1099 (1991).
144. F. Cole, P. V. Livdahl, F. Mills and L. Teng, "Design and application of a proton therapy accelerator," *Proc. of the 1987 IEEE Particle Accelerator Conference, Accelerator Engineering and Technology, March 1987* (ed. by E. R. Lindstrom and L. S. Taylor), *Washington, DC*, **Vol. 3**: 1985-1987 (1987).
145. F. T. Cole, P. V. Livdahl, F. E. Mills and L. C. Teng, "Loma Linda medical accelerator project," *Proc. of the 1989 IEEE Particle Accelerator Conference, Accelerator Science and Technology, March 1989* (ed. by F. Bennett and J. Kopta), *Chicago, IL*, 2: 737-741 (1989).
146. J. C. Rosenwald, J. L. Habrand, A. Bridier, D. Pontvert, P. Schlienger, M. Louis, J. Rouesse, A. Laugier and J. P. Camilleri, "Recent developments of a high-energy proton-therapy project in Orsay (France)," *Proc. of the 2nd European Accelerator Conference, Medical Satellite Meeting, June 1990* (ed. by P. Chauvel, A. Wambersie and P. Mandrillon), *Nice, France*, 2: S91-S93 (1990).
147. A. Bridier, S. Delacroix, L. Desjardins, J. L. Habrand, D. Lefkopoulos, M. Louis, G.Marinello, M. A, C. Nauraye, J.-C. Rosenwald, P. Schlienger, L. Schwartz and D. Valinta, "Present status and future development of the ORSAY proton-therapy center," *Proc. of the NIRS International Workshop on Heavy Charged Particle Therapy and Related Subjects* (ed. by A. Itano and T. Kanai), *July 1991, Chiba, Japan*, 166-172 (1991).
148. A. Mazal, J. L. Habrand, J. F. Desgranges, J. C. Rosenwald, S. Delacroix, M. Louis, A. Bridier, L. Desjardins, P. Schlienger, L. Schwartz, C. Nauraye, D. Valinta, D. Lefkopoulos and G. Marinello, *Orsay: status report*, Fourth Workshop on Heavy Charged Particles in Biology and Medicine and XV PTCOG Meeting, Gesellschaft für Schwerionenforschung (GSI), Darmstadt, September 23-25, 1991, Extended Abstract, Report GSI-91-29, ISSN 0171-4546, paper K10 (1991).
149. S. Vynckier, B. Delcoigne, J. M. Denis and A. Wambersie, *Verification of the influence of heterogeneities in the 85-MeV proton beam at Louvain-la-Neuve*, Fourth Workshop on Heavy

Charged Particles in Biology and Medicine and XV PTCOG Meeting, Gesellschaft für Schwerionenforschung (GSI), September 23-25, 1991, Darmstadt, Extended Abstract, Report GSI-91-29, ISSN 0171-4546, paper K3 (1991).

150. F. Richard, C. Kirkove, J. M. Denis, J. P. Meulders and A. Wambersie, *Status Report of the Proton Therapy Program at Louvain-la-Neuve (September 1991)*, Fourth Workshop on Heavy Charged Particles in Biology and Medicine and XV PTCOG Meeting, Gesellschaft für Schwerionenforschung (GSI), September 23-25, 1991, Darmstadt, Extended Abstract, Report GSI-91-29, ISSN 0171-4546, paper K7 (1991).
151. D. T. L. Jones and M. Yudelev, "Particle Therapy at the National Accelerator Center: Progress and Plans," *Proc. of the International Heavy Particle Therapy Workshop, Paul Scherrer Institute, September, 1989* (ed. by H. Blattmann), *Villigen, Switzerland*, PSI-Bericht, Nr. 69: 77-81 (1990).
152. S. Fukumoto, K. Endo, K. Muto, M. Akisada, T. Kitagawa, T. Inada, H. Tsujii, A. Maruhashi, Y. Hayakawa, Y. Takada and J. Tada, "Tsukuba Medical Proton Synchrotron," *Proc. of the International Heavy Particle Therapy Workshop (PTCOG / EORTC / ECNEU), Paul Scherrer Institut, September 1989* (ed. by H. Blattmann), *Villigen, Switzerland*, PSI-Bericht, Nr. 69: 70-74 (1990).
153. S. Fukumoto, "Present status and future of University of Tsukuba Proton Medical Research Center," *Proc. of the NIRS International Workshop on Heavy Charged Particle Therapy and Related Subjects* (ed. by A. Itano and T. Kanai), *July 1991, Chiba, Japan*, 6-12 (1991).
154. K. Kawachi, "Current heavy particle medical accelerator programs in Japan," *Proc. of the Fifth PTCOG Meeting and the International Workshop on Biomedical Accelerators, Lawrence Berkeley Laboratory, December 1-2, 1986* (ed. by W. T. Chu), *Berkeley, CA*, LBL-22962: 73-91 (1987).
155. A. Noda, E. Ego, K.Fujita, K. Fukunaga, S. Kakigi, Y. Iwashita, H. Okamoto, T. Shirai and M. Inoue, "Accelerator plan for medical treatment with charged particles at Kyoto University," *Proc. of the NIRS International Workshop on Heavy Charged Particle Therapy and Related Subjects* (ed. by A. Itano and T. Kanai), *July 1991, Chiba, Japan*, 182-188 (1991).
156. I. K. Abrosimov, A. A. Aleksandrov, G. Z. Borukhovich, V. A. Volchenkov and V. A. Eliseev, Med. Radiol. (Moscow) 32, 26-29 (1987).
157. I. I. Averbukh, A. D. Cherniakin, L. L. Danilov, V. N. Karusyuk, M. M. Karliner, V. N. Marusov, G. I. Silvestrov, V. G. Volokhov, T. A. Vsevolozhskaya and G. S. Willewald, *Project of small-dimensional 200 MeV Proton Synchrotron*, to be published (1991).
158. V. S. Khoroshkov, K. K. Onosovsky, V. M. Breev, L. L. Goldin, J. L. Kleinbock, M. F. Lomanov, V. I. Lyulevitch, I. A. Vorontsov, G. I. Klenov, V. S. Rybalko and Y. S. Ivanov, "Soviet project of PTF," *Proc. of the NIRS International Workshop on Heavy Charged*

Particle Therapy and Related Subjects (ed. by A. Itano and T. Kanai), *July 1991, Chiba, Japan*, 204-212 (1991).

159. V. S. Khoroshkov and K. K. Onossovsky, "H^- synchrotron for proton therapy facility," *Proc. of the NIRS International Workshop on Heavy Charged Particle Therapy and Related Subjects, July 1991* (ed. by A. Itano and T. Kanai), *July 1991, Chiba, Japan*, 213-220 (1991).
160. V. Khoroshkov, L. Goldin, K. Onosovsky and G. Klenov, *Moscow Proton Therapy Facility Project*, 13th PTCOG Meeting, November 1990, Lawrence Berkeley Laboratory, Univ. of Calif., Berkeley, California (unpublished) (1990).
161. K. P. Gall, P. Chapman, M. Goitein, B. Gottschalk, E. Gragoudas, A. M. Koehler, N. J. Liebsch, J. Munzenrider, M. Urie, L. Verhey and M. Wagner, "Plans for a proton medical facility at Massachusetts General Hospital," *Proc. of the NIRS International Workshop on Heavy Charged Particle Therapy and Related Subjects* (ed. by A. Itano and T. Kanai), *July 1991, Chiba, Japan*, 176-179 (1991).
162. J. Alonso, *Design study for the U. C. Davis Proton Facility*, PTCOG XIV, May 1991, Cambridge, MA (unpublished) (1991).
163. B. Prichard, private communication (1991).
164. F. T. Cole, *Notes on a visit to SSC to discuss a medical accelerator*, December 23, 1991, (unpublished) (1991).
165. G. Dobben, talk presented at the International Heavy Particle Therapy Workshop, Paul Scherrer Institute, September, 1989 (1989).
166. H. Blosser, R. Burleigh, D. Johnson, T. Kuo, F. Marti, J. Vincent, J. Wagner, Z. A, E. Blosser, G. Blosser, R.Maughan and W. Powers, "Medical accelerator projects at Michigan State University," *Proc. of the 1989 IEEE Particle Accelerator Conference, Accelerator Science and Technology* (ed. by F. Bennett and J. Kopta), *Chicago, IL*, **2**: 742-746 (1989).
167. H. Blosser, D. Johnson, D. Lawton, R. Ronningen, R. Burleigh and B. Gottschalk., *Preliminary design study exploring building features required for a proton therapy facility for the Ontario Cancer Institute*, National Superconducting Cyclotron Laboratory, Michigan State University, MSUCL-760a (1991).
168. Indiana University Cyclotron Facility, Bloomington, IN, Scientific and Technical Report 142 (1986).
169. U. Linz and R. Maier, *A first concept to use the Cooler Synchrotron COSY-Jülich for cancer therapy*, '92 European Particle Accelerator Conference (EPAC), to be published (1992).
170. F. Cera, R. Cherubini, A. M. I. Haque, G. Moschini, P. Tiveron, M. Bell, F. Ianzini, O. Sapora, M. A. Tabocchini and G. Simone, *Radiobiological Research with Charged Particles at the Laboratori Nazionali di Legnaro (LNL)*, Fourth Workshop on Heavy Charged Particles in

Biology and Medicine and XV PTCOG Meeting, Gesellschaft für Schwerionenforschung (GSI), September 23-25, 1991, Darmstadt, Extended Abstract, Report GSI-91-29, ISSN 0171-4546, paper K2 (1991).

171. G. Goodman, *talk presented at the International Heavy Particle Therapy Workshop*, Paul Scherrer Institute, Villigen, Switzerland, September, 1989 (1989).
172. P. Scalliet, "Installation of a hospital-based proton therapy center in the province of Antwerp, Belgium," *Proc. of the 2nd European Accelerator Conference, Medical Satellite Meeting, June 1990* (ed. by P. Chauvel, A. Wambersie and P. Mandrillon), *Nice, France*, 2: S94-S96 (1990).
173. W. Beeckman, Y. Jongen, A. Laisné and G. Lannoye, Nucl. Instrum. & Methods in Phys. Res. B56/57, 1201-1204 (also see "Proton Therapy, A New Concept for a Low Cost Facility — Preliminary design based on a compact, high field isochronous cyclotron," Ion Beam Applications s.a., Louvain-la-Neuve, Belgium, Report 2nd edition), (1991).
174. Y. Jongen, W. Beeckman and A. Laisne, "Development of a low-cost compact cyclotron system for proton therapy," *Proc. of the NIRS International Workshop on Heavy Charged Particle Therapy and Related Subjects* (ed. by A. Itano and T. Kanai), *July 1991, Chiba, Japan*, 189-200 (1991).
175. T. Takayama, M. Sano, T. Sato, N. Takahashi, A. Laisne, W. Beeckman, J. P. Dufour and Y. Jongen, *Compact cyclotron for proton therapy*, Quantum Equipment Division, Sumitomo Heavy Industries, Ltd., 5-2 Sobiraki-cho, Nihama-city, Ehime-ken, 792, Japan, and Ion Beam Applications, s.a., Chemin du Cyclotron, 2 B-1348, Louvain-la-Neuve, Belgium, Technical report (1991).
176. R. W. Hamm, K. R. Crandall and J. M. Potter, "Preliminary Design of a Dedicated Proton Therapy Linac," *Proc. of the IEEE 1991 Particle Accelerator Conference, Accelerator Science and Technology, May 1991* (ed. by °, 4: 2583-2585 (1991).
177. A. J. Lennox, Nucl. Instrum. & Methods in Phys. Res. B56/57, 1197-1200 (1991).
178. C. Ankenbrandt, T. Kroc, L. Michelotti, S. Peggs and C. Schmidt, *Pre-conceptual design of a proton therapy accelerator*, Fermi National Accelerator Labratory, FERMILAB-Pub-92/136 (1992).
179. K. Kawachi, T. Kanai, M. Endo, Y. Hirao and H. Tsunemoto, J. Jpn. Soc. Ther. Radiol. Oncol. 1, 19-29 (1989).
180. F. Soga, "HIMAC Project Status I — Irradiation Facility," *Proc. of the NIRS International Workshop on Heavy Charged Particle Therapy and Related Subjects* (ed. by A. Itano and T. Kanai), *July 1991, Chiba, Japan*, 36-43 (1991).
181. K. Kawachi, T. Kanai, M. Endo, F. Soga, S. Minohara, M. Sudou, H. Itoh, T. Kohno, H. Ogawa, T. Yamada, S. Yamada, Y. Sato, A. Itano, E. Takeda, M. Kanezawa, K. Noda and

Y. Hirao, *Construction of heavy ion medical Accelerator in Chiba*, presented at the NIRS International Workshop on Heavy Charged Particle Therapy and Related Subjects, July 1991, Chiba, Japan (1991).

182. K. Sato, "HIMAC Project Status I — Accelerator Complex," *Proc. of the NIRS International Workshop on Heavy Charged Particle Therapy and Related Subjects* (ed. by A. Itano and T. Kanai), *July 1991, Chiba, Japan*, 23-35 (1991).
183. H. Ohara, T. Kanai, K. Ando, K. Kasai, H. Itsukaichi, K. Fukutsu, K. Kawachi and K. Sato, "Accelerator plan for medical treatment with charged particles at Kyoto University," *Proc. of the NIRS International Workshop on Heavy Charged Particle Therapy and Related Subjects* (ed. by A. Itano and T. Kanai), *July 1991, Chiba, Japan*, 13-22 (1991).
184. T. Kanai, private communication (1992).
185. G. Gademann, B. Krebs, G. Hartmann, G. Kraft and M. Wannenmacher, "Clinical Programs of the Radiotherapy Project with Heavy Ions Heidelberg-Darmstadt," *Proc. of the International Heavy Particle Therapy Workshop, Paul Scherrer Institute, September, 1989* (ed. by H. Blattmann), *Villigen, Switzerland*, PSI-Bericht, Nr. 69: 75-76 (1989).
186. G. Gademann, G. H. Hartmann, G. Kraft, W. J. Lorenz and M. Wannenmacher, Strahlentherapie Und Onkologie 166, 34-39 (1990).
187. D. Böhne, "Biomedical activity at the SIS," *Proc. of the NIRS International Workshop on Heavy Charged Particle Therapy and Related Subjects* (ed. by A. Itano and T. Kanai), *July 199, Chiba, Japan*, (1991).
188. G. Kraft, N. Angert, W. Becher, K. Blasche, D. Böhne, B. Fischer, B. Franczak, H. Geissel, T. Haberer, W. Kraft-Weyrather, B. Langenbeck, G. Münzenberg, S. Ritter, I. Schall, D. Schardt, H. Stelzer, M. Flentje, G. Gademann and M. Wannenmacher, "Status of the Heavy Ion Therapy at GSI," *Proc. of the Fourth Workshop on Heavy Charged Particles in Biology and Medicine and XV PTCOG Meeting, Gesellschaft für Schwerionenforschung (GSI), September 23-25, 1991* (ed. by *Darmstadt*, Extended Abstract, Report GSI-91-29, ISSN 0171-4546, paper K11 (1991).
189. P. Mandrillon, A. Susini, R. Ostojic, Y. Jongen, J. P. Meulders and G. Ryckewaert, "The EULIMA project," *Proc. of the Fifth PTCOG Meeting and the International Workshop on Biomedical Accelerators, Lawrence Berkeley Laboratory, December 1-2, 1986* (ed. by W. T. Chu), *Berkeley, CA*, LBL-22962: 93-115 (1986).
190. P. Mandrillon, R. Ostojic, A. Susini, F. Farley, J. P. Schapira, G. Ryckewaert, S. Zaremba, J. C. Godot and R. Dubois, "Advances of the feasibility study of the European light ion medical accelerator: EULIMA," *Proc. of the EULIMA Workshop on the Potential Value of Light Ion Beam Therapy, Nice, France, November 1988, Centre Antoine-Lacassagne* (ed. by P. Chauvel and A. Wambersie), *Nice, France*, EUR 12165 EN: 419-468 (1988).

191. P. Mandrillon, "High Energy Medical Accelerators," *Proc. of the 2nd European Particle Accelerator Conference, June 1990* (ed. by P. Chauvel, A. Wambersie and P. Mandrillon), *Nice, France*, 2: S4-S8 (1990).
192. *EULIMA Feasibility Study Report*, February 1991, unpublished report (1991).
193. G. Cesari, P. Lefèvre and D. Vandeplassche, "The Light Ion Medical Synchrotron for EULIMA," *Proc. of the Fourth Workshop on Heavy Charged Particles in Biology and Medicine and XV PTCOG Meeting, Gesellschaft für Schwerionenforschung (GSI), September 23-25, 1991* (ed. by *Darmstadt*, Extended Abstract, Report GSI-91-29, ISSN 0171-4546, paper F2 (1991).
194. D. Böhne, Radiat. Enviro. Biophys. 31, 205-218 (1992).
195. W. Chen, *Design of a light ion medical synchrotron*, GSI, Darmstadt, Germany, GSI-92-24, ISSN 0171-4546 (1992).
196. M. Muller, *General layout of a medical accelerator with respect to specific site conditions*, GSI, Darmstadt, Germany, Technical note (unpublished) (1991).
197. V. S. Khoroshkov, L. L. Goldin, K. K. Onosovsky and G. I. Klenov, ITEP, Moscow, Technical Note (unpublished) (1991).
198. J. C. Allred, J. N. Bradbury, L. Rosen, E. V. Hungerford, H. O. W. Kidder and G. C. Phillips, Phys. Med. Biol. 23, 603-609 (1978).
199. D. Berley, L. N. Blumberg, D. C. Bonar, R. Fairchild, J. D. Fox, W.-C. Lam, D. M. Lazarus, Y. Y. Lee, C. L. Wang, A. S. Kanofsky, W. T. Chu and M. Blecher, IEEE Trans. Nucl. Sci. NS-20, 997-1001 (1973).
200. H. S. Kaplan, H. A. Schwettman, N. M. Fairbank, D.Boyd and M. A. Bagshaw, Raiology 108, 159 (1973).
201. D. A. Pistenma, P. Fessenden, D. P. Boyd, G. Luxton, R. Taber and M. A. Bagshaw, Radiology 122, 527-529 (1977).
202. C. F. von Essen, H. Blattmann, J. F. Crawford, P. Fessenden, E. Pedroni, C. Perret, M. Salzmann, K. Shortt and E. Walder, Int. J. Radiat. Oncol. Biol. Phys. 8, 1499-1509 (1982).
203. C. F. von Essen, H. Blattmann, G. Bodendoerfer, J. Mizoe, E. Pedroni, E. Walder and A. Zimmermann, Int. J. Radiat. Oncol. Biol. Phys. 11, 217-226 (1985).
204. M. M. Kligerman, G. West, J. F. Dicello, C. J. Sternhagen, J. E. Barnes, K. Loeffler, F. Dobrowolski, H. T. Davis, J. N. Bradbury, T. F. Lane, D. F. Peterson and E. A. Knapp, Am. J. Roentgenol. 126, 261 (1976).
205. M. M. Kligerman, L. Sala, A. Smith, K. E, H. Tsujii, M. Bagshaw and S. Wilson, J. Can. Assoc. Radiol. 31, 13 (1980).
206. C. F. von Essen, M. A. Bagshaw, S. E. Bush, A. R. Smith and M. M. Kligerman, Int. J. Radiat. Oncol. Biol. Phys. 13, 1389-1398 (1987).

207. H. F. Batho and R. O. Kornelson, Phys. Med. Biol. 15, 141 (1970).
208. T. Pickles, J. Bowen, P. Dixon, C. Gaffney, M. Pomeroy, D. Rheaume, F. Vernimmen and G. B. Goodman, Int. J. Radiat. Oncol. Biol. Phys. 21, 1005-1011 (1991).
209. G. Schmitt, C. von Essen, R. Greiner and H. Blattmann, Radiat Res Supplement (1985).
210. R. J. Burleigh, D. J. Clark and W. S. Flood, Experimentia Suppl. 24, 135-138 (1975).
211. H. A. Grunder and C. W. Leemann, Int. J. Radiat. Oncol. Biol. Phys. 3, 71-80 (1977).
212. Y. Umegaki, Radioisotopes 26, 51-59 (1977).
213. B. Gottschalk, IEEE. Trans. Nucl. Sci. NS-30, 3063 (1983).
214. R. Gough, J. Alonso, T. Elioff, J. Fugitt, A. Garren, H. A. Grunder, H. Lancaster, R. Sah, B. Sorensen, J. Staples and R. Yourd, IEEE Trans. Nucl. Sci. NS-30, 3067-3069 (1983).
215. R. L. Martin, Nucl. Instrum. Methods Phys. 25, 1087-1091 (1987).
216. B. Gottschalk, A. M. Koehler and M. S. Wagner, IEEE Trans. Nucl. Sci. NS-32, 3305-3307 (1985).
217. M. Goitein, R. Gentry and A. M. Koehler, Int. J. Radiat. Oncol., Biol., Phys. 9, 259-260 (1983).
218. T. R. Renner, W. T. Chu, R. A. Gough, J. Staples and J. Tanabe, IEEE Trans. Nucl. Sci. NS-32, 3327-3329 (1985).
219. C. A. Tobias, J. I. Fabrikant, E. V. Benton and W. R. Holley, "Projection Radiography and Tomography," in *Biological and Medical Research with Accelerated Heavy Ions at the Bevalac, 1977-1980* (ed. by M. C. Pirruccello and C. A. Tobias), Lawrence Berkeley Laboratory, Report LBL-11220, 335-346 (1980).
220. M. H. Phillips, K. A. Frankel, J. T. Lyman, J. I. Fabrikant and R. P. Levy, Int. J. Radiat. Oncol. Biol. Phys. 8, 211-220 (1990).
221. H. Bichsel, *Straggling of energetic heavy charged particles in thin absorbers*, University of California, Berkeley, California: Lawrence Berkeley Laboratory Report, September 1969 (1969).
222. H. Bichsel and S. Yu, IEEE Trans. Nucl. Sci. NS-19, 172-174 (1972).
223. H. W. Lewis, Phys. Rev. 85, 20 (1952).
224. M. J. Berger and S. M. Seltzer, *Multiple scattering corrections for proton range measurements*, NAS-NRC, 1133 (1964).
225. A. S. Goldhaber and H. H. Heckman, Ann. Rev. Nucl. Part. Sci. 28, 161-205 (1978).
226. L. Anderson, W. Brückner, E. Moeller, S. Nagamiya, S. Nissen-Meyer, L. Schroeder, G. Shapiro and H. Steiner, *Inclusive particle production at forward angles from collisions of light relativistic nuclei, Part I: Nuclear fragments*, Lawrence Berkeley Laboratory, May 1982, LBL-14328 (1982).

227. J. B. McCaslin, P. R. LaPlant, A. R. Smith, W. P. Swanson and R. H. Thomas, IEEE Trans. Nucl. Sci. NS-32, 3104-3106 (1985).
228. M. R. Shavers, S. B. Curtis, J. Miller and W. Schimmerling, Radiat. Res. 124, 117-130 (1990).
229. J. Llacer, C. A.Tobias, W. R. Holley and T. Kanai, Med. Phys. 11, 266-278 (1984).
230. W. Schimmerling, J. Miller, M. Wong, M. Rapkin, J. Howard, H. G. Spieler and B. V. Jarret, Radiat. Res. 120, 36-71 (1989).
231. W. Schimmerling, E. L. Alpen, P. Powers-Risius, M. Wong, R. J. Deguzeman and M. Rapkin, Radiat. Res. 112, 436-448 (1987).
232. S. B. Curtis, W. T. Chu, T. R. Renner, A. Rodriguez and T. C. H. Yang, *Model predictions using experimental physical data as input are compared with cell survival obtained in heavy charged particle beams*, Radiation Research Society Meeting, Philadelphia, PA (1988).
233. ICRU, *Basic Aspects of High Energy Particle Interactions and Radiation Dosimetry*, Int. Comm. Radiat. Units Meas., Washington, DC, Report No. 28 (1978).
234. *American Association of Physicists in Medicine, Protocols for Heavy Charged Particle Beam Dosimetry," A Report of Task Group 20, Radiation Therapy Committee*, American Institute of Physics, New York, AAPM Report No. 16 (1986).
235. S. Vynckier, D. Bonnett and D. T. Jones, *Code of Practice for Clinical Proton Dosimetry*, ECHED (European Clinical Heavy Particle Dosimetry Group), September 1989, presented at the PTCOG-ECNEU-EORTC meeting, Villigen, Switzerland (1989).
236. R. Oliver, Br. J. Radiol. 42, 231-233 (1969).
237. H. Weiss, C. C. Ling, E. R. Epp, A. Santomasso and J. M. Heslin, Radiat. Res. 61, 355-365 (1975).
238. G. T. Y. Chen, J. T. Lyman and J. Riley, Med. Phys. 4, 358 (1977).
239. J. Hill, W. R. Hendee and A. Smith, Med. Phys. 5, 325 (abstract) (1978).
240. G. T. Y. Chen, R. P. Singh, J. R. Castro, J. T. Lyman and J. M. Quivey, Int. J. Radiat. Oncol. Biol. Phys. 5, 1809-1819 (1979).
241. G. T. Y. Chen, "CT in high LET therapy planning," *Proc. of the Symposium on Computed Tomography in Radiotherapy, September 1981* (ed. by C. C. Ling and R. Morton), *Washington, DC*, Raven Press, New York, 221-228 (1983).
242. G. T. Y. Chen and M. Goitein, "Treatment planning for heavy charged particle radiotherapy," in *Advances in Radiation Therapy Treatment Planning* (ed. by A. E. Wright and A. L. Boyer), American Institute of Physics, New York, Medical Physics Monograph No. **9**, 514-541 (1983).
243. A. A. Mustafa and D. F. Jackson, Phys. Med. Biol. 28, 169-176 (1983).

244. M. M. Urie, J. M. Sisterson, A. M. Koehler, M. Goitein and J. Zoesman, Med. Phys. 13, 734-741 (1986).
245. S. B. Curtis, *The effect of track structure on OER at high LET*, Charged Particle Tracks in Liquids and Solids, Conf. Series 8, The Inst. of Physics and the Physical Society (England), 140-142 (1970).
246. E. A. Blakely, private communication (1991).
247. J. Llacer, J. B. Schmidt and C. A. Tobias, Med. Phys. 17, 151-157 (1990).
248. L. D. Skarsgard and B. Palcic, Radiology 2, 447-454 (1974).
249. E. A. Blakely, C. A. Tobias, T. C.-N. Yang, K. Smith and J. T. Lyman, Radiat. Res. 80, 122-160 (1979).
250. G. Litton, J. T. Lyman and C. A. Tobias, *Penetration of high-energy heavy ions with the inclusion of Coulomb, nuclear and other stochastic processes*, Lawrence Berkeley Laboratory, May 1968, UCRL-17392 rev., UC-34 Physics, TID-4500 (2nd Ed.) (1968).
251. C. J. Bakker and E. Segre, Phys. Rev. 81, 489-492 (1951).
252. P. Steward and R. Wallace, *Calculations of stopping power and range energy values for any heavy ion in nongaseous media*, Lawrence Berkeley Laboratory, UCRL-17314 (1966).
253. J. F. Janni, *Proton Range-Energy Tables, 1 keV-10 GeV*, Atomic Data and Nuclear Data Tables, **27**, 147-529 (1982).
254. W. H. Barkas and M. J. Berger, *Tables of energy losses and ranges of heavy charged particles*, Studies of Penetration of Charged Particles in Matter. Washington, DC: National Academy of Sciences National Research Council, NASA SP-3013 (1964).
255. National Academy of Sciences, National Research Council, Publication No. 1133 (1964).
256. H. Bischel and L. E. Porter, Phy. Rev. A 25, 2499-2510 (1982).
257. H. Bischel, "Stopping power of fast charged particles," *Proc. of the NIRS International Workshop on Heavy Charged Particle Therapy and Related Subjects* (ed. by A. Itano and T. Kanai), *July 1991, Chiba, Japan*, 144-150 (1991).
258. H. H. Anderson and J. F. Ziegler, *The Stopping and Ranges of Ions in Matter, Vol. 3, Hydrogen: Stopping Powers and Ranges in all Elements*, Pergamon, New York (1977).
259. J. F. Ziegler, *The Stopping and Ranges of Ions in Matter, Vol. 4, Helium: Stopping Powers and Ranges in all Elements*, Pergamon, New York (1977).
260. J. F. Ziegler, *The Stopping and Ranges of Ions in Matter, Vol. 5, Handbook of Stopping Cross Sections for Energetic Ions in all Elements*, New York, New York (1980).
261. D. Miller, private communication (1991).
262. S. Falkner, B. Fros, B. Larsson, A. Lindell, J. Naeslund and S. Stenson, Acta Radiol. 53, 33 (1962).
263. B. Fros, B. Larsson, A. Lindell, J. Naeslund and S. Stenson, Acta Radiol. 2, 384 (1964).

264. C. A. Tobias, J. T. Lyman, A. Chatterjee, J. Howard, H. D. Maccabee, M. R. Raju, A. R. Smith, J. M. Sperinde and G. P. Welch, Science 174, 1131-1134 (1971).
265. H. I. Amols, D. J. Liska and J. Halbig, Med. Phys. 4, 404-407 (1977).
266. D. J. Liska, Rev. Sci. Instrum. 48, 52 (1977).
267. T. Inada, Y. Hayakawa, A. Maruhash, K. Ohara, T. Kitagawa, M. Akisada, K. Kawachi and T. Kanai, Jpn. Acta Radiologica 44, 844-853 (1984).
268. R. R. Raju, J. T. Lyman, T. Brustad and C. A. Tobias, "Heavy charged-particle beams," in *Radiation Dosimetry* (ed. by F. H. Attix and E. Tochilin), Academic Press, III, 178 (1969).
269. W. T. Chu and C. A. Tobias, *Binary Filter*, private communication (1982).
270. Gottschalk, *Proton radiotherapy nozzle with combined scatterer/modulator*, presented in the Second International Charged Particle Workshop and the PTCOG meeting, Loma Linda, CA, October 1987, HCL 9/17/87 (1987).
271. W. Schimmerling, J. Alonso, R. Morgado, C. A. Tobias, H. Grunder, F. T. Upham, A. Windsor, R. A. Amer, T. C. H. Yang and J. T. Gunn, IEEE Trans. Nucl. Sci. NS-24, 1049 (1977).
272. F. J. M. Farley and C. Carli, *EULIMA beam delivery — Progress report Jan. 1991*, Laboratoire du Cyclotron, Centre Antoine Lacassagne (1991).
273. A. Akanuma, H. Majima, S. Furukawa, R. Okamoto, Y. K. Nakamura, H. Tsunemoto, S. Morita, T. Arai, A. Kurisu, T. Hiraoka, K. Kawachi and T. Kanai, Int J Radiat Oncol Biol Phys 8, 1629-1635 (1982).
274. M. Goitein, Int. J. Rad. Onc. Biol. Phys. 4, 499-508 (1978).
275. M. S. Wagner, Med. Phys. 9, 749-752 (1982).
276. M. M. Urie, M. Goitein and M. Wagner, Phys. Med. Biol. 29, 553-566 (1984).
277. R. Wada and J. R. Alonso, IEEE Trans. Nucl. Sci. NS-28, 2276-2278 (1981).
278. Y. Hayakawa, J. Tada, T. Inada, T. Kitagawa, T. Wagai and K. Yosioka, J. Acoust. Soc. Jpn. 9, 255-257 (1988).
279. L. Sulak, T. Armstrong, H. Baranger, M. Bregman, M. Levi, D. Mael, J. Strait, T. Bowen, A. E. Pifer, P. A. Polakos, H. Brandner, A. Parvulescu, W. V. Jones and J. Learned, Nucl. Instrum. Methods 161, 203-217 (1979).
280. J. Tada, Y. Hayakawa, K. Hosono and T. Inada, Med. Phys. 18 (6), 1100-1104 (1991).
281. C. Carli and F. Farley, *Charge particle beam penetrating a slab of matter optimization for minimal output emittance*, Antoine-Lacassagne Cancer Center, Nice, France, Tecnical Report (1990).
282. M. Awschalom, I. Rosenberg, T. Y. Kuo and J. L. Tom, Med. Phys. 7, 495-502 (1980).

283. C. Wang, J. T. Lyman and C. A. Tobias, *Relative biological effectiveness of 730 MeV proton particles for acute lethality of mice*, Biology and Medicine Semiannual Report: Lawrence Berkeley Laboratory Report, Spring 1962 (1962).
284. Y. Ueno and Y. G. Grigoriev, Brit. J. Radiol. 42, 475 (1969).
285. A. A. Wainson, M. F. Lomanov, N. L. Shmakova, S. I. Blokhin and S. P. Jarmonenko, Brit. J. Radiol. 45, 525-529 (1972).
286. A. H. Laing and R. J. Berry, Proc. R. Soc. Med. 67, 31-32 (1974).
287. J. Robertson, J. Williams, R. Schmidt, J. Little, D. Flynn and H. D. Suit, Cancer 35, 1664-1677 (1975).
288. J. Tepper, L. Verhey, M. Goitein and H. D. Suit, Int. J. Radiat. Oncol. Biol. Phys. 2, 1115-1122 (1977).
289. M. Urano, M. Goitein, L. Verhey, O. Mendiondo, H. D. Suit and A. M. Koehler, Int. J. Radiat. Oncol. Biol. Phys. 6, 1187-1193 (1980).
290. B. A. Konnov, V. B. Nizkovolos, D. L. Karlin, E. I. Komarov, I. A. Zacharov and T. N. Ko:zina, Radiobiologia, Radiotherapia 22, 225-232 (1981).
291. M. Urano, L. J. Verhey, M. Goitein, J. E. Tepper, H. D. Suit, O. Mendiondo, E. S. Gragoudas and A. Koehler, Int. J. Radiat. Oncol. Biol. Phys. 10, 509-514 (1984).
292. A. Perris, P. Pialoglou, A. A. Katsanos and E. G. Sideris, Int. J. Radiat. Biol. 50, 1093-1101 (1986).
293. P. L. Petti, J. T. Lyman, T. R. Renner, J. R. Castro, J. M. Collier, I. K. Daftari and B. A. Ludewigt, Med Phys, 18, 513-518 (1991).
294. A. M. Kellerer and H. H. Rossi, Curr. Top. Radiat. Res. 8, 85-158 (1972).
295. K. H. Chadwick and H. P. Leenhouts, Phys. Med. Biol. 18, 78-87 (1973).
296. B. G. Douglas and J. F. Fowler, Radiat. Res. 66, 401-426 (1976).
297. A. M. Kellerer and H. H. Rossi, Radiat. Res. 75, 471-488 (1978).
298. P. L. Petti, J. T. Lyman and J. R. Castro, Med. Phys. 18 (3), 506-512 (1991).
299. B. A. Ludewigt, W. T. Chu, M. H. Phillips and T. R. Renner, Med. Phys. 18, 36-42 (1991).
300. E. A. Blakely, "Choice of particle species," in *Radiation Oncology, Maria Design Symposium* (ed. by J. D. Chapman), Medical Accelerator Research Institute in Alberta, Edmonton, Alberta, Canada, Vol. II, 47-93 (1980).
301. E. A. Blakely, F. Q. H. Ngo, S. B. Curtis and C. A. Tobias, "Heavy-ion radiobiology: Cellular studies," in *Advances in Radiation Biology.* (ed. by J. T. Lett), Academic, New York. Also, Lawrence Berkeley Laboratory Report LBL-11861 (1983).
302. J. T. Lyman and J. Howard, *Biomedical research facilities and dosimetry*, Biological and Medical Research with Heavy Ions at the Bevalac, 1974~1977, Report LBL-5610, Lawrence Berkeley Laboratory, 26-35 (1977).

303. G. K. Y. Lam, Rev. Sci. Instrum. 53, 1067-1071 (1982).
304. R. R. Wilson, Phys. Rev. 71, 385-386 (1947).
305. A. M. Koehler and W. M. Preston, Radiology 104, 191 (1972).
306. A. M. Koehler, Radiat. Res. Suppl. 7, 53 (1967).
307. R. F. Eilbert, A. M. Koehler and J. M. Sisterson, Int. J. of Appl. Radiat. and Isotopes 27, 707-711 (1976).
308. R. Katz and S. C. Sharma, Phy. Med. Biol. 19, 413 (1974).
309. M. Bauman, G. Coutrakon, D. Lesyna, D. Miller, J. Nusbaum, J. Slater, P. DeLuca, J. Siebers, B. Ludewigt, J. Johanning and J. Miranda, *A prototype beam delivery system for the Proton Medical Accelerator at Loma Linda*, LLU report (1990).
310. C. A. Tobias, private communication (1985).
311. S. B. Curtis, A. Rodriguez, T. C.-N. Yang and E. A. Blakely, *Isosurvival testing of bar ridge filters for wobbled neon ion beams*, Biology and Medicine Division Annual Report, 1985, LBL, 149-150 (1986).
312. B. G. Karlsson, Strahlentherapie 124, 481 (1964).
313. S. I. Blokhin, L. L. Goldin, Y. L. Kleinbok, M. F. Lomanov, K. K. Onosovsky, L. M. Pavlonsky and V. S. Khoroshkov, Med. Radiol. (Moscow) 15, 64-68 (1970).
314. V. S. Khoroshkov, V. M. Breev, V. A. Zolotov, V. E. Lukyashin and G. G. Shimchuk, Med. Radiol. (Moscow) 32, 76-80 (1987).
315. Bevatron/Bevalac User's Handbook: Biology and Medicine, Lawrence Berkeley Laboratory, University of California, Berkeley, California, Pub-101 Rev. (1985).
316. E. Segre, *Experimental Nuclear Physics*, I, Wiley, New York, 282 (1953).
317. V. L. Highland, Nucl. Instrum. Methods 129, 497 (1975).
318. V. L. Highland, Nucl. Instrum. Methods 161, 171 (1979).
319. For example see: Aguilar-Benitez et al. (Particle Data Group), Phys. Lett. 170B (1986).
320. B. Gottschalk, *Multiple Coulomb Scattering of 160-MeV Protons*, HCL 11/19/90 (1990).
321. J. Carlsson and D. Rosander, Phys. Med. Biol. 18, 633-640 (1973).
322. A. M. Koehler, R. J. Schneider and J. M. Sisterson, Med. Phys. 4, 297-301 (1977).
323. B. Gottschalk, "Capabilities of passive beam-spreading techniques," *Proc. of the the Fifth PTCOG Meeting and the International Workshop on Biomedical Accelerators, December 1-2, 1986* (ed. by *Lawrence Berkeley Laboratory, Berkeley, CA*, LBL-22962: 161-168 (1986).
324. K. Crowe, L. Kanstein, J. T. Lyman and F. Yeater, *A large field medical beam at the 184-inch synchrocyclotron*, Lawrence Berkeley Laboratory, LBL-4235 (1975).
325. G. Sandberg, IEEE Trans. Nucl. Sci. NS-20, 1025 (1973).
326. A. Montelius and A. Brahme, *Charge particle beam flattening using an optimized dual scattering foil technique*, unpublished report (1987).

327. B. Gottschalk and M. S. Wagner, *Contoured scatterer for proton dose flattening*, Harvard Cyclotron Laboratory, a preliminary report 3/29/89, (1989).
328. E. A. Blakely, C. A. Tobias, P. Y. Chang, L. Lommel, M. J. Yezzi, L. M. Craise, I. S. Madfes and P. M. Martin, Radiat. Re. Soc. Abstracts, 25 (1983).
329. B. Gottschalk, A. M. Koehler and M. S. Wagner, "Upstream scattering modulation in proton therapy beams," *Proc. of the International Heavy Particle Therapy Workshop, Paul Scherrer Institute, September, 1989* (ed. by H. Blattmann), *Villigen, Switzerland*, PSI-Berich, Nr. 69: 19-23 (1989).
330. P. F. Meads Jr., IEE Trans. Nucl. Sci. NS-30, 2838-2840 (1983).
331. E. Kashy and B. Sherril, Nucl. Instrum. Methods B26, 610 (1987).
332. E. Kashy and B. Sherril, Nucl. Instrum. Methods B40, 41, 1004 (1989).
333. A. J. Jason, B. Blind and E. M. Svaton, *of the 1988 Linear Accelerator Conference, Oct. 3-7, 1988* (ed. by, CEBAF Report No. 89-001 (1988).
334. N. Tsoupas, R. Lankshear, J. C. L. Snead, T. E. Ward, M. Zucker and H. A. Enge, *Uniform beam distributions using octupoles*, BNL, Report NPB-90-15 (1990).
335. G. Silvestrov, private communication (1991).
336. B. Larsson, L. Leksell, B. Rexed and P. Sourander, Acta Radiol. 51, 52 (1959).
337. W. T. Chu, S. B. Curtis, J. Llacer, T. R. Renner and R. W. Sorensen, IEEE Trans. Nucl. Sci. NS-32, 3321-3323 (1985).
338. T. Kanai, private communication (1985).
339. T. R. Renner and W. T. Chu, Med. Phys. 14, 825-834 (1987).
340. E. L. Alpen and R. A. Gough, *The Heavy Ion Medical Accelerator: Final Design Summary*, Lawrence Berkeley Laboratory, PUB-5122 (1984).
341. T. Renner, W. Chu, M. McEvoy, M. Nyman, B. Gonzalez, R. Singh and R. Stradtner, IEEE Trans. Nucl. Sci. NS-32, 3324-3326 (1985).
342. W. T. Chu, "Biomedical facility at the Bevalac," *Proc. of the International Workshop on the NIRS Heavy Particle Medical Accelerator, March 1986* (ed. by K. K. H. Tsunemoto and H. Ohara), *Chiba, Japan*, National Institute of Radiological Sciences, Chiba, Japan, NIRS-M-63: 119-140 (1986).
343. M. Nyman, W. Chu, B. Mehlman, W. Mirer, H. Oakley, T. Renner, G. Stover and M. Tekawa, IEEE Trans. on Nucl. Sci. NS-32, 2177-2179 (1985).
344. F. C. Younger, "Permanent Magnet Wobbler for Proton Therapy," *Proc. of the Fifth PTCOG Meeting and International Workshop on Biomedical Accelerators," December 1-2, 1986* (ed. by W. T. Chu), *Lawrence Berkeley Laboratory, Berkeley, CA*, LBL-22962: 231-235 (1986).
345. C. Leemann, J. Alonso, H. Grunder, E. Hoyer, J. Kalnins, D. Rondeau, J. Staples and F. Volker, IEEE Trans. Nucl. Sci. NS-24, 1052-1054 (1977).

346. E. J. Lofgren, M. L. M. Boone et al., *Dedicated Medical Ion Accelerator Design Study, Final Report*, Lawrence Berkeley Laboratory, University of California and Arizona Medical Center, University of Arizona, December 1977, LBL-7230, TID 4500-R66, pp. 79-82 (1977).
347. P. M. Morse and H. Feshbach, Method of Theoretical Physics, McGraw Hill, New York, NY, 896-897 (Chapter 8, Part I) (1953).
348. Y. Censor, M. D. Altschuler and W. D. Powlis, Appl. Math. and Computation 25, 57-87 (1988).
349. B. K. Lind and P. Källman, Radiotherapy and Oncology 17, 359-368 (1990).
350. A. Brahme, B. Lind and P. Källman, Physica Medica VI, 53-68 (1990).
351. T. Holms, T. R. MacKie, D. Simpkin and P. Reckwerdt, Int. J. Radiat. Oncol. Biol. Phys. 20, 859-873 (1991).
352. P. Källman, B. K. Lind and A. Brahme, *An algorithm for maximizing the probability of complication free tumor control in radiation therapy*, Karolinska Institutet, Stockholm University, preprint (1991).
353. A. Brahme, P. Källman and B. Lind, "Optimization of the probability of achieving complication free tumor control using a 3D pencil beam scanning technique for proton and heavy ions," *Proc. of the NIRS International Workshop on Heavy Charged Particle Therapy and Related Subjects* (ed. by A. Itano and T. Kanai), *July 1991, Chiba, Japan*, 124-141 (1991).
354. E. Pedroni, H. Blattmann, T. Böhringer, A. Coray, S. Lin, S. Scheib and U. Schneider, "Voxel Scanning for Proton Therapy," *Proc. of the NIRS International Workshop on Heavy Charged Particle Therapy and Related Subjects* (ed. by A. Itano and T. Kanai), *July 1991, Chiba, Japan*, 94-109 (1991).
355. W. T. Chu and B. A. Ludewigt, private communication (1992).
356. W. T. Chu, T. R. Renner and B. A. Ludewigt, "Dynamic Beam Delivery for Three-Dimensional Conformal Therapy," *Proc. of the EULIMA Workshop on the Potential Value of Light Ion Beam Therapy, November 3-5, 1988* (ed. by P. Chauvel and A. Wambersie), *Nice, France*, EUR 12165 EN: 295-328 (1988).
357. E. L. Alpen, *Advanced design Research, Heavy Ion Medical Accelerator: Therapy Beam Optimization*, Lawrence Berkeley Laboratory, PUB-5113 (1984).
358. J. E. Milburn, J. T. Tanabe, T. R. Renner and W. T. Chu, "Raster Scanning for Relativistic Heavy Ions," *Proc. of the 1987 IEEE Particle Accelerator Conference, Accelerator Engineering and Technology, Washington, D. C., March 16-19, 1987* (ed. by E. R. Lindstrom and L. S. Taylor), *Washington, D. C.*, IEEE D Service Center, Piscataway, NJ, 3: 2000-2002 (1987).
359. W. T. Chu and R. W. Kuenning, "Limitations of Dynamic Beam Delivery Systems," *Proc. of the Fifth PTCOG Meeting and International Workshop on Biomedical Accelerators, December*

1-2, 1986 (ed. by W. T. Chu), *Lawrence Berkeley Laboratory, Berkeley, CA*, LBL-22962, UC-48, CONF-861271: 185-196 (1986).

360. G. Stover, M. Nyman, J. Halliwell, I. Lutz and R. Dwinell, *A Raster Scanning Power Supply System For Controlling Relativistic Heavy Ion Beams at the Bevalac Biomedical Facility*, 1987 IEEE Particle Accelerator Conference, Accelerator Engineering and Technology, March 16-19, 1987, Vol. 3, Washington, D. C., 1410-1412 (1987).
361. G. Stover, J. Halliwell, M. Nyman and R. Dwinell, *Operational Results for the Raster Scanning Power Supply System Constructed at the Bevalac Biomedical Facility*, 1989 IEEE Particle Accelerator Conference, March 1989, 3, Chicago, 1890-1892 (1989).
362. For example: such a device is supplied by Copely Controls Corp., 375 Elliot Street, Newton, MA 02164, .
363. T. R. Renner, W. T. Chu, B. A. Ludewigt, M. A. Nyman and R. Stradtner, Nucl. Instrum. Methods in Phys. Res. A281, 640-648 (1989).
364. T. R. Renner, W. Chu, B. Ludewigt, J. Halliwell, M. Nyman, R. P. Singh, G. D. Stover and R. Stradtner, *Preliminary Results of a Raster Scanning Beam Delivery System*, 1989 IEEE Particle Accelerator Conference, Accelerator and Technology, March 1989, Chicago, 672-674 (1989).
365. R. L. Martin, private communication (1992).
366. P. Grand, IEEE Trans. Nucl. Sci. NS-30, 3057-3059 (1983).
367. R. Bacher, H. Blattmann, T. Boehringer, A. Coray, E. Egger, E. Pedroni, M. Phillips and S. Scheib, "Development and First Results of Discrete Dynamic Spot Scanning with protons," *Proc. of the the International Heavy Particle Therapy Workshop (PTCOG/EORTC/ECNEU), Paul Scherrer Institut, September 1989* (ed. by H. Blattmann), *Villigen, Switzerland*, 9-12 (1989).
368. H. Blattmann, A. Coray, E. Pedroni and R. Greiner, Strahlentherapie und Onkologie 166, 45-48 (1990).
369. T. Kanai, K. Kawachi, Y. Kumamoto, H. Ogawa, T. Yamada, H. Matsuzawa and T. Inada, Med. Phys. 7, 365 - 369 (1980).
370. K. Kawachi, T. Kanai, H. Matsuzawa, Y. Kutsutani-Nakamura and T. Inada, Jpn. Acta Radiol. 42, 467-475 (1982).
371. T. Hiraoka, K. Kawashima, K. Hoshino, K. Kawachi, T. Kanai and H. Matsuzawa, Jpn. Acta Radiologica 43, 1214-1223 (1983).
372. C. A. Tobias, J. T. Lyman and J. H. Lawrence, "Some considerations of physical and biological factors in radiotherapy with high-LET radiations including heavy particles, pi mesons and fast neutrons," in *Atomic Medicine: Recent Advances in Nuclear Medicine* (ed. by J. H. Lawrence), Gurne and Stratton, Vol. 3, 167-218 (1971).

373. J. R. Castro, *Treatment of Cancer with Heavy Charged Particles*, Lawrence Berkeley Laboratory, PUB-5179 (1986).
374. M. M. Urie and M. Goitein, Med. Phys. 16, 593-601 (1989).
375. G. T. Y. Chen, S. Pitluck and J. T. Lyman, "Heavy Charged-Particle Treatment Planning," in *Biological and Medical Research with Accelerated Heavy Ions at the Bevalac, 1977-1980* (ed. by M. C. Pirruccello and C. A. Tobias), Lawrence Berkeley Laboratory, LBL-11220, UC-48, 325-331 (1980).
376. M. Goitein and G. T. Y. Chen, Med. Phys. 10, 831-840 (1983).
377. J. Lyman and P. Petti, private communication (1990).
378. J. T. Lyman, Radiat. Res. 104, S13-S19 (1985).
379. J. T. Lyman and A. B. Wolbarst, Int. J. Radiat. Oncol. Biol. Phys. 13, 103-109 (1987).
380. H. Blattmann, G. Munkel, A. Coray, T. Böhringer, K. Karasawa, W. Magdeburg, K. Nakagawa, E. Pedroni, M. Phillips, S. Scheib and W. Seelentag, "Accelerator plan for medical treatment with charged particles at Kyoto University," *Proc. of the NIRS International Workshop on Heavy Charged Particle Therapy and Related Subjects* (ed. by A. Itano and T. Kanai), *July 1991, Chiba, Japan*, 44-51 (1991).
381. I. Daftari, P. L. Petti, J. M. Collier, J. R. Castro and S. Pitluck, Med. Phys. to be published (1993); abstract, Med. Phys. 19: 830 (1992).
382. T. Kanai, K. Kawachi, H. Matsuzawa and T. Inada, Med. Phys. 10, 344-346 (1983).
383. T. Kanai, K. Kawachi, H. Matsuzawa and T. Inada, Nucl. Instrum. Methods 214, 491-496 (1983).
384. K. Kawachi, T. Kanai, H. Matsuzawa and T. Inada, Jpn. Acta Radiol. Supplementum 364, 81-88 (1983).
385. R. J. Berry and E. J. Hall, Brit. J. Radiol. 42, 102-107 (1969).
386. R. Oliver, Brit. J. Radiol. 42, 231-233 (1969).
387. T. Iwasaki, Y. Kato and S. Antoku, Radiat. Res. 57, 195-206 (1974).
388. S. Hornsey and T. Alper, Nature 210, 212-213 (1966).
389. S. B. Field and D. K. Bewley, Int. J. Radiat. Biol. 26, 259-267 (1974).
390. T. Inada, H. Nishio, S. Amino, K. Abe and K. Saito, Int. J. Radiat. Biol. 38, 139-145 (1980).
391. D. L. Dewey and J. W. Boag, Nature 183, 1450-1451 (1957).
392. W. T. Chu, *Dose-rate effects in various beam delivery systems*, presented at the Workshop on Medical Charged-Particle Beam Scanning Systems, Lawrence Berkeley Laboratory, Berkeley, CA, January 1988, unpublished (1988).

393. W. T. Chu, "High dose-rate effect from beam scanning," in *Report of the Facility Working Group, Proton Therapy CoOperative Group* (ed. by L. Verhey), Massachusetts General Hospital, Boston, MA, (1987).

394. K. Karasawa, K. Nakagawa, Y. Aoki, K. Hasezawa, Y. Onogi, A. Terahara, N. Muta, K. Sakata, A. Akanuma, M. Iio and H. Kawakami, "The Feasibility of Photon conformation Therapy with Multi-Leaf Collimaotrs in Brain (Japanese Experience)," *Proc. of the the International Heavy Particle Therapy Workshop, Paul Scherrer Institute, Villigen, Switzerland, September, 1989* (ed. by H. Blattmann),, PSI-Bericht Nr. 69: 83-89 (1990).

395. W. T. Chu, B. A. Ludewigt, K. M. Marks, M. A. Nyman, T. R. Renner, R. P. Singh and R. Stradtner, "Three-Dimensional Conformal Therapy Using Light-Ion Beams," *Proc. of the NIRS International Workshop on Heavy Charged Particle Therapy and Related Subjects* (ed. by A. Itano and T. Kanai), *July 4-5, 1991, Chiba, Japan*, 110-123 (1991).

396. T. Kanai, *the original basic design at the NIRS was a leaf with a step and the total width greater than twice the range of the primary ion beam*, private communication (1991).

397. P. Källman, B. Lind, A. Eklöf and A. Brahme, Phys. Med. Biol. 33, 1291-1300 (1988).

398. J. W. Boag, "Ionization Chambers," in *Radiation Dosimetry* (ed. by F. H. Attix and W. C. Roesch), Academic Press, New York, 2nd ed., Vol. II, Instrumentation, 1-72 (1966).

399. I. T. Myers, in *Ionization in Radiation Dosimetry*, ed. F. H. Attix, W. Roesch and E. Tochilin, 1, Academic Press, New York, 317-330 (1968).

400. L. Bragg, Proc. Roy. Soc. Ser. A 156, 578 (1936).

401. D. J. Thomas and M. Burke, Phys. Med. Biol. 30, 1201-1213 (1985).

402. P. L. Petti, L. Verhey and R. Wilson, Phys. Med. Biol. 31, 1129-1138 (1986).

403. L. J. Verhey, A. M. Koehler, J. C. McDonald, M. Goitein, I.-C. Ma, R. J. Schneider and M. Wagner, Radiat. Res. 79, 34-54 (1979).

404. L. J. Verhey and J. T. Lyman, Med. Phys. 19, 151-153 (1992).

405. ICRU, *Average Energy Required to Produce an Ion Pair*, Int. Comm. Radiat. Units Meas., Bethesda, Report No. 31 (1979).

406. Y. Hayakawa and H. Schechtman, Med. Phys. 15, 778 (1988).

407. T. R. Renner, W. T. Chu, B. Ludewigt, K. Milne, M. Nyman and R. Stradtner, "Detector systems for clinical beam delivery systems," *Proc. of the* (ed. by P. Chauvel, A. Wambersie and P. Mandrillon), *Nice, France*, S67-S69 (1990).

408. F. R. Shonka, J. E. Rose and G. Failla, *Conducting plastic equivalent to tissue, air and polystyrene*, U.N. Int. Conf. Peaceful Uses Atomic Energy, 2nd, Geneva 21, 184-187 (1958).

409. Kase, Bjarngard and Attix, *The Dosimetry of Ionizing Radiation*, vol. 2, 2nd ed., Academic Press (1966).

410. J. W. Boag, "Ionizing Cambers," in *The dosimetry of Ionizing Radiation* (ed. by K. R. Kase, B. E. Bjarngard and F.H.Attix), Academic Press, Vol. II, pp. 169-243 (1987).
411. J. W. Boag, Phys. Med. Biol. 9, 25-32 (1964).
412. F. H. Attix, Med. Phys. 17, 931-933 (1990).
413. H. Kubo, L. J. Kent and G. Krithivas, Med. Phy. 13, 242-247 (1986).
414. J. R. Cunningham and M. C. Sontag, Med. Phys. 7, 672-676 (1980).
415. J. T. Lyman, J. Howard and A. A. Windsor, Med. Phys. 2, 163 (1975).
416. E. Pedroni, R. Bacher, H. Blattmann, T. Boehringer, A. Coray, M. Phillips and S. Scheib, "Cancer therapy with 200 MeV protons at PSI. Development of a fast beam scanning method and future plans for a hospital facility," *Proc. of the EPAC 90, Medical Satellite Meeting, June 14-16, 1990* (ed. by P. Chauvel, A. Wambersie and P. Mandrillon), *Nice, France*, S100-S102 (1990).
417. AAPM Radiat. Therapy Comm. (Task Group 21), *A protocole for the determination of absorbed dose from high-energy photon and electron beams*, Med. Phys., **10**, 741-771 (1983).
418. J. W. Boag and T. Wilson, Brit. J. Appl. Phys. 3, 222 (1952).
419. P. R. Almond, Med. Phys. 8, 901 (1981).
420. J. W. Boag, Phys. Med. Biol. 27, 201-211 (1982).
421. Y. Hayakawa, C. P. Loch, J. Tada and T. Inada, Med. Phys. 16, 346-351 (1989).
422. ICRU, *The dosimetry of pulsed radiation*, Int. Comm. Radiat. Units Meas., Washington, DC, Report 34 (1979).
423. T. Hiraoka, K. Kawashima and K. Hoshino, Phys. Med. Biol. 33, Suppl. 1, 131 (1988).
424. I. A. D. Lewis and B. Collinge, Rev. Sci. Instrum. 24, 1113-1115 (1953).
425. B. Gottchalk, Nucl. Instrum. Methods 207, 417-421 (1983).
426. E. G. Shapiro, IEEE Trans. Nucl. Sci. NS-17, 335 (1970).
427. T. E. Berlin, "Vacuum chambers for radiation measurements," in *Topics in Radiation Dosimetry* (ed. by F. H. Attix), Academic Press, New Yoirk, Suppl. 1, 143 (1972).
428. G. W. Tautfest and H. R. Fechter, Rev. Sci. Instrum. 26, 229-231 (1955).
429. F. Sauli, *Principles of Operation of Multiwire Proportional and Drift Chambers*, CERN European Organization for Nuclear Research, Geneva, Switzerland, 3 May 1977, CERN 77-09 (1977).
430. G. Charpak and F. Sauli, Nucl. Instrum. and Methods 162, 405 (1979).
431. J. R. Alonso, C. A. Tobias and W. T. Chu, IEEE Trans. Nucl. Sci. NS-26, 3077-3079 (1979).
432. W. T. Chu, J. R. Alonso and C. A. Tobias, IEEE Trans. Nucl. Sci. NS-28, 2198-2200 (1981).

433. W. R. Holley, C. A. Tobias, J. I. Fabrikant, J. Llacer, W. T. Chu and E. V. Benton, *Computerized Heavy-Ion Tomography*, SPIE — The International Society for Optical Engineering, Application of Optical Instrumentation in Medicine IX, 273, San Francisco, 283-293 (1981).

434. L. A. Shepp and B. F. Logan, IEEE Trans. Nucl.Sci. NS-21, 21-43 (1974).

435. *Biological and Medical Research with Accelerated Heavy Ions at the Bevalac, 1977-1980*, ed. M. C. Pirruccello and C. A. Tobias, LBL-11220, Lawrence BerkeleyLaboratory, Berkeley, 423 pages (1980).

436. J. W. Fowler, "Solid State Electrical Conductivity Dosimeters," in *Radiation Dosimetry* (ed. by F. H. Attix and W. C. Roesch), Academic Press, New York, Volume 2 (2nd edition), 241 (1966).

437. B. Gottschalk, *Calibrating dosimeter arrays," HCL Technical Report*, Harvard Cyclotron Lab, Cambridge, MA, Note 6/10/88 (1988).

438. E. Tochilin, J. T. Lyman, F. H. Attix and E. J. West, *The dose response of glass, thermoluminescent and film dosimeters to high-energy charged particles*, Supplement to Biology and Medicine Semiannual Report, Lawrence Berkely Laboratory, Fall 1962 (1962).

439. H. Sunaga, T. Agematsu, R. Tanaka, K. Yosida and I. Kohno, Radioisotopes 37, 84-87 (1988).

440. E. Tochilin, N. Goldstein, J. T. Lyman and W. G. Miller, *The quality and LET dependance of three thermoluminescent dosimeters and their potential use as secondary standards*, Navy Radiological Defense Laboratory (1968).

441. C. A. Carlsson and C. G. Alm, Radiat. Res. 42, 207 (1970).

442. C. L. Chu, K. R. Hogstrom, G. C. Chen and R. L. Hilko, Phys. Med. Biol. 31, 145-160 (1986).

443. F. S. Fricke and E. J. Hart, "Chemical Dosimetry," in *Radiation Dosimetry* (ed. by F. H. Attix and W. C. Roesch), Academic Press, New York, 2nd ed., Vol. II, Instrumentation, 167-239 (1966).

444. A. O. Allen, *The Radiation Chemistry of Water and Aqueous Solutions*, Van Nostrand, Princeton, NJ (1961).

445. R. J. Shalek, W. K. Sinclair and J. C. Calkins, Radiat. Res. 16, 344-351 (1962).

446. S. Graffman and B. Jung, Acta Radiol. Therapy Phys. Biol. 14, 113-126 (1975).

447. J. S. Laughlin and S. Genna, "Calorimetry," in *Radiation Dosimetry* (ed. by F. H. Attix and W. C. Roesch), Academic Press, New York, Volume II, Instrumentation, 389-441 (1966).

448. ICRU, *Radiation Dosimetry: X Rays and Gamma Rays with Maximum Photon Energies between 0.6 and 50 MeV*, IInt. Comm. Radiat. Units Meas., Washington, DC, Report No. 14 (1969).

449. J. C. McDonald and S. R. Domen, Nucl. Instr. Meth. Phys. Res. 752, 35-40 (1986).
450. S. Vynckier, J.-P. Meulders, P. Robert and A. Wambersie, J. Eur. Radioth, 5, 245-247 (1984).
451. A. Kacperek and D. E. Bonnet, *The Use of a Faraday Cup in the Dosimetry of a 62 MeV Proton Beam*, (to be published), (1989).
452. F. S. Goulding, *Semiconductor detectors for nuclear spectrometry*, Lawrence Berkeley Laboratory, UCRL-16231 (1965).
453. C. Richman, Radiat. Res. 66, 453 (1976).
454. W. J. Ramm, "Scintillation Detectors," in *Radiation Dosimetry* (ed. by F. H. Attix and W. C. Roesch), Academic Press, New York, Volume II, Instrumentation, 123-166 (1966).
455. R. L. Heath, R. Hofstader and E. B. Hughes, Nucl. Instrum. and Methods 162, 431 (1979).
456. F. D. Brooks, Nucl. Instrum. and Methods 162, 477 (1979).
457. G. Coutrakon, D. Miller, B. J. Kross, D. F. Anderson, P. DeLuca and J. Siebers, Med. Phys. 18, 817-820 (1991).
458. B. J. Dropesky, G. W. Butler, C. J. Orth, R. A. Williams, M. A. Yates-Williams, G.Friedlander and S. B. Kaurman, Phys. Rev. C 20, 1844 (1979).
459. G. F. Knoll, *Radiation detection and measurement*, John Wiley & Sons, New York, p. 248 (1979).
460. G. Coutrakon, D. Miller, J. Wong, L. Gere and R. Binns, Med. Phys. 17, 543 (1990).
461. E. C. H. Silk and R. S. Barnes, Philos. Mag. 4, 970 (1959).
462. G. Somogyi, M. Toth-Szilagyi, M. Monin et al., Tenth Intern. Conf. on Solid State Nuclear Track Detectors, Pergamon Press, Oxford, 267 (1980).
463. D. A. Young, Nature 182, 375 (1958).
464. S. P. Tret'yakova, Soviet J. of Particles & Nuclei 23 (2), 156-186 (1992).
465. R. L. Fleischer, P. B. Price and R. M. Walker, *Nuclear Tracks in Solids: Priinciples and Applications*, Univ. of Calif. Press, Berkeley (1975).
466. R. M. Cassou and E. V. Benton, Nucl. Track Detection. 2, 173 (1978).
467. E. Benton, R. Henke, R. Cassou, G. T. Y. Chen and J. T. Lyman, Med. Phys. 10, 534-535 (1983).
468. R. P. Henke and E. V. Benton, Nucl. Track Detection 1, 93 (1977).
469. R. P. Henke and E. V. Benton, Nucl. Instrum. Methods 142, 521 (1977).
470. E. V. Benton, R. P. Henke and C. A. Tobias, Nucl. Track Detection. 1, 139 (1977).
471. J. R. Alonso, E. V. Benton, W. Chu, J. Llacer, J. Richier and C. A. Tobias, "Instrumentation for measuring heavy-ion fields," in *Biological and Medical Research with Accelerated Heavy*

Ions at the Bevalac, 1977-1980 (ed. by C. Pirruccello and C. A. Tobias), LBL-11220, 21-34 (1980).

472. W. Heinrich, H. Drechsel, R. Rudat, E. V. Benton and D. Hildebrand, Nucl. Instrum. Methods 190, 369-376 (1981).
473. J. Llacer, Nucl. Sci. Applications 3, 111 (1988).
474. J. Llacer, J. B. Schmidt and C. A. Tobias, Med. Phys. 17, 158-162 (1990).
475. J. Llacer and H. W. Kraner, Nucl. Instrum. and Methods 98, 467-475 (1972).
476. D. E. Greiner, Nucl. Instrum. Methods 103, 291-308 (1972).
477. G. D. Westfall, L. W. Wilson, P. J. Lindstrom, H. J. Crawford, D. E. Greiner and H. H. Hackman, Phys. Rev. C 19, 1309-1323 (1979).
478. W. Schimmerling, S. B. Curtis and K. G. Vosburgh, Radiat. Res. 72, 1-17 (1977).
479. W. Schimmerling, T. S. Subramanian, W. J. McDonald, S. N. Kaplan, A. Sadoff and G. Gabor, Nucl. Instrum. Methods 205, 531-543 (1983).
480. G. Gabor, W. Schimmerling, D. E. Greiner, F. Bieser and Lindstrom, Nucl. Instrum. Methods 130, 65 (1975).
481. M. Wong, W. Schimmerling, M. H. Phillips, B. A. Ludewigt, D. A. Landis, J. T. Walton and S. B. Curtis, Med. Phys. 17, 163-171 (1990).
482. J. W. Hilbert and N. A. Baily, Radiology 92, 168-169 (1969).
483. H. H. Rossi, "Microscopic energy distribution in irradiated matter," in *Radiation Dosimetry* (ed. by F. A. Attix and W. C. Roesch), Academic Press, New York, Vol. 1, 43-92 (1968).
484. V. A. Pitkevich and V. G. Videnskii, Radiobiologiia 16, 411-416 (1976).
485. V. G. Videnskii and V. A. Pitkevich, Radiobiologiia 16, 402-406 (1976).
486. V. G. Videnskii and V. A. Pitkevich, Med. Radiol. (Moscow) 21, 82-84 (1976).
487. P. J. Kliauga, R. D. Colvett, Y. M. Lam and H. H. Rossi, Int. J. Radiat. Oncol. Biol. Phys. 4, 1001-1008 (1978).
488. A. M. Kellerer, "Fundamentals of Microdosimetry," in *The Dosimetry of Ionizing Radiation* (ed. by K. R. Krase, B. E. Bjarngard and F. H. Attix), Academic Press, New York, I, (1985).
489. ICRU, *Microdosimetry*, Int. Comm. Radiat. Units Meas., Washington, DC, Report 36 (19??).
490. D. T. Goodhead, "Relationship of Microdosimetric Techniques to Application in Biological Systems," in *The Dosimetry of Ionizing Radiation* (ed. by K. R. Krase, B. E. Bjarngard and F. H. Attix), Academic Press, New York, II, (1985).
491. N. F. Metting, H. H. Rossi, L. A. Braby, P. J. Kliauga, J. Howard, M. Zaider, W. Schimmerling, M. Wong and M. Rapkin, Radiat. Res. 116, 183-195 (1988).
492. M. Zaider, J. F. DiCello, D. J. Brenner, M. Takai and M. R. Raju, Rad. Res. 87, 511 (1981).

493. J. F. Dicello, J. T. Lyman, J. C. Mcdonald and L. J. Verhey, Nucl. Instrum. and Methods B45, 724 (1990).
494. G. Luxton, P. Fessenden and W. Hoffmann, Radiat. Res. 79, 256-272 (1979).
495. V. M. Abazov, S. A. Gustov, V. P. Zorin, S. A. Kutuzov and I. V. Mirokhin, Med. Radiol. (Moscow) 32, 72-73 (1987).
496. R. P. Singh, W. T. Chu, B. A. Ludewigt, K. M. Marks, M. A. Nyman, T. R. Renner and R. Stradtner, *Software Quality Assurance and Software in the Biomed Control System*, Lawrence Berkeley Laboratory, Berkeley, CA, LBL Report 27948 (1989).
497. C. A. Tobias, E. V. Benton, M. P. Capp, A. Chatterjee, M. R. Cruty and R. P. Henke, Int. J. Radiat. Oncol. Biol. Phys. 3, 35-44 (1977).
498. A. Chatterjee, C. A. Tobias and J. T. Lyman, "Nuclear fragmentation in therapeutic and diagnostic studies with heavy ions," in *Spallation Nuclear Reactions with their Applications* (ed. by B. S. P. Shaw and M. Merker), Dordrecht-Holland: Reidel, Boston, 168-191 (1978).
499. A. Chatterjee, E. L. Alpen, C. A. Tobias, J. Llacer and J. Alonso, Int. J. Radiat. Oncol. Biol. Phys. 7, 503-507 (1981).
500. A. Chatterjee, W. Saunders, E. L. Alpen, J. Alonso, J. Scherer and J. Llacer, Radiat. Res. 92, 230-244 (1982).
501. E. L. Alpen, private communication (1985).
502. J. Llacer, A. Chatterjee, E. L. Alpen, W. Saunders, S. Andreae and H. C. Jackson, IEEE Trans. Med. Imaging MI-3, 80-90 (1984).
503. E. L. Alpen, W. Saunders, A. Chatterjee, J. Llacer, G. T. Chen and J. Scherer, Brit. J. Radiol. 58, 542-548 (1985).
504. A. Chatterjee, J. Llacer, M. Collier, T. Renner, S. Henderson and W. Chu, "Diagnostic application of radioactive beams," *Proc. of the Fifth PTCOG Meeting and International workshop on biomedical accelerators* (ed. by W. T. Chu), *Berkeley, CA*, 213-230 (1986).
505. S. D. Henderson, M. Collier, T. Renner, A. Chatterjee and J. Llacer, Med. Phy. 14, 468 (1987).
506. J. R. Alonso, A. Chatterjee and C. A. Tobias, IEEE Trans. Nucl. Sci. NS-26, 3003-3005 (1979).
507. J. R. Alonso, B. Feinberg, J. G. Kalnins, G. F. Krebs, M. A. McMahan and I. Tanihata, "Radioactive beam production at the Bevalac," *Proc. of the First International Conference on Radioactive Nuclear Beams, Berkeley, CA, October 16-18, 1989* (ed. by W. D. Myers, J. M. Mitschke and E. B. Norman),, World Scientific Publishing Co., Teaneck, NJ, 112 (1990).
508. J. R. Alonso, IEEE Trans. Nucl. Sci. NS-32, 1728-1731 (1985).

509. G. Berger, M. Bouvy, Th. Daras, E. Kaerts, M. Loiselet and G. Ryckewaert, *Radioactive ion beams: Results and perspectives for light ion therapy and diagnostic purposes*, 2nd European Particle Accelerator Conference, June 1990, Nice, France, 1793-1795 (1990).

510. G. Berger, Th. Daras, M. Loiselet, N. Postiau and G. Ryckewaert, *Acceleration and mass-separation of radioactive ion beams in an isochronous cyclotron*, IEEE 1991 Particle Accelerator Conference, Accelerator Science and Technology, May 1991, 4, San Francisco, CA, 2610-2612 (1991).

511. J. Llacer, H. Spieler and F. S. Goulding, *Theoretical analysis of the use of germanium detectors for time-of-flight emission tomography*, Workshop of TOF Tomography, May 1982, 448, IEEE Computer Society, St. Louis, 75-82 (1982).

512. J. Llacer, A. Chatterjee, B. Jackson, J. Lin and V. Zunzuneqi, IEEE Trans. Nucl. Sci. NS-26, 636-647 (1979).

513. J. Llacer, A. Chatterjee, E. K. Batho and J. A. Poskanzer, IEEE Trans. Nucl. Sci. NS-30, 617-625 (1983).

514. T. Haberer, W. Becher, D. Böhne, G. Kraft, B. Langenbeck, G. Lenz, D. Loos, W. Rösch, D. Schardt, R. Steiner and H. Stelzer, "Magnetic Scanning System for Heavy Ion Therapy," in *Fourth Workshop on Heavy Charged Particle in Biology and Medicine, in connection with the XV PTCOG Meeting* (ed. by G. Kraft), GSI, Darmstadt, Germany, Extended Abstracts, GSI-91-29, ISSN 0171-4546, Paper G2 (1991).

515. L. Valentine, G. Albany, J. P. Cohen and M. Gusakow, Phys. Rev. Letters 7, 163 (1963).

516. G. W. Bennett, A. C. Goldberg, G. S. Levine, J. Guthy, J. Balsamo and J. O. Archambeau, Nuc.r Instrum. Methods 125, 333-338 (1975).

517. G. W. Bennett and J. O. Archambeau, Med. Phys. 4, 115-117 (1977).

518. G. W. Bennett, J. O. Archambeau, B. E. Archambeau, J. I. Meltzer and C. L. Wingate, Science 200, 1151-1153 (1978).

519. D. West and A. C. Sherwood, Nature 236, 157-159 (1972).

520. K. M. Crowe, T. F. Budinger, J. L. Cahoon, V. P. Elischer, R. H. Huesman and L. L. Kanstein, IEEE Trans. Nucl. Sci. NS-22, 1752-1754 (1975).

521. E. V. Benton, R. P. Henke, C. A. Tobias, W. R. Holley and J. I. Fabrikant, *Charged-particle radiography*, Solid State Nuclear Track Detectors, 725 (1980).

522. A. M. Cormack and A. M. Koehler, Phys. Med. Biol. 21, 560-569 (1976).

523. S. L. Kramer, IEEE Trans. Nucl. Sci. NS-28, 1910-1915 (1981).

524. C. A. Tobias, E.V.Benton and M.P.Capp, in *Recent Advances in Nuclear Medicine* (ed. by J. H. Lawrence and T. F. Budinger), Grune & Stratton, Inc., 5, 71 (1978).

525. F. G. Sommer, M. P. Capp, C. A. Tobias, E. V. Benton, K. H. Woodruff, R. P. Henke, W. Holley and H. K. Genant, Investigative Radiology 13, 163 (1978).

526. M. P. Capp, F. G. Sommer, C. A. Tobias and E. V. Benton, Recent and Future Developments in Medical Imaging, SPIE 152 (1978).
527. W. R. Holley, R. P. Henke, G. E. Gauger, B. Jones, E. V. Benton, J. I. Fabrikant and C. A. Tobias, "Heavy particle computed tomography," *Proc. of the Sixth Computer Radiology Conference* (ed. by, June 1979 (1979).
528. J. I. Fabrikant, C. A. Tobias, M. P. Capp, E. V. Benton and W. R. Holley, Application of Optical Instrumentation in Medicine VIII, SPIE 233, 255 (1980).
529. J. Llacer, IEEE Trans. Nucl. Sci. NS-26, 596-602 (1979).
530. J. Llacer, W. Chu, C. A. Tobias, J. I. Fabrikant and J. R. Alonso, "Active Heavy-Ion Radiography and Computerized Tomography," in *Biological and Medical Research with Accelerated Heavy Ions at the Bevalac, 1977-1980* (ed. by M. C. Pirruccello and C. A. Tobias), Lawrence Berkeley Laboratory, Report LBL-11220, 367-374 (1980).
531. W. T. Chu, J. R. Alonso and C. A. Tobias, *Imaging with a Multiplane Multiwire Proportional Chamber Using Heavy Ion Beams*, International Workshop on Physics and Engineering in Medical Imaging, Pacific Grove, California, March 1982,, IEEE Computer Society, Los Angeles, 221-224 (1982).
532. W. T. Chu, "Imaging Using Accelerated Heavy Ions," *Proc. of the Workshop on Computerized Tomography and Multi-Dimensional Digital Image Processing, Korea Advance Institute of Science and Technology, Seoul, Korea, May 1982* (ed. by Z. H. Cho),, 21-27 (1983).

LAWRENCE BERKELEY LABORATORY
UNIVERSITY OF CALIFORNIA
TECHNICAL INFORMATION DEPARTMENT
BERKELEY, CALIFORNIA 94720